Università degli Studi Di Cagliari

Dottorato di Ricerca

INGEGNERIA INDUSTRIALE

CICLO XXIX

Titolo Tesi

SUPERVISION AND DIAGNOSIS OF INDUSTRIAL SYSTEMS

Settore/i scientifico disciplinari di afferenza

ING-INF/04 AUTOMATICA

Presentata da: **Gianluca Fadda**

Coordinatore Dottorato: **Prof. Francesco Aymerich**

Tutor: **Prof. Elio Usai**

Esame finale anno accademico 2015 - 2016

Tesi discussa nella sessione d'esame marzo - aprile 2017

Alla mia famiglia

Abstract

This Thesis focuses on two specific research areas, both related to the subject of supervision and diagnosis of industrial systems.

One topic is the fault detection and diagnosis, a subfield of the control engineering which concerns itself with monitoring a system, identifying when a fault occurred, and pinpointing both the type and location of fault. Within this context, this research addresses the issue of discriminating between different faults which could affect both sensors and actuators of a generic system, by developing a novel proposal based on two main concepts, namely sliding mode observer and residual signature. The validity of the proposed fault diagnosis scheme was tested successfully on a steam separator unit of a thermal power plant. This proposal and its first results have been presented in the works [Fadda et al., 2015b] and [Fadda et al., 2015a], whereas a first theoretic background to support this hybrid scheme was recently provided in [Fadda et al., 2016].

The other topic is the data reconciliation and parameter estimation, a crucial technology which allows for obtaining and validating reliable process models. Within this other context, in this research the joint problem of performing in real-time the reconciliation of measurements and the estimation of the model's parameters, by exploiting the concept of temporal redundancy, has been examined, and a suitable filtering approach which exploits the concepts of quasi-steady-state and Kalman filter has been developed. An important contribution to the state-of-the-art results in the opportunity of decoupling the two tasks of dynamic data reconciliation and parameter estimation by means of two different schemes, which allow for turning on the parameter estimation filter only when a stable estimate of the state has been achieved. Also in this case, the effectiveness of the proposal has been evaluated on a real industrial application, related to monitoring the healthy conditions of a pyrolysis reactor. A scientific paper about this contribution will be submitted soon.

It is worth to remark that this research has been partially supported by the projects PGR00152-RObust Decentralised Estimation fOr large-scale systems (RODEO), of the Italian Ministry for Foreign Affairs and International Cooperation, and by Region Sardinia project n°CRP-24709 "SIAR - Sistemi Interconnessi per l'Automazione su Reti" (L. R. 7/2007).

Acknowledgements

First and foremost, I am really grateful to my advisor, Prof. Elio Usai, for his trust, motivation, and guidance. Based on his vast knowledge, he supported me throughout the entire period of this research with patience, whilst allowing me the liberty to work in my own way. I could not have imagined having a better advisor and mentor for my Ph.D study.

Furthermore, I would like to express my sincere gratitude also to my other mentor, Prof. José Romagnoli, an outstanding person who gave me the valuable opportunity to work with him and his brilliant research group within a traineeship period at the Louisiana State University. An important part of this dissertation would not have been possible without his priceless help and continuous support.

A special thanks goes to my fellow lab mates in the Automatic Control Group of Cagliari: Alessandro Pilloni, who has provided me with a lot of help and support with my research, Antonello Baccoli, for the stimulating discussions and for all the fun we have had in the last years, Alessandro Pisano and Mauro Franceschelli for their valuable comments and suggestions.

My sincere thanks goes also to my fellow lab mates in the Process Systems Engineering group at the Louisiana State University: Santiago Salas, Wenbo Zhu, Jorge Chebeir, Michael Thomas, Aryan Geraili Nejadfomeshi and Navid Ghadipasha, including the Associate Director of the International Services at LSU, Ms. Loveness Schafer, for their invaluable kindness, helpfulness and hospitality. Thank you all for making my visit in the U.S. so comfortable and memorable.

Particular thanks to Prof. Zeljko Durovic and and his whole staff, including Veljko Papic, Predrag Tadić, and Predrag Todorov, as well my two co-authors Sanja Vujnović and Alexsandra Marjanović, for their hospitality and precious support throughout my visiting periods at the University of Belgrade, within the RODEO project.

I am truly grateful to my boss Giovanni Mascia, for encouraging me to start this Ph.D, and for believing in me throughout all these years.

Last but not the least, I would like to thank all of my family for their continued help and support, and my girlfriend for her encouragement, understanding, and patience even during hard times of this study.

Finally, I appreciate the financial support provided me by the University of Cagliari, which made possible my traineeship in the U.S.

Contents

List of Figures

List of Tables

List of Abbreviations

AC Alternate Current.
ANN Artificial Neutral Network.

BFDF Beard Fault Detection Filter.

CK Correlated Kurtosis.
CUSUM CUmulative SUM.

DC Direct Current.
DD Data-Driven.
DDR Dynamic Data Reconciliation.
DFT Discrete Fourier Transform.
DR Data Reconciliation.
DTCWT Dual-tree complex wavelet transform.
DTW Dynamic Time Warping.

EIV Error-In-Variable.
EKF Extended Kalman Filter.

FD Frquency-Domain.
FDD HFault Detection and Diagnosis.
FDI Fault Detection and Isolation.
FFT Fast Fourier Transform.
FIR Finite Impulse Response.
FL Fuzzy Logic.
FPGA Field Programmable Fate Array.

GUI Graphical User Interface.

HHT Hilbert-Huang transform.

ICA Independent Component Analysis.

KF Kalman Filter.
KNN K-Nearest-Neighborhood.

LBP Local Binary Patterns.
LD Linear Dynamic.
LPG Liquid Petroleum Gas.
LSE Least Square Estimation.
LTI Linear Time Invariant.

MB Model-Based.
MCSA Motor-Current Signature Analysis.
MIMO Multiple In Multiple Out.

NLP Non-Linear Programming.
NN Neural Network.

ODR Orthogonal Distance Regression.

PCA Principal Component Analysis.
PE Parameter Estimation.
PLS Partial Least Squares.
PMSG Permanent Magnet Synchronous Generator.

QP Quadratic Programming.
QSS Quasi-Steady-State.
QTA Qualitative Trend Analysis.

SB Signal-Based.
SDG Signed Directed Graphs.
SIFT Scale Invariant Feature Transform.
SISO Single Input Single Output.
SMO Sliding Mode Observer.
SQP Sequential Quadratic Programming.
SS State-Space.
STFT Short-Time Fourier Transform.
SVM Support Vector Machine.

T-PLS Total Projection to Latent Structures.
TD Time-Domain.
TFD Time-Frquency-Domain.
TLE Transfer Line Exchanger.

UIO Unknown input observers.

WT Wavelet Transform.
WVD Wigner-Ville distribution.

Introduction

The first two Sections of this Chapter aim to provide the main purposes of this work, and the outline of this Thesis, respectively. Some of the topics in the present dissertation were presented both in national and international conferences and papers. The last Section of this Chapter contains the list of the Author's publications derived from the present work.

Background and Motivation

Optimization in terms of costs and productivity has been always one of the most important goals and the common objective for many industrial activities. The fast and steady progress in many technological fields is getting every day to more complex industrial plants and the corresponding control systems also are getting more sophisticated in both hardware and software components. Furthermore, the increasing demand in terms of higher safety, availability and reliability of the plant is another critical aspect to be taken into account. The process monitoring, that is the supervision, control, and diagnosis of industrial processes is the line of research where all the aspects mentioned above are considered. This dissertation focuses its attention on two specific subjects of the process monitoring, which are respectively the Fault Detection, Isolation and Diagnosis (FDD) and the Data Reconciliation (DR) and Parameter Estimation (PE) in industrial applications.

The increasing of complexity in an industrial plant results in an higher probability of plant failure and in a larger amount of errors and faults in the process measurement. As a consequence, the ability of automatically detect and isolate malfunctions both in the process and in the plant instrumentation as early as possible are demanding task which is receiving considerable interest both from the industrial as well as the academic point of view.

Indeed, the early fault diagnosis while the process is still operating in a controllable region could help avoiding the evolution of abnormal events, thus consequently productivity losses could be reduced as well as major breakdowns or catastrophes.

Thesis Outline

The whole content of this dissertation was arranged in two main parts. The part I, called "State of the Art", provides a survey on the concepts and theoretical preliminaries needed to understand the remains of this Thesis. Based on the available information reported in the literature, the broad features of the main methodologies will be reviewed, without going into details. However, only those approaches which result to be strictly related to the Author's proposal will be reviewed in detail, in order to highlight some important concept exploited in the following of the dissertation. The part II, called "Author's Contributions", presents and discusses the results and novel proposals of this research. In the following, the subject

of each Chapter is briefly explained:

Part I: State of the Art

- Chapter 1. **Fault Detection, Isolation and Diagnosis**: The introductory Sections provide some basic concepts and definitions related to the topic of fault detection and diagnosis in industrial plants. Then, a comprehensive review of model-based, signal-based, and data-driven fault diagnosis methods is presented. Finally, hybrid approaches are briefly discussed. The objective is to introduce the reader to the part of the research developed in the Chapters 3 and 4.

- Chapter 2. **Data Reconciliation and Parameter Estimation**: At first, some basic concepts and definitions, related to the topics of data reconciliation and parameter estimation are introduced. Then, a rapid overview of different data reconciliation methods, where both steady-state and dynamic approaches are taken into account. Finally, the parameter estimation problem is also considered, as well as some approaches to implement the parameter estimation along the data reconciliation. The objective is to introduce the reader to the part of the research developed in the Chapters 5 and 6.

Part II: Author's Contributions

- Chapter 3. **Hybrid Fault Detection and Diagnosis**: This Chapter focuses on the novel hybrid FDD proposal developed in this research to achieve a complete fault isolation and diagnosis. The general architecture is depicted at fist, then the two main modules of the FDD scheme are described in detail, i.e. the residual generator, based on the concept of Sliding Mode Observer (SMO), and the residual evaluator, based on the concept of residual signature analysis. Finally, the ongoing part of this research is discussed.

- Chapter 4. **Practical Application: Steam Separator**: This Chapter discusses the development of a practical application, which confirms the validity of the proposal explained in Chapter 3. The linearized model of the system, i.e. a steam separator unit of a thermal power plant, is presented at first. Then, two different SMOs for sensor and actuator fault detection are developed, and their corresponding residual sets are designed to achieve the fault diagnosis. Finally, the experimental results are shown and commented.

- Chapter 5. **Real-time DDR State-Parameter Estimation**: This Chapter focuses on the novel approach developed in this research to implement a real-time version of the data reconciliation technique along with the parameter estimation. The two fundamental concepts behind this proposal, i.e. Quasi-Steady-State (QSS) model and Dynamic Data Reconciliation (DDR), are introduced at first. Then, the novel procedure is explained in detail, and two different state-parameter decoupling strategies are proposed.

- Chapter 6. **Practical Application: Pyrolysis Reactor**: A practical application, which confirms the validity of the proposal explained in Chapter 5, is developed and discussed. The considered process, i.e. a pyrolysis reactor, is depicted, then a suitable model is provided. Finally, the experimental results are shown and commented.

Author's publications

- **[Fadda et al., 2015b]** Fadda, G., Pilloni, A., Pisano, A., Usai, E., Marjanović, A., and Vujnović, S. In *Recent Advances in Sliding Modes (RASM), 2015 International Workshop on*, pages 1–7.

- **[Fadda et al., 2015a]** Fadda, G., Franceschelli, M., Pilloni, A., Pisano, A., Usai, E., Durovic, Z., Marjanović, A., Papic, V., Tadić, P., and Vujnović, S. In *Italy Serbia Day: Growth and Development through Science and Technology*, pages 45–50.

- **[Fadda et al., 2016]** Fadda, G., Piiloni, A., Pisano, A., Usai, E., Marjanović, A., and Vujnović, S. In *Control and Fault-Tolerant Systems (SysTol), 2016 3rd Conference on*, pages 245–250.

Part I

State of the Art

Chapter 1

Fault Detection, Isolation and Diagnosis

In the last decades, a great number of methodologies have been developed on the topic of fault detection and diagnosis, ranging from analytical methods to artificial intelligence and statistical approaches. Several attempts to classify such methods can be found in literature, based on different perspectives. The three-part series of papers [Venkatasubramanian et al., 2003c], [Venkatasubramanian et al., 2003a] and [Venkatasubramanian et al., 2003b], provided a comparative study where a broad classification of fault diagnosis methods into three general categories was proposed, i.e. quantitative model-based methods, qualitative model-based methods, and process history based methods. In [Angeli and Chatzinikolaou, 2004], [Dai and Gao, 2013], [Yin et al., 2014a], fault diagnostic methods were reviewed respectively from the data-driven perspective. The organization of this Chapter follows the classification scheme firstly proposed in [Frank, 1990], then integrated in [Frank, 1996], and recently updated by a two-part survey [Gao et al., 2015a], [Gao et al., 2015b], where a comprehensive review for real-time fault diagnosis, with particular attention on the results reported in the last decade, is given. Therefore, the Chapter is structured as follows: at first, in Section 2.1 some important definitions about the topic of this dissertation, i.e. the *Supervision* and *Fault Diagnosis* of Industrial Systems, are briefly introduced; then, in Sections 1.2, 1.3, and 1.4, fault diagnosis approaches are reviewed comprehensively from a model-based, signal-based, and data-driven perspective, respectively. Finally, in the Section 1.5, hybrid approaches which exploit the combination and integration of two or more of such fault diagnosis methodologies are briefly discussed.

1.1 Basic Concepts and Definitions

The terminology used in this Thesis intends to be as much as possible consistent with that proposed by the *IFAC* Technical Committee on Fault Detection, Supervision and Safety of Technical Processes (*SAFEPROCESS*). The following set of definitions was firstly suggested by [Isermann and Ballé, 1997], based on the discussion within the Committée during the period 1991 – 1995. Many other works in the literature, such as for example the books of [Simani et al., 2010], [Chen and Patton, 1999] and [Isermann, 2006] agree with this nomenclature.

States and Signals

- *Fault*: An unpermitted deviation of at least one characteristic property or parameter of the system from the acceptable/usual/standard condition.

- *Failure*: A permanent interruption of a system's ability to perform a required function under specified operating conditions.
- *Malfunction*: An intermittent irregularity in the fulfilment of a system's desired function.
- *Error*: A deviation between a measured or computed value (of an output variable) and the true, specified or theoretically correct value.
- *Disturbance*: An unknown (and uncontrolled) input acting on a system.
- *Perturbation*: An input acting on a system, which results in a temporary departure from the current state.
- *Residual*: A fault indicator, based on a deviation between measurements and model-equation-based computations.
- *Symptom*: A change of an observable quantity from normal behavior.

Functions

- *Fault Detection*: Determination of the faults present in a system and the time of detection.
- *Fault Isolation*: Determination of the kind, location and time of detection of a fault. Follows fault detection.
- *Fault Identification*: Determination of the size and time-variant behavior of a fault. Follows fault isolation.
- *Fault diagnosis*: Determination of the kind, size, location and time of detection of a fault. Includes fault detection, isolation and identification.
- *Monitoring*: A continuous real-time task of determining the conditions of a physical system, by recording information, recognizing and indicating anomalies in the behavior.
- *Supervision*: Monitoring a physical system and taking appropriate actions to maintain the operation in the case of faults.
- *Protection*: Means by which a potentially dangerous behavior of the system is suppressed if possible, or means by which the consequences of a dangerous behavior are avoided.

Models

- *Quantitative model*: Use of static and dynamic relations among system variables and parameters in order to describe a system's behavior in quantitative mathematical terms.
- *Qualitative model*: Use of static and dynamic relations among system variables and parameters in order to describe a system's behavior in qualitative terms such as causalities or if-then rules.

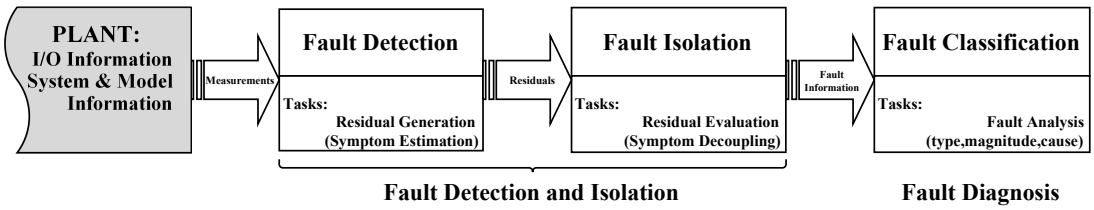

Figure 1.1: Schematic representation of a generic FDD Procedure

- *Diagnostic model*: A set of static or dynamic relations which link specific input variables - the symptoms - to specific output variables - the faults.
- *Analytical redundancy*: Use of two or more (but not necessarily identical) ways to determine a variable, where one way uses a mathematical process model in analytical form.

System Properties

- *Reliability*: Ability of a system to perform a required function under stated conditions, within a given scope, during a given period of time.
- *Safety*: Ability of a system not to cause danger to persons or equipment or the environment.
- *Availability*: Probability that a system or equipment will operate satisfactorily and effectively at any point of time.
- *Dependability*: A form of availability that has the property of always being available when required. It is the degree to which a system is operable and capable of performing its required function at any randomly chosen time during its specified operating time, provided that the item is available at the start of that period.

As explained by [Frank, 1996], the main purpose of a FDD system is to prevent the failing of the overall plant, by detecting abnormal or unexpected situations and their causes early enough. The general scheme of FDD system which achieves this result is shown in the Figure 1.1. Thus, the general solution is marked out by the following three facilities, according to the definitions given in Section 2.1, i.e. 1) *Fault Detection*, 2) *Fault Isolation*, 3) *Fault Diagnosis*. The two-stage architecture for the Fault Detection and Isolation (FDI) procedure was firstly suggested by [Chow and Willsky, 1980], and now is widely accepted also by the fault diagnosis community. As depicted in the Figure 1.1, it comprises two tasks, which are called respectively: *Residual Generation* and *Residual Evaluation*, where the residual is defined according to the nomenclature of Section 2.1. Therefore, according to [Frank, 1996], the classification of Fault Detection methods depends on the approach applied to implement the residual generation task, whereas the classification of Fault Isolation strategies refers to the methodology used to evaluate residuals.

1.2 Model-Based Methodologies

1.2.1 Introduction

As stated by [Simani et al., 2010], [Chen and Patton, 1999], [Patton et al., 2010] a traditional way to achieve the FDI, often referred to as *hardware* (or *physical/parallel*) *redundancy*, is

based on the replication of sensors, actuators, computers, software, and other components to measure and/or control a particular set of variables. Typically, a voting scheme is applied to the identical components of this redundant system in order to decide if and when a fault has occurred, and its likely location amongst redundant system components. As pointed out by [Isermann and Ballé, 1997] and [Isermann, 1997], the main problems encountered with hardware redundancy are the extra equipment and maintenance cost, as well as the additional space required to accommodate the equipment. During the last decades, advances in modern control theory and progresses of computer technology led to powerful techniques for mathematical modeling, system identification and state estimation, which have provided novel schemes for FDD. Indeed, as referred by [Chen and Patton, 1999], [Patton et al., 1989] [Patton et al., 2010], and also stated by [Simani et al., 2010], a more convenient approach can be implemented, rather than replicating each hardware individually. Indeed, by exploiting the concept of *analytical* or *functional redundancy* among various measured variables of the monitored process, firstly proposed by [Beard, 1971], the dissimilar measured values can be used together to cross-check each other, by means of analytical relationships about the system being monitored, i.e., based on a mathematical model of the system, which can be obtained by using either physical principles or systems identification techniques. When such a concept of redundancy is applied to correct the measurements acquired by the sensors as little as possible, in order to satisfy the algebraic constraints which describe the process model, it usually refers to the *Data Reconciliation* subject, which will be discussed in the Chapter 2. In most of the analytical redundancy schemes, the resulting difference generated from the consistency checking of different variables is called as a *residual*, or *symptom*, signal, according to the previous nomenclature. As a consequence, according to [Frank, 1996], [Gertler, 1998], [Chen and Patton, 1999], [Simani et al., 2010], a residual signal should provide a zero value as long as the process is evolving within its nominal dynamic, whereas it should diverge from zero as soon as a fault affecting the checked variable has occurred. Since analytical redundancy exploits a mathematical model of the monitored process, according to [Frank, 1990], [Gertler, 1998], [Patton et al., 1989], [Chen and Patton, 1999], [Simani et al., 2010], it is often referred to as the *model-based approach* to fault diagnosis. The major advantage of the analytical redundancy approach is that no additional hardware components are needed, because an FDI algorithm can be implemented via software on the process control computer [Chen and Patton, 1999].

In [Gao et al., 2015a], model-based fault diagnosis methods are classified on the basis of the different models used, as follows:

- *deterministic fault diagnosis methods*,
- *stochastic fault diagnosis methods*,
- *fault diagnosis for discrete-events and hybrid systems*
- *fault diagnosis for networked and distributed systems*

In this Section, only deterministic and stochastic fault diagnosis methods will be reviewed.

1.2.2 Fault Modeling

As stated by [Simani et al., 2010], [Chen and Patton, 1999], every FDI model-based approach needs at first to determine a mathematical model of the system to be supervised,

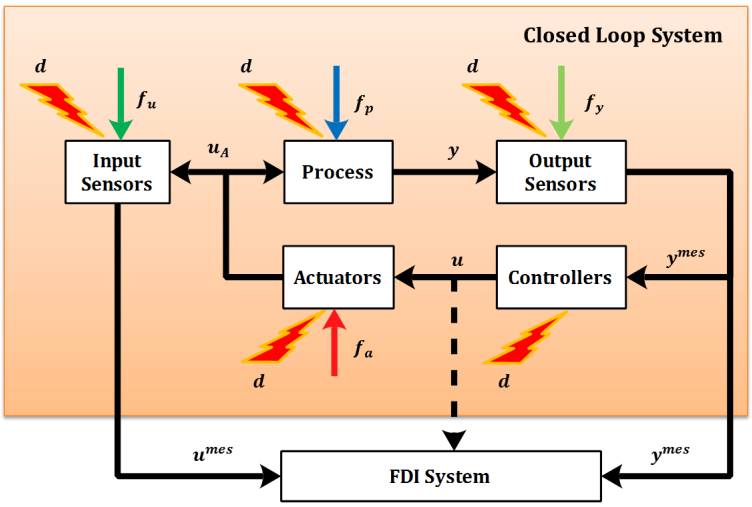

Figure 1.2: Schematic representation of a generic faulty system

including all the possible fault cases. Furthermore, [Patton et al., 1989] pointed out that the representation used to include fault effects in the process model, often depends more upon the detection method used than upon the real nature of the process dynamics. Therefore, a realistic approach and a good starting point for the subsequent fault diagnosis presupposes the understanding of the nature of the real faults, their system location, and their mapping into the generated residuals, or their description in terms of symptoms. In a first step, this can be provided only by the inspection of real processes, the understanding of the physics and a fault-symptom-tree analysis. In the Figure 1.2, a general scheme of a closed-loop faulty system, suitable to discuss the design of the FDI techniques presented in this Thesis, is provided.

The whole system in Figure 1.2 can be splitted in several different functional blocks, as follows: *actuators*, *process*, *output sensors*, *input sensors* and *controllers*. The working conditions of the system are monitored by means of the measurement signals acquired by the input and output sensors, i.e. $\boldsymbol{u}^{mes}(t)$ and $\boldsymbol{y}^{mes}(t)$, respectively, and the control signals $\boldsymbol{u}(t)$ provided by the controllers devices to the actuators. Usually, all these signals are supposed to be available for the FDI system. When this condition is not satisfied, as highlight by [Simani et al., 2010], the missing of information about the system working conditions could make the design of the FDI scheme a complicated task. E.g., the control action applied by robust controllers, desensitizes the effects of faults and makes the diagnosis task difficult if some important data could not be acquired from the sensors installed on the plant. The actual inputs and outputs signals of the process, i.e. $\boldsymbol{u}(t)$ and $\boldsymbol{y}(t)$ respectively, are usually not directly available, but they can be only measured by the input and output sensors. Therefore, as remarked in [Simani et al., 2010], the design of an FDI system can be considered as an observation problem of $\boldsymbol{u}^{mes}(t)$ and $\boldsymbol{y}^{mes}(t)$.

As depicted in Figure 1.2, with reference to the occurrence of malfunctions, the location of faults, and their modelling, the parts of a system which are usually considered as potentially affected by faults are:

- Process
- Actuators
- Input Sensors

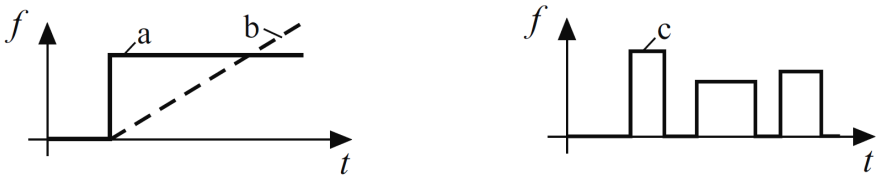

Figure 1.3: Time dependency of faults: abrupt (a); incipient (b); intermittent (c)

- Output Sensors

Remark 1. *As mentioned by [Simani et al., 2010], the controller device is typically considered as a fault-free component. Indeed, when the control signal $u(t)$ provided by the controller to the actuator is not directly available to the FDI system, and the actuator results to be a component of the whole control device, e.g., when the control action is performed by a digital computer, under this assumption, the actuator can be treated as the subsystem where faults are likelier to occur, whilst the controller device remains free from faults. Hence, the behavior of the controller device can be usually neglected in the design of a fault diagnosis scheme.*

The appearance of faults could be related to many different reasons, such as those summarized by [Isermann, 2006]:

- wrong design, wrong assembling;
- wrong operation, missing maintenance;
- ageing corrosion, wear during normal operation

With regard to the operation phase, the faults can be classified, as suggested by [Isermann, 2006], depending on their different way to appear, and their corresponding change effect applied on the physical quantities, as follows:

- *deterministic faults*
  - *abrupt*: when the fault appears suddenly, thus its bias effect can be modeled by means of a step signal, having small or large size
  - *incipient*: when the fault appears gradually, thus its drift effect can be modeled by means of a ramp signal
- *stochastic faults*
  - *intermittent*: when the fault appears in a non deterministic way

The different time dependency of faults is depicted in Figure 1.3.

It is worth to note that, according to [Simani et al., 2010], the faults affecting input and output sensors can be further classified as follows, with regard to their way to affect the system dynamics, as depicted in Figure 1.4

- *additive faults*:

$$\zeta^{mes} = \zeta + f \tag{1.1}$$

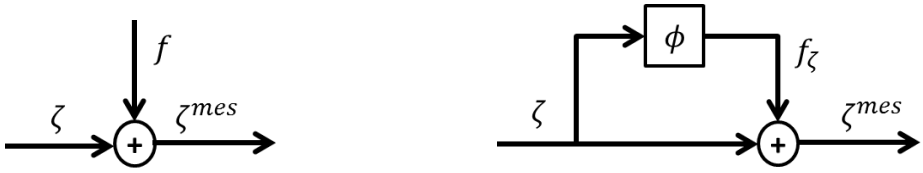

Figure 1.4: Fault models for input and output sensors: additive fault (a); multiplicative fault (b);

- *multiplicative faults*:

$$\zeta^{mes} = (1+\phi)\zeta = \zeta + f_\zeta \tag{1.2}$$

where: $\zeta \in \mathbb{R}$ and $\zeta^{mes} \in \mathbb{R}$ denote respectively the actual and measured value of a generic physical quantity, whereas $f \in \mathbb{R}$ and $f_\zeta \in \mathbb{R}$ are two different fault symptoms affecting ζ, and $\phi \in \mathbb{R}$ is an (unknown) time-varying function representative of the fault with respect to ζ. The analytical models of $\phi(t)$ can have the following expressions:

- *step fault signal*:

$$\phi(t) = \frac{\zeta_\%}{100}\delta_{-1}(t-t_f) \tag{1.3}$$

- *ramp fault signal*:

$$\phi(t) = \frac{\zeta_\%}{100}\left(\frac{t}{t_r}\right)[\delta_{-1}(t-t_f) - \delta_{-1}(t-t_f-t_r)] \tag{1.4}$$

- *random-walk fault signal*:

$$\phi(t) = \int_{t_f}^{t} v_q(\tau)d\tau \Big|_{-\zeta_\%/100}^{\zeta_\%/100} \delta_{-1}(t-t_f) \tag{1.5}$$

where $\zeta_\%$ denotes the fault amplitude, expressed as percentage of full-scale related to the measurement device, $\delta_{-1}(\cdot)$ is the Heaviside's step function, t_f is the fault occurrence time, t_r is the fault rise time, and $v_q(t)$ is a white noise process having autocorrelation function $E\{v_q(t_1)v_q(t_2)\} = q\delta(t_1-t_2)$. As stated above, step, ramp and random-walk fault signals can be used to simulate abrupt, slow and irregular variations of the physical parameters, respectively. When dealing with multiplicative faults, note that, if $\phi \neq 0$, then $f_\zeta \neq 0$; thus $f_\zeta = \phi\zeta$ is the fault symptom corresponding to the multiplicative fault ϕ. Additive faults reflect static changes of signals, whereas multiplicative faults refer to dynamic changes of signals, most of the times due to variations affecting the model parameters. Due to this fact, multiplicative faults result to be harder to detect with respect to additive faults.

According to the modeling approach mentioned by [Ding, 2008], a State-Space representation of a generic faulty Multiple In Multiple Out (MIMO) Linear Time Invariant (LTI) system, suitable for the FDI approaches discussed in the following of this Thesis, can be expressed as:

$$\begin{cases} \dot{\boldsymbol{x}} = A\boldsymbol{x} + B\boldsymbol{u} + E_d\boldsymbol{d} + E_f\boldsymbol{f} \\ \boldsymbol{y} = C\boldsymbol{x} + D\boldsymbol{u} + F_d\boldsymbol{d} + F_f\boldsymbol{f} \end{cases} \tag{1.6}$$

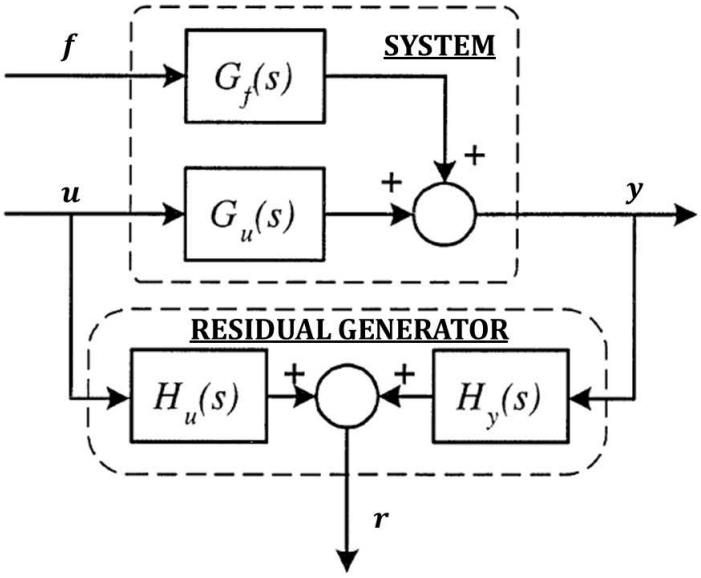

Figure 1.5: Schematic representation of a generic residual generator

where $\boldsymbol{x} \in \mathbb{R}^n$ is the state vector, $\boldsymbol{u} \in \mathbb{R}^m$ is the input vector, $\boldsymbol{y} \in \mathbb{R}^p$ is the output vector, and $\{A \in \mathbb{R}^{n\times n}, B \in \mathbb{R}^{n\times m}, C \in \mathbb{R}^{p\times n}, D \in \mathbb{R}^{p\times m}\}$ are the matrices related to the standard fault-free state-space representation, whereas $\boldsymbol{f} \in \mathbb{R}^q$ is the known fault vector, provided that the type of fault is not specified, whereas $\boldsymbol{d} \in \mathbb{R}^s$ denotes the vector of disturbances, or unknown inputs, and finally $\{E_f \in \mathbb{R}^{n\times q}, F_f \in \mathbb{R}^{p\times q}\}$, $\{E_d \in \mathbb{R}^{n\times s}, F_d \in \mathbb{R}^{p\times s}\}$ are known constant matrices, indicating the place where the faults and the disturbances occur, respectively, and their respective influence on the system. For the sake of clarity, the time dependency of all the considered signals was omitted.

The three different types of faults taken into account by this model reflect those depicted in Figure 1.2, as follows:

- Actuator faults: are those which cause changes in the actuators, namely $\boldsymbol{f_a}$. They can be modeled by setting $E_f = B$ and $F_f = D$.
- Process faults: are those used to indicate malfunctions within the process, namely $\boldsymbol{f_p}$. Depending on their type and location, they can be modeled by setting $E_f = E_p$ and $F_f = F_p$.
- Output Sensor faults: are those which directly act on the process measurements, namely $\boldsymbol{f_s} \equiv \boldsymbol{f_y}$. They can be modeled by setting $F_f = I$.

Thus, for a system with sensor, actuator and process faults, we define:

$$\boldsymbol{f} = \begin{bmatrix} \boldsymbol{f_a} \\ \boldsymbol{f_p} \\ \boldsymbol{f_s} \end{bmatrix}, \; E_f = [B, E_p, 0], \; F_f = [D, F_p, I] \tag{1.7}$$

1.2.3 Residual Generation in Model-Based FDI

Each of the model-based approaches reviewed in this Section implements in a different way the residual generation task. Nevertheless, each of these residual generators refers to the

same general representation, which considers a generic linear time-invariant system, so that it can be represented in the frequency domain in terms of the input-output relation:

$$Y(s) = G_u(s)U(s) + G_d(s)D(s) + G_f(s)F(s) \tag{1.8}$$

where $Y(s)$, $U(s)$, $F(s)$, $D(s)$ denote the Laplace transforms of the output vector $\boldsymbol{y}(t)$, the input vector $\boldsymbol{u}(t)$, the fault vector $\boldsymbol{f}(t)$ and the disturbance vector $\boldsymbol{d}(t)$, respectively, whereas $G_u(s)$, $G_f(s)$, $G_d(s)$ denote respectively the transfer matrices from $\boldsymbol{u}(t)$, $\boldsymbol{f}(t)$, $\boldsymbol{d}(t)$ to $\boldsymbol{y}(t)$.

The general structure of a residual generator based on the system description (1.8) is shown in Figure 1.5.

According to [Chen and Patton, 1999], this structure refers to the following mathematical expression for the residual signal:

$$R(s) = [H_u(s)\ H_y(s)] \begin{bmatrix} U(s) \\ Y(s) \end{bmatrix} = H_u(s)U(s) + H_y(s)Y(s) \tag{1.9}$$

where $R(s)$ denote the Laplace transforms of the residual signal $r(t)$, whereas $H_u(s)$ and $H_y(s)$ are both transfer matrices which can be implemented by using stable linear systems. According to the definition given in Section 2.1, the residual signal is designed in order to implement the following condition:

$$r(t) = 0 \quad \Leftrightarrow \quad \boldsymbol{f}(t) = 0 \tag{1.10}$$

In order to satisfy the condition (1.10), the transfer matrices $H_u(s)$ and $H_y(s)$ must satisfy the following constraint:

$$H_u(s) + H_y(s)G_u(s) = 0 \tag{1.11}$$

Thus, as stated in [Chen and Patton, 1999], the design of the residual generator refers to the choice of the transfer matrices $H_u(s)$ and $H_y(s)$ which satisfy the constraint (1.11). As a consequence, different residual generators can be obtained by means of different $H_u(s)$ and $H_y(s)$. Therefore, $H_u(s)$ and $H_y(s)$ are two design parameters which have to be chosen in such a way the fault detection can be performed by means of the following threshold test:

$$\begin{aligned} J(r(t)) < T(t) \ &\Rightarrow \ \boldsymbol{f}(t) = 0 \\ J(r(t)) \geq T(t) \ &\Rightarrow \ \boldsymbol{f}(t) \neq 0 \end{aligned} \tag{1.12}$$

where $J(r)$ is a suitable residual evaluation function, whereas $T(t)$ is its corresponding threshold function. Hence, if the threshold test is positive, i.e. the residual evaluation function exceeds the value of the threshold function, a fault is likely occurring. Many different ways of defining residual evaluation functions and determining static or adaptive threshold functions can be found in literature, based on empirical or theoretical considerations.

According to Figure 1.5, and to the design constraint (1.11), when one or more faults occur, the dynamic of the residual signal becomes:

$$r(s) = H_y(s)G_f(s)\boldsymbol{f}(s) = G_{rf}(s)\boldsymbol{f}(s) = \sum_{i=1}^{q} G_{rf_i}(s)f_i(s) \tag{1.13}$$

where $G_{rf}(s) = H_y(s)G_f(s)$ is defined as the *fault transfer matrix*, that is a transfer matrix which represents the relation between the residual and faults, whereas $G_{rf_i}(s)$ is the i-th

column of the fault transfer matrix $G_{rf}(s)$ and $f_i(s)$ is the i-th component of the fault vector $f(s)$.

Therefore, in order to detect the i-th fault f_i, by means of the residual $r(s)$, the i-th column of the fault transfer matrix $G_{rf}(s)$ should be non-zero, that is:

$$G_{rf_i}(s) \neq 0 \tag{1.14}$$

According to [Chen and Patton, 1999], the constraint (1.14) is defined as the *fault detectability condition* of the residual $r(s)$ to the fault f_i. If the i-th fault satisfies the fault detectability condition, then f_i is said to be *detectable* in the residual $r(s)$.

Nevertheless, as proven by [Chen and Patton, 1999], the satisfaction of the fault detectability condition (1.14), does not guarantee a reliable fault detection, which instead needs the satisfaction of a stricter constraint, called *strong fault detectability condition*, that is:

$$G_{rf_i}(0) \neq 0 \tag{1.15}$$

If the i-th fault satisfies the strong fault detectability condition, then f_i is said to be *strongly detectable* in the residual $r(s)$.

As mentioned in [Chen and Patton, 1999], the satisfaction of the only fault detectability condition, denotes an unsatisfactory design of the residual generator, because in this case it may happen that the effect of the fault on the residual disappears, although the fault effect on the system still exists.

1.2.4 Residual Evaluation in Model-Based FDI

As pointed up in [Chen and Patton, 1999], although the fault detection can be achieved by means of a single residual signal, usually the fault isolation requires a residual set. If a fault can be distinguished from the others by using a residual set, hence this fault is said to be *isolable* by the residual set. If the residual set can isolate all faults, thus the residual set achieves the required *isolability* property. In order to fulfil the fault isolation task, in [Gertler, 1992] two different enhancement concepts have been introduced, namely *Structured Residual Set* and *Fixed Direction Residual Set*. Both these concepts refer to a geometric framework in which a *residual vector* spans the *residual space*, as depicted in Figure 1.6. The components of this vector are those signals in the residual set. According to [Gertler, 1992], [Chen and Patton, 1999], [Sobhani-Tehrani and Khorasani, 2009], [Patton et al., 2010], in a structured residual set each signal is designed to be affected only by a specific subset of faults, although remaining insensitive to the other ones. In a fixed direction residual set instead, each signal is designed to be affected only by one specific fault, although remaining insensitive to the other ones.

From a geometrical point of view, as explained by [Gertler, 1998], when using a structured residual set, in response to a single fault the residual vector is confined to a subspace spanned by a subset of the vector's components, because only a fault-specific subset of residuals becomes non-zero. When using a fixed direction residual set instead, in response to a particular fault, the residual vector holds on a fault-specific direction (or subspace), which should be maintained also in dynamic transients.

The design procedure of a structured residual set consists of two steps: in the first step, the sensitivity and insensitivity relationships between residuals and faults, according to the assigned isolation task, are specified; in the second step, a set of residual generators is then

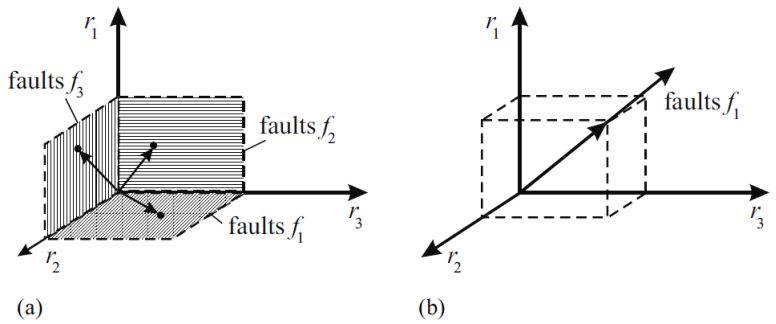

Figure 1.6: Schematic representation of two types of enhanced residuals: (a) structured residuals; (b) directional residuals

designed, according to the relationships previously defined. In a structured residual set the diagnostic analysis results to be simplified, because this task is reduced to determining which of the residuals differ from zero. Indeed, for each residual, the threshold test can be performed separately, taking to a Boolean decision table, which can then be used to fulfil the isolation task.

In structured residuals, each element $r_i(t)$ of the residual set $R = \{r_1(t), \ldots, r_n(t)\}$ is connected to a different binary variable ε_i as follows:

$$\varepsilon_i(t) = \begin{cases} 0 & if |r_i(t)| < k_i \\ 1 & if |r_i(t)| \geq k_i \end{cases} \quad i = \{1, \ldots, n\} \tag{1.16}$$

where k_i is the triggering limit used to test the residual r_i when a fault occurs. Hence, the vector $\vec{\varepsilon}(t) = [\varepsilon_1(t), \ldots, \varepsilon_n(t)]^T$ results to be the fault code, or signature. The fault isolation is then achieved by comparing the actual signature generated by $\vec{\varepsilon}$ when a fault occurs to a pre-defined set of signatures.

The concept of directional residual may also be expressed in a mathematical way, by recalling the notation given by [Gertler, 1998], and mentioned also by [Chen and Patton, 1999], that is:

$$\vec{r}(t|f_i(t)) = \alpha_i(t) \cdot \vec{l}_i \quad i = \{1, ..., n\} \tag{1.17}$$

In this notation, the constant vector $\vec{l}_i(t)$ is the *signature direction* of the i-th fault in the residual space $\mathbb{R}^n$, and $\alpha_i(t)$ is a scalar function that depends on the size and dynamics of the fault. In general, a *fault signature* can be thought as the pattern which is generated by a residual set when a specific fault occur. As pointed out by [Chen and Patton, 1999], the main idea behind this geometric approach is to isolate faults by comparing the direction or subspace where lies the residual vector with the known fault signature directions or subspaces. [Chen and Patton, 1999] also mention that to gain a reliable fault isolation, each fault signature has to be uniquely related to one fault. A residual set in which each residual is sensitive to one fault only, results to be both structured and directional. This last type of residual sets, are referred to as diagonal or basis residuals.

As mentioned in [Frank, 1996], other methods to evaluate residuals generated by model-based approaches are those involving:

- threshold logic
- pattern recognition

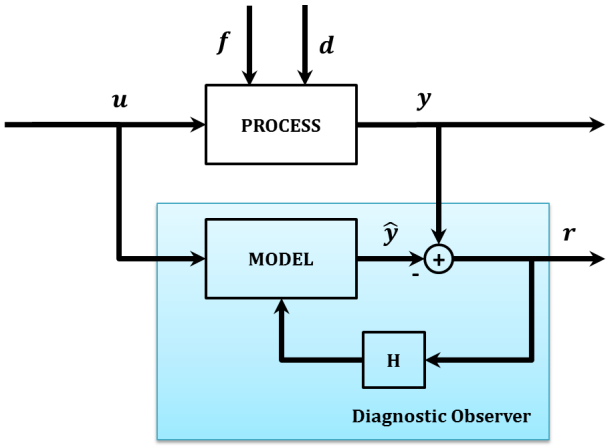

Figure 1.7: Schematic representation of the observer-based fault diagnosis approach

- fuzzy decision making
- neural networks

The most common residual evaluation methods result to be those based on threshold tests. Constant threshold have been applied in many applications; nevertheless in [Ding and Frank, 1991], [Emami-Naeini et al., 1988], it has been shown that better performances in terms of robustness despite unknown inputs, reduction of false alarms, and ability to detect small faults, can be achieved by using time-varying thresholds which can be adapted based on the operating conditions of the process.

1.2.5 Observer-Based Approach

As explained in [Frank, 1990] and [Frank, 1996], the main idea behind a residual generation task implemented by an observer-based approach consist in the estimation of the system's outputs from the measurements or a subset of the measurements, i.e. by means of one or more observers, when dealing with deterministic models (or Kalman filters, when dealing with stochastic models, e.g. when noise is considered), and then in the use of the estimation error (or innovation), or a functional of it, as the residual signal for the detection and isolation of the faults.

An important aspect remarked in [Frank, 1996] is that a diagnostic observer is not a *state observer*, but it is an *output observer*. This difference implies that a diagnostic observer can be designed also in the frequency domain, without the application of the state-space theory, which is needed instead to design the state feedback in the case of incomplete measurement of the state vector. Therefore, this consideration reveals the structural equivalence between the observer-based approach and the stable factorization approach presented in Section 1.2.7.

The schematic diagram of the general configuration, i.e. a linear full order diagnostic observer, is depicted in Figure 1.7. The residual signal $\boldsymbol{r}$ is generated by comparing the actual measurements, denoted by the output vector $\boldsymbol{y}$ of the process, with their estimates, denoted by the output vector $\hat{\boldsymbol{y}}$ of the nominal model, then it is filtered by the gain matrix H and finally fed back to the model, in order to compensate unmatched initial conditions and stabilize the observer, if the process dynamic is not stable. Therefore, by assuming the model of the faulty process as the linearized state-space representation given in 1.6, the

corresponding full-order observer results to be:

$$\begin{cases} \dot{\hat{\boldsymbol{x}}} = A\hat{\boldsymbol{x}} + B\boldsymbol{u} + H(\boldsymbol{y} - \hat{\boldsymbol{y}}) \\ \hat{\boldsymbol{y}} = C\hat{\boldsymbol{x}} + D\boldsymbol{u} \end{cases} \tag{1.18}$$

Hence, the equations related to the state estimation error $\boldsymbol{e} = \boldsymbol{x} - \hat{\boldsymbol{x}}$ and the output estimation error $\boldsymbol{r} = \boldsymbol{y} - \hat{\boldsymbol{y}}$ result to be, respectively:

$$\dot{\boldsymbol{e}} = (A - HC)\boldsymbol{e} + E_d\boldsymbol{d} + E_f\boldsymbol{f} - HF_d\boldsymbol{d} - HF_f\boldsymbol{f} \tag{1.19}$$

$$\boldsymbol{r} = C\boldsymbol{e} + F_d\boldsymbol{d} + F_f\boldsymbol{f} \tag{1.20}$$

From (1.19) and (1.20), it is apparent $\boldsymbol{r}$ is a function of both $\boldsymbol{f}$ and $\boldsymbol{d}$, that is the residual signal is sensitive both to faults and unknown inputs. As pointed out by [Gertler, 1998], since in every practical application unknown input signals are always present and unavoidable, i.e. $\boldsymbol{d} \neq \boldsymbol{0}$, because of model's parameter variation, measurement noises as well as exogenous unmodelled disturbances, the residual always differs from zero even if there is no fault, i.e. $\boldsymbol{f} = \boldsymbol{0}$. Thus, the matrix H is usually designed in such a way the fault detection can be performed by means of the threshold test 1.12, where the threshold value is assigned larger than the effect of the unknown inputs $\boldsymbol{d}(t)$ in the fault-free case. The feedback gain matrix H is also a design parameter which allows to reach robustness, that is to decouple (in the ideal case) the effects of faults from the effects of unknown inputs. When dealing with noisy measurements or nonlinear processes, equivalent schemes based on reduced order observers, Kalman filters or nonlinear observer can be used.

As denoted in [Frank, 1996], the objective of a robust observer-based residual generator which aims to achieve also the fault isolation, is to produce structured or directional residual sets such that individual faults are mapped into different patterns or directions, respectively, independent of each other and also, for the sake of robustness, of the unknown input vector $\boldsymbol{d}$. The most powerful technique to reach distinguishability among faults is to implement the total decoupling. As stated in [Frank, 1996], such a decoupling can be achieved either in the time domain or in the frequency domain. The latter refers to the stable factorization approach presented in Section 1.2.7. The decoupling strategy in the time domain refers to the concept of *fault detection filter*, firstly proposed by [Beard, 1971] and [Jones, 1973]. The goal of the fault detection filter is to map the residual related to a particular fault into a single direction or plane in the residual space, so that this fault results to be decoupled from the other faults. In order to achieve this result, the gain matrix H must be designed in such a way the direction of each of the residuals has very attractive unidirectional properties. Let consider the full-order observer previously defined in (1.18), and let make some assumptions, i.e. $D = 0$, $\boldsymbol{d} = 0$, since originally unknown inputs were not taken into account in this concept. According to the modeling approach presented in Section 1.2.2:

- a fault on the i-th actuator can be modelled as follows:

$$\dot{\boldsymbol{x}} = A\boldsymbol{x} + B\boldsymbol{u} + b_i f_a \tag{1.21}$$

  where b_i is the i-th column of the $E_f = B$ matrix and f_a is a time-varying scalar which denotes the dynamic of the i-th actuator fault. In this case, the equations related to the state estimation error and the output estimation error result to be, respectively:

$$\dot{\boldsymbol{e}} = (A - HC)\boldsymbol{e} + b_i f_a \tag{1.22}$$

$$\boldsymbol{r} = C\boldsymbol{e} \tag{1.23}$$

- a fault on the j-th output sensor can be modelled as follows:

$$\boldsymbol{y} = C\boldsymbol{x} + I_j f_y \tag{1.24}$$

where I_j is the j-th column of the $F_f = I$ matrix and f_y is a time-varying scalar which denotes the dynamic of the j-th output sensor fault. In this case, the equations related to the state estimation error and the output estimation error result to be, respectively:

$$\dot{\boldsymbol{e}} = (A - HC)\boldsymbol{e} - h_j f_y \tag{1.25}$$

$$\boldsymbol{r} = C\boldsymbol{e} + I_j f_y \tag{1.26}$$

where h_j is the j-th column of the gain matrix H.

As stated in [Chen and Patton, 1999], the fault detection filter must be designed in order to make the quantity $C\boldsymbol{e}$ assume a fixed direction in the output space when either $b_i f_a \neq 0$ or $I_j f_y \neq 0$ occurs, that is the residual has uni-directional properties. Thus, by following [Frank, 1994], the gain matrix H is designed such that the following conditions are satisfied:

(a1) $\text{rank}[Cb_i,\ C(A-HC)b_i,\ \ldots,C(A-HC)^{n-1}b_i] = 1$

(a2) $\text{rank}[Ch_j,\ C(A-HC)h_j,\ \ldots,C(A-HC)^{n-1}h_j] = 1$

(b) all the eigenvalues of $(A-HC)$ can be arbitrarily assigned

The satisfaction of condition (**a1**), i.e. the rank of the controllability matrix of (A, b_i) pair must be equal to one, guarantees that the fault on the i-th actuator will force the residual $\boldsymbol{r}$ to grow in the direction Cb_i, whereas the satisfaction of condition (**a2**), i.e. the rank of the controllability matrix of (A, h_j) pair must be equal to one, guarantees that the fault on the j-th output sensor will force the residual $\boldsymbol{r}$ to belong to the subspace spanned by $\{Ch_j, I_j\}$. The satisfaction of condition (**b**) instead, i.e. the matrix $(A-HC)$ can be stabilized, guarantees the stability of the filter. The fault detection filter has been actually the first raw implementation of the directional residual vector concept defined in Section 1.2.4. Indeed, the directions Cb_i and Ch_j are known as the *fault signature directions* in the residual space. As pointed up in [Frank, 1990], since the important information for the fault detection is in the direction of the residual rather than in its dynamic, the use of a fault detection filter does not requires the knowledge of the fault dynamic. Hence, a fault is isolated when the residual projections along the known fault signature directions or in the known fault signature subspaces are sufficiently large. However, since the fault detection filter does not account for the effects of the unknown inputs, it cannot be used to implement a robust residual evaluation. As stated in [Frank, 1994], all observer-based residual generators with perfect decoupling among the faults and from unknown inputs can be treated as special cases of a unified approach, known as the Unknown Input Observer (UIO) scheme. UIOs are well known from control theory. Under certain conditions they allow to decouple the effect of unknown inputs from the estimate of the state. Following [Frank, 1990], let consider the general model of the faulty

process given in 1.6, assuming $D = 0$; the corresponding UIO which meets the robustness requirements as defined above can be represented in the following form:

$$\begin{cases} \dot{\boldsymbol{z}} = M\boldsymbol{z} + J\boldsymbol{u} + N\boldsymbol{y} \\ \boldsymbol{r} = L_z\boldsymbol{z} + L_y\boldsymbol{y} \end{cases} \tag{1.27}$$

with the residual $\boldsymbol{r}$ having the following properties:

$$\begin{cases} \boldsymbol{f}(t) = 0 \implies \lim\limits_{t\to+\infty} \boldsymbol{r}(t) = 0 \qquad \forall\{\boldsymbol{u}, \boldsymbol{d}, \boldsymbol{x}_0, \boldsymbol{z}_0\} \\ \boldsymbol{f}(t) \neq 0 \implies \boldsymbol{r}(t) \neq 0 \end{cases} \tag{1.28}$$

and the state $\boldsymbol{z}$ of the UIO supposed to be a linear transformation of the faulty model's state $\boldsymbol{x}$ in the unfaulty case, after the response to unlike conditions has died out:

$$\boldsymbol{z} = T\hat{\boldsymbol{x}} \tag{1.29}$$

that is the observer is supposed to estimate a linear transformation of the original state. A necessary and sufficient condition for the existence of such an ideal UIO is given in [Patton et al., 1989]. If these conditions are satisfied, the dynamic of the state estimation error $\boldsymbol{e} = T\boldsymbol{x} - T\hat{\boldsymbol{x}}$ and the residual $\boldsymbol{r}$ become, respectively:

$$\begin{aligned} \dot{\boldsymbol{e}} &= T\dot{\boldsymbol{x}} - \dot{\boldsymbol{z}} = T(A\boldsymbol{x} + B\boldsymbol{u} + E_d\boldsymbol{d} + E_f\boldsymbol{f}) - MT\hat{\boldsymbol{x}} - J\boldsymbol{u} - N(C\boldsymbol{x} + F_d\boldsymbol{d} + F_f\boldsymbol{f}) + \\ &+ (MT\boldsymbol{x} - MT\boldsymbol{x}) = \\ &= M\boldsymbol{e} + (TA - NC - MT)\boldsymbol{x} + (TB - J)\boldsymbol{u} + (TE_d - NF_d)\boldsymbol{d} + (TE_f - NF_f)\boldsymbol{f} \end{aligned} \tag{1.30}$$

$$\boldsymbol{r} = L_zT\hat{\boldsymbol{x}} + L_yC\boldsymbol{x} + (L_zT\boldsymbol{x} - L_zT\boldsymbol{x}) = -L_z\boldsymbol{e} + (L_zT + L_yC)\boldsymbol{x} \tag{1.31}$$

Hence, to make the observer (1.27) a residual generator, the linear transformation T and the matrices $\{M, N, J, L_z, L_y\}$ must be designed in order to satisfy the following set of equations:

$$\begin{cases} TA - MT = NC \\ J = TB \\ L_zT + L_yC = 0 \end{cases} \tag{1.32}$$

To meet instead the robustness requirements, the linear transformation T and the matrices of the observer $\{N, L_y\}$ must satisfy also the following set of equations:

$$\begin{cases} TE_d = 0 \quad , \quad TE_f \neq 0 \\ NF_d = 0 \quad , \quad NF_f \neq 0 \\ L_yF_d = 0 \quad , \quad L_yF_f \neq 0 \end{cases} \tag{1.33}$$

As shown in [Patton et al., 1989], the design problem given by the two equation sets (1.32), (1.33) can be solved by using either the Kronecker canonical state representation approach or the eigenstructure approach.

If all the design conditions are satisfied, including also the pole assignment of the observer in order to satisfy (1.28), the dynamic of the residual signal becomes:

$$\dot{\boldsymbol{r}} = -L_z\dot{\boldsymbol{e}} = -L_z(TE_f - NF_f)\boldsymbol{f} = L_zNF_f\boldsymbol{f} - L_zTE_f\boldsymbol{f} \tag{1.34}$$

As underlined in [Frank, 1996], an important precondition for the solvability of this problem is the availability of a sufficient number of measurements. Indeed, in order to decouple q faults and s unknown inputs from each other, it needs at least $q+s$ independent measurements which reflect the faults. Furthermore, in many practical situations unfortunately, the physical conditions to satisfy (1.28), that is to design a UIO able to achieve a perfect decoupling, do not exist. Usually, only a compromise between fault detection sensitivity and robustness with respect to unknown inputs can be implemented. In this case, an optimal approximation of a performance criterion which takes into account the sensitivity with respect to the disturbance vector $\boldsymbol{d}$, as well as the sensitivity with respect to the fault vector $\boldsymbol{f}$, can be found. This optimization problem can be solved either in the time domain or in the frequency domain, by means of algorithms such as those suggested in [Wüennenberg, 1990].

Note that, as stated in [Frank, 1990], this approach is superior to the detection filter approach in that it accounts for modelling errors also, and to the parity space approach in that it also takes into account the sensitivity to the faults.

As stated in [Gao et al., 2015a], a bank of observer-based residuals is generally required in order to achieve the fault isolation, which can be implemented mainly by the two following schemes, both exploiting in a different way the concept of structured residual set discussed in Section 1.2.4:

- *Dedicated Observer Scheme*: [Clark et al., 1975] given a certain set of faults to isolate, $\{f_1,\dots,f_i,\dots,f_q\}$, $i=1,\dots,q$, the i-th observer is designed in such a way its corresponding scalar residual r_i results to be sensitive to the fault f_i only. Therefore, the corresponding *dedicated residual set* is designed according to the following fault sensitivity conditions:

$$r_i(t) = R(f_i(t)) \quad i=1,\dots,q \tag{1.35}$$

  where $R(\cdot)$ denotes a suitable functional, and then in such a way the fault isolation can be achieved by means of the following threshold test:

$$r_i(t) > T_i(t) \;\Rightarrow\; f_i(t) \neq 0 \quad i=1,\dots,q \tag{1.36}$$

  where $T_i(t)$ are thresholds. As claimed in [Chen and Patton, 1999], this residual structure is very simple and all faults can be detected simultaneously, however it is difficult to design in practice. Even when such a structured residual set can be designed, there is normally no design freedom left to achieve other desirable performances such as robustness against unknown inputs [Frank, 1990].

- *Generalized Observer Scheme*: [Frank, 1987] the i-th observer is designed in such a way its corresponding residual signal r_i results to be sensitive to all but one fault, and independent of the unknown input vector d. Therefore, the corresponding *generalized residual set* is designed according to the following fault sensitivity conditions:

$$\begin{cases} r_1(t) = R(f_2(t),\dots,f_q(t)) \\ \vdots \\ r_i(t) = R(f_1(t),\dots,f_{i-1}(t),f_{i+1}(t),\dots,f_q(t)) \\ \vdots \\ r_q(t) = R(f_1(t),\dots,f_{q-1}(t)) \end{cases} \tag{1.37}$$

where denotes a suitable functional, and then in such a way the fault isolation can be achieved by means of the following threshold test:

$$\begin{cases} r_i(t) \leq T_i(t) \\ r_j(t) > T_j(t) \quad \forall j = 1,\ldots,i-1,i+1,\ldots,q \end{cases} \Rightarrow f_i(t) \neq 0 \qquad i = 1,\ldots,q \tag{1.38}$$

As claimed in [Frank, 1994], by using a GOS of q observers, the corresponding structured residual set allows again a unique fault isolation; however, in contrast to DOS, only for a single fault at a time. Nevertheless, in this the additional design freedom can now be used to make the FDI scheme robust to up to $(q-2)$ unknown inputs.

Other important contributions to the generation of structured and directional residuals in the framework of diagnostic observers include: [Massoumnia, 1986], [White and Speyer, 1986], [Park et al., 1994], [Edelmayer et al., 1997].

In this research, a particular class of nonlinear observers, namely SMOs, was investigated to implement the residual generation task. Indeed, SMOs are able to generate *injection signals* to estimate the symptoms of faults in spite of matched uncertainties, whereas in the presence of unmatched uncertainties, although the total insensitive property is lost, their effects can be optimally reduced by combining them with other optimization techniques as in [Castaños and Fridman, 2006], [Yan and Edwards, 2007], [Orani et al., 2010], [Bejarano et al., 2011], [Pillosu et al., 2012], [Pisano et al., 2014].

As stated in [Alwi et al., 2011], this result is achieved by a suitable filtering of the so-called *equivalent output error injection*, which represents the average control signal provided by the nonlinear output error injection term in order to maintain the sliding motion on the controlled system. Since the introduction of a sliding motion on the observer forces its outputs to exactly track the plant measurements, even in the presence of actuator faults, an accurate estimation of the states results still possible.

Remark 2. *The main differences between SMOs and the other observer-based methods, reflect the fact that in the SMO, the equivalent output error injection signal can allow to estimate the fault signal, while the standard residual, which is the signal based on the output estimation error, result to be zero during the sliding motion.*

As a consequence, in principle, SMOs allow to achieve simultaneous and accurate estimation of both state and faults, whereas traditional linear observers using output error based residuals, require a trade-off between robustness with respect to the state estimation, and sensitivity to the fault detection. SMOs for sensor FDI are presented in [Edwards et al., 2000, Tan and Edwards, 2002] for minimum phase linear systems. Recently these limitation are removed in [Yan and Edwards, 2007], where nonlinear systems with stable Jacobian matrix plus model uncertainties are considered. However, all those approaches are thought to deal only with faults acting on the output's sensors. If both output and input measurements are faulty, the injection signals are hardly able to estimate/discern among faults. However, these signals still embed, in some sense, information of them. By exploiting this fact, the FDD proposal depicted in Chapter 3 has been developed.

1.2.6 Parity Space Approach

According to the explanation given in [Frank, 1990] and [Frank, 1996], the main idea behind a residual generation which exploits the parity space approach is to test the consistency,

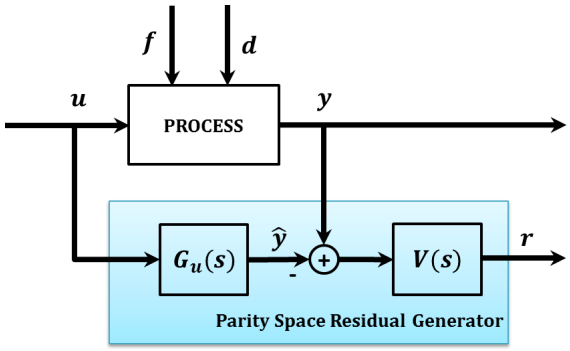

Figure 1.8: Schematic representation of a residual generator in the parity space approach

i.e. to perform the *parity check*, of properly modified analytical redundancy equations of the system, called *parity equations*, by using the actual measurement signals. By this way, the faults can be detected from the inconsistency of the parity equations, which is revealed by the residual vector. The modification of the system equations aims at the decoupling of the residuals from the system states and among different faults to enhance their diagnosability. The parity equation approach can be applied to either time-domain state-space model or frequency-domain input-output model. The early contributions to the parity space approach were provided in [Potter and Sunman, 1977], [Desai and Ray, 1984]. In [Chow and Willsky, 1984], parity equations were derived from the state-space model of the system. Starting from this point of view, in [Gertler, 1992],[Staroswiecki et al., 1993] the structural equivalence between observer-based and parity space residual generation approaches has been proven. Furthermore, in [Wünnenberg and Frank, 1987], it has been shown that the parity space approach leads to a special class of observer-based residual generators called *deadbeat observers*. As shown in [Gertler, 1992], also more general observers can be obtained. Further contributions focusing on relations based on transfer functions have been provided in [Gertler and Singer, 1990], [Gertler, 1992], [Delmaire et al., 1994] , [Gertler and Kunwer, 1995], [Gertler, 1995], [Staroswiecki et al., 1993]. In practical situations the parity space approach may results easier to handle than the observer-based approach, because in the latter case more design constraints have to be satisfied.

The basic configuration of the parity space approach in input-output format first described in [Gertler, 1992] is shown in Figure 1.8. Therefore, the residual signal can be represented as follows:

$$R(s) = V(s)[Y(s) - G_u(s)U(s)] \tag{1.39}$$

where $V(s)$ denotes a linear filter which allows to implement the decoupling. In [Gertler, 1992] it has been proven that if the decoupling filter $V(s)$ is designed according to the following form:

$$V(s) = Q(s)\hat{M}_u(s) \tag{1.40}$$

where $\hat{M}_u(s)$ and $Q(s)$ are defined according to (1.41), then the structure depicted in Figure 1.8 becomes equivalent to that of the diagnostic observer shown in Figure 1.9. As mentioned in [Frank, 1996], the robustness achieved by a suitable design of the filter V consists in a selection of those parity equations which reflect an independency, or at least a week dependency, upon the modelling errors.

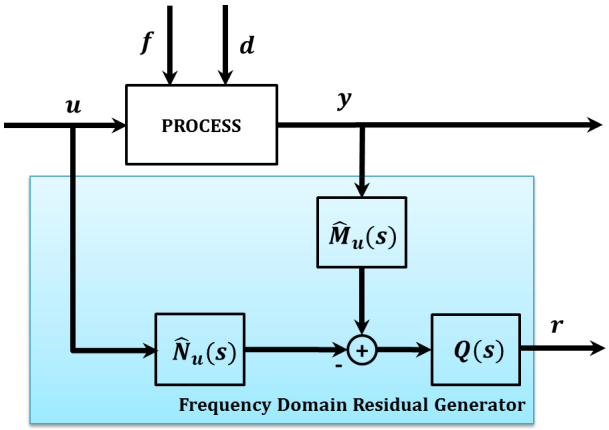

Figure 1.9: Schematic representation of a residual generator in the frequency domain

1.2.7 Stable Factorization Approach

As explained in [Gao et al., 2015a], the basic idea behind the stable factorization approach is to generate in the frequency domain a residual signal based on the stable coprime factorization of the transfer function matrix of the monitored system, which is made sensitive to the fault, but robust against disturbances by selecting an optimal weighting factor. This method was first proposed by [Viswanadham et al., 1987], and further extended by [Ding and Frank, 1990]. Recently, developments of the stable factorization approach have been provided by [Abid et al., 2011] for nonlinear systems and by [Hu and Tsai, 2008], [Ming-Cong et al., 2010] for applications in auto-balancing two-wheeled cart and thermal process, respectively. Also in [Gao et al., 2015a] the structural equivalence among parity space, diagnostic observers and stable factorization approaches is confirmed. E.g., the realization of the coprime factorization includes the design of a state-feedback gain. Moreover, also the decoupling strategy mentioned in Section 1.2.5 can be easily implemented in the frequency domain. Indeed, according to the definitions given in Section 1.2.3, several design method to find the matrices $H_u(s)$ and $H_y(s)$ have been proposed, such as those in [Ding and Frank, 1991], [Frank, 1993].

According to [Frank, 1996], a straightforward method is that based upon the following factorization of $R(s)$:

$$R(s) = Q(s)[\hat{M}_u(s)Y(s) - \hat{N}_u(s)U(s)] \tag{1.41}$$

where $\hat{M}_u(s)$, $\hat{N}_u(s)$ are left coprime factors of $H_u(s)$, obtained by means of the factorization $H_u(s) = \hat{M}_u(s)^{-1}\hat{N}_u(s)$, and $Q(s)$ denotes a filter which can be designed in order to achieve the frequency requirements of the residual signal. The resulting structure of this residual generator is depicted in Figure 1.9. The substitution of $Y(s)$ in (1.41) according to (1.8) brings to the following result:

$$R(s) = Q(s)\hat{M}_u(s)[G_d(s)D(s) + G_f(s)F(s)] \tag{1.42}$$

Hence, by means of this factorization approach, the residual only depends on the faults and the unknown inputs. In order to reach perfect decoupling among the faults and between faults and unknown inputs, according to [Ding and Frank, 1991], $Q(s)$ and $\hat{M}_u(s)$ must be designed such that:

$$Q(s)\hat{M}_u(s) = Q(s)\hat{M}_u(s)G_f(s) = diag(t_1(s), \ldots, t_q(s)) \tag{1.43}$$

where $t_i(s)$, $i = 1,\ldots,q$, are arbitrary time functions, and

$$Q(s)\hat{M}_u(s)G_d(s) = 0 \tag{1.44}$$

Methods to find $Q(s)$ and $\hat{M}_u(s)$ suitable to solve this problem have been proposed in [Ding and Frank, 1991],[Frank and Ding, 1993]. If the perfect decoupling cannot be achieved, the same compromise between sensitivity with respect to faults and robustness with respect to unknown inputs discussed in Section 1.2.5 for the time domain can be obtained, i.e. by solving an optimization problem based on the same performance criterion. Thus, as suggested in [Ding and Frank, 1991], in the frequency domain the approximate decoupling strategy is implemented by maximizing the following performance index:

$$\frac{\|\partial \boldsymbol{r}/\partial \boldsymbol{f}\|}{\|\partial \boldsymbol{r}/\partial \boldsymbol{d}\|} = \frac{\|Q(s)\hat{M}_u(s)G_f(s)\|}{\|Q(s)\hat{M}_u(s)G_d(s)\|} \tag{1.45}$$

where $\|\partial \boldsymbol{r}/\partial \boldsymbol{f}\|$ and $\|\partial \boldsymbol{r}/\partial \boldsymbol{d}\|$ denote the norms of sensitivity functions with respect to the fault vector $\boldsymbol{f}$ and the unknown input vector $\boldsymbol{d}$, respectively. As mentioned in [Frank, 1996], the solution of this problem can be achieved by means of modern methods of H_∞ optimization. Extensions based on this idea where made in the context of parity relations by [Gertler and Kunwer, 1995], [Staroswiecki et al., 1993] and others. As claimed in [Frank, 1996], the design methods based on the frequency domain appear to be much simpler and better tailored for engineering applications, since they allow to exploit well established frequency domain techniques for the fault isolation. E.g., the design of the filter $Q(s)$ allows to select the portions of the spectral domain which provide a maximum ratio of the fault detection sensitivity to the sensitivity with respect to unknown inputs, whatever the dependence of the residual upon the spectral domain of the process signals may be.

1.2.8 Parameter Estimation Approach

As stated in [Frank, 1990], an alternative approach to those which implement residual generators based on the state estimation is that based on the parameter estimation. The main assumption of this approach is that the faults reflect their effect in the physical parameters of the actual process, e.g. friction, mass, viscosity, capacitance, inductance, etc... The fault detection is implemented according to the following procedure: an on-line estimation of the actual process parameters is performed repeatedly, by means of well known parameter estimation methodologies, then these results are compared with those obtained on the reference model initially estimated under fault-free conditions; any difference among values of parameters is an indicator of change in the process and may be interpreted as a fault. Important contributions in the development and application of this approach can be found in [Isermann, 1984], [Isermann, 1993]. As denoted in [Gao et al., 2015a], the fault diagnosis methods based on the parameter estimation result to be very straightforward if the model parameters reveal an explicit mapping with the physical coefficients. Recent development of this approach can be found in [Doraiswami et al., 2010], [Döhler and Mevel, 2013], [Akhenak et al., 2013]. In [Gao et al., 2007], an integration of descriptor estimator and parametric eigenstructure assignment was used to improve robustness against measurement noises, modelling errors and process disturbances. As underlined in [Frank, 1996], an important advantage brought by the parameter estimation approach is that it allows to know the size of the deviations, which is an important information for the fault diagnosis. Nevertheless, as a drawback, the

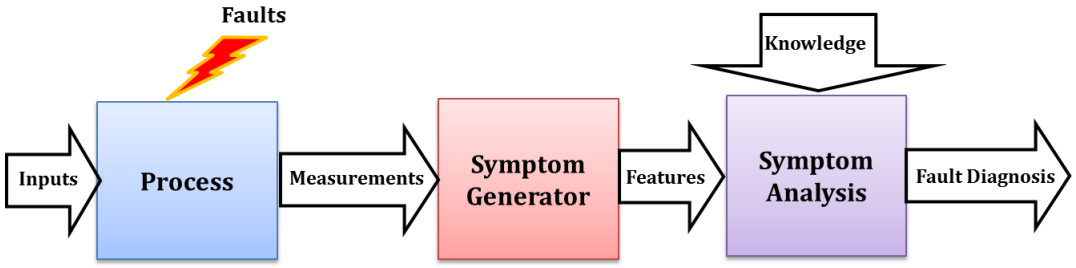

Figure 1.10: Schematic representation of the SB approach to FDD

parameter estimation approach requires a system always excited in order to estimate the parameters, and this may be a problem when dealing with processes operating at stationary conditions. Moreover, the determination of physical parameters from mathematical parameters, which results to be necessary when no classification method can be used, is in general not unique and only feasible if the order of the model is low. The results provided in [Frank, 1996] reveal that a close relationship and several interesting similarities can be found among observer-based, parity space-based and parameter estimation-based approaches. The existence of correlations among all these approaches have been confirmed in other works also, such as [Staroswiecki et al., 1993], [Delmaire et al., 1994], [Magni, 1995]. Furthermore, an interesting generalization of these results was described by [Gertler, 1995], and the discussion is still ongoing. Of course this close relationship appears to be logical, because all of them evaluate the same signals, i.e. the inputs and outputs of the actual process. Since the application of one method in place of another may be more o less efficient depending on the specific situation, hence these approaches are often used together in practical applications, in order to maximize the overall performances of the FDI system. As suggested in [Frank, 1996], a useful combination of these different techniques in practical applications is the use of diagnostic observers or parity equations for a rapid fault detection and isolation, whereas the parameter estimation is started when the fault diagnosis needs to be performed, e.g. to determine the size and type of the faults.

1.3 Signal-Based Methodologies

1.3.1 Introduction

The Signal-Based (SB) methodologies denote all those approaches which employ a suitable processing on the measured signals rather than explicit input-output models in order to achieve the FDI. By assuming that certain process signals bring information about the faults of interest, which are reflected in the measurements under form of symptoms, the main idea behind these methods is to extract a suitable set of *features*, i.e. relevant information, from these signals, then to carry out the fault diagnosis by checking the consistency between the known healthy signal pattern and the signal symptom of the real-time process extracted either by using Time-Domain (TD), Frequency-Domain (FD), or Time-Frequency-Domain (TFD) signal processing techniques. As stated in [Gao et al., 2015a], signal based fault diagnosis methods are largely employed in a wide range of real-time applications, such as the monitoring and diagnosis of induction motors, power converters and mechanical components in a system. A schematic representation of the SB approach to FDD is depicted in Figure 1.10.

The features to be extracted for the so-called *pattern analysis*, i.e. analysis of the fault

symptoms, can be either:

- time-domain signals (e.g.: mean, standard deviation, trend, slope, ...)
- frequency-domain signals: (e.g. spectral power density, frequency spectral lines, ...)
- magnitudes (e.g.: peak, root mean square, ...)

Hence, as done in [Gao et al., 2015a], signal-based fault diagnosis methods can be classified as follows:

- Time-Domain Signal-Based (TD SB) approach
- Frequency-Domain Signal-Based (FD SB) approach
- Time-Frequency Signal-Based (TF SB) approach.

1.3.2 Time-Domain Approach

The TD approach refers to all of those methods which perform the fault diagnosis by extracting time-domain features. Typically, such kind of approach is applied to monitor continuous dynamical processes, as confirmed by the following list of references, grouped in the following two categories based on the dimensionality of the featured extracted from the measured signals.

1.3.2.1 One-Dimension TD SB Methods

In [Chen and Lu, 2013] a fault diagnosis method was developed for power converters of switched reluctance motors based on the analysis of the measured root-mean-square current characteristics between healthy conditions and the situations under single/dual transistor short circuit or open circuit. In [Freire et al., 2013] instead, the absolute value of the derivative of the Park's vector phase angle was used as a fault indicator for wind turbine applications, i.e. to diagnose multiple open-circuit faults in two converters of PMSGs drives. In [Shahbazi et al., 2013] a fault diagnosis method was addressed for open and short circuits switch in non-isolated DC-DC converters, based on the slope of the induction current over time, and a real-time implementation on FPGA digital target was used to validate the proposal. In [Estima and Cardoso, 2013] another real-time algorithm was proposed to detect and locate multiple power switch open circuit faults in inverted-fed AC motor drives, based on the analysis of the measured motor phase currents and their corresponding reference signals. In [Bouzid and Champenois, 2013] it was shown that, under balanced supply voltage, the phase angle and the magnitudes of the negative and zero-sequence currents can be considered together as a set of reliable indicators of stator faults in the induction motors. In [Samara et al., 2008], a statistical method was presented for the detection of sensor abrupt faults in aircraft control systems, where the covariance of the sensing signals was used for feature extraction. A TD SB diagnostic algorithm for the supervision of gear faults was recently developed in [Hong and Dhupia, 2014], by combining fast Dynamic Time Warping (DTW) with Correlated Kurtosis (CK) techniques. In this application, the fast DTW algorithm is employed to extract the periodic impulse excitations caused from the faulty gear tooth, then the extracted signal is re-sampled by using the CK technique for the subsequent diagnostic analysis. By exploiting the periodicity of the geared faults, the CK algorithm can identify the position of the local gear fault in the gearbox.

1.3.2.2 Two-Dimension TD SB Methods

In [Chong et al., 2011], a FDI method under the pattern classification framework was proposed, where the vibration signal was translated into an image, then the local features were extracted from this two-dimensional signal by means of the Scale Invariant Feature Transform (SIFT) technique. Another approach based on two-dimensional features was recently proposed in [Shahriar et al., 2013] for the fault diagnosis of induction motors. In this method, the TD vibration signals acquired from the operating motor are firstly converted into gray-scale images, then the discriminating texture features are extracted from these two-dimensional signals by exploiting the Local Binary Patterns (LBP) technique. Finally, the extracted texture features are send to a classifier to perform the fault diagnosis. In this application, when converting signals into images, it has been noticed the added noise acts as illumination variation. Since both SIFT and LBP techniques reveal illumination invariance capability to some extent, the two proposed methods in [Chong et al., 2011], [Shahriar et al., 2013] result to be robust enough even when dealing with high levels of background noises.

1.3.3 Frequency-Domain Approach

The FD approach refers to all of those methods where the fault diagnosis is achieved by exploiting tools for the spectral analysis such as the Discrete Fourier Transformation (DFT). As reported in [Gao et al., 2015a], one of the most powerful frequency-domain methods is the Motor-Current Signature Analysis (MCSA), used for the diagnosis of motor faults. The MCSA method, which is well reviewed in [Benbouzid, 2000], [Nandi et al., 2005], exploits the spectral analysis of the stator current to detect rotor faults associated with broken rotor bars and mechanical balance, without requiring access to the motor. Recent development of the current based spectrum signature analysis for fault diagnosis applications can be found in [Joksimović et al., 2013], [Gong and Qiao, 2013].

Vibration signal analysis is instead a common method to monitor and diagnose the condition of mechanical equipment such as the gear box, since in this case a key indicator about working condition of the machine results to be actually the sound produced by the equipment. In [Pan et al., 2012], an algorithm based on the improved FD blind de-convolution flow technique was proposed as an acoustic fault detection method for a gear box. More recently, in [Feng and Zuo, 2013], Fourier spectrum and the demodulated spectra of amplitude envelope were employed together in order to detect and locate multiple gear faults in planetary gearboxes.

1.3.4 Time-Frequency-Domain Approach

The TFD approach refers to all of those combinations of TD and FD techniques applied in order to achieve the fault diagnosis.

As pointed out in [Gao et al., 2015a], when the machines are working under an unloaded condition, unbalanced supply voltages, varying load, or load torque oscillations, the measured signals typically appear transient and dynamic under the concerned time section. Hence, the analysis of the stationary quantities to monitor or detect faults could become less effective and reliable, either using a pure TD or FD approach. For such real-time monitoring and fault diagnosis applications, since transient signals are located on a time-varying frequency spectrum, suitable time-frequency decomposition tools are needed. As an example, in [Feng et al., 2013] an effective fault diagnosis tool based on the information revealed by

the feature extracted from non-stationary signals was proposed. In this application, the signal frequency components are identified by means of a time-frequency analysis able to reveal their time variant features.

As reported in [Gao et al., 2015a], several time-frequency analysis methods have been proposed and applied for the machinery fault diagnosis. The most common methods are those based on the following techniques:

- Short-Time Fourier Transform (STFT)
- Wavelet Transform (WT)
- Hilbert-Huang Transform (HHT)
- Wigner-Ville Distribution (WVD)

The method based on the STFT proposed in [Nandi et al., 2011], which allows to determine signal frequency contents of local sections when the signal changes in time, is widely applied to detect both stator and rotor faults in inductor motors. However, as mentioned by [Gao et al., 2015a], the STFT requires high computational resources to achieve good resolution. In [Gritli et al., 2013] the effectiveness of a method based on the WT for tracking fault frequency components under non-stationary conditions has been proven. Indeed, as a linear decomposition, the WT can provide a good resolution in time for high-frequency components of a signal and a good resolution in frequency for low-frequency components. In [Cabal-Yepez et al., 2013], the integration of STFT and discrete WT has been proposed to achieve early diagnosis and prognosis of the abnormalities in industrial systems. In [Gao et al., 2015a], is remarked that the practical application of STFT and WT may result limited by some design elements which need to be correctly defined. E.g., the selection of a suitable window size in STFT is required, but generally it is not known a priori. Furthermore, the selection of a suitable basic wavelet function in WT has a direct effect on the effective capability to identify transient elements which are hidden within a dynamic signal. The HHT method is not constrained by the limitations with respect to the time and frequency resolutions suffered by STFT and WT. The method based on HHT proposed in [Yan and Gao, 2006], on the basis of the instantaneous frequencies resulting from the intrinsic-mode functions of the signal being analyzed, has provided quite interesting results in terms of fault severity evaluation. The WVD technique features a relatively low computational cost and high resolution, since the entire signal is exploited to obtain the energy at each time-frequency bin. The application of WVD in fault diagnosis methods has been successfully tested along with current analysis [Burnett et al., 1996] and vibration analysis [Tang et al., 2010]. A relevant drawback of the conventional WVD is the appearance of cross terms in the distribution of artifacts, which in some cases preclude the practical application of methods based on such a technique. In [Climente-Alarcon et al., 2014] an improved fault diagnosis algorithm based on the WVD was recently proposed, based on the combination of the conventional WVD along with advanced notch FIR filters, which can effectively minimize the cross terms and provide seamless high-resolution time-frequency diagrams. As a consequence, the diagnosis of rotor asymmetries and eccentricities in induction machines directly connected to the grid can be achieved even in the worst cases. In [Xiang and Yan, 2014], a self-adaptive WVD method based on local mean decomposition has been presented, which can evidently remove the cross-terms of WVD to improve the performance in terms of defect diagnosis.

1.4 Data-Driven Methodologies

1.4.1 Introduction

As denoted in [Frank, 1996], [Gao et al., 2015b], both MB and SB approaches may be difficult to apply under real conditions where no accurate mathematical models of the system can be obtained, or no suitable signal patterns can be extracted. For the most part of typical industrial processes, rather than a model or a signal pattern, a large amount of historical data is usually available. Therefore, an alternative way to implement FDI systems is that to exploit the underlying knowledge contained in the large volume of available historic data, which implicitly represents the relationships among the process variables. As pointed out in [Gao et al., 2015b], model-based, signal-based and knowledge-based algorithms all have to use real-time data when performing real-time monitoring and on-line fault diagnosis. However, only knowledge-based fault diagnosis approaches need to employ a large volume of historic data available. From this point of view, knowledge-based fault diagnosis is also referred to as *Data-Driven* (DD) fault diagnosis. As stated in [Frank, 1996], DD methods can be applied to implement all the three tasks of the generic FDD procedure discussed in Section 2.1, namely residual generation, residual evaluation and fault analysis, although in this case these phases are not always as clearly separable as in the MB methodology. According to [Gao et al., 2015b], DD fault diagnosis methods can be classified in the two following categories, based on the nature of the extraction process of the knowledge base:

- *Qualitative Fault Diagnosis Methods*
- *Quantitative Fault Diagnosis Methods*

1.4.2 Qualitative Fault Diagnosis Methods

As mentioned in [Gao et al., 2015b], the most known and common qualitative fault diagnosis methods are those based on expert systems. Expert systems emerged in the late 1960s as a branch of the artificial intelligence, which is a way to represent the human expertise by means of a rule-based approach. Fault diagnosis methods based on expert systems was first proposed in [Henley, 1984], [Chester et al., 1984], where the evaluation of the on-line monitored data was performed according to a set of rules, learned from the past experience of human experts. The main advantages provided by the expert systems are: the ease of development, the transparent reasoning, the ability to reason under uncertainty, and the capability to explain the solutions provided. However, as it has been noticed in [Gao et al., 2015b], faults diagnosis methods based on expert systems results to be system specific, with low generality and low expandability. Some attempts to overcome this limitations has been provided. In [Bo et al., 2012], a task-based diagnosis expert system was proposed, in which object-oriented knowledge representation methods were applied so that the rules of a specific machine can be flexibly customized on the basis of a general rule set. In [Kodavade and Apte, 2012], a universal fault diagnostic expert system framework was presented, based on the integration of the object-oriented paradigm into a rule based expert system.

In many industrial applications, process malfunctions may reflect distinct trends in the measurements, which can be suitably employed to identify such deviations from the nominal conditions. Indeed, another common set of qualitative fault diagnosis methods refers to those which implement the classification and analysis of the process trends. The Qualitative Trend Analysis (QTA), comprehensively reviewed in [Venkatasubramanian et al., 2003b], is a DD

technique which consists in the identification of process trends from noisy process data and in the subsequent comparison of such extracted information to a set of known fault trends stored in a database. As mentioned in [Gao et al., 2015b], the QTA technique has been widely applied to implement the fault diagnosis in complex industrial applications, such as those related to chemical processes. Recently, improved versions of the QTA have been integrated with other qualitative tools, such as the Signed Directed Graphs (SDG), in order to enhance their respective advantages while compensate their respective disadvantages. An integrated framework which combines the completeness property of the SDG and the high diagnostic resolution property of the QTA was proposed in [Maurya et al., 2007] for the diagnosis of incipient faults. Another approach based on the integration of SDG and QTA, which meets the fundamental diagnosis requirements such as correctness, completeness and real-time, but also provides a good resolution, was proposed in [Dong et al., 2010] to make the fault diagnosis of a distillation power unit.

1.4.3 Quantitative Fault Diagnosis Methods

All the quantitative knowledge-based methods share the same general approach, which essentially consist in the formulation of the fault diagnosis by solving a suitable pattern recognition problem. Quantitative information, called *features*, can be either extracted by using statistical or non-statistical methods. Therefore, according to [Gao et al., 2015b], the quantitative knowledge-based fault diagnosis methods can be roughly classified into the two following sub-categories:

- Statistical Analysis DD FDD Methods
- Nonstatistical Analysis DD FDD Methods

1.4.3.1 Statistical Analysis DD FDD Methods

Under the statistical framework, the quantitative knowledge-based fault diagnosis methods are mainly based on the following multivariate statistical techniques:

- Principal Component Analysis (PCA)
- Partial Least Squares (PLS)
- Independent Component Analysis (ICA)

Other common methods are those based on statistical pattern classifiers, and a more recent strategy called Support Vector Machine (SVM). As mentioned in [Gao et al., 2015b], all the above methods require a large amount of training data to capture the key characteristics of the process by using statistical analysis. PCA is the most popular technique employed in statistical-based fault diagnosis methods, because of its ability to handle huge amount of highly correlated data, and its simple implementability. According to the definition provided in [Sari, 2014], the PCA is an optimal linear dimensionality reduction technique, in terms of capturing the main variations in data. The dimensionality reduction of the original data set is achieved by projecting all the available data into the subspace spanned by a suitable set of orthogonal vectors, known as *loading vectors*, which reveals most of the variance in the data, without losing important information, so that the major trends in the original data set can be properly described. Fault diagnosis methods based on PCA have been extensively

investigated in literature and have successful applications in complex industrial systems, as confirmed by the following references. In [Wang et al., 2008], a nonlinear extension of PCA was developed for the diagnostic of diesel engines. In [Elshenawy and Awad, 2012], a fault diagnosis method based on recursive PCA was presented for a time-varying industrial process. Probabilistic fault diagnosis techniques based on the ability of PCA to de-noise original signals and improve the signal-to-noise ratio PCA were proposed in [Jiang et al., 2014] to monitor a rolling bearing with an outer race fault. In [Zhang et al., 2013], the integration of y-indices, residual errors and faulty sensor identification indices with PCA yielded to propose two different approaches for the diagnostic of gas turbine engines, both easy to implement and computationally efficient. PLS, also known as *Projection to Latent Structure*, is another dominant tool employed in statistical-based fault diagnosis methods for complex industrial processes. As pointed out in [Sari, 2014], compared to PCA, which aims to capture the correlation among the process variables, then to find the subspace which contains the most variations, PLS instead, aims to determine at first which subspace is the most correlated with a *predicted block*, then to describes the most variations in a *predictor block*. As referred in [Sari, 2014], a typical application of such an approach is to consider the process measurements as the predictor block and the product quality measurements as the predicted block. The product quality is often measured off-line in the laboratory and is not available on-line. Thus, PLS can be used both to predict the product quality and to monitor the process. Recent development of fault diagnosis an monitoring methods based on PLS can be found in literature. In [Ding et al., 2013], a DD scheme of key performance indicator prediction and diagnosis for both static and dynamic processes was proposed as an alternative solution to the standard PLS method, with simplified computation procedures. In [Zhao et al., 2014], an improved structure based on a further decomposition for the obtained PLS structure, namely Total Projection to Latent Structures (T-PLS), was presented. This diagnostic method based on T-PLS, can well detect quality-relevant faults in industrial processes subjected to a variety of raw materials and changeable control conditions. As stated in [Gao et al., 2015b], ICA plays an important role in the real-time monitoring and diagnosis of many industrial processes, since it allows to deal with latent variables which do not follow a Gaussian distribution. Recently, a fault isolation method based on the kernel ICA was proposed in [Zhang et al., 2014] for non-Gaussian nonlinear processes. In [Tsai et al., 2013], by applying ICA to basis images defect detection was investigated for solar modules. In [Guo et al., 2014], fault diagnosis technique based on ICA was applied to monitor and diagnose rolling element bearing. As pointed out in [Gao et al., 2015b], SVM is a recent machine learning technique relying on the statistical learning theory, which is able to achieve high generalization and dealing with problems with low samples and high input features. SVM is considered as a suitable technique potentially able to classify all kinds of data sets. The first attempts to apply SVM for fault diagnosis and monitoring purposes were made by [AYDMJ and Duin, 1999], [Rychetsky et al., 1999]. Several recent results about fault diagnosis applications based on SVM can be found in literature, e.g.:[Yin et al., 2014b], [Namdari et al., 2014], [Sahri and Yusof, 2014].

1.4.3.2 Nonstatistical Analysis DD FDD Methods

The most common computational approach employed in the main part of the nonstatistical data-driven fault diagnosis methods is the Artificial Neutral Network (ANN). Following the explanation given in [Frank, 1996], the ANN is based on a collection of single processing units, called *neurons*, which become active as soon as their inputs exceed certain thresholds.

The neurons are arranged in subsets, called *layers*, which are connected in such a way the signals at the input are propagated through the network to the output. The choice of the *activation function* of each neuron contributes to the overall nonlinear behavior of the network. Thus, the ANN is typically defined by three different types of parameters:the interconnection pattern between the different layers of neurons, the learning process for updating the weights of the interconnections and the activation function that converts a neuron's weighted input to its output activation. In terms of topology, the ANN can be classified into:

- Radial Basis Networks
- Recurrent Dynamic Networks
- Self-Organizing-Maps
- Back-Propagation Networks
- Extension Networks

In terms of learning strategy, two different approaches can be applied, i.e. supervised and unsupervised learning. As explained in [Gao et al., 2015b], when using the supervised learning, the knowledge-base is extracted from the historical data to emulate the nominal system behavior, which is then compared in real-time to that of the actual process, in order to check for deviations from the nominal conditions. When using unsupervised learning instead, the knowledge-bases related to the nominal and faulty conditions are all extracted, then are used, during the real-time monitoring. The most popular supervised learning strategy in ANN has been the back-propagation algorithm. Indeed, several papers address the problem of fault diagnosis using back-propagation neural networks. E.g., the works of [Watanabe et al., 1989], [Venkatasubramanian and Chan, 1989], [Ungar et al., 1990], [Hoskins et al., 1991] are among the first attempts to demonstrate the usefulness of fault diagnosis methods based on ANN in chemical engineering. A survey of ANN-based fault diagnosis methods for steady-state processes was presented by [Venkatasubramanian et al., 1990]. The extension to dynamic processes was later provided by [Vaidyanathan and Venkatasubramanian, 1992]. Several different network architectures have been proposed to achieve the fault diagnosis. For instance, a multi-resolution hierarchical neural network has been proposed in [Bakshi and Stephanopoulos, 1993] whereas self-organizing neural network structures have been proposed in [Carpenter and Grossberg, 1988] and [Whiteley and Davis, 1994]. Recent developments of ANN-based fault diagnosis methods in several different real-time applications, such as combustion engines, steam turbine generators, nuclear process, induction machines and power network quality, are reported in [Gao et al., 2015b].

Another common approach employed in many nonstatistical data-driven fault diagnosis methods is the Fuzzy Logic (FL). The main idea behind the FL is to approximate the human way of reasoning, by partitioning a feature space into fuzzy sets, then using fuzzy rules to implement the deductive analysis. According to [Chen and Patton, 1999], the most appealing feature of FL is to be a powerful tool for modeling not well specified data; therefore this approach results to be highly suited for applications where a complete information about the system is not available to the designer. Recent developments have shown the interest to combine FL with other knowledge-based techniques such as expert systems or ANN in order to solve engineering-oriented diagnosis issues [Nan et al., 2008] or getting better diagnosis performances [Wijayasekara et al., 2014].

1.5 Hybrid Methodologies

It is apparent that each of the three different methodologies discussed in the previous Sections of this Chapter presents its own advantages and constraints. MB approaches need only a few data to make fault diagnosis, but their implementation usually is not straightforward, and the performances depend on the accuracy of the model. Both SB and DD methods can be applied when a model is unavailable or is not enough compliant with the real system, specially if the industrial application is complex. Nevertheless, on the one hand, since SB techniques perform the fault diagnosis by extracting suitable features from the output signals, they result less robust than MB methods, when dealing with noises such as unknown inputs or unbalanced conditions. On the other hand, DD techniques achieve the fault diagnosis by means of expensive procedures in terms of computational resources, which require a lot of historical data. In the last years, several attempts to make hybrid FDD systems, which aim to suitably combine or integrate such approaches, in order to exploit the advantages of each method and increase the overall performances in terms of diagnostic capabilities, have been investigated for a wide range of engineering applications.

In [He et al., 2013], a SB-DD integration was proposed to diagnose plastic bearing faults. Specifically, the outer race fault was isolated by applying a statistical approach, whereas other types of faults were isolated by means of frequency-domain fault features, extracted with the Fast Fourier Transform (FFT), as well as time-domain features, extracted by a TD SB algorithm, and given as inputs to a K-Nearest-Neighborhood (KNN) classifier to achieve the fault diagnosis. Another SB-DD method was presented in [Soualhi et al., 2013] for the FDD of induction motors. In this application, different signal processing techniques, including spectral analysis, were developed to extract features sensitive to electrical and mechanical faults, whereas a DD classifier, denoted as *Artificial Ant Clustering*, was employed to classify different operation modes. The new data were then compared with such a knowledge base in order to perform the fault diagnosis. The integration of SB and DD approaches was exploited also in [Seshadrinath et al., 2014] to diagnose inter-turn faults in induction machines. At first, features were extracted from the measured vibration signals, by means of the Dual-Tree Complex Wavelet Transform (DTCWT), then their classification in healthy and faulty features was performed through PCA and probabilistic ANN. Another interesting SB-DD application was presented in [Ebrahimi et al., 2014], where WT, PCA and fuzzy SVM were exploited to achieve, separately, each of the following three tasks: 1) the feature extraction, 2) the dimension reduction and elimination of linear dependence among the extracted features, 3) the fault classification.

The integration of MB and DD method was also investigated, as in [Sheibat-Othman et al., 2014], where such an hybrid fault diagnosis method was proposed for chemical reactors, typically subjected to high nonlinearities and high variability of dynamics. Indeed, at first the fault detection was achieved by implementing a SVM, but with this method it was difficult to detect faults generated by the highly transitional dynamics. Thus, in order to improve the fault isolation capability, a combination of the SVM with an observer based on a simplified initial model was exploited, where the model was corrected and updated by the information provided by the SVM.

1.6 Conclusion

In this Chapter, a general overview of the first subject discussed in this dissertation has been provided. At first, a basic set of definitions was given to introduce the reader to those concepts widely used in the topic of fault detection, isolation and diagnosis. Then, the different methodologies which nowadays include almost the whole state-of-the-art about the FDD systems, i.e. MB, SB, and DD, have been discussed and compared. For each of these methodologies, the main approaches and techniques were reviewed, by underlying their respective advantages and constraints. Since in this research the integration of different fault diagnosis methodologies was exploited, a brief discussion about the hybrid approaches and the most recent proposals provided by the fault diagnosis community in this promising direction were also investigated.

Chapter 2

Data Reconciliation and Parameter Estimation

The research area of gross error detection in sensor data and subsequent validation is closely related to the topic of fault detection and diagnosis. The gross error detection, or sensor validation, refers to the identification of faulty, or failed, sensors in the process. Two major types of gross errors can be found in practical applications. The first type of gross error refers to the instrument performance, and includes measurement bias, drifting, uncalibration, and total instrument failure. The second type of gross error refers to the constraints related to the model, and includes unaccounted loss of energy and material resulting from leaks, process equipment, or model uncertainties due to inaccurate parameters. Several techniques have been proposed in the literature for the detection and elimination of these two types of gross errors, as stated in [Narasimhan and Jordache, 1999].

Data reconciliation, or rectification, is the task of providing estimates for the true values of the sensor readings. Since fault diagnosis includes sensor failures also in its scope, hence, data validation and rectification can be considered as a specific case of a more general fault diagnosis problem. Data Reconciliation (DR) technology is widely applied nowadays in various chemical, petrochemical, and other material processing industries. It is applied off-line, or in connection with on-line applications, such as process optimization and advanced process control.

Both unmeasured variables and model parameters can be estimated by data reconciliation, providing that enough measured data is available in order to make them observable. Applications such as simulation and optimization of existing process equipment rely on a model of the equipment. These models, usually, contain parameters which have to be estimated from the available plant data. This is also known as model tuning, for which accurate data is essential. The use of erroneous measurements in model tuning can give rise to incorrect model parameters, which can nullify the benefits achievable through optimization.

According to [Narasimhan and Jordache, 1999], three different ways to apply the data reconciliation and gross error detection technologies to industrial applications can be distinguished:

- Process unit balance reconciliation and gross error detection
- Parameter estimation and data reconciliation
- Plant-wide material and utilities reconciliation

This Chapter focuses attention only on those approaches which perform the data reconciliation and parameter estimation tasks. The Section 2.1 introduces to some basic concepts and definitions, related to the topics of data reconciliation and parameter estimation. The Section 2.2 provides a rapid overview of different DR methods, referring to systems operating at steady-state conditions. In Section 2.3 instead, dynamic data reconciliation procedures are reviewed. Finally, in Section 2.4, the parameter estimation problem is also considered, ad some approaches which allow to estimate parameters along with the data reconciliation procedure are discussed.

2.1 Basic Concepts and Definitions

Efficient, profitable, and safe plant operations depend on accurate and reliable process data. DR is a technique that has been developed to improve the accuracy of measurements by reducing the effect of random errors in the data. The principal difference between DR and other filtering techniques is that the former explicitly makes use of process model constraints, and obtains estimates of process variables by adjusting process measurements, so that the estimates satisfy the constraints. The reconciled estimates are expected to be more accurate than the measurements and, more importantly, they are also consistent with the known relationships between process variables, as defined by the constraints. In order for data reconciliation to be effective, there should be no gross errors, either in the measurements, or in the process model constraints. Gross error detection is a companion technique to DR, which has been developed in order to identify and eliminate gross errors. Thus, DR and gross error detection are applied together to improve accuracy of measured data.

DR and gross error detection both achieve the reduction of errors, only by exploiting the redundancy properties of measurements. Typically, in any process, the variables are related to each other through physical constraints, such as material or energy conservation laws. Given a set of such system constraints, a minimum number of error-free measurements is required, in order to compute all of the system parameters and variables. If there are more measurements than this minimum, then redundancy exists in the measurements, which can be exploited. This property is usually called *spatial redundancy*, and when it exists, the system of equations is said to be overdetermined. DR cannot be performed without the spatial redundancy. With no extra measured information, the system is just determined, and no correction to erroneous measurements is possible. Furthermore, if fewer variables than those needed to determine the system are measured, the system is undetermined, and the values of some variables can be estimated only through other means, or if additional measurements are provided. A second type of redundancy, refers to the fact that measurements of process variables are made continually in time at a high sampling rate, producing more data than necessary to determine a steady-state process. This property is usually called *temporal redundancy*. If the process is assumed to be in a steady state, then temporal redundancy can be exploited, by simply averaging the measurements, and applying steady-state DR to the averaged values.

If the process state is dynamic, however, its evolution is described by differential equations corresponding to mass and energy balances, which inherently capture both the temporal and spatial redundancy of measured variables. For such process, Dynamic Data Reconciliation (DDR) and gross error detection techniques have been developed, to obtain accurate estimates consistent with the differential model equations of the system.

As stated above, DR improves the accuracy of process data, by adjusting the measured

values so that they satisfy the process constraints. The amount of adjustment made to the measurements is minimized, since the random errors in the measurements are expected to be small. In the general case, not all variables of the process are measured, due to economic or technical limitations. The estimates of unmeasured variables, as well as model parameters, are also obtained as part of the reconciliation problem. The estimation of unmeasured values based on the reconciled measured values is also known as *data coaptation*.

2.2 Steady-State Data Reconciliation

2.2.1 Introduction

According to [Romagnoli and Sánchez, 2000], the following definitions are provided. Assuming the absence of gross errors, the measurement vector can be written as follows:

$$\mathbf{y} = \mathbf{x} + \boldsymbol{\varepsilon} \tag{2.1}$$

where $\mathbf{y} \in \mathbb{R}^n$ is the measurement vector, $\mathbf{x} \in \mathbb{R}^n$ is the vector of the actual values of the variables, and $\boldsymbol{\varepsilon} \in \mathbb{R}^n$ is the vector which denotes the unknown random measurements errors. Usually, some assumptions about the statistical properties of the measurement errors are also made, i.e. the random errors are assumed to follow a multivariate normal distribution with zero mean and known variance-covariance matrix. Therefore:

- The expected value of the measurement errors is zero, i.e. $E(\boldsymbol{\varepsilon}) = \mathbf{0}$
- The subsequent measurements are independent, i.e. $E(\boldsymbol{\varepsilon}_i \boldsymbol{\varepsilon}_j^T) = \mathbf{0} \quad \forall i \neq j$
- The covariance matrix of the measurement errors is known and positive definite, i.e. $Cov(\boldsymbol{\varepsilon}) = \boldsymbol{\Sigma} = E(\boldsymbol{\varepsilon}_i \boldsymbol{\varepsilon}_i^T)$

where $E(\cdot)$ is the expectation operator. It is worth to notice that, since both $\mathbf{x}$ and $\mathbf{y}$ are vectors in the $\mathbb{R}^n$ space, at this stage, all the process variables are assumed to be measured.

As explained before, additional information must be introduced in practice, under the form of process model equations, since the process variables must conform to some relationships arising from the physical characteristics of the model. These *constraint equations* are usually represented as a set of nonlinear algebraic equations:

$$\begin{aligned} \mathbf{f}(\mathbf{x}, \mathbf{u}) &= \mathbf{0} \\ \mathbf{g}(\mathbf{x}, \mathbf{u}) &\leq \mathbf{0} \end{aligned} \tag{2.2}$$

where $\mathbf{u} \in \mathbb{R}^p$ indicates the vector of unmeasured process variables, $\mathbf{f}(\cdot) \in \mathbb{R}^m$ denotes the set of m equality constraints representing the process model and $\mathbf{g}(\cdot) \in \mathbb{R}^q$ denotes the set of q the inequality constraints.

In general, data reconciliation can be formulated by the following constrained weighted least-squares optimization problem:

$$\begin{aligned} &\min_{\mathbf{x},\mathbf{u}} \ (\mathbf{y} - \mathbf{x})^T \boldsymbol{\Sigma}^{-1} (\mathbf{y} - \mathbf{x}) \\ &\text{s.t.} \ \begin{cases} \mathbf{f}(\mathbf{x}, \mathbf{u}) = \mathbf{0} \\ \mathbf{g}(\mathbf{x}, \mathbf{u}) \leq \mathbf{0} \\ \mathbf{x}^{\mathrm{L}} \leq \mathbf{x} \leq \mathbf{x}^{\mathrm{U}} \\ \mathbf{u}^{\mathrm{L}} \leq \mathbf{u} \leq \mathbf{u}^{\mathrm{U}} \end{cases} \end{aligned} \tag{2.3}$$

where $\{\mathbf{x}^L, \mathbf{x}^U\}$ and $\{\mathbf{u}^L, \mathbf{u}^U\}$ denote the lower and upper bounds of $\mathbf{x}$ and $\mathbf{u}$, respectively.

As pointed out in [Romagnoli and Sánchez, 2000], if the measurement errors are normally distributed, the resolution of problem (2.3) provides the maximum likelihood estimates of process variables. Therefore, they result to be minimum-variance unbiased estimators. Different methodologies are required to solve the problem (2.3), depending on whether the constraints are a linear or a nonlinear set of equations. Some of these methods will be reviewed in the following of this Section.

2.2.2 Linear Data Reconciliation

As mentioned in [Romagnoli and Sánchez, 2000], two different situations have to be considered in linear data reconciliation. Indeed, sometimes, all the variables included in the process model are measured, but more frequently, some of them cannot be measured. Both cases will be briefly reviewed in the next two Paragraphs.

2.2.2.1 Linear DR with all variables measured

In this case, the problem (2.3) can be reformulated as:

$$\begin{aligned} &\min_{\mathbf{x},\mathbf{u}} \ (\mathbf{y}-\mathbf{x})^T \boldsymbol{\Sigma}^{-1} (\mathbf{y}-\mathbf{x}) \\ &\text{s.t.} \ \ \mathbf{A}\mathbf{x} = \mathbf{0} \end{aligned} \tag{2.4}$$

where $A \in \mathbb{R}^{m \times n}$ is a matrix of known constants. In this case all variables are redundant. Several different resolution methods are available in literature for this problem. Good surveys about them can be found in [Romagnoli and Sánchez, 2000], [Mah, 2013].

In this paragraph only two approaches will be discussed, which are the traditional one, called *batch resolution*, and an alternative one, based on the *Q-R factorization*.

Batch Solution

Introducing the measurement errors into the process constraints, by means of (2.2), the optimization problem (2.4) becomes:

$$\begin{aligned} &\min_{\boldsymbol{\varepsilon}} \ \boldsymbol{\varepsilon}^T \boldsymbol{\Sigma}^{-1} \boldsymbol{\varepsilon} \\ &\text{s.t.} \ \ \mathbf{A}(\mathbf{y}-\boldsymbol{\varepsilon}) = \mathbf{0} \end{aligned} \tag{2.5}$$

The solution of this problem is obtained by applying the Lagrange multipliers method, where the Lagrangian is:

$$L = \boldsymbol{\varepsilon}^T \boldsymbol{\Sigma}^{-1} \boldsymbol{\varepsilon} - 2\lambda^T \mathbf{A}(\mathbf{y}-\boldsymbol{\varepsilon}) \tag{2.6}$$

Since $\boldsymbol{\Sigma}$ is positive definite and the constraints are linear, the minimization conditions are:

$$\begin{aligned} \frac{\partial L}{\partial \boldsymbol{\varepsilon}} &= 2\boldsymbol{\Sigma}^{-1}\boldsymbol{\varepsilon} + 2\mathbf{A}^T\lambda = \mathbf{0} \ \ &\Rightarrow \ \ \boldsymbol{\Sigma}^{-1}\boldsymbol{\varepsilon} = -\mathbf{A}^T\lambda \\ \frac{\partial L}{\partial \lambda} &= \mathbf{A}(\mathbf{y}-\boldsymbol{\varepsilon}) = \mathbf{0} \ \ &\Rightarrow \ \ \mathbf{A}\boldsymbol{\varepsilon} = \mathbf{A}\mathbf{y} \end{aligned} \tag{2.7}$$

hence:

$$\begin{aligned} \boldsymbol{\varepsilon} &= -\boldsymbol{\Sigma}\mathbf{A}^T\lambda \\ \mathbf{A}(-\boldsymbol{\Sigma}\mathbf{A}^T\lambda) &= \mathbf{A}\mathbf{y} \;\Rightarrow\; \lambda = -(\mathbf{A}\boldsymbol{\Sigma}\mathbf{A}^T)^{-1}\mathbf{A}\mathbf{y} \end{aligned} \tag{2.8}$$

Hence, the estimate of the process variables, i.e. $\hat{\mathbf{x}}$, is then obtained by substituting the result of (2.8) in (2.1), that is:

$$\hat{\mathbf{x}} = \mathbf{y} - \boldsymbol{\Sigma}\mathbf{A}^T(\mathbf{A}\boldsymbol{\Sigma}\mathbf{A}^T)^{-1}\mathbf{A}\mathbf{y} \tag{2.9}$$

Q-R Factorizations

In this procedure, the constrained problem (2.5) is transformed into an unconstrained one. By means of the Q-R orthogonal factorization algorithm, depicted in [Romagnoli and Sánchez, 2000], and applied to matrix $\mathbf{A}$, the following result can be obtained:

$$\mathbf{A}\Pi = \mathbf{Q}\mathbf{R} \tag{2.10}$$

where $\mathbf{Q} \in \mathbb{R}^{m\times m}$ is an orthogonal matrix, $\mathbf{R} \in \mathbb{R}^{m\times n}$ is an upper-triangular matrix, and $\Pi \in \mathbb{R}^{n\times n}$ is a permutation matrix of $\mathbf{A}$, and the following partitioning arise:

$$\mathbf{Q} = [\mathbf{Q}_1\ \mathbf{Q}_2]\ ,\ \mathbf{R} = \begin{bmatrix} \mathbf{R}_{11} & \mathbf{R}_{12} \\ \mathbf{0} & \mathbf{0} \end{bmatrix}\ ,\ \Pi^T\mathbf{x} = \begin{bmatrix} \mathbf{x}_r \\ \mathbf{x}_{n-r} \end{bmatrix} \tag{2.11}$$

where $r = \text{rank}(\mathbf{R}_{11}) = \text{rank}(\mathbf{A})$, $\mathbf{Q}_1 \in \mathbb{R}^{m\times r}$ has r orthonormal columns, $\mathbf{R}_{11} \in \mathbb{R}^{r\times r}$ is a nonsingular upper triangular matrix, and $\mathbf{x}_{n-r}$ is an arbitrary vector. In [Romagnoli and Sánchez, 2000] it has been shown that the general solution of the undetermined system $\mathbf{A}\mathbf{x} = \mathbf{0}$ ca be obtained as:

$$\mathbf{x}_r = -\mathbf{R}_{11}^{-1}\mathbf{R}_{12}\mathbf{x}_{n-r} \tag{2.12}$$

As a consequence, the vector of the objective function related to the problem (2.5), i.e. $(\mathbf{y}-\mathbf{x})$, can be expressed as follows:

$$\begin{aligned} (\mathbf{y}-\mathbf{x}) &= \mathbf{y} - [\mathbf{I}_1\ \ \mathbf{I}_2]\begin{bmatrix} \mathbf{x}_r \\ \mathbf{x}_{n-r} \end{bmatrix} = \mathbf{y} + \mathbf{I}_1\mathbf{R}_1^{-1}\mathbf{R}_2\mathbf{x}_{n-r} - \mathbf{I}_2\mathbf{x}_{n-r} = \\ &= \mathbf{y} + (\mathbf{I}_1\mathbf{R}_1^{-1}\mathbf{R}_2 - \mathbf{I}_2)\mathbf{x}_{n-r} \end{aligned} \tag{2.13}$$

where:

$$\mathbf{I}\Pi = [\mathbf{I}_1\ \ \mathbf{I}_2]\ ,\ \tilde{\mathbf{I}} = \mathbf{I}_1\mathbf{R}_1^{-1}\mathbf{R}_2 - \mathbf{I}_2 \tag{2.14}$$

being $\mathbf{I} \in \mathbb{R}^{n\times n}$ the identity matrix and $\tilde{\mathbf{I}} \in \mathbb{R}^{n\times(n-r)}$ a matrix with independent columns.

Hence, the unconstrained minimization problem can be stated as:

$$\min\ (\mathbf{y} + \tilde{\mathbf{I}}\mathbf{x}_{n-r})^T\boldsymbol{\Sigma}^{-1}(\mathbf{y} + \tilde{\mathbf{I}}\mathbf{x}_{n-r}) \tag{2.15}$$

and the solution of this problem can be computed by means of the standard method of Lagrange multipliers seen above in the batch solution, that is:

$$\hat{\mathbf{x}}_{n-r} = -(\tilde{\mathbf{I}}^T\boldsymbol{\Sigma}^{-1}\tilde{\mathbf{I}})^{-1}\tilde{\mathbf{I}}^T\boldsymbol{\Sigma}^{-1}\mathbf{y} \tag{2.16}$$

finally, the estimate $\hat{\mathbf{x}}_r$, is then obtained by substituting the value of (2.16) in (2.12).

2.2.2.2 Linear DR with unmeasured variables

In many practical applications, usually, only a subset of process variables are measured. Hence, all the unmeasured variables must be estimated. In this paragraph, the approaches discussed for the linear data reconciliation problem involving only measured variables will be applied, in order to provide a general solution of the linear data reconciliation problem, which can deal both with measured and unmeasured variables.

Following [Romagnoli and Sánchez, 2000], the main idea is based on the decoupling of the unmeasured variables from the measured ones, by means of Q-R orthogonal factorizations. By this way the overall estimation problem is divided in two subproblems.

$$\mathbf{A}_1\mathbf{x}+\mathbf{A}_2\mathbf{u}=\mathbf{0} \tag{2.17}$$

where $\mathbf{x}\in\mathbb{R}^n$ denotes the vector of the n measured variables, $\mathbf{u}\in\mathbb{R}^p$ denotes the vector of the p unmeasured variables, $\mathbf{A}_1\in\mathbb{R}^{m\times n}$ and $\mathbf{A}_2\in\mathbb{R}^{m\times p}$ are compatible matrices.

By means of the Q-R orthogonal factorization algorithm depicted in the previous paragraph, applied to matrix $\mathbf{A}_2$, the following result can be obtained:

$$\mathbf{A}_2\Pi=\mathbf{QR} \tag{2.18}$$

where $\mathbf{Q}\in\mathbb{R}^{m\times m}$, $\mathbf{R}\in\mathbb{R}^{m\times p}$, and $\Pi\in\mathbb{R}^{p\times p}$ have the same meaning of the matrices depicted (2.11). Hence, in this case will be: $r=\text{rank}(\mathbf{R}_{11})=\text{rank}(\mathbf{A}_2)$, and the vector of unmeasured variables, i.e. $\mathbf{u}\in\mathbb{R}^n$, will be partitioned into two subsets:

$$\Pi^T\mathbf{u}=\begin{bmatrix}\mathbf{u}_s\\ \mathbf{u}_{p-s}\end{bmatrix} \tag{2.19}$$

Hence, multiplying the linearized constraints (2.17) by $\mathbf{Q}^T=\mathbf{Q}^{-1}$, the following result arises:

$$\begin{aligned}&\mathbf{Q}_1^T\mathbf{A}_1\mathbf{x}+\mathbf{R}_{11}\mathbf{u}_s+\mathbf{R}_{12}\mathbf{u}_{p-s}=\mathbf{0}\\ &\mathbf{Q}_2^T\mathbf{A}_1\mathbf{x}=\mathbf{0}\end{aligned} \tag{2.20}$$

Thus, by applying the standard reconciliation procedure on the decoupled subsystem of the measured variables $\mathbf{u}$, the solution will be the same as in (2.9), that is:

$$\hat{\mathbf{x}}=\mathbf{y}-\mathbf{\Sigma}(\mathbf{Q}_2^T\mathbf{A}_1)^T[(\mathbf{Q}_2^T\mathbf{A}_1)\mathbf{\Sigma}(\mathbf{Q}_2^T\mathbf{A}_1)^T]^{-1}(\mathbf{Q}_2^T\mathbf{A}_1)\mathbf{y} \tag{2.21}$$

The unmeasured variables can be explicitated from the first equation of (2.20), as follows:

$$\mathbf{u}_s=-\mathbf{R}_{11}^{-1}(\mathbf{Q}_1^T\mathbf{A}_1\hat{\mathbf{x}}+\mathbf{R}_{12}\mathbf{u}_{p-s})=-\mathbf{R}_{11}^T\mathbf{Q}_1^T\mathbf{A}_1\hat{\mathbf{x}}-\mathbf{R}_{11}^{-1}\mathbf{R}_{12}\mathbf{u}_{p-s} \tag{2.22}$$

where the $\mathbf{u}_{p-s}$ components are set arbitrarily. Two different cases have to be considered:

1. $\text{Rank}(\mathbf{R}_{11})=p$
2. $\text{Rank}(\mathbf{R}_{11})<p$

In case 1), all the unmeasured process variables are estimable, and then a unique solution can be obtained for their estimation, by means of the rectified measured values (2.21) and of the balance equations (2.22).

In case 2), some unmeasured process variables cannot be estimated, and an infinite number of solutions are possible. Thus, the basic solution is:

$$\begin{aligned} \mathbf{u}_s &= -\mathbf{R}_{11}^T \mathbf{Q}_1^T \mathbf{A}_1 \mathbf{x} \\ \mathbf{u}_{p-s} &= \mathbf{0} \end{aligned} \tag{2.23}$$

2.2.3 Nonlinear Data Reconciliation

As mentioned in [Romagnoli and Sánchez, 2000], a plant under steady-state operating conditions is commonly represented by a non-linear system of algebraic equations, made up of energy and mass balances, as well as thermodynamic relationships, and sometimes other physical behaviors of the system also. In these cases, the data reconciliation is based on the solution of a nonlinear constrained optimization problem. The general problem (2.3) can be formulated also by using a more compact notation:

$$\begin{aligned} &\min_{\mathbf{z}} \ \boldsymbol{\Sigma}(\mathbf{z}) \\ &\text{s.t.} \quad \begin{cases} \mathbf{f}(\mathbf{z}) = \mathbf{0} \\ \mathbf{g}(\mathbf{z}) \leq \mathbf{0} \\ \mathbf{z}^{\mathrm{L}} \leq \mathbf{z} \leq \mathbf{z}^{\mathrm{U}} \end{cases} \end{aligned} \tag{2.24}$$

where $\mathbf{z} \in \mathbb{R}^{n+p}$ is the vector of optimization variables, which includes both the measured and unmeasured process variables, and $\boldsymbol{\Sigma}(\mathbf{z})$ is the objective function. According to [Romagnoli and Sánchez, 2000], the necessary conditions for an optimal solution of the problem are equivalent to those for optimizing the Lagrange function, which is defined as:

$$L(\mathbf{z}, \lambda, \mu) = \boldsymbol{\Sigma}(\mathbf{z}) + \sum_{i=1}^{m} \lambda_i f_i(\mathbf{z}) + \sum_{j=1}^{q} \mu_j g_j(\mathbf{z}) \tag{2.25}$$

The following are the well known Kuhn-Tucker (KT) conditions:

- Linear dependency of the gradients:

$$\nabla \boldsymbol{\Sigma}(\mathbf{z}) + \sum_{i=1}^{m} \lambda_i \nabla f_i(\mathbf{z}) + \sum_{j=1}^{q} \mu_j \nabla g_j(\mathbf{z}) = \mathbf{0} \tag{2.26}$$

- Constraint feasibility:

$$\begin{aligned} f_i(\mathbf{z}) &= \mathbf{0} \quad , \quad i = 1, \ldots, m \\ g_j(\mathbf{z}) &\leq \mathbf{0} \quad , \quad j = 1, \ldots, q \end{aligned} \tag{2.27}$$

- Complementary conditions:

$$\mu_j g_j(\mathbf{z}) \leq 0 \quad , \quad j = 1, \ldots, q \tag{2.28}$$

- Nonnegativity conditions for inequality multipliers:

$$\mu_j \geq 0 \quad , \quad j = 1, \ldots, q \tag{2.29}$$

where λ_i and μ_j are the Lagrange and Kuhn-Tucker multipliers, respectively.

The sufficient conditions for obtaining a global solution of the nonlinear programming problem are those requiring both the objective function and the constraint set to be convex. If these conditions are not satisfied, there is no guarantee that the local optimum will be the global optimum. In the following, the applicability of two different techniques for solving the nonlinear data reconciliation problem is discussed.

2.2.3.1 Successive Linearizations

The method developed for problems with linear constraints can be extended also to deal with nonlinearly constrained problems. According to [Romagnoli and Sánchez, 2000], the main idea is to linearize the nonlinear equality constraints, i.e. $\mathbf{f}(\mathbf{x},\mathbf{u}) = \mathbf{0}$, by means of a Taylor series expansion around an estimation of the solution $(\mathbf{x}_k, \mathbf{u}_k)$. Usually, measurement values are used as initial estimations for the measured process variables. Therefore, the following linear system of equations can be obtained:

$$\mathbf{A}_1\mathbf{x} + \mathbf{A}_2\mathbf{u} = \mathbf{c} \tag{2.30}$$

where:

$$\mathbf{A}_1 = \left.\frac{\partial \mathbf{f}}{\partial \mathbf{x}}\right|_{(\mathbf{x}_k,\mathbf{u}_k)} , \; \mathbf{A}_2 = \left.\frac{\partial \mathbf{f}}{\partial \mathbf{u}}\right|_{(\mathbf{x}_k,\mathbf{u}_k)} , \; \mathbf{c} = \mathbf{A}_1\mathbf{x}_k + \mathbf{A}_2\mathbf{u}_k - \mathbf{f}(\mathbf{x}_k,\mathbf{u}_k) \tag{2.31}$$

As mentioned in [Romagnoli and Sánchez, 2000], orthogonal factorizations may be applied to solve the general problem (2.3) if the system of equality constraints $\mathbf{f}(\mathbf{x},\mathbf{u}) = \mathbf{0}$ is made up of linear mass balances, bilinear component and energy balances. After replacing the bilinear terms of the original model by the corresponding mass and energy flows, a linear data reconciliation problem results. Thus, the unmeasured variables can be eliminated by means of the orthogonal factorization procedure. Once the subset of equations containing only measured variables has been identified, the original problem is reduced to the linear one in (2.5), that is:

$$\begin{aligned} &\min_{\mathbf{x},\mathbf{u}} \; (\mathbf{y}-\mathbf{x})^T\boldsymbol{\Sigma}^{-1}(\mathbf{y}-\mathbf{x}) \\ &\text{s.t.} \; \mathbf{G}\mathbf{x} = \mathbf{b} \end{aligned} \tag{2.32}$$

where: $\mathbf{G} = \mathbf{Q}_2^T\mathbf{A}_1$ and $\mathbf{b} = \mathbf{Q}_2^T\mathbf{c}$.

Hence, the corresponding solution, which results to be the optimal point for the linear constraints, is:

$$\hat{\mathbf{x}} = \mathbf{y} - \boldsymbol{\Sigma}\mathbf{G}^T(\mathbf{G}\boldsymbol{\Sigma}\mathbf{G}^T)^{-1}(\mathbf{G}\mathbf{y} - \mathbf{b}) \tag{2.33}$$

$$\mathbf{u}_s = -\mathbf{R}_{11}^{-1}\mathbf{Q}_1^T\mathbf{c} - \mathbf{R}_{11}^T\mathbf{Q}_1^T\mathbf{A}_1\hat{\mathbf{x}} - \mathbf{R}_{11}^{-1}\mathbf{R}_{12}\mathbf{u}_{p-s} \tag{2.34}$$

Several iterations are then performed, by linearizing the constraints about the previous iterate, until a solution which satisfies the nonlinear constraints is obtained. The successive linearisation method has the advantage to be simple and fast in terms of computational requirements. In addition, it can be modified to choose a step size to minimize a pre-specified penalty function. However, variable bounds cannot be handled, because it may fail to converge to the desired minimum and it might oscillate when multiple minima exist.

2.2.3.2 Nonlinear Programming Techniques

Non-Linear Programming (NLP) algorithms are applied when dealing with general nonlinear objective function, not just a weighted least squares objective function, since they can explicitly handle nonlinear constraints, inequality constraints, and variable bounds. Typical algorithms include Sequential Quadratic Programming (SQP) techniques, such as NPSOL [Gill et al., 1986], and reduced gradient methods, such as GRG2 [Lasdon and Waren, 1977]. The main features of both approaches are described.

Sequential Quadratic Programming

According to [Romagnoli and Sánchez, 2000], a SQP technique involves the resolution of a sequence of explicit Quadratic Programming (QP) subproblems. The solution of each subproblem produces the search direction $\mathbf{d}_k$, which has to be taken to reach the next iterate $\mathbf{z}_{k+l}$ from the current iterate $\mathbf{z}_k$. A one-dimensional search is then accomplished in the direction $\mathbf{d}_k$ to obtain the optimal step size. To apply the procedure, the nonlinear constraints $\mathbf{f}(\mathbf{x},\mathbf{u}) = \mathbf{0}$ are linearized by means of a Taylor series expansion and the related linear optimization problem is resolved to find the solution, i.e. $\mathbf{d}_k$, which minimizes a quadratic objective function subject to linear constraints. According to [Romagnoli and Sánchez, 2000], the QP subproblem is formulated as follows:

$$\begin{aligned} \min_{\mathbf{d}} \ & \frac{1}{2}\mathbf{d}_k^T \mathbf{HL}(\mathbf{z}_k,\lambda_k)\mathbf{d}_k + \nabla\boldsymbol{\Sigma}^T(\mathbf{z}_k)\mathbf{d}_k \\ \text{s.t.} \ & \nabla\mathbf{f}(\mathbf{z}_k)\mathbf{d}_k + \mathbf{f}(\mathbf{z}_k) = \mathbf{0} \end{aligned} \tag{2.35}$$

where $\mathbf{HL}(\mathbf{z}_k,\lambda_k)$ is the Hessian matrix of the Lagrange function formulated for the problem (2.3), $\nabla\boldsymbol{\Sigma}$ and $\nabla\mathbf{f}(\mathbf{z}_k)$ denote the gradients of the objective function and of the constraints, respectively.

Reduced Gradient Method

This technique is based on the resolution of a sequence of optimization subproblems for a reduced set of variables. According to [Romagnoli and Sánchez, 2000], the process constraints are used to solve a set of variables, i.e. $\mathbf{z}_D$, called basic, or dependent, in terms of the others, i.e. $\mathbf{z}_I$, which are known as nonbasic, or independent. By means of these variables, the problem (2.3) is transformed into another one of fewer dimensions:

$$\begin{aligned} \min_{\mathbf{z}_I} \ & \boldsymbol{\Sigma}(\mathbf{z}_I) \\ \text{s.t.} \ & \mathbf{z}_I^L \leq \mathbf{z}_I \leq \mathbf{z}_I^U \end{aligned} \tag{2.36}$$

where $\mathbf{\Sigma}(\mathbf{z}_I)$ denotes the reduced objective function, whereas its reduced gradient is formulated as:

$$\mathbf{\Sigma}_R^T = \left[\frac{\partial \mathbf{\Sigma}_{\mathbf{z}_I}}{\partial \mathbf{z}_I}\right]^T - \left[\frac{\partial \mathbf{\Sigma}_{\mathbf{z}_I}}{\partial \mathbf{z}_D}\right]^T \left[\frac{\partial \mathbf{f}}{\partial \mathbf{z}_D}\right]^{-1} \left[\frac{\partial \mathbf{f}}{\partial \mathbf{z}_I}\right] \tag{2.37}$$

Initially, the search direction, i.e. $\mathbf{d}$, in the space of the independent variables, is determined from the elements of $\mathbf{\Sigma}_R^T$, then the search components for the dependent ones are computed. A one-dimensional search is accomplished to obtain a solution for $\mathbf{z}_I$. The remaining dependent variables of $\mathbf{z}_D$ are evaluated as functions of $\mathbf{z}_I$, by means of the process constraints.

The main disadvantage of these NLP algorithms is the large requirement in terms of computation time, needed to perform the successive linearisation algorithm. Nevertheless, such methods can be applied in a wide range of applications, since they are able to manage nonlinear objective functions, equality and inequality constraints, as well as bounds on variables. The performance of NLP algorithms is better when the problems are well-scaled. Since very often order and magnitude of variables are different, thus a scaling is usually required. Furthermore, if constraints have different magnitudes, they need to be scaled, in order to obtain constraints' residuals of the same magnitude. The accuracy of the solution provided by the NLP software depends on the problem to be solved.

2.3 Dynamic Data Reconciliation

2.3.1 Introduction

In the previous Section the data reconciliation problem was considered for systems assumed to be operating at steady state. As a consequence, only one set of data was supposed to be available. As pointed out in [Romagnoli and Sánchez, 2000], in many practical situations, the occurrence of various disturbances makes the steady-state assumption not verified anymore, since it generates a dynamic or quasi-steady-state response of the process. A continuous monitoring of a process operating under dynamic or quasi-steady-state conditions is needed, to take into account correctly these changes in the operating conditions. If the process is sampled at fixed frequency, then along with the spatial redundancy defined above also the temporal redundancy takes place. As stated in [Romagnoli and Sánchez, 2000], in this case, by applying in two different times, t_1 and t_2, the data reconciliation methods presented in the previous Section, the estimates of the process variables are said to be obtained independently, that is, no previous information is considered in the estimation procedure. This means the past information is discarded, thus the temporal redundancy is ignored. In this Section, the data reconciliation problem for dynamic evolving processes is considered. The temporal redundancy is taken into account by using filtering techniques.

2.3.2 Linear Dynamic System Model

According to [Romagnoli and Sánchez, 2000], a dynamic system can be modeled as follows:

$$\begin{aligned} \dot{\mathbf{x}} &= \mathbf{f}(\mathbf{x}) + \mathbf{w}(t) \\ \mathbf{y} &= \boldsymbol{\phi}(\mathbf{x}) + \boldsymbol{\varepsilon}(t) \end{aligned} \tag{2.38}$$

with initial conditions set as: $\mathbf{x}(0) = \mathbf{x}_0$, and where $\mathbf{f}(\mathbf{x})$ and $\phi(\mathbf{x})$ denote the functions which model the internal and the output dynamic of the system, respectively, $\mathbf{x} \in \mathbb{R}^n$ is the state vector, $\mathbf{y} \in \mathbb{R}^m$ is the measurement vector, and $\mathbf{w} \in \mathbb{R}^n$, $\boldsymbol{\varepsilon} \in \mathbb{R}^m$ are the vector which denote the unknown modeling and observation errors, respectively, both supposed to be Gaussian white noise processes. Hence:

$$\begin{aligned} \mathbf{w}(t) &\approx N[\mathbf{0};\mathbf{Q}(t)] \quad , \quad \mathbf{Q}(t) = \mathbf{Q}^T(t) > \mathbf{0} \\ \boldsymbol{\varepsilon}(t) &\approx N[\mathbf{0};\mathbf{R}(t)] \quad , \quad \mathbf{R}(t) = \mathbf{R}^T(t) > \mathbf{0} \end{aligned} \tag{2.39}$$

where $N[\cdot]$ stands for normal distribution, which parameters in the brackets are the mean and the spectral density, respectively, whereas $\mathbf{Q}(t)$ and $\mathbf{R}(t)$ denote the spectral density matrices of $\mathbf{w}(t)$ and $\boldsymbol{\varepsilon}(t)$, respectively.

For the continuous formulation, the covariance matrices of the model and observation errors are defined as:

$$\begin{aligned} E[\mathbf{w}(t)\mathbf{w}^T(t)] &= \mathbf{Q}(t)\Delta(t-\xi) \\ E[\boldsymbol{\varepsilon}(t)\boldsymbol{\varepsilon}^T(t)] &= \mathbf{R}(t)\Delta(t-\xi) \end{aligned} \tag{2.40}$$

where $E(\cdot)$ is the expectation operator and Δ is the Dirac delta function.

The distinctive aspect of the dynamic case with respect to the static one, is the time evolution of the estimate $\hat{\mathbf{x}}$ and its error covariance matrix $\boldsymbol{\Sigma}$, which can be expressed as follows, according to [Romagnoli and Sánchez, 2000]:

$$\begin{aligned} \dot{\hat{\mathbf{x}}} &= \hat{\mathbf{f}}(\mathbf{x},t) \\ \dot{\boldsymbol{\Sigma}}(t) &= E(\mathbf{x}\mathbf{f}^T) - \hat{\mathbf{x}}\hat{\mathbf{f}}^T + E(\mathbf{f}\mathbf{x}^T) - \hat{\mathbf{f}}\hat{\mathbf{x}}^T + \mathbf{Q}(t) \\ \mathbf{x}(0) &= \mathbf{x}_0 \quad , \quad \boldsymbol{\Sigma}(0) = \boldsymbol{\Sigma}_0 \end{aligned} \tag{2.41}$$

The implementation of practical algorithms for the computation of the estimate $\hat{\mathbf{x}}$ and its error covariance $\boldsymbol{\Sigma}$ requires methods that do not depend on knowing the entire probability density function $p(\mathbf{x},t)$ for $\mathbf{x}(t)$. A method often used consists in the expansion of $\mathbf{f}$ in (2.38) as a Taylor series around a certain point $\hat{\mathbf{x}}$ close to $\mathbf{x}$. Carrying out the first-order expansion on the current estimate of the state vector, the following result arises:

$$\mathbf{f}(\mathbf{x},t) = \mathbf{f}(\hat{\mathbf{x}},t) + \mathbf{A}(\hat{\mathbf{x}},t)(\mathbf{x}-\hat{\mathbf{x}}) + \ldots \tag{2.42}$$

where the generic component of the $\mathbf{A}$ matrix is:

$$A_{ij}(\hat{\mathbf{x}},t) = \left.\frac{\partial f_i(\mathbf{x},t)}{\partial x_j}\right|_{\mathbf{x}(t)=\hat{\mathbf{x}}(t)} \tag{2.43}$$

Following [Romagnoli and Sánchez, 2000], by applying the expectation operation on both sides of (2.42) and substituting the result into the first equation of (2.41) it yields:

$$\dot{\hat{\mathbf{x}}} = \mathbf{f}(\hat{\mathbf{x}},t) \quad , \quad \mathbf{x}(0) = \mathbf{x}_0 \tag{2.44}$$

Substituting (2.44) into the second equation of (2.41), an expression for the differential equation of the estimation error covariance matrix $\boldsymbol{\Sigma}$ is obtained:

$$\begin{aligned} \dot{\boldsymbol{\Sigma}}(t) &= \mathbf{A}(\hat{\mathbf{x}},t)\boldsymbol{\Sigma}(t) + \boldsymbol{\Sigma}(t)\mathbf{A}^T(\hat{\mathbf{x}},t) + \mathbf{Q}(t) \\ \boldsymbol{\Sigma}(\mathbf{0}) &= \boldsymbol{\Sigma}_0 \quad ; \quad \boldsymbol{\Sigma}_0 = \boldsymbol{\Sigma}_0^T > \mathbf{0} \end{aligned} \tag{2.45}$$

According to [Romagnoli and Sánchez, 2000], the two approximate expressions (2.44) and (2.45), which denote the temporal evolving of the estimate and the error covariance, respectively, are referred in the literature to as the Extended Kalman Filter (EKF) propagation equations. In order to implement the algorithm, usually it results more convenient to approximate (2.44) and (2.45) with their corresponding discrete form. Thus, respectively:

$$\mathbf{x}_{k+1} = \mathbf{F}_k \mathbf{x}_k + (\mathbf{w})_k \tag{2.46}$$

where $(\mathbf{w})_k \sim N[\mathbf{0}, \mathbf{Q}_k]$ is now a stochastic sequence, with $\mathbf{Q}_k = \mathbf{Q}(t)\Delta'$. Being $\Delta' = t_{k+1} - t_k$ the time step, and Δ the sampling interval, hence $i = \Delta/\Delta'$ denotes the number of time steps contained in the sampling interval.

$$\mathbf{\Sigma}_{k+1} = \mathbf{F}_k \mathbf{\Sigma}_k \mathbf{F}_k^T + \mathbf{Q}_k \tag{2.47}$$

where $\mathbf{F}_k$ represents the transition matrix related to the system equation (2.44).

As stated in [Romagnoli and Sánchez, 2000], the statistical properties of the random process $\mathbf{x}$, i.e. mean $\hat{\mathbf{x}}$ and covariance $\mathbf{\Sigma}$, can be evaluated in the time interval $t_k < t < t_{k+l}$, but in this process there is an input noise $\mathbf{w}$ which increases the error, damaging the quality of the estimate. If at a time t_{k-1} the updated values of the mean and the estimate error covariance are available, i.e. $\hat{\mathbf{x}}(t_{k-1}|t_{k-1})$ and $\mathbf{\Sigma}(t_{k-1}|t_{k-1})$, where the argument means *at time t_{k-1}, given information up to time t_{k-l}*, these values are then used as initial values to evaluate the temporal evolution of the mean and covariance in the time interval $t_{k-1} < t < t_k$, by means of the model equations (2.44), (2.45). According to [Romagnoli and Sánchez, 2000], once the predicted values are computed, i.e. $\hat{\mathbf{x}}_{k/k-1}$ and $\mathbf{\Sigma}_{k/k-1}$, then the minimum variance estimate of the state vector, i.e. $\hat{\mathbf{x}}_k$, can be obtained as the solution of the following minimization problem:

$$\min \; J = \mathbf{a}_k^T \mathbf{\Sigma}_{k/k-1}^{-1} \mathbf{a}_k + \boldsymbol{\varepsilon}_k^T \mathbf{R}_k^{-1} \boldsymbol{\varepsilon}_k \tag{2.48}$$

where $\mathbf{a}_k = \mathbf{x}_k - \hat{\mathbf{x}}_{k/k-1}$ and $\boldsymbol{\varepsilon}_k = \mathbf{y}_k - \mathbf{C}\mathbf{x}_k$ denote the objective functions related to the modeling prediction errors and the observation errors, respectively.

According to [Romagnoli and Sánchez, 2000], the solution of the minimization problem (2.48) is given by the formula:

$$\hat{\mathbf{x}}_k = \mathbf{\Sigma}_k [\mathbf{\Sigma}_{k/k-1}^{-1} \hat{\mathbf{x}}_{k/k-1} + \mathbf{C}^T \mathbf{R}_k^{-1} \mathbf{y}_k] \tag{2.49}$$

where:

$$\mathbf{\Sigma}_k = [\mathbf{\Sigma}_{k/k-1}^{-1} + \mathbf{C}^T \mathbf{R}_k^{-1} \mathbf{C}]^{-1} \tag{2.50}$$

As pointed out in [Romagnoli and Sánchez, 2000], since $\mathbf{\Sigma}$ is a positive definite symmetric matrix, its trace can be taken as a measure of the estimate error covariance. Furthermore, it should be noted that the solution of the minimization problem, i.e. the recursive equations (2.49) and (2.50), simplifies to the updating step of a Kalman Filter (KF).

2.3.3 Quasi-Steady-State System Model

In this Section, the data reconciliation analysis is referred to systems operating at Quasi-Steady-State (QSS) conditions, which reflect those situations where the dominant time constant of the systems' dynamic response is much smaller than the period with which disturbances affect the system. The disturbances able to induce such kind of behavior in the

operating conditions of the process, may refer to slow variations in the heat transfer coefficients, catalytic activity in reactors, etc..., or the source of a disturbance may be a sudden but lasting change. Therefore, a process can be considered as operating in QSS conditions, when it exhibits slow, or occasionally sharp, transitions between steady states. According to [Stanley and Mah, 1977], the model for such kinds of processes can be expressed as follows:

- a set of n transition equations:

$$\mathbf{x}_{k+1} = \mathbf{I}\mathbf{x}_k + \mathbf{n}_k \quad ; \quad k = 0, 1, \ldots \tag{2.51}$$

  where $\mathbf{x}_k$ and $\mathbf{n}_k$ are the state vector and the process noise vector at time t_k, respectively;

- a set of l measurement equations:

$$\mathbf{y}_k = \mathbf{C}\mathbf{x}_k + \boldsymbol{\varepsilon}_k \quad ; \quad k = 0, 1, \ldots \tag{2.52}$$

  where $\mathbf{y}_k$ and $\boldsymbol{\varepsilon}_k$ are the output vector and the measurement error vector at time t_k, respectively;

- a set of m steady-state algebraic balance equations:

$$\mathbf{A}_k\mathbf{x}_k + \mathbf{w}_k = \mathbf{0} \quad ; \quad k = 0, 1, \ldots \tag{2.53}$$

  where $\mathbf{A}_k$ and $\mathbf{w}_k$ are the matrix related to the linear approximation of the model, and the modeling error vector at time t_k, respectively.

As in the static case, the state and all the error vectors in the model are supposed to be uncorrelated and normally distributed random variables, with known covariance matrix, that is:

$$\begin{aligned} \mathbf{x}_k &\sim N[\bar{\mathbf{x}}_0, \boldsymbol{\Sigma}_0] \\ \mathbf{n}_k &\sim N[0, \mathbf{S}] \\ \boldsymbol{\varepsilon}_k &\sim N[0, \mathbf{R}] \\ \mathbf{w}_k &\sim N[0, \mathbf{Q}] \end{aligned} \tag{2.54}$$

If the predicted values are available at time t_k, by following the same reasoning explained in Section 2.3, the minimum variance estimate of the state vector, i.e. $\hat{\mathbf{x}}_k$, is obtained as the solution of the following minimization problem:

$$\min \; J = \mathbf{a}_k^T \boldsymbol{\Sigma}_{k/k-1}^{-1} \mathbf{a}_k + \boldsymbol{\varepsilon}_k^T \mathbf{R}_k^{-1} \boldsymbol{\varepsilon}_k + \mathbf{w}_k^T \mathbf{Q}_k^{-1} \mathbf{w}_k \tag{2.55}$$

where $\mathbf{a}_k = \mathbf{x}_k - \hat{\mathbf{x}}_{k/k-1}$, $\boldsymbol{\varepsilon}_k = \mathbf{y}_k - \mathbf{C}\mathbf{x}_k$ and $\mathbf{w}_k = -\mathbf{A}\mathbf{x}_k$ denote the objective functions related to the prediction errors, the observation errors, and the modeling errors, respectively. As in Section 2.3, the solution of the minimization problem is given by the formula (2.49), where in this case the estimate of the error covariance is computed as:

$$\boldsymbol{\Sigma}_k = [\boldsymbol{\Sigma}_{k/k-1}^{-1} + \mathbf{C}^T \mathbf{R}_k^{-1} \mathbf{C} + \mathbf{A}^T \mathbf{Q}_k^{-1} \mathbf{A}]^{-1} \tag{2.56}$$

The values of $\hat{\mathbf{x}}_k$ and $\boldsymbol{\Sigma}_k$ computed by means of the equations (2.49) and (2.56), respectively, are used as initial values to evaluate the temporal evolution of the mean and covariance in the time interval $t_k < t < t_{k+1}$, that is:

$$\hat{\mathbf{x}}_{k+1/k} = \hat{\mathbf{x}}_k \tag{2.57}$$

$$\boldsymbol{\Sigma}_{k+1/k} = [\boldsymbol{\Sigma}_k + \mathbf{Q}_k] \tag{2.58}$$

According to [Romagnoli and Sánchez, 2000], the initial values for the recursive computations are assumed to be available, and given by $\hat{\mathbf{x}}_0 = \overline{\mathbf{x}}_0$ and $\boldsymbol{\Sigma}_0 = \boldsymbol{\Sigma}(0)$. As in Section 2.3, the solution of the minimization problem again simplifies to the updating steps of a static Kalman filter. As pointed out in [Romagnoli and Sánchez, 2000], for the linear case, matrices $\mathbf{A}$ and $\mathbf{C}$ do not depend on $\mathbf{x}$, thus the covariance matrix of errors can be computed in advance, without having actual measurements. Instead, when the problem is nonlinear, these matrices depend on the last available estimate of the state vector, and the Extended Kalman Filter (EKF) takes place.

2.4 Joint Data Reconciliation Parameter Estimation

2.4.1 Introduction

A problem associated with the data reconciliation is the estimation of various model parameters. Indeed, data reconciliation and gross error detection algorithms make use of plant models, which might have totally unknown parameters, or parameters subject to changing during the plant operation. Most of these parameters, such as heat transfer coefficients, fouling factors, distillation column tray efficiencies, compressor efficiencies, etc..., are fixed values for the process optimization; therefore, a high accuracy in their estimated values is required.

One approach to the parameter estimation problem is to solve it simultaneously with the reconciliation problem. The model parameters can be treated as regular unmeasured variables, or as tuning parameters, which are adjusted in NLP-type algorithms to match the plant measurements. The major problem with this approach is that in the presence of gross errors, the parameters may be adjusted to wrong values, or some measurements can wrongly be declared in gross error, because of errors in model parameters. To obtain an accurate solution for both measured variables and model parameters, an iterative process is usually required, which is time consuming, especially with rigorous models. An alternative approach is to separate and sequentially solve the two problems. First, data reconciliation and gross error detection is performed using only overall material and energy balances. The model parameters are then estimated using the reconciled values. This is similar to projecting out the unmeasured model parameters from the reconciliation problem, along with their associated model equations. The parameter estimates obtained using the sequential approach are identical to those obtained using the simultaneous approach, if there are no a priori estimates of the parameters available. Moreover, the parameter estimates obtained using the sequential approach may not always satisfy bounds on parameter values. An iterative procedure may be used to eliminate such problems. This approach was applied to parameter estimation problems in connection with advanced process control applications. The computational time is a serious constraint for such applications, and usually only one iteration is applied.

The parameter estimation is also an important aspect of activities such as process design, evaluation, and control. Since, usually, the data acquired from the field do not satisfy the process constraints, Error-In-Variable (EIV) methods typically are used to obtain both parameter and reconciled data estimates which are consistent with the model. Such approaches represent a special class of optimization problem, because the structure of least squares is

exploited in the development of the optimization procedure. A review of this subject can be found in [Biegler et al., 1986].

This Section discusses the joint parameter estimation and data reconciliation problem. First, the typical parameter estimation problem, in which the independent variables are error-free, is analyzed. The main aspects related to the processing of the information are considered. Later, the more general formulation in terms of the error-in-variable method, where measurement errors in all variables are considered in the parameter estimation problem, is examined.

As stated in [Romagnoli and Sánchez, 2000], the nature of a parameter estimation problem depends on the mathematical model used to match the experimental data. Indeed, a model contains both state variables, e.g.: concentrations, temperatures, pressures, etc..., and parameters, e.g.: rate constants, dispersion coefficients, activation energies, etc.... Furthermore, the state variables can be decomposed into two different groups: independent and dependent variables. Thus, the following vectors of variables and parameters can be defined:

- $\boldsymbol{\theta} = [\theta_1, \ldots, \theta_g]^T$: vector of parameters whose numerical values are unknown
- $\mathbf{x} = [x_1, \ldots, x_n]^T$: vector of state variables
- $\mathbf{y} = [y_1, \ldots, y_p]^T$: vector of observed variables, which are the actually measured process variables.

This decomposition leads to two different problems. According to the definitions given in [Romagnoli and Sánchez, 2000], a single experiment consists of the measurement of each of the n observed variables for a given set of all the state variables, i.e. dependent and independent variables. If all the independent state variables are error-free, only errors in the dependent variables $\mathbf{y}$ need to be minimized. Therefore, in this case, the model result to be explicit, since the vector of observed variables $\mathbf{y}$ can be expressed as an explicit function of the state $\mathbf{x}$ and the parameters $\boldsymbol{\theta}$, as follows:

$$\mathbf{y} = \mathbf{f}(\mathbf{x}, \boldsymbol{\theta}) \tag{2.59}$$

where $\mathbf{f} \in \mathbb{R}^p$ is a vector which contains a set of p functions of known form.

Since in this case g parameters need to be estimated, thus at least g observations must be performed. By assuming that M different experiments are done, then each individual experiment provides a different set of values, that is:

$$\mathbf{y}_j = \mathbf{f}(\mathbf{x}_j, \boldsymbol{\theta}) \quad , \quad j = 1, \ldots, M \tag{2.60}$$

It is worth to notice that this approach is quite general, since also those applications where the states and parameters are related by ordinary differential equations can be taken into account, by referring to the following formulation:

$$\frac{dx_i}{dt} = f_i(t, \mathbf{x}(t), \boldsymbol{\theta}) \quad , \quad x_i(0) = x_{i_0} \quad , \quad i = 1, \ldots, n \tag{2.61}$$

The simplest case of this parameter estimation problem results when all state variables $x_i(t)$ and their derivatives its $\dot{x}_i(t)$ are measured directly, since the estimation task involves only n algebraic equations. On the other hand, if the derivatives are not available by direct measurement, the integrated forms need to be used, which again yield a system of algebraic equations. When some of the independent state variables are subject to errors instead, the model results to be implicit, and the distinction between independent and dependent variables is no longer clear. In this case, errors for all variables need to be minimized.

2.4.2 Sequential Processing

In the sequential processing approach to parameter estimation, an initial estimate of $\boldsymbol{\theta} \in \mathbb{R}^g$ is obtained from a minimal data set, in which the number of observations is equal to the number of components of $\boldsymbol{\theta}$, that is:

$$\mathbf{y}_0 = \begin{bmatrix} y_{10} \\ \vdots \\ y_{g0} \end{bmatrix} \tag{2.62}$$

Hence, the initial estimate, i.e. $\hat{\boldsymbol{\theta}}_0$, can be computed from the model of the system, that is:

$$\mathbf{f}_0(\hat{\boldsymbol{\theta}}_0) = \begin{bmatrix} f_{10}(\boldsymbol{\theta}) \\ \vdots \\ f_{g0}(\boldsymbol{\theta}) \end{bmatrix} + \boldsymbol{\varepsilon}_0 = \mathbf{y}_0 \tag{2.63}$$

where each element of $\mathbf{f}_0$ denotes the prediction of an observed variable at time $t = t_0$, and $\boldsymbol{\varepsilon}_0$ is the measurement error related to the minimal data set $\mathbf{y}_0$. In order to obtain the covariance matrix of the initial estimate error, the same approach discussed in paragraph 2.3.2 can be applied. Thus, the prediction function $\mathbf{f}_0(\hat{\boldsymbol{\theta}}_0)$ can be expanded as a Taylor series around the true value of the parameter set, i.e. $\boldsymbol{\theta}$. Hence, by retaining only the constant and linear terms:

$$\mathbf{f}_0(\hat{\boldsymbol{\theta}}_0) = \mathbf{f}_0(\boldsymbol{\theta}) + \mathbf{D}_0(\boldsymbol{\theta})(\hat{\boldsymbol{\theta}}_0 - \boldsymbol{\theta}) \tag{2.64}$$

where:

$$\mathbf{D}_0(\boldsymbol{\theta}) = \nabla \mathbf{f}_0(\boldsymbol{\theta}) \tag{2.65}$$

By defining $\boldsymbol{\Delta}_0 = (\hat{\boldsymbol{\theta}}_0 - \boldsymbol{\theta})$, (2.64) can be written also as:

$$\mathbf{D}_0(\boldsymbol{\theta})\boldsymbol{\Delta}_0 = \mathbf{f}_0(\hat{\boldsymbol{\theta}}_0) - \mathbf{f}_0(\boldsymbol{\theta}) = \boldsymbol{\varepsilon}_0 \tag{2.66}$$

Hence, the covariance matrix of the initial measurement error $\boldsymbol{\varepsilon}_0$ can be expressed as:

$$\boldsymbol{\Psi} = E[\boldsymbol{\varepsilon}_0 \boldsymbol{\varepsilon}_0^T] = E[\mathbf{D}_0(\boldsymbol{\theta})\boldsymbol{\Delta}_0 \boldsymbol{\Delta}_0^T \mathbf{D}_0^T(\boldsymbol{\theta})] \tag{2.67}$$

By defining the covariance matrix of the parameter estimation error as: $\boldsymbol{\Sigma}_0 = E[\boldsymbol{\Delta}_0 \boldsymbol{\Delta}_0^T]$, the covariance matrix of the initial estimate can be expressed as a function of the known covariance matrix of the measurement errors, as follows:

$$\boldsymbol{\Sigma}_0 = [\mathbf{D}_0^T(\boldsymbol{\theta})\boldsymbol{\Psi}^{-1}\mathbf{D}_0(\boldsymbol{\theta})]^{-1} \tag{2.68}$$

At the subsequent time $t = t_l$, following the initial estimation, a new observation $\mathbf{y}_1$ can be computed. At this point, the objective function to be minimized can be written, by combining the new data with the previous estimate, according to [Romagnoli and Sánchez, 2000]:

$$\begin{aligned} J(\boldsymbol{\theta}/\boldsymbol{\theta}_0, \boldsymbol{\varepsilon}_1) &= \boldsymbol{\theta}_0^T \boldsymbol{\Sigma}_0^{-1} \boldsymbol{\theta}_0 + \boldsymbol{\varepsilon}_1^T \boldsymbol{\Psi}^{-1} \boldsymbol{\varepsilon}_1 = \\ &= (\hat{\boldsymbol{\theta}}_0 - \boldsymbol{\theta})^T \boldsymbol{\Sigma}_0^{-1} (\hat{\boldsymbol{\theta}}_0 - \boldsymbol{\theta}) + [\mathbf{y}_1 - \mathbf{f}_1(\boldsymbol{\theta})]^T \boldsymbol{\Psi}^{-1} [\mathbf{y}_1 - \mathbf{f}_1(\boldsymbol{\theta})] \end{aligned} \tag{2.69}$$

where $\mathbf{f}_1(\boldsymbol{\theta})$ denotes the predicted value of the observation $\mathbf{y}_1$ at time $t = t_1$ based on the value of the system parameters.

According to [Romagnoli and Sánchez, 2000], the new covariance matrix of the error estimate when the measurement at time $t = t_1$ is processed as a function of the previous one, can be expressed as:

$$\begin{aligned} \boldsymbol{\Sigma}_1 &= [\boldsymbol{\Sigma}_0^{-1} + \mathbf{D}_1^T(\boldsymbol{\theta})\boldsymbol{\Psi}^{-1}\mathbf{D}_1(\boldsymbol{\theta})]^{-1} \\ \Rightarrow \quad \boldsymbol{\Sigma}_1^{-1} &= \boldsymbol{\Sigma}_0^{-1} + \mathbf{D}_1^T(\boldsymbol{\theta})\boldsymbol{\Psi}^{-1}\mathbf{D}_1(\boldsymbol{\theta}) \end{aligned} \tag{2.70}$$

The process can be iterated at each step by introducing or deleting new observations. By induction, according to [Romagnoli and Sánchez, 2000], the covariance matrix for the error estimate at the $k-$th step can be written as:

$$\begin{aligned} \boldsymbol{\Sigma}_{k+1} &= [\boldsymbol{\Sigma}_k^{-1} + \mathbf{D}_{k+1}^T(\boldsymbol{\theta})\boldsymbol{\Psi}^{-1}\mathbf{D}_{k+1}(\boldsymbol{\theta})]^{-1} \\ \Rightarrow \quad \boldsymbol{\Sigma}_{k+1}^{-1} &= \boldsymbol{\Sigma}_k^{-1} + \mathbf{D}_{k+1}^T(\boldsymbol{\theta})\boldsymbol{\Psi}^{-1}\mathbf{D}_{k+1}(\boldsymbol{\theta}) \end{aligned} \tag{2.71}$$

where the positive signs stand for the addition of information.

As mentioned in [Romagnoli and Sánchez, 2000], this procedure can be extended in general to different kinds of variables also, other than time, such as temperature, pressure, or some other qualitative variable such as the type of catalyst. In this way a whole range of operating conditions can be covered, by processing the information at each stage in a sequential manner, using the information available from previous calculations.

2.4.3 Error-in-Variable Methods

In the EVM, the measurement errors in all variables are taken into account in the parameter estimation. EVM provides consistent estimates with respect to the model of both parameters and reconciled data. Often, the regression models result to be implicit and undetermined, that is:

$$\mathbf{f}(\mathbf{x}, \mathbf{y}, \boldsymbol{\theta}) = \mathbf{0} \tag{2.72}$$

where $\mathbf{x}$ and $\mathbf{y}$ denote the independent and dependent variables, respectively, whereas $\boldsymbol{\theta}$ denotes the parameter set.

As stated in [Tjoa and Biegler, 1992], the estimation problem is often referred to as parameter estimation with implicit models or Orthogonal Distance Regression (ODR). Therefore, such an approach consist in the minimization of a suitably weighted least squares function, which includes both independent and dependent variables.

By defining the vector containing both independent and dependent variables as:

$$\mathbf{z} = \begin{bmatrix} \mathbf{y} \\ \mathbf{x} \end{bmatrix} \tag{2.73}$$

an implicit model including m equations, denoted by the vector $\mathbf{f} = [f_1, \ldots, f_m]^T$, n process variables, denoted by the vector $\mathbf{z} = [z_1, \ldots, z_n]^T$, and g parameters, denoted by the vector $\boldsymbol{\theta} = [\theta_1, \ldots, \theta_g]^T$, can be described as follows:

$$\mathbf{f}(\mathbf{z}, \boldsymbol{\theta}) = \mathbf{0} \tag{2.74}$$

In the experiments, the observed measurements of all values, denoted by the vector $\tilde{\mathbf{z}}$, can all be affected by errors, that is:

$$\tilde{\mathbf{z}}_j = \mathbf{z}_j + \boldsymbol{\varepsilon}_j \quad , \quad j = 1, \ldots, M \tag{2.75}$$

where M denotes the number of experiments.

Following [Romagnoli and Sánchez, 2000], assuming that the measurement errors $\boldsymbol{\varepsilon}_j$ are normally distributed and uncorrelated, with zero mean and known positive definite covariance matrix $\boldsymbol{\Psi}_j$, the parameter estimation problem can be formulated as a minimization problem with respect to $\hat{\mathbf{z}}_j$ and $\hat{\boldsymbol{\theta}}$, as follows:

$$\begin{aligned} \min_{\mathbf{z}_j, \boldsymbol{\theta}} \quad & \sum_{j=1}^{M} (\tilde{\mathbf{z}}_j - \mathbf{z}_j)^T \boldsymbol{\Psi}_j^{-1} (\tilde{\mathbf{z}}_j - \mathbf{z}_j) \\ \text{s.t.} \quad & \mathbf{f}(\mathbf{z}_j, \boldsymbol{\theta}) = \mathbf{0} \quad , \quad j = 1, \ldots, M \end{aligned} \tag{2.76}$$

As mentioned in [Romagnoli and Sánchez, 2000], several alternative algorithms have been proposed in the literature to solve efficiently the optimization problem (2.76), related to the application of EVM. The main approaches can be distinguished as:

- Simultaneous solution methods
- Nested EVM
- Two-stage EVM

Simultaneous Solution

As stated in [Romagnoli and Sánchez, 2000], the most straightforward approach to solve nonlinear EVM problems is to apply nonlinear programming techniques to make a simultaneous estimation of both $\mathbf{z}_j$ and $\boldsymbol{\theta}$. In the standard formulation of the weighted least squares parameter estimation there are only g optimization variables, which correspond to the number of unknown parameters. Instead, the simultaneous parameter estimation and data reconciliation formulation provides $(nM + g)$ optimization variables. As a consequence, since the dimensionality of the problem directly increases with the number of data sets, it can become large. A *feasible path* optimization approach can be very expensive to solve such a NLP problem, since an iterative calculation is required to solve the undetermined model. A more efficient way is to use an *infeasible path* approach. However, many of these large-scale NLP methods are efficient only in solving problems with few degrees of freedom. A decoupled SQP method, based on a globally convergent SQP algorithm, was proposed by [Tjoa and Biegler, 1992].

Nested EVM

In this approach, proposed by [Kim et al., 1990] following ideas similar to those of [Reilly and Patino-Lea1, 1981], the two problems of parameter estimation and data reconciliation are decoupled; however, the latter is optimized at each iteration of the parameter estimation. The algorithm is made by the following two steps:

- **Step 1**: If $k = 1$, set $\hat{\mathbf{z}} = \tilde{\mathbf{z}}$, $\hat{\boldsymbol{\theta}} = \boldsymbol{\theta}_0$, then go to Step 2

- **Step 2**: Find the minimum of the function for Solve the two nested minimization problems:

$$\begin{aligned} J_1 = \min_{\boldsymbol{\theta}} \quad & \sum_{j=1}^{M} (\tilde{\mathbf{z}}_j - \mathbf{z}_j)^T \boldsymbol{\Psi}_j^{-1} (\tilde{\mathbf{z}}_j - \mathbf{z}_j) \\ \text{s.t.} \quad J_2 = \min_{\hat{\mathbf{z}}_j} \quad & \sum_{j=1}^{M} (\tilde{\mathbf{z}}_j - \mathbf{z}_j)^T \boldsymbol{\Psi}_j^{-1} (\tilde{\mathbf{z}}_j - \mathbf{z}_j) \\ \text{s.t.} \quad & \mathbf{f}(\mathbf{z}_j, \boldsymbol{\theta}) = \mathbf{0} \quad , \quad j = 1, \ldots, M \end{aligned} \tag{2.77}$$

As pointed out by [Kim et al., 1990], the difference between this algorithm and the proposal of [Reilly and Patino-Lea1, 1981], is that the successive linearization solution is replaced with a nonlinear programming problem. The nested NLP is solved as a set of decoupled NLPs, and the size of the largest optimization problem to be solved is reduced to the order of n.

Two-Stage EVM

The two-stage algorithm follows the work of [Valko and Vajda, 1987], which basically decouples the two problems. Starting from the definition of the general EVM problem in (2.76), the vectors $\mathbf{z}_1, \ldots, \mathbf{z}_M$ minimize the constrained problem at fixed $\boldsymbol{\theta}$, if and only if each $\mathbf{z}_j$, $j = 1, \ldots, M$, is the solution of the following problem:

$$\begin{aligned} \min \quad & J(\mathbf{z}) = (\tilde{\mathbf{z}} - \mathbf{z})^T \boldsymbol{\Psi}^{-1} (\tilde{\mathbf{z}} - \mathbf{z}) \\ \text{s.t.} \quad & \mathbf{f}(\mathbf{z}, \boldsymbol{\theta}) = \mathbf{0} \end{aligned} \tag{2.78}$$

where the index j is dropped, since the problem (2.78) is solved separately for each $j = 1, \ldots, M$.

By linearizing the constraints in (2.78) around some estimate $\hat{\mathbf{z}}$, the estimation error can be defined in terms of the following linear approximation:

$$\mathbf{e} = \mathbf{f}(\hat{\mathbf{z}}, \boldsymbol{\theta}) + \mathbf{N}(\hat{\mathbf{z}}, \boldsymbol{\theta})(\tilde{\mathbf{z}} - \hat{\mathbf{z}}) = \mathbf{0} \tag{2.79}$$

where $\mathbf{N}$ denotes the Jacobian matrix of $\mathbf{f}$ with respect to the variables $\mathbf{z}$. Thus, by keeping $\hat{\mathbf{z}}$ fixed, and setting $\mathbf{d} = (\tilde{\mathbf{z}} - \mathbf{z})$, in place of the generic nonlinear problem (2.78) it can be solved the following linearized problem:

$$\begin{aligned} \min \quad & \mathbf{d}^T \boldsymbol{\Psi}^{-1} \mathbf{d} \\ \text{s.t.} \quad & -\mathbf{N}(\hat{\mathbf{z}}, \boldsymbol{\theta})\mathbf{d} + \mathbf{f}(\tilde{\mathbf{z}}, \boldsymbol{\theta}) + \mathbf{N}(\hat{\mathbf{z}}, \boldsymbol{\theta})(\tilde{\mathbf{z}} - \hat{\mathbf{z}}) \end{aligned} \tag{2.80}$$

whose solution, according to [Romagnoli and Sánchez, 2000] is:

$$\hat{\mathbf{d}} = \boldsymbol{\Psi}\mathbf{N}^T (\mathbf{N}\boldsymbol{\Psi}\mathbf{N}^T)^{-1} [\mathbf{f} + \mathbf{N}(\tilde{\mathbf{z}} - \hat{\mathbf{z}})] \tag{2.81}$$

The problem can be solved using the successive linearization technique presented in Section 2.2.3, until the convergence is achieved. The fixed point in the iteration, i.e. $\hat{\mathbf{z}}$, is the solution of (2.78). Thus, by putting the equation (2.81) into (2.80), the corresponding objective function J can be expressed as follows:

$$J(\hat{\mathbf{z}}) = [\mathbf{f} + \mathbf{N}(\tilde{\mathbf{z}} - \hat{\mathbf{z}})]^T (\mathbf{N}\boldsymbol{\Psi}\mathbf{N}^T)^{-1} [\mathbf{f} + \mathbf{N}(\tilde{\mathbf{z}} - \hat{\mathbf{z}})] \tag{2.82}$$

The equation (2.82) contains explicit information about the effect of the parameters on the objective function of (2.78). This fact has been exploited in the following procedure:

- **Step 1**: If $k = 1$, set $\hat{\mathbf{z}}_{j_k} = \tilde{\mathbf{z}}_j \ \ \forall j = 1, \ldots, M$, then go to Step 2
- **Step 2**: Find the minimum $\boldsymbol{\theta}_{k+1}$ of the function:

$$J(\boldsymbol{\theta}) = \sum_{j=1}^{M} [\mathbf{f}_j + \mathbf{N}_j(\tilde{\mathbf{z}}_j - \hat{\mathbf{z}}_{j_k})]^T (\mathbf{N}_j \boldsymbol{\Psi} \mathbf{N}_j^T)^{-1} [\mathbf{f}_j + \mathbf{N}_j(\tilde{\mathbf{z}}_j - \hat{\mathbf{z}}_{j_k})] \tag{2.83}$$

  where $\mathbf{f}_j = \mathbf{f}(\mathbf{z}_j, \boldsymbol{\theta})$ and $\mathbf{N}_j = \frac{\partial \mathbf{f}(\mathbf{z}_j, \boldsymbol{\theta})}{\partial \mathbf{z}_j}|_{\mathbf{z}_j = \hat{\mathbf{z}}_{j_k}}$. If $k > 1$ and $\|\boldsymbol{\theta}_k - \boldsymbol{\theta}_{k+1}\| \leq T_b$, then finish; otherwise go to Step 3.

- **Step 3**: At fixed $\boldsymbol{\theta}_{k+1}$, perform the data reconciliation for each $j = 1, \ldots, M$ by applying the successive linearizations procedure:

$$\hat{\mathbf{z}}_j^{new} = \hat{\mathbf{z}}_j - \boldsymbol{\Psi} \mathbf{N}_j^T (\mathbf{N}_j \boldsymbol{\Psi} \mathbf{N}_j^T)^{-1} [\mathbf{f}_j + \mathbf{N}_j(\tilde{\mathbf{z}}_j - \hat{\mathbf{z}}_j)] \tag{2.84}$$

  Compute (2.84) until the convergence is achieved, then set $\hat{\mathbf{z}}_{j_k} = \hat{\mathbf{z}}_j^{new}$, $k = k + 1$ and return to Step 2.

As stated in [Romagnoli and Sánchez, 2000], by means of this algorithm, the entire procedure can be easily implemented, since existing programs can be putted together, such as the successive linearizations step, which can be implemented by the already available data reconciliation strategy. An alternative formulation was proposed by [Kim et al., 1990], where the successive linearization approach in Step 3 is replaced with a nonlinear programming problem.

2.5 Conclusion

This Chapter has provided a general overview of the second subject of this dissertation, which refers to the data reconciliation and parameter estimation methodologies for industrial process monitoring applications. Since data reconciliation and parameter estimation together aim to validate the process measurements acquired by sensors, they are both directly related to the fault diagnosis topic. The main concepts and definitions of the DR technology have been introduced and discussed at first. Thus, the main linear and nonlinear steady-state techniques have been briefly reviewed, as well as the two fundamental methods which implement a DDR approach, including the QSS system model, exploited in this research. Then, the parameter estimation problem has been considered along with the data reconciliation task. Thus, the main joint data reconciliation and parameter estimation approaches, which are currently applied in many of the methods available in the literature, have been examined.

Part II

Author's Contributions

Chapter 3

Hybrid Fault Detection and Diagnosis

3.1 Hybrid FDD Architecture

When faults which could affect both the q inputs and p outputs measurements of a generic MIMO system cannot be separated in frequency, conventional MB approaches can only perform at most the detection of the fault occurrence. However, although these techniques are able to provide some estimation of the fault symptoms, they do not allow in general to discriminate among every fault. This follows from the fact that MB algorithms may generate a number of residuals that is equal to the number of the system outputs. Consequently, only p independent faults can be isolated simultaneously [Pilloni et al., 2013]. Note that, if more than p faults occur, the residuals produced by a MB residual generator, e.g. a SMO [Pilloni et al., 2012] or a properly designed KF [Simani et al., 2010], still carry information about the whole set of faults. However, those information could be extracted if an augmented residual space is designed and its temporal dimension is exploited. In this Chapter a novel hybrid FDD approach able to achieve a complete fault isolation and diagnosis is presented. The architecture of the proposed scheme is depicted in figure 3.1, and the main modules of this FDD scheme are described in detail in the following Sections. The residual generation is achieved by taking advantage of the sliding mode tool presented in Section 3.2, whereas, the residual evaluation task, which is discussed in Section 3.3, is performed by extending the residual signature concept towards a time-varying setting over a suitably designed augmented residual space. Then, in the Section 3.3.4, different strategies, which are still under development for the analysis of residuals, are briefly introduced.

3.2 Fault Detection by Residual Generation

In order to generate residuals which are able to deal with both sensor and actuator faults, and at the same time which are robust enough towards uncertainties, the SMO design approach proposed by [Yan and Edwards, 2007] was exploited. The scheme of this robust residual generator is shown in figure 3.2, and a detailed description of it is given in the following of this Section.

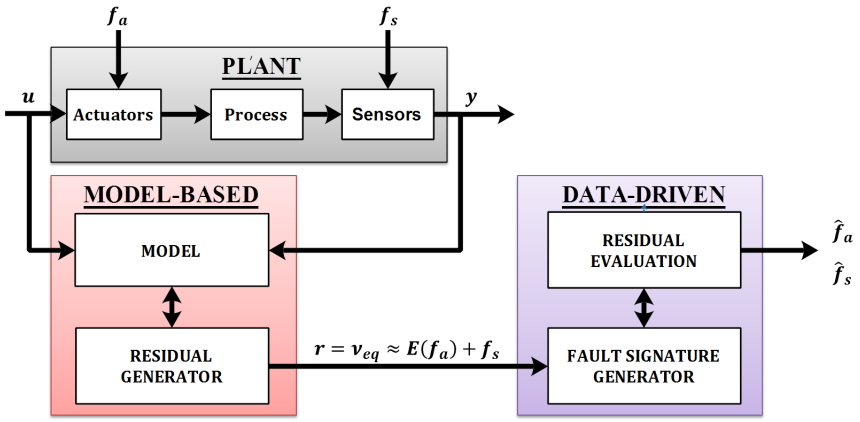

Figure 3.1: Hybrid FDD Architecture scheme

3.2.1 Robust Residual Generation by SMO

Let consider the following model for a generic nonlinear faulty system:

$$\begin{aligned} \dot{\boldsymbol{x}} &= G(\boldsymbol{x},\boldsymbol{u}) + \Delta G(\boldsymbol{x}) \\ \boldsymbol{y} &= h(\boldsymbol{x}) + \boldsymbol{f}_s \end{aligned} \tag{3.1}$$

where $\boldsymbol{x} \in \Omega \subset \mathbb{R}^n$ is the state vector, $\boldsymbol{u} \in \mathbb{R}^m$ is the input vector, $\boldsymbol{y} \in \mathbb{R}^p$ is the output vector, whereas the vector pair $\{G(\boldsymbol{x},\boldsymbol{u}), h(\boldsymbol{x})\}$ depicts the nominal system's dynamic, supposed to be smooth and bounded around a neighborhood Ω of the system working point. All the uncertainties and disturbances, as well as faults affecting the actuators, are taken into account by the vector $\Delta G(\boldsymbol{x})$, while $\boldsymbol{f}_s$ is the vector of faults, supposed to be bounded, which directly affect the output sensors, and that is:

$$\|\boldsymbol{f}_s(t)\| \leq \rho(t) \tag{3.2}$$

where $\rho(t)$ is an known continuous function and $\|\cdot\|$ is the Euclidean norm operator.

According to definitions given in [Yan and Edwards, 2007], if the nominal system denoted by the pair $\{G(\boldsymbol{x},\boldsymbol{u}), h(\boldsymbol{x})\}$ is uniformly observable with uniform observability index the set of nonnegative integer scalars $\{r_1, r_2, \cdots, r_p\}$ such that $\sum_{i=1}^{p} r_i = n$, then a diffeomorphism in the domain Ω, that is $T(\Omega) : \boldsymbol{x} \mapsto \boldsymbol{z}$ can be designed as follows:

$$\begin{aligned} \boldsymbol{z}_{i1} &= h_i(\boldsymbol{x}) \\ \boldsymbol{z}_{i2} &= L_{G(\boldsymbol{x},\boldsymbol{u})} h_i(\boldsymbol{x}) \\ &\vdots \\ \boldsymbol{z}_{i_{r_i}} &= L^{r_i-1}_{G(\boldsymbol{x},\boldsymbol{u})} h_i(\boldsymbol{x}). \end{aligned} \tag{3.3}$$

where $L^{j}_{G(\boldsymbol{x},\boldsymbol{u})} h_i(\boldsymbol{x}) = \frac{\partial^j h_i(\boldsymbol{x})}{\partial \boldsymbol{x}^j} G(\boldsymbol{x},\boldsymbol{u})$ is the j-th order Lie derivative of the i-th output of the system $h_i(\boldsymbol{x})$ along the vector field $G(\boldsymbol{x},\boldsymbol{u})$, and $\boldsymbol{z}_i = (\boldsymbol{z}_{i_1}, \boldsymbol{z}_{i_2}, \cdots, \boldsymbol{z}_{i_{r_i}})$ for indices $i = 1, \cdots, p$, $j = 1, \cdots, r_i - 1$, whereas $\boldsymbol{z} = (\boldsymbol{z}_1, \boldsymbol{z}_2, \cdots, \boldsymbol{z}_p)$.

In accordance with [Yan and Edwards, 2007], in the new coordinates $\boldsymbol{z}$ defined by the transformation (3.3), the dynamics of the system (3.1) can be expressed in its corresponding

Brunovsky canonical representation, that is:

$$\begin{cases} \dot{\boldsymbol{z}} = \boldsymbol{\mathcal{A}}\boldsymbol{z} + \boldsymbol{\mathcal{B}}\Phi(\boldsymbol{z},\boldsymbol{u}) + \Psi(\boldsymbol{z}) \\ \boldsymbol{y} = \boldsymbol{\mathcal{C}}\boldsymbol{z} + \boldsymbol{f}_s \end{cases} \tag{3.4}$$

where $\boldsymbol{\mathcal{A}} = diag(A_1, \cdots, A_p) \in \mathbb{R}^{n\times n}$, $\boldsymbol{\mathcal{B}} = diag(B_1, \cdots, B_p) \in \mathbb{R}^{n\times p}$ and $\boldsymbol{\mathcal{C}} = diag(C_1, \cdots, C_p) \in \mathbb{R}^{p\times n}$, whose matrices $A_i \in \mathbb{R}^{r_i\times r_i}$, $B_i \in \mathbb{R}^{r_i\times 1}$ and $C_i \in \mathbb{R}^{1\times r_i}$ $(i = 1, \cdots, p)$ are defined as follows:

$$A_i = \begin{bmatrix} 0 & 1 & 0 & \cdots & 0 \\ 0 & 0 & 1 & \cdots & 0 \\ \vdots & \vdots & \vdots & & \vdots \\ 0 & 0 & 0 & \cdots & 1 \\ 0 & 0 & 0 & \cdots & 0 \end{bmatrix}, \; B_i = \begin{bmatrix} 0 \\ 0 \\ \vdots \\ 0 \\ 1 \end{bmatrix}, \; C_i = \begin{bmatrix} 1 & 0 & \cdots & 0 \end{bmatrix} \tag{3.5}$$

whereas the vectors $\Phi(\boldsymbol{z},\boldsymbol{u}) \in \mathbb{R}^p$ and $\Psi(\boldsymbol{z}) \in \mathbb{R}^n$ are respectively:

$$\Phi(\boldsymbol{z},\boldsymbol{u}) = \begin{bmatrix} \phi_1(\boldsymbol{z},\boldsymbol{u}) \\ \phi_2(\boldsymbol{z},\boldsymbol{u}) \\ \vdots \\ \phi_p(\boldsymbol{z},\boldsymbol{u}) \end{bmatrix} = \begin{bmatrix} L^{r_1}_{G(\boldsymbol{x},\boldsymbol{u})} h_1(\boldsymbol{x}) \\ L^{r_2}_{G(\boldsymbol{x},\boldsymbol{u})} h_2(\boldsymbol{x}) \\ \vdots \\ L^{r_p}_{G(\boldsymbol{x},\boldsymbol{u})} h_p(\boldsymbol{x}) \end{bmatrix}_{x=T^{-1}(\boldsymbol{z})} \tag{3.6}$$

$$\Psi(\boldsymbol{z}) = \begin{bmatrix} \psi_1(\boldsymbol{z}) \\ \psi_2(\boldsymbol{z}) \\ \vdots \\ \psi_p(\boldsymbol{z}) \end{bmatrix} = \left[\frac{\partial T(\boldsymbol{x})}{\partial \boldsymbol{x}} \Delta G(\boldsymbol{x}) \right]_{x=T^{-1}(\boldsymbol{z})} \tag{3.7}$$

where $\phi_i \in \mathbb{R}$, and $\psi_i \in \mathbb{R}^{r_i}$ $\forall i = 1, 2, \cdots, p$.

The nonlinear function $\Phi(\boldsymbol{z},\boldsymbol{u})$ can be splitted in two different parts; the first one related to the linear component of the function, while the second one taking into account the residual nonlinear component. In other words, $\Phi(\boldsymbol{z},\boldsymbol{u})$ can be expressed also in terms of a pair of design matrices $\{\Lambda, \Gamma\}$ as follows:

$$\Phi(\boldsymbol{z},\boldsymbol{u}) = -\Lambda\boldsymbol{z} + \Gamma(\boldsymbol{z},\boldsymbol{u}) \tag{3.8}$$

where:

- $\Lambda = diag(\Lambda_1, \Lambda_2, \cdots, \Lambda_p) \in \mathbb{R}^{p\times n}$ with $\Lambda_i = (\alpha_{i0}, \alpha_{i1}, \cdots, \alpha_{i(r_i-1)}) \in \mathbb{R}^{1\times r_i}$ is a diagonal matrix designed such that the roots of the polynomial algebraic equation:

  $$\lambda^{r_i} + \alpha_{i(r_i-1)}\lambda^{(r_i-1)} + \cdots + \alpha_{i1}\lambda + \alpha_{i0} = 0 \tag{3.9}$$

  have all negative real part $\forall i = 1, 2, \cdots, p$.

  By making this choice, each of the $(A_i - B_i\Lambda_i)$ matrices results to be stable. Consequently, $(\boldsymbol{\mathcal{A}} - \boldsymbol{\mathcal{B}}\Lambda)$ is Hurwitz.

- $\Gamma(\boldsymbol{z},\boldsymbol{u}) \in \mathbb{R}^p$ is a suitable vector chosen such that the decomposition (3.4) preserves the own nominal dynamic of the system (3.1), that is: $G(\boldsymbol{x},\boldsymbol{u}) = (\boldsymbol{\mathcal{A}} - \boldsymbol{\mathcal{B}}\Lambda)\boldsymbol{z} + \boldsymbol{\mathcal{B}}\Gamma(\boldsymbol{z},\boldsymbol{u})$.

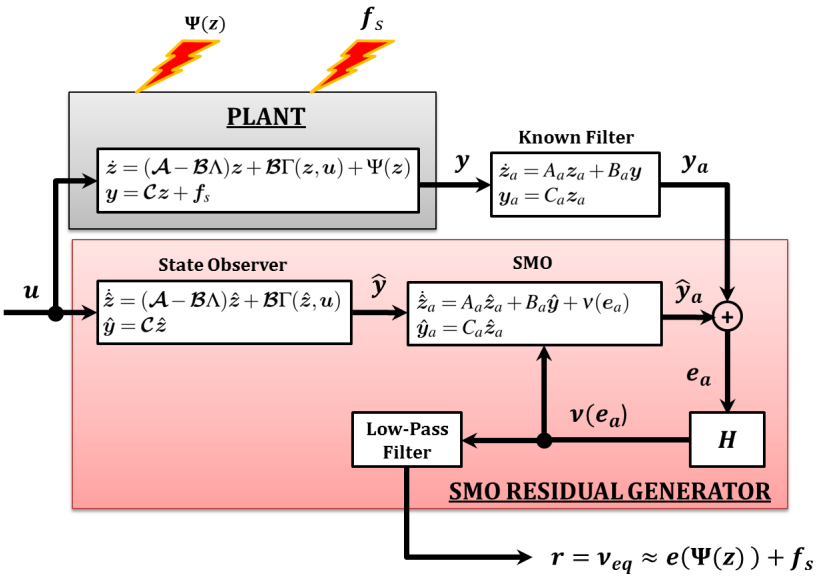

Figure 3.2: SMO Residual Generator scheme

It is worth to note that the following constraint:

$$\|\Gamma(z,u) - \Gamma(\hat{z},u)\| \leq \mathscr{L}_\Gamma \|z - \hat{z}\| \tag{3.10}$$

needs to be satisfied for any z, $\hat{z} \in T(\Omega) \subset \mathbb{R}^n$, where $\mathscr{L}_\Gamma \in \mathbb{R}^+$ is a continuous function, in order to make feasible the design of the observer as explained in section 3.2.2.

3.2.2 Observer Design

If (3.8) and (3.10) are both satisfied, the following augmented system can be obtained:

$$\begin{aligned} \dot{z} &= (\mathcal{A} - \mathcal{B}\Lambda)z + \mathcal{B}\Gamma(z,u) + \Psi(z) \\ \dot{z}_a &= A_a z_a + B_a \mathcal{C} z + B_a f_s \\ y_a &= C_a z_a \end{aligned} \tag{3.11}$$

where $z_a \in \mathbb{R}^p$ and $y_a \in \mathbb{R}^p$ are respectively the state and output's vectors of a linear filter described by the set of matrices $\{A_a \in \mathbb{R}^{p\times p}$, $B_a \in \mathbb{R}^{p\times p}$, $C_a \in \mathbb{R}^{p\times p}\}$ which are three design parameters to be defined later.

Notice that, this filter has two main advantages: it enables the conversion of the output sensors faults in (3.1) into *pseudo-actuator faults* with respect to (3.11), and it allows the arbitrary reduction of the measurements noise.

Let consider now the following observer dynamic:

$$\begin{aligned} \dot{\hat{z}} &= (\mathcal{A} - \mathcal{B}\Lambda)\hat{z} + \mathcal{B}\Gamma(\hat{z},u) \\ \dot{\hat{z}}_a &= A_a \hat{z}_a + B_a \mathcal{C}\hat{z} + \nu(t, y_a, \hat{y}_a) \\ \hat{y}_a &= C_a \hat{z}_a \end{aligned} \tag{3.12}$$

where ν is the sliding mode control algorithm, defined as the unit-vector:

$$\nu := k(t) C_a^T \frac{y_a - \hat{y}_a}{\|y_a - \hat{y}_a\|} \tag{3.13}$$

with the scalar gain $k(t)$ being designed later.

Let:

$$\boldsymbol{e}(t) = \boldsymbol{z}(t) - \hat{\boldsymbol{z}}(t) \tag{3.14}$$

and

$$\boldsymbol{e}_a(t) = \boldsymbol{z}_a(t) - \hat{\boldsymbol{z}}_a(t) \tag{3.15}$$

It follows from (3.11) and (3.12) that the two dynamics of errors (3.14) and (3.15) can be expressed respectively as:

$$\dot{\boldsymbol{e}} = (\boldsymbol{\mathcal{A}} - \boldsymbol{\mathcal{B}}\Lambda)\boldsymbol{e} + \boldsymbol{\mathcal{B}}[\Gamma(\boldsymbol{z},\boldsymbol{u}) - \Gamma(\hat{\boldsymbol{z}},\boldsymbol{u})] + \Psi(\boldsymbol{z}) \tag{3.16}$$

and:

$$\dot{\boldsymbol{e}}_a = A_a\boldsymbol{e}_a + B_a\boldsymbol{\mathcal{C}}\boldsymbol{e} + B_a\boldsymbol{f}_s - \nu(t,\boldsymbol{y}_a,\hat{\boldsymbol{y}}_a) \tag{3.17}$$

At this point, two different types of faulty scenario need to be considered.

3.2.2.1 Output Sensors Faults

In this scenario, only faults on the output sensors are taken into account. Therefore, the error dynamic (3.16) becomes:

$$\dot{\boldsymbol{e}} = (\boldsymbol{\mathcal{A}} - \boldsymbol{\mathcal{B}}\Lambda)\boldsymbol{e} + \boldsymbol{\mathcal{B}}[\Gamma(\boldsymbol{z},\boldsymbol{u}) - \Gamma(\hat{\boldsymbol{z}},\boldsymbol{u})] \tag{3.18}$$

Proposition 1. *Let define $Q \in \mathbb{R}^{n\times n}$ as the following symmetric, i.e. $Q^T = Q$, negative definite matrix, i.e. $Q < 0$:*

$$Q = P(\boldsymbol{\mathcal{A}} - \boldsymbol{\mathcal{B}}\Lambda) + (\boldsymbol{\mathcal{A}} - \boldsymbol{\mathcal{B}}\Lambda)^T P + \varepsilon_1(\mathscr{L}_\Gamma)^2 I_n + \frac{1}{\varepsilon_1} P\boldsymbol{\mathcal{B}}\boldsymbol{\mathcal{B}}^T P \tag{3.19}$$

If the assumptions (3.8) and (3.10) are both satisfied, then the dynamic of the error system (3.18) is stable if there exist a matrix $P > 0$ and a constant scalar $\varepsilon_1 > 0$ such that $Q < 0$.

Proof. Let consider the candidate Lyapunov function $V(t) = \boldsymbol{e}^T(t)P\boldsymbol{e}(t) \in \mathbb{R}$, where $P \in \mathbb{R}^{n\times n}$ is a symmetric, i.e. $P^T = P$, positive definite matrix, i.e. $P > 0$, such that the time-derivative of the Lyapunov function along the trajectories of system (3.18) is negative semi-definite, that is $\dot{V}(t) \leq 0$, $\forall t > 0$.

$$\begin{aligned}
\dot{V}|_{(3.18)} &= \boldsymbol{e}^T P\dot{\boldsymbol{e}} + \dot{\boldsymbol{e}}^T P\boldsymbol{e} = \\
&= \boldsymbol{e}^T P\{(\boldsymbol{\mathcal{A}} - \boldsymbol{\mathcal{B}}\Lambda)\boldsymbol{e} + \boldsymbol{\mathcal{B}}[\Gamma(\boldsymbol{z},\boldsymbol{u}) - \Gamma(\hat{\boldsymbol{z}},\boldsymbol{u})]\} + \\
&+ \{\boldsymbol{e}^T(\boldsymbol{\mathcal{A}} - \boldsymbol{\mathcal{B}}\Lambda)^T + [\Gamma(\boldsymbol{z},\boldsymbol{u}) - \Gamma(\hat{\boldsymbol{z}},\boldsymbol{u})]^T\boldsymbol{\mathcal{B}}^T\}P\boldsymbol{e} = \\
&= \boldsymbol{e}^T[P(\boldsymbol{\mathcal{A}} - \boldsymbol{\mathcal{B}}\Lambda) + (\boldsymbol{\mathcal{A}} - \boldsymbol{\mathcal{B}}\Lambda)^T P]\boldsymbol{e} + \\
&+ \boldsymbol{e}^T P\boldsymbol{\mathcal{B}}[\Gamma(\boldsymbol{z},\boldsymbol{u}) - \Gamma(\hat{\boldsymbol{z}},\boldsymbol{u})] + [\Gamma(\boldsymbol{z},\boldsymbol{u}) - \Gamma(\hat{\boldsymbol{z}},\boldsymbol{u})]^T\boldsymbol{\mathcal{B}}^T P\boldsymbol{e}
\end{aligned} \tag{3.20}$$

If the quantity X^TY is a scalar, hence: $X^TY = (X^TY)^T = Y^TX$. Because the quantities $\boldsymbol{\mathcal{B}}^T P\boldsymbol{e}$ and $\Gamma(\boldsymbol{z},\boldsymbol{u})$ are both vectors $\in \mathbb{R}^p$, by setting $X = [\Gamma(\boldsymbol{z},\boldsymbol{u}) - \Gamma(\hat{\boldsymbol{z}},\boldsymbol{u})]$, $Y = \boldsymbol{\mathcal{B}}^T P\boldsymbol{e}$, then (3.20) becomes:

$$\dot{V}|_{(3.18)} = \boldsymbol{e}^T[P(\boldsymbol{\mathcal{A}} - \boldsymbol{\mathcal{B}}\Lambda) + (\boldsymbol{\mathcal{A}} - \boldsymbol{\mathcal{B}}\Lambda)^T P]\boldsymbol{e} + 2[\Gamma(\boldsymbol{z},\boldsymbol{u}) - \Gamma(\hat{\boldsymbol{z}},\boldsymbol{u})]^T\boldsymbol{\mathcal{B}}^T P\boldsymbol{e} \tag{3.21}$$

From the well known Young's inequality $2X^TY \leq \varepsilon_1 X^TX + \frac{1}{\varepsilon_1}Y^TY$, where $\varepsilon_1 > 0$ is a constant value which provides an additional design freedom, then (3.21) becomes:

$$\begin{aligned}\dot{V}|_{(3.18)} \leq\ & e^T[P(\mathcal{A}-\mathcal{B}\Lambda)+(\mathcal{A}-\mathcal{B}\Lambda)^TP]e+ \\ & +\varepsilon_1[\Gamma(z,u)-\Gamma(\hat{z},u)]^T[\Gamma(z,u)-\Gamma(\hat{z},u)]+\frac{1}{\varepsilon_1}(\mathcal{B}^TPe)^T\mathcal{B}^TPe\end{aligned} \tag{3.22}$$

Because of (3.10), then (3.22) becomes:

$$\dot{V}|_{(3.18)} \leq e^T[P(\mathcal{A}-\mathcal{B}\Lambda)+(\mathcal{A}-\mathcal{B}\Lambda)^TP]e+\varepsilon_1(\mathscr{L}_\Gamma)^2\|z-\hat{z}\|^2+\frac{1}{\varepsilon_1}e^TP\mathcal{B}\mathcal{B}^TPe \tag{3.23}$$

and since $\|z-\hat{z}\|^2 = \|e\|^2 = e^TI_ne$, consequently:

$$\dot{V}|_{(3.18)} \leq e^T\underbrace{\left[P(\mathcal{A}-\mathcal{B}\Lambda)+(\mathcal{A}-\mathcal{B}\Lambda)^TP+\varepsilon_1(\mathscr{L}_\Gamma)^2I_n+\frac{1}{\varepsilon_1}P\mathcal{B}\mathcal{B}^TP\right]}_{=Q}e \tag{3.24}$$

□

If (3.24) is satisfied, it implies that e is bounded, that is:

$$\sup_{0\leq t\leq\infty}\|e(t)\| \leq b \tag{3.25}$$

for some positive scalar b. As claimed in [Yan and Edwards, 2007], because of the scalar ε_1 in (3.24), without loss of generality it can be assumed that $P > I_n$ rather than just being positive definite.

At this point, in order to design the SMO, the following two-step design procedure is then applied.

The first step of this procedure is to design the sliding surface such that the system has the desired performance when constrained to move on it. In this case, a suitable sliding surface is:

$$\mathscr{S} = \{(e,e_a) \mid e_a = 0\} \tag{3.26}$$

Indeed, because of (3.24) and (3.25), the sliding mode dynamics of the two error systems (3.18) and (3.17) associated with the sliding surface (3.26) are both stable.

The second step is then to design of a sliding mode controller/observer gain such that the system can be driven onto the sliding surface and a sliding motion maintained thereafter.

Proposition 2. *According to the sliding mode theory, the only requirement needed to guarantee the stability of the observer* (3.12) *is to choose a suitable gain* $k(t)$ *in* (3.13) *such that the error systems* (3.18) *and* (3.17) *can be driven both to the sliding surface* (3.26) *in a finite time. This happens if the inequality* (3.24) *holds, and* $k(t)$ *satisfies the following constraint:*

$$k(t) \geq \|B_a\mathcal{C}\|b+\|B_a\|\rho(t)+\eta \quad , \quad \eta > 0 \tag{3.27}$$

where η *is an additional design parameter.*

Proof. Let $V_a(t) = \frac{1}{2}\|\boldsymbol{e}_a(t)\|^2 = \frac{1}{2}\boldsymbol{e}_a^T\boldsymbol{e}_a$ be a candidate Lyapunov function to evaluate the stability of the error dynamic (3.17), then:

$$\dot{V}_a|_{(3.17)} = \frac{1}{2}\left(\dot{\boldsymbol{e}}_a^T\boldsymbol{e}_a + \boldsymbol{e}_a^T\dot{\boldsymbol{e}}_a\right) \tag{3.28}$$

If the quantity X^TY is a scalar, hence: $X^TY = (X^TY)^T = Y^TX$. By setting $X = \dot{\boldsymbol{e}}_a$, $Y = \boldsymbol{e}_a$, then it results: $\dot{\boldsymbol{e}}_a^T\boldsymbol{e}_a = \boldsymbol{e}_a^T\dot{\boldsymbol{e}}_a$. Consequently, (3.28) can be rewritten as:

$$\begin{aligned}\dot{V}_a|_{(3.17)} &= \boldsymbol{e}_a^T\dot{\boldsymbol{e}}_a = \boldsymbol{e}_a^T[A_a\boldsymbol{e}_a + B_a\boldsymbol{\mathcal{C}}\boldsymbol{e} + B_a\boldsymbol{f}_s - \boldsymbol{\nu}(t,\boldsymbol{y}_a,\hat{\boldsymbol{y}}_a)] = \\ &= \boldsymbol{e}_a^TA_a\boldsymbol{e}_a + \boldsymbol{e}_a^TB_a\boldsymbol{\mathcal{C}}\boldsymbol{e} + \boldsymbol{e}_a^TB_a\boldsymbol{f}_s - \boldsymbol{e}_a^T\boldsymbol{\nu}(t,\boldsymbol{y}_a,\hat{\boldsymbol{y}}_a)\end{aligned} \tag{3.29}$$

Since, A_a is a design matrix which can be defined as Hurwitz, i.e. $A_a < 0$, it follows that:

$$\boldsymbol{e}_a^TA_a\boldsymbol{e}_a \leq 0. \tag{3.30}$$

Therefore, from (3.29) and (3.30), the following inequality arises:

$$\dot{V}_a|_{(3.17)} \leq \boldsymbol{e}_a^TB_a\boldsymbol{\mathcal{C}}\boldsymbol{e} + \boldsymbol{e}_a^TB_a\boldsymbol{f}_s - \boldsymbol{e}_a^T\boldsymbol{\nu}(t,\boldsymbol{y}_a,\hat{\boldsymbol{y}}_a) \tag{3.31}$$

From (3.13) and by taking into account the bound constraints on the fault vector $\boldsymbol{f}_s$, i.e. (3.2), and on the error signal $\boldsymbol{e}$, i.e. (3.25), then (3.31) becomes:

$$\dot{V}_a|_{(3.17)} \leq \|\boldsymbol{e}_a\|\|B_a\boldsymbol{\mathcal{C}}\|b + \|\boldsymbol{e}_a\|\|B_a\|\rho - \boldsymbol{e}_a^Tk(t)C_a^T\frac{\boldsymbol{y}_a - \hat{\boldsymbol{y}}_a}{\|\boldsymbol{y}_a - \hat{\boldsymbol{y}}_a\|} \tag{3.32}$$

From (3.15), it follow that:

$$\begin{aligned}\|\boldsymbol{y}_a - \hat{\boldsymbol{y}}_a\| &= \sqrt{(\boldsymbol{y}_a - \hat{\boldsymbol{y}}_a)^T(\boldsymbol{y}_a - \hat{\boldsymbol{y}}_a)} = \sqrt{(C_a\boldsymbol{z}_a - C_a\hat{\boldsymbol{z}}_a)^T(C_a\boldsymbol{z}_a - C_a\hat{\boldsymbol{z}}_a)} = \\ &= \sqrt{[(C_a(\boldsymbol{z}_a - \hat{\boldsymbol{z}}_a)]^T[(C_a(\boldsymbol{z}_a - \hat{\boldsymbol{z}}_a)]} = \sqrt{(C_a\boldsymbol{e}_a)^T(C_a\boldsymbol{e}_a)} = \\ &= \sqrt{\boldsymbol{e}_a^TC_a^TC_a\boldsymbol{e}_a}\end{aligned} \tag{3.33}$$

and since C_a is a design matrix which can be defined as orthogonal, i.e. $C_a^TC_a = C_aC_a^T = I_p$, by setting $C_a = I_p$, consequently:

$$\|\boldsymbol{y}_a - \hat{\boldsymbol{y}}_a\| = \sqrt{\boldsymbol{e}_a^TI_p\boldsymbol{e}_a} = \sqrt{\boldsymbol{e}_a^T\boldsymbol{e}_a} = \|\boldsymbol{e}_a\| \tag{3.34}$$

Hence, from (3.33) and (3.34), then (3.32) can be rewritten as:

$$\begin{aligned}\dot{V}_a|_{(3.17)} &\leq \|\boldsymbol{e}_a\|\|B_a\boldsymbol{\mathcal{C}}\|b + \|\boldsymbol{e}_a\|\|B_a\|\rho(t) - k(t)(\boldsymbol{e}_a^TC_a^T)\frac{(C_a\boldsymbol{e}_a)}{\|\boldsymbol{y}_a - \hat{\boldsymbol{y}}_a\|} = \\ &= \|\boldsymbol{e}_a\|\|B_a\boldsymbol{\mathcal{C}}\|b + \|\boldsymbol{e}_a\|\|B_a\|\rho(t) - k(t)\frac{\|\boldsymbol{e}_a\|^2}{\|\boldsymbol{e}_a\|} = \\ &= \|\boldsymbol{e}_a\|\|B_a\boldsymbol{\mathcal{C}}\|b + \|\boldsymbol{e}_a\|\|B_a\|\rho(t) - k(t)\|\boldsymbol{e}_a\| = \\ &= \|\boldsymbol{e}_a\|\underbrace{[\|B_a\boldsymbol{\mathcal{C}}\|b + \|B_a\|\rho(t) - k(t)]}_{=-\eta} = -\eta\|\boldsymbol{e}_a\|\end{aligned} \tag{3.35}$$

According to [Shtessel et al., 2013], (3.35) is the so-called *reachability condition*, i.e. $e_a^T \dot{e}_a \leq -\eta \|e_a\|$, which must be satisfied in order to guarantee that the sliding motion on the surface (3.26) is achieved and maintained after some finite time. Thus, the gain $k(t)$ must be designed in order to satisfy the following constraint:

$$\begin{aligned} -\eta &= \|B_a \mathcal{C}\| b + \|B_a\| \rho(t) - k(t) \\ \Rightarrow k(t) &\geq \|B_a \mathcal{C}\| b + \|B_a\| \rho(t) + \eta \end{aligned} \tag{3.36}$$

Hence the proof is complete. □

Once the sliding motion takes place, then:

$$e_a = \dot{e}_a = 0 \tag{3.37}$$

Hence, from (3.17) it yields:

$$B_a \mathcal{C} e + B_a f_s - \nu_{eq} = 0 \tag{3.38}$$

where ν_{eq} is the so-called *equivalent output error injection*, which plays the same role assumed in the sliding mode control theory by the equivalent control [Utkin, 1992]. The equivalent output injection signal represents the average behavior which needs to adopt the discontinuous function (3.13) in order to keep on the sliding motion. The filter design parameter B_a can be chosen according to (1.7). Hence, by setting $B_a = I_p$, (3.38) becomes:

$$\mathcal{C} e + f_s - \nu_{eq} = 0 \quad \Rightarrow \quad f_s = -\mathcal{C} e + \nu_{eq} \tag{3.39}$$

As claimed in [Yan and Edwards, 2007], given the structure of the unit-vector ν in (3.13), the corresponding ν_{eq} signal can be approximated to any accuracy by the following low-pass filter:

$$\nu_{eq} \approx \nu_\sigma = k(t) C_a^T \frac{y_a - \hat{y}_a}{\|y_a - \hat{y}_a\| + \sigma} \tag{3.40}$$

where $k(t)$ satisfies (3.27) and $\sigma > 0$ is a suitable scalar.

Thus, by defining the estimation of the vector fault f_s as:

$$\hat{f}_s = \nu_\sigma \tag{3.41}$$

Then from (3.40) and (3.41):

$$f_s - \hat{f}_s = -\mathcal{C} e + (\nu_{eq} - \nu_\sigma) \tag{3.42}$$

Since because of (3.24) $e(t)$ is exponentially stable, i.e. $\lim_{t \to +\infty} e(t) = 0$, hence from (3.42) it results a precise reconstruction of the output sensor fault f_s can be achieved by making σ as small as possible, that is:

$$\|\nu_{eq} - \nu_\sigma\| \quad \Rightarrow \quad f_s - \hat{f}_s \approx 0 \quad \Rightarrow \quad \hat{f}_s \approx f_s \tag{3.43}$$

Remark 3. *Because the signal $\hat{f}_s$ depends on y_a and $\hat{y}_a$ only, which can both be obtained online, this fault reconstruction scheme is convenient for a practical implementation.*

Remark 4. *Others sliding mode control algorithm could be used in place of the unit-vector structure in (3.13), such as the componentwise super-twisting injection signal [Levant, 1998].*

3.2.2.2 Actuators and Output Sensors Faults

In this scenario, both the faults on actuators and output sensors are taken into account. Therefore, the dynamics of the error system $\boldsymbol{e}$ and $\boldsymbol{e}_a$ are the general ones in (3.16) and (3.17), respectively. In this case, some additional requirements need to be satisfied in order to guarantee the stability of the SMO. The following constraint introduces a bound on the magnitude of the faults on the actuators:

$$\sqrt{\Psi(\boldsymbol{z})^T P \Psi(\boldsymbol{z})} \leq \frac{1}{2} d \quad \forall z \in T(\Omega) \tag{3.44}$$

where $P > I_n$ is the matrix which satisfies (3.24) and d is another design parameter set as a constant value. In this scenario, in contrast with the previous one, the exponential convergence to zero of $\boldsymbol{e}(t)$ cannot be guarantee, but only the convergence into a closed set, whose amplitude should be strictly related to the magnitude of the perturbed term $\Psi(\boldsymbol{z})$.

Proposition 3. *If the inequality* (3.24) *and the constraint* (3.44) *hold, for any value of the arbitrarily small positive constant* $\varepsilon_2 > 0$*, after a time* $t \geq T_1$*,* $\boldsymbol{e}(t)$ *will remain confined into the set:*

$$\mathscr{B} = \left\{ \boldsymbol{e} | \boldsymbol{e}^T P \boldsymbol{e} \leq \left(\frac{d + \varepsilon_2}{\alpha} \right)^2 \right\} \tag{3.45}$$

where $\alpha = -\lambda_{max}(P^{-1/2} Q P^{-1/2})$ is the maximum eigenvalue of the matrix $P^{-1/2} Q P^{-1/2}$ with Q defined as in (3.19).

Proof. As done in the proof of preposition 1, let consider the candidate Lyapunov function: $V = \boldsymbol{e}^T P \boldsymbol{e}$ to evaluate the stability of the error dynamic (3.16). Then, by applying the same steps:

$$\begin{aligned}
\dot{V}|_{(3.16)} &= \boldsymbol{e}^T P \dot{\boldsymbol{e}} + \dot{\boldsymbol{e}}^T P \boldsymbol{e} = \\
&= \boldsymbol{e}^T P \{ (\boldsymbol{\mathcal{A}} - \boldsymbol{\mathcal{B}}\Lambda) \boldsymbol{e} + \boldsymbol{\mathcal{B}} [\Gamma(\boldsymbol{z}, \boldsymbol{u}) - \Gamma(\hat{\boldsymbol{z}}, \boldsymbol{u})] + \Psi(\boldsymbol{z}) \} + \\
&+ \{ \boldsymbol{e}^T (\boldsymbol{\mathcal{A}} - \boldsymbol{\mathcal{B}}\Lambda)^T + [\Gamma(\boldsymbol{z}, \boldsymbol{u}) - \Gamma(\hat{\boldsymbol{z}}, \boldsymbol{u})]^T \boldsymbol{\mathcal{B}}^T + \Psi^T(\boldsymbol{z}) \} P \boldsymbol{e} = \\
&= \boldsymbol{e}^T [P(\boldsymbol{\mathcal{A}} - \boldsymbol{\mathcal{B}}\Lambda) + (\boldsymbol{\mathcal{A}} - \boldsymbol{\mathcal{B}}\Lambda)^T P] \boldsymbol{e} + 2[\Gamma(\boldsymbol{z}, \boldsymbol{u}) - \Gamma(\hat{\boldsymbol{z}}, \boldsymbol{u})]^T (\boldsymbol{\mathcal{B}}^T P \boldsymbol{e}) + \\
&+ 2(P\boldsymbol{e})^T \Psi(\boldsymbol{z})
\end{aligned} \tag{3.46}$$

From (3.24), the following inequality arises:

$$\dot{V}|_{(3.16)} \leq \boldsymbol{e}^T Q \boldsymbol{e} + 2(P\boldsymbol{e})^T \Psi(\boldsymbol{z}) \tag{3.47}$$

The inequality (3.47) can be rewritten in terms of $P^{1/2}$ as follows:

$$\begin{aligned}
\dot{V}|_{(3.16)} &\leq \boldsymbol{e}^T Q \boldsymbol{e} + 2\boldsymbol{e}^T P \Psi(\boldsymbol{z}) = \\
&= \boldsymbol{e}^T (P^{1/2} P^{-1/2}) Q (P^{-1/2} P^{1/2}) \boldsymbol{e} + 2\boldsymbol{e}^T (P^{1/2} P^{1/2}) \Psi(\boldsymbol{z}) = \\
&= \boldsymbol{e}^T P^{1/2} (P^{-1/2} Q P^{-1/2}) P^{1/2} \boldsymbol{e} + 2\boldsymbol{e}^T P^{1/2} (P^{1/2} \Psi(\boldsymbol{z})) = \\
&= (P^{1/2}\boldsymbol{e})^T (P^{-1/2} Q P^{-1/2}) (P^{1/2}\boldsymbol{e}) + 2(P^{1/2}\boldsymbol{e})^T (P^{1/2} \Psi(\boldsymbol{z}))
\end{aligned} \tag{3.48}$$

Since quadratic forms always satisfy the Rayleigh principle [Shtessel et al., 2013], namely:

$$\lambda_{min}(W)\|\boldsymbol{x}\|^2 \leq \boldsymbol{x}^T W \boldsymbol{x} \leq \lambda_{max}(W)\|\boldsymbol{x}\|^2 \tag{3.49}$$

Then, by setting $W = P^{-1/2}QP^{-1/2}$, $\boldsymbol{x} = P^{1/2}\boldsymbol{e}$, and applying the Euclidean norm operator $\|\cdot\|$, the inequality (3.48) becomes:

$$\dot{V}|_{(3.16)} \leq \lambda_{max}(P^{-1/2}QP^{-1/2})\|P^{1/2}\boldsymbol{e}\|^2 + 2\|P^{1/2}\boldsymbol{e}\|\|P^{1/2}\Psi(\boldsymbol{z})\| \tag{3.50}$$

Since also V and (3.44) can be all rewritten in terms of $P^{1/2}$, that is:

$$V = \boldsymbol{e}^T(P^{1/2}P^{1/2})\boldsymbol{e} = (\boldsymbol{e}^T P^{1/2})(P^{1/2}\boldsymbol{e}) = (P^{1/2}\boldsymbol{e})^T(P^{1/2}\boldsymbol{e}) = \|P^{1/2}\boldsymbol{e}\|^2 \tag{3.51}$$

$$\sqrt{\Psi(z)^T P \Psi(z)} = \sqrt{(\Psi(z)^T P^{1/2})(P^{1/2}\Psi(z))} = \|P^{1/2}\Psi(z)\| \leq \frac{1}{2}d \tag{3.52}$$

Then, by applying (3.51), (3.52), and setting $\alpha = -\lambda_{max}(P^{-1/2}QP^{-1/2})$, the inequality (3.50) becomes:

$$\dot{V}|_{(3.16)} \leq -\alpha V + d\sqrt{V} \tag{3.53}$$

Therefore, the condition which guarantees the stability of the error $\boldsymbol{e}(t)$ is:

$$\dot{V}|_{(3.16)} \leq (d - \alpha\sqrt{V})\sqrt{V} \tag{3.54}$$

If $\boldsymbol{e}(t) \notin \mathscr{B}$, from (3.45) it implies that, $\forall \varepsilon_2 > 0$:

$$\begin{aligned} V > \left(\frac{d+\varepsilon_2}{\alpha}\right)^2 \;\Rightarrow\; \sqrt{V} > \frac{d+\varepsilon_2}{\alpha} \\ \Rightarrow\; \alpha\sqrt{V} > d + \varepsilon_2 \;\Rightarrow\; (d - \alpha\sqrt{V}) < -\varepsilon_2 \end{aligned} \tag{3.55}$$

Hence, the following inequality:

$$\dot{V}|_{(3.16)} \leq -\varepsilon_2\sqrt{V} \tag{3.56}$$

guarantees the validity of the proposition 3, and consequently the proof is completed. □

By applying the design procedure depicted in Section 3.2.2.1, since the dynamic (3.17) of $\boldsymbol{e}_a(t)$ is the same in both cases, the constraint to be satisfied by the gain $k(t)$ in (3.13) so that the error systems (3.16) and (3.17) can be driven both to the sliding surface (3.26) in a finite time is still (3.36).

Remark 5. *In the fault configuration considered in Section 3.2.2.1, i.e. $\Psi(\boldsymbol{z}) = 0$, the sliding motion results to be asymptotically stable, because of: $\lim_{t\to+\infty} \boldsymbol{e}(t) = 0$. When faults on the actuators are taken into account instead, i.e. $\Psi(\boldsymbol{z}) \neq 0$, it results $\boldsymbol{e}(t) \in \mathscr{B}$ $\forall t \geq T_1$, that is the sliding motion is ultimately bounded. Therefore, in this case, once the sliding motion takes place, from (3.42) the following approximation can be obtained by making σ as small as possible:*

$$\|v_{eq} - v_\sigma\| \approx 0 \;\Rightarrow\; \boldsymbol{f}_s - \hat{\boldsymbol{f}}_s \approx -\mathcal{C}\boldsymbol{e} \;\Rightarrow\; \hat{\boldsymbol{f}}_s \approx \boldsymbol{f}_s + \mathcal{C}\boldsymbol{e} \tag{3.57}$$

Remark 6. *According to (1.7), when the unknown term $\Psi(\boldsymbol{z})$ refers to faults on the actuators, it can be expressed also as:*

$$\Psi(\boldsymbol{z}) = \boldsymbol{\mathcal{B}} \boldsymbol{f}_a \tag{3.58}$$

Hence, since the error dynamic depends on the input measurement fault term, i.e. $\boldsymbol{e} = \boldsymbol{e}(\Psi(\boldsymbol{z}))$, the functional dependence of the error dynamics from the uncertainties on the input channels, when they refer to actuator faults, can be represented in a more generic form by using the following expression:

$$\boldsymbol{\mathcal{C}} \boldsymbol{e} = E(\boldsymbol{f}_a) \tag{3.59}$$

where $E(\cdot)$ is a functional representative of the filtering action applied to the unknown signal $\boldsymbol{f}_a$ due to the particular structure of the system.

At this point, a convenient way to determine optimal values for the design parameters is then presented. Let consider the following inequality:

$$\begin{aligned} Q + \frac{1}{\gamma} P < 0 \quad &\Rightarrow \quad P^{-1/2} Q P^{-1/2} + \frac{1}{\gamma} P^{-1/2} \underbrace{P}_{=P^{1/2}P^{1/2}} P^{-1/2} < 0 \\ \Rightarrow \quad P^{-1/2} Q P^{-1/2} + \frac{1}{\gamma} I_n < 0 \quad &\Rightarrow \quad P^{-1/2} Q P^{-1/2} < -\frac{1}{\gamma} I_n \end{aligned} \tag{3.60}$$

where Q and P are the design matrices defined in Proposition 1 and $\gamma \in \mathbb{R}$ is a positive scalar. Thus, in terms of eigenvalues:

$$\begin{aligned} \lambda_{max}(P^{-1/2} Q P^{-1/2}) = -\alpha < -\frac{1}{\gamma} \\ \Rightarrow \quad \gamma > \frac{1}{\alpha} \end{aligned} \tag{3.61}$$

As a consequence, to find the design matrix P, which implies to minimize γ in the equation (3.60), results also in decreasing the radius of the boundness set (3.45). According to [Yan and Edwards, 2007], a suitable way to solve the design problem is to find matrices P and X which minimize the scalar $\gamma > 0$, and such that the following constraints are satisfied:

$$\begin{bmatrix} P(\boldsymbol{\mathcal{A}} - \boldsymbol{\mathcal{B}}\Lambda) + (\boldsymbol{\mathcal{A}} - \boldsymbol{\mathcal{B}}\Lambda)^T P + \varepsilon_1 (\mathscr{L}_\Gamma)^2 I_n + X & P\boldsymbol{\mathcal{B}} \\ \boldsymbol{\mathcal{B}}^T P & -\varepsilon_1 I_p \end{bmatrix} < 0 \tag{3.62}$$

$$I_n < P \tag{3.63}$$

$$P < \gamma X \tag{3.64}$$

where $X \in \mathbb{R}^{n \times n}$ is a so-called *'slack'* variable. This is a convex optimization problem and can be solved by means of Linear Matrix Inequality (LMI) techniques. Indeed, by recalling the definition of *Shur complement*, let $M \in \mathbb{R}^{(p+q)\times(p+q)}$ a matrix block, such as:

$$M = \begin{bmatrix} \bar{A} & \bar{B} \\ \bar{C} & \bar{D} \end{bmatrix} \tag{3.65}$$

where $\bar{A} \in \mathbb{R}^{p\times p}$, $\bar{B} \in \mathbb{R}^{p\times q}$, $\bar{C} \in \mathbb{R}^{q\times p}$, $\bar{D} \in \mathbb{R}^{q\times q}$ are block submatrices and D is invertible. Then, the Schur complement of the block D of the matrix M is:

$$M/\bar{D} = \bar{A} - \bar{B}\bar{D}^{-1}\bar{C} \tag{3.66}$$

Hence, the Shur component of the matrix in (3.62) is:

$$\underbrace{P(\mathcal{A}-\mathcal{B}\Lambda)+(\mathcal{A}-\mathcal{B}\Lambda)^T P+\varepsilon_1(\mathscr{L}_\Gamma)^2 I_n + X}_{\bar{A}} - \underbrace{(P\mathcal{B})}_{\bar{B}}\underbrace{(-1/\varepsilon_1)}_{\bar{D}^{-1}}\underbrace{(\mathcal{B}^T P)}_{\bar{C}} \tag{3.67}$$

If the constraint (3.62) is satisfied, then it will result:

$$P(\mathcal{A}-\mathcal{B}\Lambda)+(\mathcal{A}-\mathcal{B}\Lambda)^T P+\varepsilon_1(\mathscr{L}_\Gamma)^2 I_n + \frac{1}{\varepsilon_1}P\mathcal{B}\mathcal{B}^T P < -X \tag{3.68}$$

If also constraints (3.63) and (3.64) are satisfied, then it will result:

$$I_n < P < \gamma X \;\Rightarrow\; -\gamma X < -P < -I_n \;\Rightarrow\; -X < -\frac{1}{\gamma}P < -\frac{1}{\gamma}I_n \tag{3.69}$$

Therefore, the inequality (3.60) is satisfied.

3.3 Fault Isolation and Diagnosis by Residual Evaluation

In order to achieve a complete FDD, a novel analysis, which extends the standard concept of *directional residual* introduced in the Section 1.2.4, has been developed. Such residual evaluation method has been applied to the injection signals generated by the SMO, as depicted in the previous Section. Given a generic MIMO system, the faults affecting its inputs can be defined as $\boldsymbol{f}_u \equiv \boldsymbol{f}_a$, whereas the faults affecting its outputs as $\boldsymbol{f}_y \equiv \boldsymbol{f}_s$. If the fault symptoms $\boldsymbol{f}_u$ and $\boldsymbol{f}_y$ are bounded, it has been shown that their occurrence can be easily detected by exploiting the concept of the equivalent output error injection signal [Utkin, 1992], as follows:

$$\exists \nu(\boldsymbol{e_a}) : (\boldsymbol{e}_a, \dot{\boldsymbol{e}}_a) = 0 \;\Rightarrow\; \nu_{eq} \approx E(\boldsymbol{f}_u) + \boldsymbol{f}_y \tag{3.70}$$

By recalling the standard definition of residual provided in Section 1.2.5 for a generic observer-based residual generator, the residual $\boldsymbol{r}$ generated by means of the SMO scheme should be defined as the difference between the output $\boldsymbol{y_a}$ and its estimate $\hat{\boldsymbol{y}}_{\boldsymbol{a}}$, i.e. the error signal $\boldsymbol{e_a}$, given as input to the feedback block H, according with the scheme depicted in Figure 1.7. In this approach instead, as showed in Figure 3.2, the residual signal is defined as the output of the filter H, that is:

$$\boldsymbol{r} = H\boldsymbol{e_a} = H(\boldsymbol{y_a} - \hat{\boldsymbol{y}}_{\boldsymbol{a}}) = \nu(\boldsymbol{e_a}) \tag{3.71}$$

By comparing (3.70) and (3.71) it is apparent that resorting to the equivalent output injection in SMO corresponds to those fault isolation approaches depicted in Section 1.2 where a suitable filter is designed to exploit frequency separation properties among faults, measurement noises and/or unknown inputs. However, since also the SMO scheme is an observer-based method, it is affected by the same precondition needed for the solvability of the decoupling problem discussed in Section 1.2.5, which is the availability of a sufficient

number of measurements. Indeed, when faults affect both the q inputs and p outputs channels of a generic MIMO system, their occurrence can be detected by the residual observer-based residual generator scheme designed in the previous section. However, although this techniques is able to provide some estimation of the fault symptoms, in general it does not allow to discriminate among every fault, since the maximum number of residuals which can be generated, i.e. the output injections, is equal to the number of the system's outputs. Therefore, only p faults can be independently detected. However, when more than p faults occur, these residuals signals still carry the information about all faults. Thus, whenever a new fault occurs, the goal is to discern among the following three scenarios:

1. $\boldsymbol{r} \approx E(f_u) \Rightarrow$ input fault;
2. $\boldsymbol{r} \approx f_y \Rightarrow$ output fault;
3. $\boldsymbol{r} \approx E(f_u) + f_y \Rightarrow$ (input + output) fault.

It is apparent that the third scenario is a combination of two isolated faults. The probability of simultaneous fault occurrences on both input and output at the same instant of time is very low, then it is often neglected [Tadić et al., 2012]. Nevertheless, in order to complete the FDD task, it needs to classify both faults by post-processing the residual $\boldsymbol{r}$ such that decoupling between the different fault symptoms is attained.

3.3.1 Residual Evaluation by Signature Analysis

The residual evaluation method developed in this work refers to the geometric approach to FDI discussed in Section 1.2.4. Indeed, also this approach refers to a suitable set of residuals $R = \{r_i\}$ $(i = 1, ..., n)$ as a basis of the residual space, whose dimensionality n is equal to the number of detectable faults f_i. The corresponding *residual vector* $\vec{r}$, whose components are all fault-sensitive, is defined as:

$$\vec{r}(t) = [r_1(t), r_2(t), ..., r_n(t)]^T = \vec{r}(f_1(t), f_2(t), ..., f_n(t)) \tag{3.72}$$

The isolation of faults is achieved by exploiting the main idea behind the decoupling strategy introduced by Beard and Jones in the early 1970s and discussed in Section 1.2.4. Precisely, the fault isolation is performed by analysing the fault signature of the residual vector, namely the fixed direction or the subspace where $\vec{r}$ take its trajectory when a generic faulty symptom f_i occurs. However, as it happens for the fault detection filter of Beard and Jones, when one or more components of $\vec{r}$ result to be dynamically sensitive to several faults f_i, this design method could be not effective, because the requested one-to-one correspondence among fixed direction of signatures and faulty symptoms is not guaranteed. To overcome this limit, in this proposal the concept of signature direction has been extended. Referring to the standard definition of directional residual, i.e. (1.17), the signature direction is not considered anymore as a constant time-independent vector, i.e. $\vec{l}_i$, but as a more general time-varying vector, i.e. $\vec{L}_i(t)$, which is able to depict any shape during its time evolution. Thus, the new mathematical notation introduced for this extended directional residual vector is:

$$\vec{r}(t|f_i(t)) = \vec{L}_i(t) \; ; \; i = \{1, ..., n\} \tag{3.73}$$

It is worth to note that in this case, in addition to the one-to-one correspondence between fault signatures and fault sources, another condition to be guaranteed in order to have a

reliable fault isolation is the distinctiveness among the signatures, i.e., the shapes, generated by different faults. By this way, the fault isolation problem is then converted into a *fault classification* problem, that could be solved by using suitable pattern recognition techniques. Indeed, the pattern generated by the residual vector when a specific fault occurs is now a characteristic trajectory in the residual space. Hence, fault isolation could be achieved by determining which one of the known *fault trajectories* is the most similar to that taken by the residual vector during a certain amount of time after the fault occurred. The time needed for the generation of suitable fault patterns is an important aspect to take into account. The length of the temporal window needed by the residual generator in order to produce enough data will depend on the specific dynamic of the system and on some parameters of the SMO. In order to better understand all the general aspects mentioned above, let consider at first the simplest case, that is a SISO system. As stated before, at this level of analysis, the simultaneous occurrence of different faults is not taken into account. The residual space needed for a SISO system with faults considered both at the input and output side is $\mathbb{R}^2$. On one hand, by applying the SMO-based scheme, the residual generator provides only a scalar output injection, which is sensitive to both faulty symptoms. On the other hand, the residual evaluation approach requires to design a residual set $R = \{r_1, r_2\}$ such that the following residual vector:

$$\vec{r}(t) = [r_1(t), r_2(t)]^T = \vec{r}(f_u(t), f_y(t)) \tag{3.74}$$

and the corresponding fault signatures:

$$\begin{cases} \vec{r}(t|f_u(t)) = \vec{L}_u(t) \\ \vec{r}(t|f_y(t)) = \vec{L}_y(t) \end{cases} \tag{3.75}$$

could be defined.

In the next two paragraphs, two different ways of designing a suitable residual set by using the injection signal, i.e. $v_{eq}(t)$, and the measured output, i.e. $y^{mes}(t)$, are proposed. In order to simplify the notation, the time dependency of all the considered signals is omitted.

3.3.2 Residual Set R_a

In this approach, the residual $r_1(t)$ is designed to be the signal directly related to the fault on the output channel, i.e. $f_y(t)$. The missing residual $r_2(t)$ instead, is designed to be directly related to the fault on the input channel, i.e. $f_u(t)$. In general terms, this result can be obtained by applying a proper filtering action on the signal $v_{eq}(t)$. Thus, by designing this filter as the inverse of the functional in (3.59), i.e. $E^{-1}(\cdot)$, the following residual set can be defined:

$$R_a : \begin{cases} r_{a1}(f_u, f_y) = v_{eq} \approx E(f_u) + f_y \\ r_{a2}(f_u, f_y) = \overline{v}_{eq} = E^{-1}(v_{eq}) \approx f_u + E^{-1}(f_y) \end{cases} \tag{3.76}$$

With this choice, in nominal conditions, the residual set R_a becomes:

$$f_u = 0\ ,\ f_y = 0 \ \Rightarrow \ \begin{cases} r_{a1} \approx 0 \\ r_{a2} \approx 0 \end{cases} \tag{3.77}$$

Therefore, since $\vec{r}_a(t) \approx [0\ ,\ 0]^T$, in this case the residual vector will stay around the origin of the residual space $\mathbb{R}^2$ and, as expected, any trajectory will be depicted.

When a fault occurs on the output channel, the two components of the residual set R_a will raise the following configuration:

$$f_u = 0\ ,\ f_y \neq 0 \ \Rightarrow \ \begin{cases} r_{a1} \approx f_y \\ r_{a2} \approx E^{-1}(f_y) \end{cases} \tag{3.78}$$

Consequently, the residual vector $\vec{r}_a$ will start to generate on the residual space $\mathbb{R}^2$ the fault signature:

$$\vec{r}_a(t|f_y) = \vec{L}_a(f_y) \approx \langle f_y, E^{-1}(f_y) \rangle \tag{3.79}$$

where the function-valued vector $\vec{L}_a(f_y)$ will reflect the dynamic of the faulty symptom affecting the output channel, filtered by $E^{-1}(\cdot)$, i.e. the inverse of the functional defined in (3.59). When a fault occurs on the input channel instead, the following configuration will appear:

$$f_u \neq 0\ ,\ f_y = 0 \ \Rightarrow \ \begin{cases} r_{a1} \approx E(f_u) \\ r_{a2} \approx f_u \end{cases} \tag{3.80}$$

Hence, the residual vector $\vec{r}_a$ will start to generate on the residual space $\mathbb{R}^2$ the fault signature:

$$\vec{r}_a(t|f_u) = \vec{L}_a(f_u) \approx \langle E(f_u), f_u \rangle \tag{3.81}$$

where the function-valued vector $\vec{L}_a(f_u)$ will reflect the dynamic of the faulty symptom affecting the input channel, filtered by $E(\cdot)$, i.e. the functional defined in (3.59). Therefore, since $\vec{r}_a$ generates two different fault signatures corresponding to the fault symptoms f_u and f_y, the residual set R_a can be used to isolate faults affecting the input and output channels of a SISO system.

Nevertheless, with this configuration it is not possible to discriminate between two different types of fault f_u and f_y such as: $f_y \approx E(f_u)$, because in this case both symptoms will generate the same fault signature, i.e. $\vec{L}_a(f_y) \approx \vec{L}_a(f_u) \approx \langle E(f_u), f_u \rangle$. In order to overcome this limit, the following residual set was then designed:

3.3.3 Residual Set R_b

Also in this approach, the component $r_1(t)$ result to be directly related to the fault on the output channel. Nevertheless, in this case, the missing component $r_2(t)$ sensitive to the fault on the input channel is obtained by exploiting the relationship between injection signal, i.e. v_{eq}, and measured output, i.e. y^{mes}, as follows:

$$R_b : \begin{cases} r_{b1}(f_u, f_y) = v_{eq} \approx E(f_u) + f_y \\ r_{b2}(f_u, y) = v_{eq}^{\perp} = y^{mes} - v_{eq} \approx y - E(f_u) \end{cases} \tag{3.82}$$

With this choice the following relationship can be exploited:

$$r_{b1} + r_{b2} = v_{eq} + v_{eq}^{\perp} = y^{mes} \tag{3.83}$$

The trajectories of the residual vector $\vec{r}_b$, having as components those of the set R_b, will evolve according to a the following reasoning. In nominal conditions, the residual set R_b becomes:

$$f_u = 0\ ,\ f_y = 0 \ \Rightarrow \ \begin{cases} r_{b1} \approx 0 \\ r_{b2} \approx y \end{cases} \tag{3.84}$$

Therefore, since $\vec{r}_b(t) \approx [0\ ,\ y]$, in this case the residual vector will depict on the residual space $\mathbb{R}^2$ the actual dynamic of the system. Then, assuming steady state nominal conditions, i.e. $y = \bar{y}$, the residual vector will stay fixed on the point of the residual space $\mathbb{R}^2$ corresponding to this steady state, and its trajectory will not evolve.

When a fault on the output channel occurs, then the configuration assumed by the residual set R_b becomes:

$$f_u = 0\ ,\ f_y \neq 0 \ \Rightarrow \ \begin{cases} r_{b1} \approx f_y \\ r_{b2} \approx y \end{cases} \tag{3.85}$$

Hence, the residual vector $\vec{r}_b$ will start to generate on the residual space $\mathbb{R}^2$ the fault signature:

$$\vec{r}_b(t|f_y) = \vec{L}_b(f_y) \approx \langle f_y, y \rangle \tag{3.86}$$

where the function-valued vector $\vec{L}_b(f_y)$ will reflect the dynamic of the faulty measurement, which of course will result to be a $2D$ shape strictly correlated to the faulty symptom f_y. When a fault on the input channel occurs instead, the configuration of the residual set R_b becomes:

$$f_u \neq 0\ ,\ f_y = 0 \ \Rightarrow \ \begin{cases} r_{b1} \approx E(f_u) \\ r_{b2} \approx y - E(f_u) \end{cases} \tag{3.87}$$

Hence, both components of $\vec{r}_b$ are affected in the same way by the faulty symptom. As a consequence, after a certain amount of time, depending on the type and intensity of the fault, the trajectory of $\vec{r}_b$ will tend to converge to the following curve $S \in \mathbb{R}^2$:

$$S = \{(r_{b1}, r_{b2}) \in \mathbb{R}^2 \mid r_{b2} = -r_{b1} + \bar{y}\} \tag{3.88}$$

where $\bar{y}$ denotes the nominal dynamic of the system. When dealing with system operating at steady state nominal conditions, the trajectory of the curve S becomes a subspace of $\mathbb{R}^2$, that is the straight line having slope -1 and r_{b2}-intercept $\bar{y}$. In this case the fault signature generated by $\vec{r}_b$ will be:

$$\vec{r}_b(t|f_u) = \vec{L}_b(f_u) \approx \langle E(f_u), y - E(f_u) \rangle \tag{3.89}$$

where the function-valued vector $\vec{L}_b(f_u)$ will result to be a $2D$ shape convergent to the curve (3.88).

The curve S results to be the key factor of the residual set R_b, because by analysing if the trajectory of $\vec{r}_b$ converges on this portion of the residual space $\mathbb{R}^2$ it will be possible to discriminate if a signature reflects a fault on the input or the output of the system.

3.3.4 Features Extraction

In order to improve the performances of the FDD system in terms of fault isolation and diagnosis, in this work the opportunity to apply suitable signal processing techniques to residual signals and signatures was also investigated. This research is still undergoing and no experimental results are still available; nevertheless the two different draft of proposals under development are briefly discussed in this Section.

3.3.4.1 Data-Driven Approach

The alternative definition of signature provided in Section 3.3.1 is the key element of the novel hybrid approach to FDI investigated in this research. Indeed, it gives the opportunity to implement the whole residual evaluation task by exploiting a wide range of pattern recognition techniques, typically used in other contexts like handwritten signature verification [Faundez-Zanuy, 2007], [Fierrez et al., 2007], [Jain et al., 2002], [Lee et al., 2004], curve/shape matching and time series analysis [Efrat et al., 2007], [Keogh and Ratanamahatana, 2005], [Nakamura et al., 2013], [Marteau, 2009], and motion trajectory analysis [Wu and Li, 2009], [Vlachos et al., 2002]. As stated in the previous Section, the whole hybrid FDI proposal can be thought also as a pattern recognition scheme, where the residual generator block can be interpreted like a *pattern generator* module, while the residual evaluation block can be treated and developed as a *pattern classification* module. The main objective of the latter is to analyze the patterns generated by the previous module when a fault occurs, in order to extract some features that allow for comparing the current signature among the other ones, stored in the faults database, which the considered pattern recognition system will be able to classify. The study of suitable DD approaches is still ongoing. The most promising pattern recognition techniques seem to be those developed in the field of biometric recognition of handwritten signature [Fierrez et al., 2007], in order to find other discriminative information which can be extracted from the fault signatures. These methods can be broadly divided into two main categories:

- feature-based
- function-based

The first class of methods refers to a holistic vector representation, consisting of a set of global features which are derived from the signature trajectories [Lee et al., 1996, Ketabdar et al., 2005]. The second class of methods refers to time sequences describing local properties of the signature, i.e. position trajectory, velocity, acceleration, which are used for recognition [Jain et al., 2002, Nalwa, 1997, Li et al., 2006]. Several features could be tested in order to improve the performance of the fault classifier.

3.3.4.2 Signal-Based Approach

This idea refers to the fact that residual signals can be considered also as discrete time-series, since they are generated by a software-implemented algorithm, i.e. the SMO. Therefore, their temporal evolution can be evaluated also by exploiting some concepts related to the SB methodologies reviewed in Section 1.3. This research is exploiting the concept of *time series segmentation*. A good survey about this topic is provided in [Keogh et al., 2004], whereas in [Martí et al., 2014] an interesting application of such an approach in order to implement an efficient anomaly detection on a oil platform turbo-machinery is presented. As stated in [Martí et al., 2014], depending on the application, the segmentation of time-series is applied to locate stable periods of time, to identify change points, or to simply compress the original time series into a more compact representation.

The traditional approach to residual evaluation based on signature analysis refers to those trajectories in the residual space $\mathbb{R}^p$ which are updated based on the sampling frequency of the residual generator. Therefore, assuming to collect for each of the p residual signals a dataset of N samples, instead of referring to the residual signature, i.e. the N points depicted

in the residual space $\mathbb{R}^p$ by the residual vector, the idea is to process the p time series related to the residual set in order to extract more information, by means of a suitable segmentation.

According to definitions given in [Bouchard, 2006], a time series can be expressed as a set of n pairs, each of them consisting of a vector and a scalar, as follows:

$$T = \{(v_1, t_1), \dots (v_n, t_n)\} \tag{3.90}$$

where v_i is the value of the generic m-dimensional function at time t_i, $(i = 1, \dots, n)$. A more practical definition of a time series refers to the concept of *regular time series*, where the amount of time between two consecutive pairs is constant. A segment is a contiguous subset of a time series that is itself a time series, which can be formally expressed as:

$$S = \{s_1, \dots, s_{n_0}\} \tag{3.91}$$

where $s_i = (v_{i+j}, t_{i+j})$, $\forall i = \{1, \dots, n_0\}$ for a fixed value of the offset $0 \leq j \leq (n - n_0)$. As pointed out in [Bouchard, 2006], a segmentation is not a partition, thus not all the time value pairs in a time series T are included in a segment S. As a consequence, a time series T can be splitted in a set of segments, such as: $T = \{S_1, \dots, S_k\}$. Different applications have different time-series and segmentation criteria. At this stage of the research, only a basic segmentation strategy has been applied to residual signals in order to evaluate empirically the effective potential of such an approach in terms of fault isolation.

The main assumption of the proposal is that more information can be extracted from each residual if the corresponding time series is splitted into a set of segments, and a suitable metric or feature for each period is computed, in order to evaluate the behavior of the residual in each time window. By this way, the resulting fault signature will reflect also the peculiarities of the dynamic patterns assumed by every component of the residual vector in each of the time windows, thus it will be able to provide more information en respect to the conventional fault signature.

The proposed approach does not implement any of those automatic segmentation strategies reviewed in [Bouchard, 2006], but refers instead to a static choice of the fixed size n_0 for all the segments on the basis of empirical considerations. By this way, also the on-line implementation results to be straightforward.

Formally, the proposed segmentation strategy can be expressed as follows: given a time series $r(t) = \{(r_1, t_1), \dots (r_N, r_N)\}$ of N samples, where $w_k = (r_k, t_k)$, $\forall k = \{1, \dots, N\}$ denotes the generic sample of the residual signal, the i-th segment of the partitioning is defined as:

$$W_i = \{w_{1+M\times(i-1)}, \dots, w_{M\times i}\}, \forall i = \{1, \dots, N_0\} \tag{3.92}$$

where M is the number of samples in each of the segments W_i, whereas $N_0 = N/M \in \mathbb{N}$ is the total number of segments in the time series $r(t)$.

Each of the W_i segments can be referred to as *observing window*. A suitable metric, or feature, denoted as F, and representative of the local dynamic behavior of the residual signal within the observing window, has to be selected at this point. As a result, by computing the selected feature F for each of the N_0 observing windows W_i, a new dataset, denoted as D, can be obtained. This new set of N_0 samples can be formally expressed as a time series, as follows:

$$D = \{(F(W_1), W_1), \dots (F(W_{N_0}), W_{N_0})\} \tag{3.93}$$

where $F(W_i)$ denotes the value of the feature F related to the observing window W_i, $(i = 1, \dots, N_0)$.

By doing this way, it is apparent that the residual generator has been converted into a pattern generator . Therefore, the fault diagnosis can be performed by means of a suitable SB methodology, according to the general scheme depicted in Section 1.3.1. As a consequence, the resulting FDD system can be considered as a novel hybrid architecture, where the fault detection is based on a MB methodology, whereas the fault isolation and diagnosis refers to the implementation of a SB approach.

Another interesting point of view, which refers again to the fault detection by residual signature analysis, is being evaluated in this research. This novel proposal refers to the fact that the time series D can be considered itself as a residual signal, which results to be just a filtered version of the original one, and hence it can be used as a component of a new residual vector. As stated above, the expected result is that the new trajectories in the residual space will be more able to represent the peculiarities of each different fault typology.

Referring to Section 1.3, it has been shown that several different kind of features can be evaluated for the pattern analysis. Therefore, the feature F to be extracted from the observing window result to be a key parameter in the design of such a fault diagnosis system. It is worth to remark that also the size of the observing window, i.e. M, is an important design parameter which hardly affects the isolation capabilities of the new signatures, since its value directly influences the dynamic properties which can be hidden or highlight. At the moment, a methodological formulation of this approach which aims to provide more details about the design procedure is still under study.

3.4 Conclusion

In this Chapter a new hybrid FDD scheme has been presented. The whole proposal can be splitted in two main parts: the residual generation and the residual evaluation stage. The first stage is implemented by exploiting a MB method based on SMO, while the second one introduces a graphical approach which exploits an alternative definition of fault signature. This hybrid FDD approach can be expressed also as a pattern recognition scheme, where the residual generator block is the pattern generator module, whereas the residual evaluation block refers to as the pattern classification module. In this Chapter, it was shown that a fault classification scheme can be designed for a generic SISO system, by exploiting the output injection signal of the corresponding SMO. Faults affecting both the input and output channels can be isolated, overcoming the limitations related to a direct use of the output injection signal as residual for FDI. For a generic MIMO system, having m inputs and p outputs, the dimension of the residual space is equal to $q = m + p$, but only p residuals can be directly generated. In this case, a proper manipulation of the output injections and other available measurements must be designed in order to find the remaining $m = q - p$ components needed by the residual set. A systematic procedure to find an optimal set of components making the residual vector able to depict signatures which are suitable for the fault isolation is the most challenging aspect of this proposal, and it is still under study.

Chapter 4

Practical Application: Steam Separator

In this Chapter, the development of an FDD system which exploits the design approach discussed in Chapter 3 is applied to a typical industrial application related to the electricity generation field. Even though the growth of renewable power stations, currently, in some countries, a large portion of the overall power supply is still provided by thermal power plants. E.g., as mentioned by [Aldian Ambark Shashoa et al., 2013], in Serbia thermal power plants are the largest generators of electricity, contributing to more than the 65% of whole demand. Due to this fact, designing fault diagnosis systems which could prevent accidents and down time by allowing early detection of faults is a crucial task.

In the literature, most of the works dealing with the problem of FDI in thermal power plant propose solutions formulated in the framework of statistical decision making, such as likelihood ratio test [Chetouani, 2011], Bayes decision [Sun et al., 2012], CUmulative SUM (CUSUM) classification [Tadić et al., 2012] and SVM [Chen et al., 2011]. Although statistical approaches have a long tradition in FDI, those approaches are limited for processes in the steady state. Therefore, their efficiency for the detection of faults in dynamic systems has limits [Ding, 2008]. To overcome such a limitation, MB solutions for FDI have received considerably attention in the last decades.

This work deals with the problem of MB-FDI in water-steam power plants where, due to extreme pressures and temperatures, sensors and actuators are prone to failures. Both fault in the output channels, e.g. water flow and water level sensors, and in the input channels, e.g. steam flow sensor and feedwater actuator, are analyzed. Although SMOs are renowned in FDI for their ability to generate injection signals able to reproduce faulty behaviors, when both output and input measurements are faulty, they are hardly able to estimate the faults or to discern among them. However, those signals still embed, in some sense, an aggregate information about the faults nature. To overcome this limitation and achieve FDI, the proposed approach is to process the injection terms generated by a suitably designed SMO, by a procedure able to identify a distinguishing signature for each fault. Both faults in the sensor and actuator characteristics are considered. The performances of the proposed scheme have been evaluated through simulations which used real data taken from the TEKO B1 Thermal Power Plant of Kostolac (Serbia), whose nominal power is 330 MW.

This Chapter is organized as follows: in Section 4.1 a linearized model of the plant is presented; then, in Section 4.2 two different SMOs for sensor and actuator fault detection are developed, based on the scheme depicted in Section 3.2, whereas in Section 4.3 the practical implementation of the residual evaluation based on the signature analysis discussed in Section 3.3 is developed. The experimental results of the proposed FDD application are finally discussed in Section 4.4.

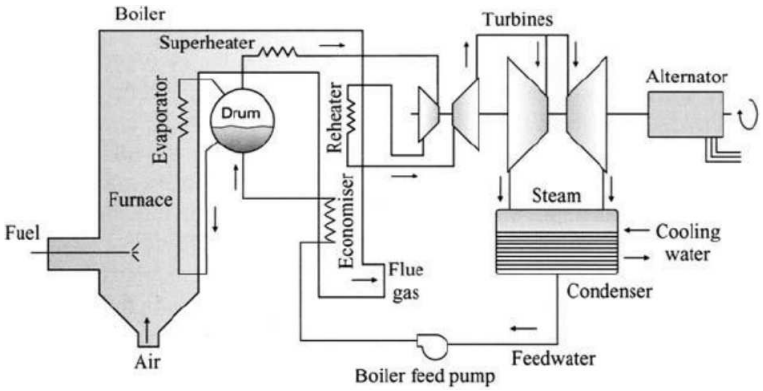

Figure 4.1: Thermal power plant schematic representation

4.1 Process Description, Modeling and Validation

The steam separator is a critical component in thermal power plants having schematic representation such that depicted in Figure 4.1. The processes which take place in a steam separator are highly nonlinear and involve several different parts. The boiler is the main unit, where the chemical energy of fossil fuel is converted into heat energy of steam. It denotes the core of the following water-steam cycle. The water, partially heated through an economizer, is provided to the steam drum by a set of feed pumps. Other pumps of the same feedwater system discharge the water into a system of pipes inside the boiler. In the boiler, the water is converted into steam. Before it leaves the boiler, the steam is then delivered to a superheater. The superheated steam, finally goes on to the turbines. The steam separator unit under analysis is the same considered in [Aldian Ambark Shashoa et al., 2013]. The drum's geometry is cylindrical, with an height of 24 [m] and a diameter of 2 [m]. Nominal temperatures inside the furnace are as high as 1400 [°C]. Nominal temperatures and pressures of the steam are 540 [°C] and $165 \div 175$ [bar] respectively. One of the process requirements is to maintain the water level in the drum at an height of 8 [m], independently to the other variables. This goal is achieved by implementing a closed loop scheme in which a cascaded PID receiving as input the difference signal between the required and the measured water level, is able to provide as output the control signal for the feedwater pump discharge. Consequently, the most important measurements for this control system are:

- the feedwater flow at the steam drum inlet;
- the steam flow at the steam drum outlet;
- the water level in the steam drum.

All these physical quantities are measured indirectly, via differential pressures. Water and steam flows are both measured by differential pressure transmitters (Siemens Sitrans PDSIII7MF4533), having measurement range of $0 \div 500$ [mbar] and accuracy of 0.075%, which are located on the inlet and outlet of the steam drum, respectively. The water level instead, is measured by differential pressure gauges (Siemens Sitrans PDSIII7MF4433), having measurement range of $0 \div 1570$ [mbar] and accuracy of 0.075%, which are located at the bottom of the steam drum.

As done in [Aldian Ambark Shashoa et al., 2013], faults where the corresponding error is multiplicative, i.e. the measurement results to be scaled, have been considered. Based on

the operator's experience, they represent the most frequent faults which could affect a steam separator measurement system. Such faults are also the most difficult to detect, because they cause only a degradation of the measurement quality instead of an abrupt change in the measurement; they are virtually undetectable by standard methods, e.g. those algorithms which only check limits.

Therefore, the system architecture of the steam separator can be thought as a cascade control scheme where the objective is to control both the volume of water and the inlet of water mass-flow rate inside the steam drum. In the system model depicted in figure 4.2, four main blocks can be easily recognized, which are respectively:

- the water-level PID controller, which generates the set-point for the feedwater system;
- the feedwater system, consisting of a nested closed loop multistage centrifugal pump system whose output is used to adjust the boiler's water level;
- the water piping, which conducts the water inside the boiler;
- the steam drum, where the water is converted into steam.

As stated above, the dynamics of the system under analysis result to be nonlinear. Therefore, in order to apply the FDD design procedure presented in chapter 3, a linearized version of the model is needed.

The next subsections provide a State-Space representation of the corresponding linear model identified for each of the needed blocks mentioned above, that is:

$$\begin{aligned} \dot{x} &= Ax + Bu \\ y &= Cx + Du \end{aligned} \tag{4.1}$$

Notice that, each State-Space representation is expressed in its phase variables canonical form, e.g. the output of each system exits from a chain of integrators, that is:

$$A = \begin{bmatrix} 0 & 1 & 0 & 0 \\ 0 & 0 & \ddots & 0 \\ 0 & 0 & 0 & 1 \\ * & * & * & * \end{bmatrix}, \quad C = \begin{bmatrix} 1 & 0 & \cdots & 0 \end{bmatrix} \tag{4.2}$$

For each subsystem, the identification procedure was conducted by exploiting practical methods for the characterization of dynamical systems, such as step-response-like tests. For this task, real data acquired from the plant over a period of 24 hours during which there were no faults have been employed.

4.1.1 Feedwater System Linear Model

As previously stated, the feedwater system consists of a nested and enough fast closed-loop system whose input is generated by the water-level regulator, i.e. an adjustable water-flow set-point, whereas its output is used to adjust the boiler's water level. According to figure 4.2, this sub-system can be modeled as a SISO system having the set-point for the feedwater system, namely $q_w^{PID}(t)$, as the input signal, and the water flow going into the water piping system, namely $q'_w(t)$, as the output signal. By means of a simple black-box step-response test, which consists in the comparison between the step-test responses of the

real and linearized version of this sub-system under the same operating conditions, the real dynamics has been approximated by a second-order linear model, as follows:

$$\frac{q'_w(s)}{q_w^{PID}(s)} \approx \frac{k}{1+2\frac{\xi}{\omega_n}+\frac{s^2}{\omega_n^2}} \tag{4.3}$$

where the variable s denotes the representation in terms of Laplace transforms, and the model's parameter and their corresponding values are:

- DC Gain: $k = 2$;
- Damping Ratio: $\xi = 0.53$;
- Natural Frequency: $\omega_n = 0.2903$.

The corresponding State Space representation of this model is:

$$\left[\begin{array}{c|c} A_w & B_w \\ \hline C_w & D_w \end{array}\right] = \left[\begin{array}{cc|c} 0 & 1 & 0 \\ \text{-0.843} & \text{-0.3077} & 0.1685 \\ \hline 1 & 0 & 0 \end{array}\right] \tag{4.4}$$

The only difference in the step-test response of the real and the approximated model of the feedwater system was related to the presence of some steady-state self-sustained oscillations in the original system due to the nonlinearities inside the PID water flow regulator, such as the anti-windup saturation components. Since a linearized approximation of the system was needed, these nonlinear behaviours have been neglected.

4.1.2 Water Piping Linear Model

The water piping conducts the water flow into the boiler. According to figure 4.2, the water piping can be modeled as a SISO system having the water flow going from the feedwater system, namely $q'_w(t)$, as the input signal, and the water flow going into the steam drum, namely $q_w(t)$, as the output signal. This system has been modeled as a pure delay. Therefore, in order to get a linear approximation of it, the following Padé first-order approximation of a pure delay has been considered:

$$\frac{q_w(s)}{q'_w(s)} \approx \frac{\left(1-\frac{\Delta T_w}{2}\cdot s\right)}{\left(1+\frac{\Delta T_w}{2}\cdot s\right)} \tag{4.5}$$

where the variable s denotes the representation in terms of Laplace transforms, $\Delta T_w = 10$ [sec] is the water time delay, and the corresponding State Space representation of this model is:

$$\left[\begin{array}{c|c} A_{pw} & B_{pw} \\ \hline C_{pw} & D_{pw} \end{array}\right] = \left[\begin{array}{c|c} \Delta T_w/2 & \Delta T_w \\ \hline 1 & \text{-1} \end{array}\right] \tag{4.6}$$

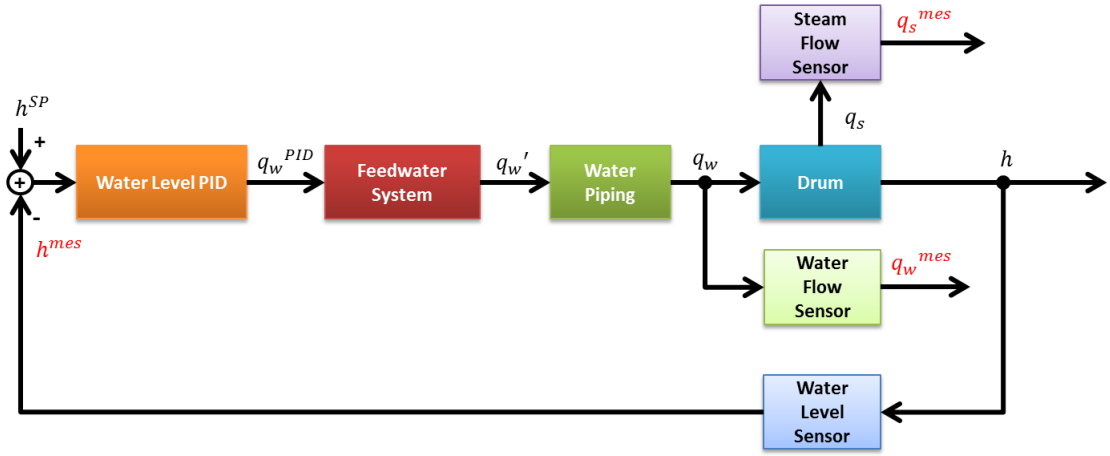

Figure 4.2: Nonlinear Steam Separator System Model

4.1.3 Steam Drum Linear Model

The steam drum is the main part of the boiler, where the water is converted into steam and also residual drops of water are removed from the steam. According to figure 4.2, this sub-system can be modeled as a SISO system having as input signal the overall flow going into the drum, computed as the difference between the water flow pumped into the drum and the steam flow leaving the steam drum, namely the difference signal $q_w(t) - q_s(t)$, and as output signal the water level inside the drum, namely $h(t)$. In accordance with [Aldian Ambark Shashoa et al., 2013], the dynamic of the steam drum has been modeled as a pure integrator as follows:

$$\frac{h(s)}{q_w(s) - q_s(s)} \approx \frac{1}{1000 \cdot \left(d^2 \frac{\pi}{4}\right) s} \approx 0.0003 \frac{1}{s} \tag{4.7}$$

where the variable s denotes the representation in terms of Laplace transforms, and d is the steam drum's diameter

The corresponding State Space representation of this models is:

$$\left[\begin{array}{c|cc} A_d & B_d \\ \hline C_d & D_d \end{array}\right] = \left[\begin{array}{c|cc} 0 & 1 & -1 \\ \hline 1 & 0 & 0 \end{array}\right] \tag{4.8}$$

4.1.4 Steam Separator Forward Path Linearized Model

The attention was focused on the forward path of the steam separator, that is where the separation between water and steam occurs. In accordance with the scheme in figure 4.4, this forward path results to be the series of the following sub-systems, respectively: feedwater system, water piping, and steam drum. By properly combining the linearized version of those dynamics, the following 4th order stable MIMO (2in - 2 out) LTI dynamic model has been derived:

$$\begin{aligned} \dot{\boldsymbol{x}} &= A\boldsymbol{x} + B_1 u_1 + B_2 u_2 \\ \boldsymbol{y} &= C\boldsymbol{x} \end{aligned} \tag{4.9}$$

where $\boldsymbol{x} = [x_1, x_2, x_3, x_4]^T \in \Omega \subset \mathbb{R}^4$ represents the system's state, with: $x_1 = h(t)$, $x_2 = q_w(t)$, $x_3 = q_w'(t)$ and $x_4 = \dot{q_w}'(t)$, whereas $u_1 = q_s(t)$ and $u_2 = q_w^{PID}(t)$ are its inputs and

$\boldsymbol{y} = [y_1, y_2]^T = [h(t), q_w(t)]^T \in \mathbb{R}^2$ are its output vector. Ω is a neighborhood of the system working point.

As stated above, the system under analysis is highly complex. Indeed, besides the processes which take place are nonlinear, also the water-steam boundary is not clear, because the drum contains a mixture of both in a diphasic state and, in addition, the steam pressure affects the water level [Aldian Ambark Shashoa et al., 2013]. However, given the ultimate goal to provide a simple and sufficiently accurate mathematical description of the process, and reminding that, due to the control action of the system, the water level is maintained around a nominal value of $\bar{y}_1 \approx h^{SP} = 8$ [m], with approximatively $\bar{y}_2 = y_2(\infty) \approx 200$ [m^3/sec] of nominal inlet water flow, see e.g. the bottom plots in Figure 4.3, a linear approximation of the plant around this nominal working point has been identified, according to [Aldian Ambark Shashoa et al., 2013, Kvaščev et al., 2011].

Matrices $A \in \mathbb{R}^{4\times4}$, $B_1 \in \mathbb{R}^{4\times1}$, $B_2 \in \mathbb{R}^{4\times1}$, $C \in \mathbb{R}^{2\times4}$, in accordance with the previous treatment, are denoted as follows:

$$\left[\begin{array}{c:cc} A & B_1 & B_2 \\ \hdashline C & & \end{array}\right] = \left[\begin{array}{cccc:cc} 0 & 0.0003 & 0 & 0 & -0.0003 & 0 \\ 0 & 0 & 1 & 0 & 0 & 0 \\ 0 & 0 & 0 & 1 & 0 & -0.1685 \\ 0 & -0.0169 & -0.1458 & -0.5077 & 0 & 0.1193 \\ \hdashline 1 & 0 & 0 & 0 & & \\ 0 & 1 & 0 & 0 & & \end{array}\right] \tag{4.10}$$

In accordance with definitions provided in Section 3.2.1, the pair (A, C) of the nominal system (4.10) is observable with observability indices $\{r_1 = 1, r_2 = 3\}$ such that $\sum_{i=1}^{2} r_i = 4$. Worth also to remark that matrix A has a zero column, i.e., the inherent integrating effect of drum is preserved.

To confirm the effectiveness of the proposed model, the two bottom plots of Figure 4.3 show a comparison between the measured and the estimated system's outputs. During the test, the system model (4.10) was fed by real inputs collected over a period of 3 hours of operation, which are reported in the two top plots of Figure 4.3. The model's output closely follow the measured variables and thus the proposed model is validated.

4.1.5 Sensor Fault Modeling

Due to the fact that nowadays control signals are available to the supervisory system, e.g. SCADA, and the PID/PLC integrates diagnostic routines, u_2 can be assumed as fault-free. Data from the field are stored in the SCADA system with a sampling period of 1 [sec].

Taking into account the operating conditions, e.g. extreme pressures and temperatures, sedimentation of substances and erosion of material, the most frequent class of faults are not related to ageing, but to performance degradation of the measurement devices. Such faults or measurement errors are multiplicative and result to be hardly detectable, even virtually undetectable by simple methods based on thresholds checking, e.g. $4 \div 20$ [mA] signalling protocol.

From that, since all the field measurement, i.e. u_1, y_1 and y_2, may be faulty, according to

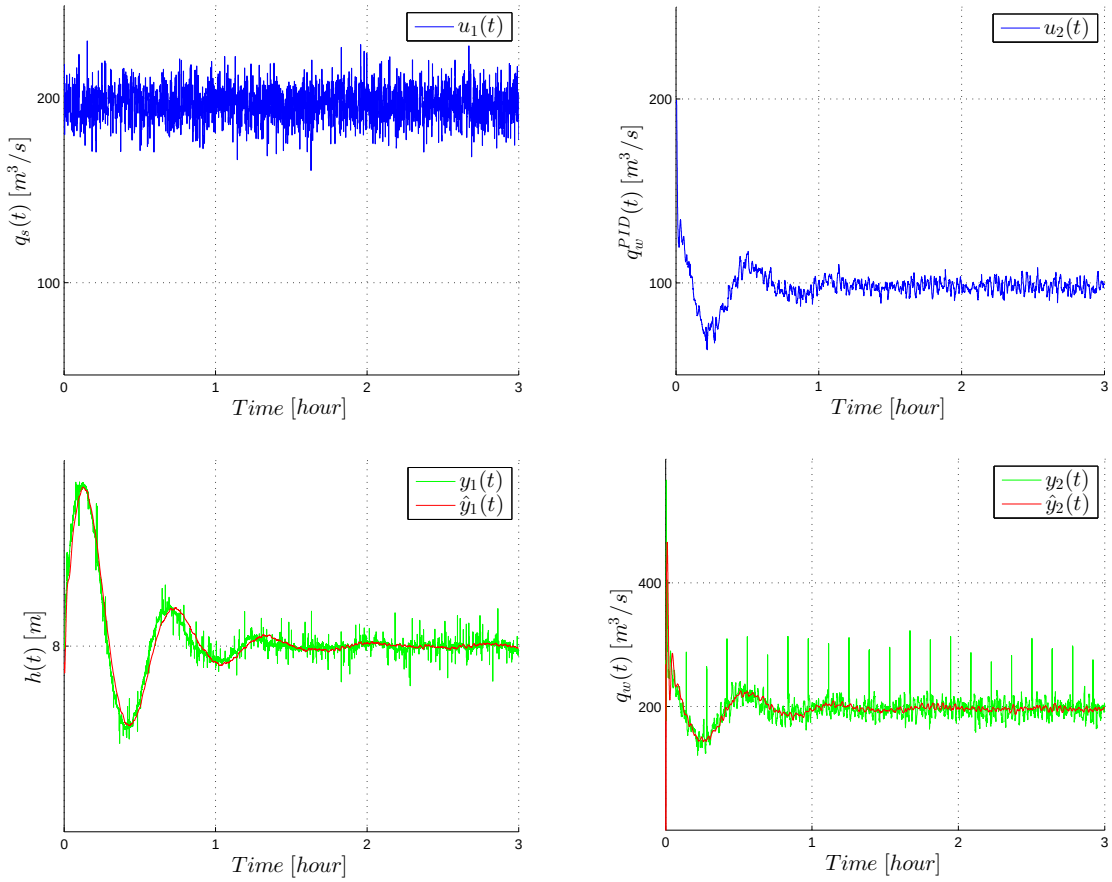

Figure 4.3: **Top:** System's inputs. **Bottom:** Comparison between measured (green) and estimated (red) outputs.

definitions provided in Section 1.2.2, the system (4.9) can be rewritten as follows:

$$\begin{aligned} \dot{\boldsymbol{x}} &= A\boldsymbol{x} + B_1 u_1 + B_2 u_2 + B_1 f_{u_1} \\ \boldsymbol{y} &= C\boldsymbol{x} + \boldsymbol{f}_y \end{aligned} \tag{4.11}$$

where

$$f_{u_1} = \xi u_1 \quad , \quad \boldsymbol{f}_y = [f_{y_1}\ ,\ f_{y_2}]^T = [\mu_1 x_1\ ,\ \mu_2 x_2]^T \tag{4.12}$$

represent respectively the faulty symptoms in the input and output measurements. Worth also to remark that, due to working constraints, the whole set of system trajectories are always bounded during operation, i.e. the water level and water flow are approximatively constant, therefore it holds:

$$\|f_{u_1}(t)\| \leq \sigma(t) \quad , \quad \|\boldsymbol{f}_y(t)\| \leq \rho(t) \tag{4.13}$$

where $\sigma(t)$ and $\rho(t)$ are known continuous function associated to the sensors full-scale. Hence, the measurement acquired by the three sensors in Figure 4.2 are denoted by the following quantities:

$$\begin{aligned} q_s^{mes} &= u_1^{mes} = u_1 + f_{u_1} = (1+\xi)u_1 \\ h^{mes} &= y_1^{mes} = y_1 + f_{y_1} = (1+\mu_1)y_1 \\ q_w^{mes} &= y_2^{mes} = y_2 + f_{y_2} = (1+\mu_2)y_2 \end{aligned} \tag{4.14}$$

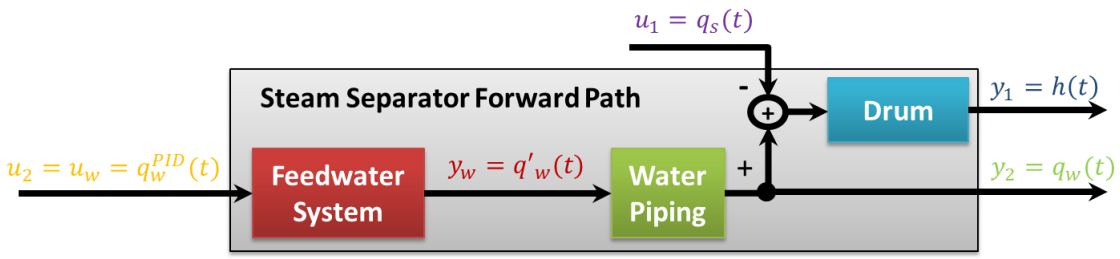

Figure 4.4: Inputs and outputs of the Steam Separator Forward Path and Feedwater System models

It is worth also to note that, if there is no fault, all symptoms are zero, i.e. $f_{u_1} = 0, \boldsymbol{f}_y = 0$. Thus, the faulty model (4.11) degenerates into the nominal one in (4.9).

4.1.6 Actuator Fault Modeling

In order to verify as much as possible the effectiveness of the proposed FDD approach, in this application also the controller device has been modeled as a potentially faulty component, even though, as mentioned in Sections 1.2.2 and 4.1.5, such systems are typically considered fault-free. This further condition has been taken into account in addition to the fault modeling approach depicted in Section 4.1.5, by focusing on the sub-dynamic of the steam separator related to the feedwater system. Referring to the Section 4.1.1, the feedwater system has been modeled as the following second order stable SISO LTI dynamic system:

$$\begin{aligned} \dot{\boldsymbol{x}}_w &= A_w \boldsymbol{x}_w + B_w u_w \\ y_w &= C_w \boldsymbol{x}_w \end{aligned} \tag{4.15}$$

where $\boldsymbol{x}_w = [x_{1_w}, x_{2_w}]^T \in \Omega_w \subset \mathbb{R}^2$ represents the system's state, with: $x_{1_w} = q'_w(t)$, $x_{2_w} = \dot{q_w}'(t)$, whereas $u_w = q_w^{PID}(t)$ and $y_w = q'_w(t)$ are the system's input and output, respectively. Ω_w is a neighborhood of the system working point.

Therefore, different residuals have been generated for this purpose, based on a different SMO which works in parallel to the SMO designed for the forward path of the steam separator. Recalling the remark 1 of Section 1.2.2, since in this case the control action is performed by a digital computer, the actuators installed on the feedwater system can be considered as a component of the whole controller device. As a consequence, the fault on the PID controller can be modeled as an actuator fault affecting the feedwater system. Thus, taking into account the same approach considered in Section 4.1.5 for modeling the faults on sensors, and according to definitions provided in Section 1.2.2, the system (4.15) can be rewritten as follows:

$$\begin{aligned} \dot{\boldsymbol{x}}_w &= A_w \boldsymbol{x}_w + B_w u_w + B_w f_{u_w} \\ y_w &= C_w \boldsymbol{x}_w + f_{y_w} \end{aligned} \tag{4.16}$$

where

$$f_{u_w} := \xi_w u_w \quad , \quad f_{y_w} := \mu_w y_w \tag{4.17}$$

denote the faulty symptoms in the PID controller output, and in the water flow sensor installed before the water piping, i.e. the input and the output of the feedwater system, respectively. According to the remark of Section 4.1.5, the same boundness conditions hold:

$$\|f_{u_w}(t)\| \leq \sigma_w(t) \quad , \quad \|f_{y_w}(t)\| \leq \rho_w(t) \tag{4.18}$$

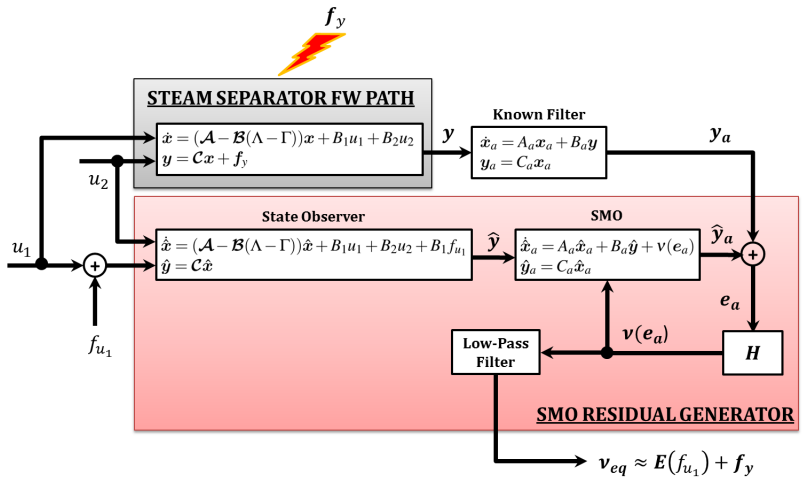

Figure 4.5: Steam Separator Forward Path SMO Residual Generator

where $\sigma_w(t)$ and $\rho_w(t)$ are known continuous function associated to the full-scale of their respective device.

Hence, the process signals in Figure 4.2 are denoted by the following quantities:

$$\begin{aligned} q_w^{PID} &= u_w^{PID} = u_w + f_{u_w} = (1+\xi_w)u_w \\ q'_w &= y_w^{mes} = y_w + f_{y_w} = (1+\mu_w)y_w \end{aligned} \tag{4.19}$$

Again, when there is no fault, both symptoms are zero, i.e. $f_{u_w} = 0$, $f_{y_w} = 0$. Thus, the faulty model (4.16) degenerates into the nominal one in (4.15).

4.2 SMO Design

For both the steam separator forward path and the feedwater system, the residual generator has been implemented according with the scheme discussed in Section 3.2.

4.2.1 Steam Separator Forward Path SMO

At first, the following remark about the modeling of the fault signal f_{u_1} need to be considered.

Remark 7. *In the Steam Separator forward path faulty model (4.11), the fault signal f_{u_1} refers to a sensor fault in place of an actuator fault on the input channel. As a consequence, since the scenario considers both input and output measurement faults, the original scheme in Figure 3.2 was modified as depicted in Figure 4.5.*

Therefore, according with Section 3.2.1, the model (4.11) becomes:

$$\begin{aligned} \dot{\boldsymbol{x}} &= A\boldsymbol{x} + B_1u_1 + B_2u_2 \\ \boldsymbol{y} &= C\boldsymbol{x} + \boldsymbol{f}_y \end{aligned} \tag{4.20}$$

and its corresponding Brunowsky canonical representation is:

$$\begin{aligned} \dot{\boldsymbol{x}} &= (\boldsymbol{\mathcal{A}} - \boldsymbol{\mathcal{B}}\Lambda)\boldsymbol{x} + \boldsymbol{\mathcal{B}}\Gamma\boldsymbol{x} + B_1u_1 + B_2u_2 \\ \boldsymbol{y} &= \boldsymbol{\mathcal{C}}\boldsymbol{x} + \boldsymbol{f}_y \end{aligned} \tag{4.21}$$

where matrices $\{\boldsymbol{\mathcal{A}}\ ,\ \boldsymbol{\mathcal{B}}\ ,\ \boldsymbol{\mathcal{C}} = C\}$, are selected in accordance with (3.5), Λ is an arbitrary matrix such that $(\boldsymbol{\mathcal{A}} - \boldsymbol{\mathcal{B}}\Lambda)$ is Hurwitz, whereas Γ is chosen such that $A = (\boldsymbol{\mathcal{A}} - \boldsymbol{\mathcal{B}}(\Lambda - \Gamma))$. Furthermore, according to (3.10), the following constraint needs to be satisfied in order to make feasible the design of the observer:

$$\|\Gamma \boldsymbol{x} - \Gamma \hat{\boldsymbol{x}}\| \leq \beta \|\boldsymbol{x} - \hat{\boldsymbol{x}}\| \tag{4.22}$$

for any $\boldsymbol{x}$, $\hat{\boldsymbol{x}} \in \Omega \subset \mathbb{R}^4$, with $\beta \in \mathbb{R}^+$. Worth to remark that the decomposition (4.21) preserves the own dynamic of the system in (4.20) and, since the system (4.9) is in an observable canonical form, i.e. $y_1 \equiv x_1$ and $y_2 \equiv x_2$, no further transformation $T(\Omega) : \boldsymbol{x} \mapsto \boldsymbol{z}$ is required.

The augmented dynamics of (4.21) is:

$$\begin{aligned} \dot{\boldsymbol{x}} &= (\boldsymbol{\mathcal{A}} - \boldsymbol{\mathcal{B}}\Lambda)\boldsymbol{x} + \boldsymbol{\mathcal{B}}\Gamma\boldsymbol{x} + B_1 u_1 + B_2 u_2 \\ \dot{\boldsymbol{x}}_a &= A_a \boldsymbol{x}_a + B_a \boldsymbol{\mathcal{C}}\boldsymbol{x} + B_a \boldsymbol{f}_y \\ \boldsymbol{y}_a &= C_a \boldsymbol{x}_a \end{aligned} \tag{4.23}$$

where $\boldsymbol{x}_a \in \mathbb{R}^2$ and $\boldsymbol{y}_a \in \mathbb{R}^2$ are respectively the state and output's vectors of a suitably designed filter described by matrices $\{A_a\ ,\ B_a = I_2\ ,\ C_a = I_2\}$.

The corresponding observer dynamic of (4.23) is:

$$\begin{aligned} \dot{\hat{\boldsymbol{x}}} &= (\boldsymbol{\mathcal{A}} - \boldsymbol{\mathcal{B}}\Lambda)\hat{\boldsymbol{x}} + \boldsymbol{\mathcal{B}}\Gamma\hat{\boldsymbol{x}} + B_1 u_1 + B_2 u_2 + B_1 f_{u_1} \\ \dot{\hat{\boldsymbol{x}}}_a &= A_a \hat{\boldsymbol{x}}_a + B_a \boldsymbol{\mathcal{C}}\hat{\boldsymbol{x}} + \nu(t, \boldsymbol{y}_a, \hat{\boldsymbol{y}}_a) \\ \hat{\boldsymbol{y}}_a &= C_a \hat{\boldsymbol{x}}_a \end{aligned} \tag{4.24}$$

where $\nu(t, \boldsymbol{y}_a, \hat{\boldsymbol{y}}_a)$ is the so-called unit-vector SMC algorithm defined in 3.13.

In accordance with definitions given in (3.14) and (3.15), from (4.23) and (4.24) it results:

$$\dot{\boldsymbol{e}} = (\boldsymbol{\mathcal{A}} - \boldsymbol{\mathcal{B}}(\Lambda - \Gamma))\boldsymbol{e} - B_1 f_{u_1} \tag{4.25}$$

$$\dot{\boldsymbol{e}}_a = A_a \boldsymbol{e}_a + \boldsymbol{\mathcal{C}}\boldsymbol{e} + \boldsymbol{f}_y - \nu(\boldsymbol{e}_a) \tag{4.26}$$

where the input measurement fault term $B_1 f_{u_1}$ in (4.25) makes the role of the disturbance vector $\Psi(\boldsymbol{z})$ in (3.16).

Hence, the two error dynamics (4.25) and (4.26) have respectively the same form as in (3.16), and (3.17) and the whole observer design procedure can be applied with any difference. As a consequence, it results that by an analogous analysis as in Section 3.2.2, the design parameters of the SMO can be found by solving the following LMI convex optimization problem:

$$\begin{gathered} \min_{P,X}\ \gamma \qquad \text{subject to :} \\ \begin{bmatrix} (\boldsymbol{\mathcal{A}} - \boldsymbol{\mathcal{B}}\Lambda)^T P + P(\boldsymbol{\mathcal{A}} - \boldsymbol{\mathcal{B}}\Lambda) + \varepsilon_1 \beta^2 I_4 + X & P\boldsymbol{\mathcal{B}} \\ \boldsymbol{\mathcal{B}}^T P & -\varepsilon_1 I_2 \end{bmatrix} < 0 \\ I_4 < P \quad , \quad P < \gamma X \end{gathered} \tag{4.27}$$

where $X \in \mathbb{R}^{4\times 4}$ is a symmetric positive definite "slack" variable, whereas $\varepsilon_1 > 0$ and $\gamma > 0$ are arbitrary constants.

Hence, a sliding motion is achieved after a finite transient along the manifold (3.26). From that, since $\dot{\boldsymbol{e}}_a = \boldsymbol{e}_a = 0$, according to Preposition 3 in Section 3.2.2.2, the reduced order error state $\boldsymbol{e}$ results to be optimally, uniformly bounded with respect to:

$$\mathscr{B} = \left\{ \boldsymbol{e} \mid \boldsymbol{e}^T P \boldsymbol{e} \leq \gamma^2 (d + \varepsilon_2)^2 \right\} \quad \forall \varepsilon_2 > 0 \tag{4.28}$$

where d is a known constant satisfying the following constraint related to the magnitude of the faults on the input channels, according to (3.44):

$$\|P^{1/2}B_1 f_{u_1}\| \leq \frac{1}{\gamma}\|B_1\sigma(t)\| \leq \frac{1}{2}d \tag{4.29}$$

Furthermore, once the sliding mode condition is achieved, the fault symptoms in the output measurement vector $\boldsymbol{y}$ can be estimated by exploiting the concept of equivalent control, i.e. (3.39), since it results:

$$\nu_{eq} = \mathcal{C}\boldsymbol{e} + \boldsymbol{f}_y \tag{4.30}$$

where ν_{eq} is obtained by low-pass filtering of the discontinuous signal $\nu(t)$, as in (3.40).

By substituting the matrix $\mathcal{C} = C$, the two components of the equivalent output error injection vector $\nu_{eq} = [\nu_{eq1}\ ,\ \nu_{eq2}]^T$ assume the following explicit form:

$$\begin{aligned} \nu_{eq1} &= e_1 + f_{y_1} \\ \nu_{eq2} &= e_2 + f_{y_2} \end{aligned} \tag{4.31}$$

where the two components of the error vector $\boldsymbol{e} = [e_1\ ,\ e_2]^T$ are the solution of the following ODEs:

$$\begin{aligned} \dot{e}_1 &= -0.0003 f_{u_1} \\ \dddot{e}_2 + 0.5077\ddot{e}_2 + 0.1458\dot{e}_2 + 0.0169 e_2 &= 0 \end{aligned} \tag{4.32}$$

As a consequence, it result that e_2 is vanishing, and then ν_{eq2} is able to exactly estimate the fault symptom associated to the water flow measurement. On the other hand, due to the particular structure of the system, see Figure 4.4 and the first row of the matrix in (4.10), the injection term associated to the steam drum includes both the fault symptoms associated to this dynamic, which are the measurement errors related to the water level and the steam flow sensors. Actually, it results:

$$\begin{aligned} \nu_{eq1}(t) &= -0.0003 \int_0^t f_{u_1}(\tau)d\tau + f_{y_1}(t) \\ \nu_{eq2}(t) &= f_{y_2}(t) \end{aligned} \tag{4.33}$$

Remark 8. *In order to correctly extract the whole information about the faults, a further filtering effect of the signal $\nu(\boldsymbol{e}_a)$ must be avoided. Hence, since the relative degree between the filter output $\boldsymbol{y}_a$ and the output injection $\nu(\boldsymbol{e}_a)$ is 1, the componentwise super-twisting control law [Levant, 1998]*

$$\nu_i(e_{ai}(t)) = k_{i1}|\ e_{ai}(t)\ |^{1/2}\text{sign}(e_{ai}(t)) + k_{i2}\int \text{sign}(e_{ai}(\tau))d\tau \tag{4.34}$$

with $i = 1,2$ has been used in place of (3.13). This allows to avoid the low pass filtering of $\nu(\boldsymbol{e}_a)$ in order to extract the equivalent control ν_{eq}, as the next condition

$$\nu_i(e_{ai}(t)) = \nu_{eq_i}(t) \tag{4.35}$$

is in force after the sliding mode has been established along the manifold $\boldsymbol{e}_a(t) = 0$.

The Figure 4.6 shows the effectiveness of the proposed approach in terms of fault detection capability, and at the same time confirms the fact that the two residuals generated by the SMO are influenced by the whole set of faults, i.e. those affecting the steam flow, water level and water flow sensors.

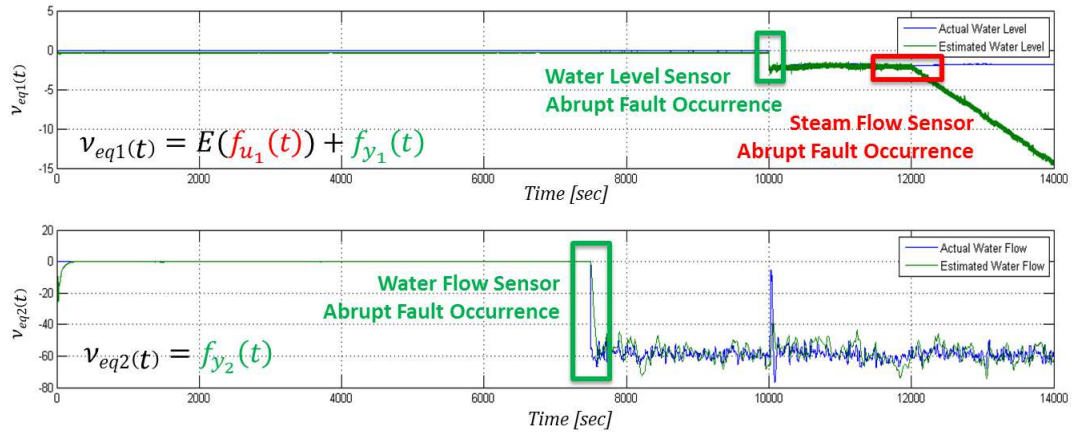

Figure 4.6: Fault Detection results by using the Steam Separator Forward Path SMO

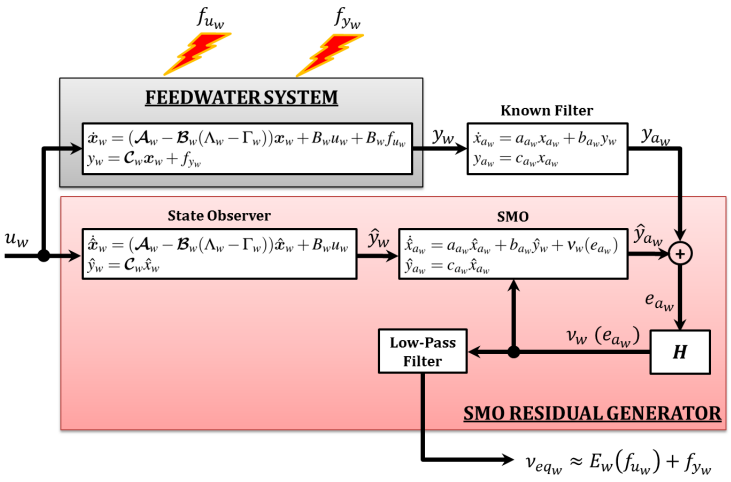

Figure 4.7: Feedwater System SMO Residual Generation

4.2.2 Feedwater System SMO

Remark 9. *Since in the feedwater system faulty model (4.16) both the sensor and the actuator can be affected by faults, thus the scheme of the SMO residual generator related to a generic system, depicted in Figure 3.2, and the scheme related to the feedwater system SMO residual generator, depicted in Figure 4.7, reflect the same configuration.*

According with Section 3.2.1, the model (4.16) can be decomposed in its corresponding Brunowsky canonical representation, that is:

$$\begin{aligned} \dot{x}_w &= (\mathcal{A}_w - \mathcal{B}_w\Lambda_w)x_w + \mathcal{B}_w\Gamma_w x_w + B_w u_w + B_w f_{u_w} \\ y_w &= \mathcal{C}_w x_w + f_{y_w} \end{aligned} \tag{4.36}$$

where matrices $\{\mathcal{A}_w\ ,\ \mathcal{B}_w\ ,\ \mathcal{C}_w = C_w\}$, are selected in accordance with (3.5), Λ_w is an arbitrary matrix such that $(\mathcal{A}_w - \mathcal{B}_w\Lambda_w)$ is Hurwitz, whereas Γ_w is chosen such that $A_w = (\mathcal{A}_w - \mathcal{B}_w(\Lambda_w - \Gamma_w))$. Furthermore, according to (3.10), the following constraint needs to be satisfied in order to make feasible the design of the observer:

$$\|\Gamma_w x_w - \Gamma\hat{x}_w\| \leq \beta_w \|x_w - \hat{x}_w\| \tag{4.37}$$

for any $\boldsymbol{x}_w$, $\hat{\boldsymbol{x}}_w \in \Omega_w \subset \mathbb{R}^2$, with $\beta_w \in \mathbb{R}^+$. Worth to remark that the decomposition (4.36) preserves the own dynamic of the system in (4.16) and, since the system (4.15) is in an observable canonical form, i.e. $y_w \equiv x_{1_w}$, no further transformation $T(\Omega_w) : \boldsymbol{x}_w \mapsto \boldsymbol{z}_w$ is required.

The augmented dynamic of (4.36) is:

$$\begin{aligned} \dot{\boldsymbol{x}}_w &= (\boldsymbol{\mathcal{A}}_w - \boldsymbol{\mathcal{B}}_w\Lambda_w)\boldsymbol{x}_w + \boldsymbol{\mathcal{B}}_w\Gamma_w\boldsymbol{x}_w + B_w u_w + B_w f_{u_w} \\ \dot{x}_{a_w} &= a_{a_w}x_{a_w} + b_{a_w}\boldsymbol{\mathcal{C}}_w\boldsymbol{x}_w + b_{a_w}f_{y_w} \\ y_{a_w} &= c_{a_w}x_{a_w} \end{aligned} \tag{4.38}$$

where $x_{a_w} \in \mathbb{R}$ and $y_{a_w} \in \mathbb{R}$ are respectively the state and the output of a suitably designed filter described by the scalars $\{a_{a_w}\ ,\ b_{a_w} = 1\ ,\ c_{a_w} = 1\}$.

The corresponding observer dynamic of (4.38) is:

$$\begin{aligned} \dot{\hat{\boldsymbol{x}}}_w &= (\boldsymbol{\mathcal{A}}_w - \boldsymbol{\mathcal{B}}_w\Lambda_w)\hat{\boldsymbol{x}}_w + \boldsymbol{\mathcal{B}}_w\Gamma_w\hat{\boldsymbol{x}}_w + B_w u_w \\ \dot{\hat{x}}_{a_w} &= a_{a_w}\hat{x}_{a_w} + b_{a_w}\boldsymbol{\mathcal{C}}_w\hat{\boldsymbol{x}}_w + \nu_w(t, y_{a_w}, \hat{y}_{a_w}) \\ \hat{y}_{a_w} &= c_{a_w}\hat{x}_{a_w} \end{aligned} \tag{4.39}$$

where $\nu_w(t, y_{a_w}, \hat{y}_{a_w})$ is the so-called unit-vector SMC algorithm defined in 3.13.

In accordance with definitions given in 3.14 and 3.15, it follows from (4.38) and (4.39) that:

$$\dot{\boldsymbol{e}}_w = (\boldsymbol{\mathcal{A}}_w - \boldsymbol{\mathcal{B}}_w(\Lambda_w - \Gamma_w))\boldsymbol{e}_w + B_w f_{u_w} \tag{4.40}$$

$$\dot{e}_{a_w} = a_{a_w}e_{a_w} + \boldsymbol{\mathcal{C}}_w\boldsymbol{e}_w + f_{y_w} - \nu_w(e_{a_w}) \tag{4.41}$$

where the input measurement fault term $B_w f_w$ in (4.40) makes the role of the disturbance vector $\Psi(\boldsymbol{z})$ in (3.16).

Hence, the two error dynamics (4.40) and (4.41) have respectively the same form as in (3.16), and (3.17) and the whole observer design procedure can be applied with any difference. As a consequence, it results that by an analogous analysis as in Section 3.2.2, the design parameters of the SMO can be found by solving the following LMI convex optimization problem:

$$\begin{gathered} \min_{P_w, X_w}\ \gamma_w \qquad \text{subject to :} \\ \left[\begin{array}{cc} (\boldsymbol{\mathcal{A}}_w - \boldsymbol{\mathcal{B}}_w\Lambda_w)^T P_w + P_w(\boldsymbol{\mathcal{A}}_w - \boldsymbol{\mathcal{B}}_w\Lambda_w) + \varepsilon_{1_w}\beta_w^2 I_2 + X_w & P_w\boldsymbol{\mathcal{B}}_w \\ \boldsymbol{\mathcal{B}}_w^T P_w & -\varepsilon_{1_w} \end{array}\right] < 0 \\ I_2 < P_w \quad , \quad P_w < \gamma_w X_w \end{gathered} \tag{4.42}$$

where $X_w \in \mathbb{R}^{2\times 2}$ is a symmetric positive definite "slack" variable, whereas $\varepsilon_{1_w} > 0$ and $\gamma_w > 0$ are arbitrary constants.

Hence, a sliding motion is achieved after a finite transient along the manifold (3.26). From that, since $\dot{e}_{a_w} = e_{a_w} = 0$, according to Preposition 3 in Section 3.2.2.2, the reduced order error state $\boldsymbol{e}_w$ results to be optimally, uniformly bounded with respect to:

$$\mathscr{B}_w = \left\{ \boldsymbol{e}_w \mid \boldsymbol{e}_w^T P_w \boldsymbol{e}_w \le \gamma_w^2 \left(d_w + \varepsilon_{2_w}\right)^2 \right\} \quad \forall \varepsilon_{2_w} > 0 \tag{4.43}$$

where d_w is a known constant satisfying the following constraint related to the magnitude of the faults on the input channels, according to (3.44):

$$\|P_w^{1/2} B_w f_{u_w}\| \le \frac{1}{\gamma}\|B_w\sigma_w(t)\| \le \frac{1}{2}d_w \tag{4.44}$$

Furthermore, once the sliding mode condition is achieved, the fault symptoms in the output measurement signal y_w can be estimated by exploiting the concept of equivalent control, i.e. (3.39), since it results:

$$\nu_{eq_w} = e_w + f_{y_w} \tag{4.45}$$

where ν_{eq_w} is obtained by low-pass filtering of the discontinuous signal $\nu_w(t)$, as in (3.40), and e_w is the solution of the following ODE:

$$\ddot{e}_w + 0.3077\dot{e}_w + 0.0843 e_w = -0.1685 f_{u_w} \tag{4.46}$$

As a consequence, it result that, due to the particular structure of the system, the injection term ν_{eq_w} includes both symptoms of the faults related to the PID controller and the feedwater dynamic: Therefore, (4.45) can be expressed also as:

$$\nu_{eq_w}(t) = E_w(f_{u_w}(t)) + f_{y_w}(t) \tag{4.47}$$

Remark 10. *In order to correctly extract the whole information about the faults, a further filtering effect of $\nu_w(e_{a_w})$ must be avoided. Hence, since the relative degree between the filter output y_{a_w} and the output injection $\nu_w(e_{a_w})$ is 1, the componentwise super-twisting control law [Levant, 1998]*

$$\nu_w\left(e_{a_w}(t)\right) = k_{1_w} \mid e_{a_w}(t) \mid^{1/2} \text{sign}(e_{a_w}(t)) + k_{2_w} \int \text{sign}(e_{a_w}(\tau)) d\tau \tag{4.48}$$

has been used in place of (3.13). This allows to avoid the low pass filtering of $\nu_w(e_{a_w})$ in order to extract the equivalent control ν_{eq_w}, as the next condition

$$\nu_w(e_{a_w}(t)) = \nu_{eq_w}(t) \tag{4.49}$$

is in force after the sliding mode has been established along the manifold $e_{a_w}(t) = 0$.

The Figure 4.8 shows the effectiveness of the fault detection capability for the feedwater system also, and at the same time confirms the fact that the residual signal generated by the observer in this case is influenced by both faults acting on the input and output of the system, i.e. those affecting the PID controller and the water flow sensor installed at the beginning of the water piping.

4.3 Residual Set Design

4.3.1 Steam Separator Forward Path Fault Signatures

According with the scheme in Figure 4.5, the following two-dimensional residual vector was generated by the SM-based residual generator depicted in Section 4.2.1:

$$\boldsymbol{r} = \nu_{eq} \;\Rightarrow\; [r_{y_1}\ ,\ r_{y_2}] = [\nu_{eq_1}\ ,\ \nu_{eq_2}] \;\Rightarrow\; \begin{cases} \nu_{eq_1}(t) = r_{y_1}(f_{y_1}(t), f_{u_1}(t)) \\ \nu_{eq_2}(t) = r_{y_2}(f_{y_2}(t)) \end{cases} \tag{4.50}$$

As discussed in Section 4.2, the two components of the residual vector $\boldsymbol{r}$ are influenced by the whole set of faults, i.e. those affecting the steam-flow, water-level and water-flow sensors. However, as expected, since the number of faults is greater than the number of residuals, two on three faults influence the same residual. Thus, only the fault occurrence

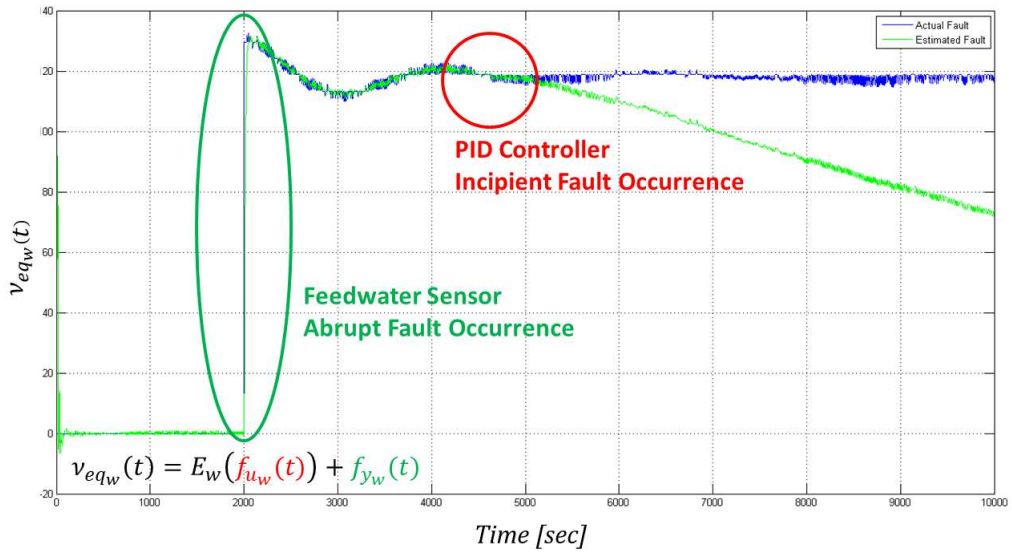

Figure 4.8: Fault Detection results by using the Feedwater System SMO

can be detected, but it is not possible to discriminate between a fault on the steam flow and a fault on the water level, both detected by the injection signal v_{eq1}, whereas the water flow sensor fault can be directly isolated by using only the injection signal v_{eq2}.

Indeed, the isolation of the water flow sensor's fault $f_{y_2}(t)$ can be achieved by a simple threshold checking, typical of a dedicated observer scheme, that is to determine if the considered residual has exceeded or not its threshold, as explained in Section 1.2.5. Hence, in the considered case, a fault in the water flow sensor is detected and isolated if it results:

$$r_{y_2}(t) \geq T_w \;\Rightarrow\; f_{y_2}(t) \neq 0 \tag{4.51}$$

Furthermore, residual r_{y_2} directly gives the shape of the fault such that fault diagnosis can be directly achieved for the water flow sensor.

Threshold checking for residual r_{y_1} cannot guarantee the isolation of the water level and steam flow sensor faults, due to the same sensitivity of r_{y_1} to both faults. Since the sub-dynamic of the steam separator forward path model which affects the output injection v_{eq1} is the steam drum depicted in Section 4.1.3, which is a SISO system, therefore the residual evaluation approach discussed in Section 3.3 can be applied to residual r_{y_1} in order to achieve the complete fault isolation. Both the residual sets R_a and R_b have been designed. According to 3.3.2, in order to obtain the missing component of the residual set R_a, a suitable filtering action on the injection signal v_{eq1} need to be designed.

Remark 11. *Due to the particular structure of the steam drum, the filtering action applied by the functional $E(\cdot)$ to the signal f_{u_1} have the same dynamic of the model, that is a pure integrator:*

$$E(f_{u_1}) = \mathcal{C}e \approx -0.0003 \int_0^t f_{u_1}(\tau)d\tau \tag{4.52}$$

Therefore, the inverse filtering effect en respect to $E(\cdot)$ is a pure differentiator.

By taking into account the Remark 11, and assuming that the dynamics of the fault on the level measurement device is slowly varying with respect to both the system and observer

dynamics, the effect of the fault on the steam flow measurement device can be isolated by differentiating the output injection v_{eq1}.

Since v_{eq1} in (4.33)-(4.34) is continuous but not differentiable, in order to make possible the use of a Levant's robust differentiator [Levant, 1998], and also to reduce the noise propagation, it is filtered by:

$$\begin{aligned} \dot{x}_b &= A_b x_b + B_b v_{eq1} \\ y_b &= C_b x_b \end{aligned} \tag{4.53}$$

where (A_b, B_b, C_b) represents a properly designed low-pass filter having relative degree $m \geq 1$. Then, the output y_b is differentiated by the Levant's robust differentiator [Levant, 1998]

$$\begin{aligned} \dot{z}_1 &= z_2 - \lambda_1 |\, z_1 - y_b \,|^{1/2} \text{sign}(z_1 - y_b) \\ \dot{z}_2 &= -\lambda_2 \text{sign}(z_1 - y_b) \end{aligned} \tag{4.54}$$

with properly chosen gains λ_1, λ_2. Once the differentiator converges, the following condition holds:

$$z_2 = \dot{y}_b \approx \dot{v}_{eq1} = E^{-1}(v_{eq1}) \tag{4.55}$$

Thus, the residual set R_a has been designed as follows:

$$R_a : \begin{cases} r_{a1}(f_{u_1}, f_{y_1}) = v_{eq1} \approx -0.0003 \int_0^t f_{u_1}(\tau) d\tau + f_{y_1} \\ r_{a2}(f_{u_1}) = \bar{v}_{eq1} = z_2 \approx f_{u_1} - 0.0003 \dot{f}_{y_1} \end{cases} \tag{4.56}$$

With this choice, in nominal conditions, the residual set R_a becomes:

$$f_{u_1} = 0 \;,\; f_{y_1} = 0 \;\; \Rightarrow \;\; \begin{cases} r_{a1} \approx 0 \\ r_{a2} \approx 0 \end{cases} \tag{4.57}$$

Therefore, since $\vec{r}_a(t) \approx [0 \;,\; 0]^T$, in this case the residual vector will stay around the origin of the residual space $\mathbb{R}^2$ and, as expected, no trajectory will be depicted.

When a fault occurs on the output channel y_1, the two components of the residual set R_a will raise the following configuration:

$$f_{u_1} = 0 \;,\; f_{y_1} \neq 0 \;\; \Rightarrow \;\; \begin{cases} r_{a1} \approx f_{y_1} \\ r_{a2} \approx \dot{f}_{y_1} \end{cases} \tag{4.58}$$

Consequently, the residual vector $\vec{r}_a$ will start to generate on the residual space $\mathbb{R}^2$ the fault signature:

$$\vec{r}_a(t | f_{y_1}) = \vec{L}_a(f_{y_1}) \approx \langle f_{y_1} \;,\; \dot{f}_{y_1} \rangle \tag{4.59}$$

where the function-valued vector $\vec{L}_a(f_{y_1})$ will reflect the dynamic of the faulty symptom affecting the channel y_1, filtered by the inverse of the functional $E(\cdot)$, which, according to (4.52), is a pure differentiator.

When a fault occurs on the input channel u_1 instead, the following configuration will appear:

$$f_{u_1} \neq 0 \;,\; f_{y_1} = 0 \;\; \Rightarrow \;\; \begin{cases} r_{a1} \approx -0.0003 \int_0^t f_{u_1}(\tau) d\tau \\ r_{a2} \approx f_{u_1} \end{cases} \tag{4.60}$$

Hence, the residual vector $\vec{r}_a$ will start to generate on the residual space $\mathbb{R}^2$ the fault signature:

$$\vec{r}_a(t|f_{u_1}) = \vec{L}_a(f_{u_1}) \approx \left\langle -0.0003 \int_0^t f_{u_1}(\tau)d\tau \ , \ f_{u_1} \right\rangle \tag{4.61}$$

where the function-valued vector $\vec{L}_a(f_{u_1})$ will reflect the dynamic of the faulty symptom affecting the channel u_1, filtered by the functional $E(\cdot)$, i.e. the pure integrator in (4.52).

Therefore, R_a results to be a suitable residual set when it needs to isolate fault affecting both the water level and the steam flow sensor, since the corresponding vector $\vec{r}_a$ is able to generate fault signatures which reflect different dynamics and then which result to be distinguishable.

Nevertheless, as stated in Section 3.3.2, with this configuration it is not possible to discriminate between an abrupt fault on the steam flow sensor, and an incipient fault on the water level sensor, such that: $f_{y_1} \approx \int_0^t f_{u_1}(\tau)d\tau$, because both faults will generate the same fault signature, i.e. $\vec{L}_a(f_{y_1}) \approx \vec{L}_a(f_{u_1}) \approx \langle -0.0003 \int_0^t f_{u_1}(\tau)d\tau, f_{u_1} \rangle$.

In order to overcome this limit, the following residual set was then designed:

$$R_b : \begin{cases} r_{b1}(f_{u_1}, f_{y_1}) = \nu_{eq1} \approx -0.0003 \int_0^t f_{u_1}(\tau)d\tau + f_{y_1} \\ r_{b2}(f_{u_1}, f_{y_1}) = \nu_{eq1}^{\perp} = y_1^{mes} - \nu_{eq1} \approx y_1 + 0.0003 \int_0^t f_{u_1}(\tau)d\tau \end{cases} \tag{4.62}$$

The trajectories of the directional residual vector $\vec{r}_b$, having as components those of the set R_b, will evolve according to the following reasoning. In nominal conditions, as shown in Figure 4.2, at steady state the level of the drum is keep equal to the set point value by the water level PID, i.e. $h^{SP} = y_1^{SP}$. Hence the residual set R_b becomes:

$$f_{u_1} = 0 \ , \ f_{y_1} = 0 \ \Rightarrow \ \begin{cases} r_{b1} \approx 0 \\ r_{b2} \approx y_1^{SP} \end{cases} \tag{4.63}$$

Therefore, $\vec{r}_b$ will stay fixed around the point of the residual space $\mathbb{R}^2$ corresponding to this steady state and its trajectory will not evolve, i.e. $\vec{r}_b(t) \approx [0 \ , \ y_1^{SP}]^T$.

When a fault on the level sensor occurs, then the level of the drum, i.e. y_1, will start changing, until the control loop will not bring back the system to the steady state. When the level will have reached its new constant value, then $\vec{r}_b$ will stay fixed on the point of the residual space corresponding to the new steady state, until the fault f_{y_1} will be on. The configuration assumed by the components of R_b will be then:

$$f_{u_1} = 0 \ , \ f_{y_1} \neq 0 \ \Rightarrow \ \begin{cases} r_{b1} \approx f_{y_1} \\ r_{b2} \approx y_1 \end{cases} \tag{4.64}$$

The important thing to remark is that during this transient, $\vec{r}_b$ will generate on the residual space $\mathbb{R}^2$ the fault signature:

$$\vec{r}_b(t|f_{y_1}) = \vec{L}_b(f_{y_1}) \approx \langle f_{y_1} \ , \ y_1 \rangle \tag{4.65}$$

where the function-valued vector $\vec{L}_b(f_{y_1})$ will be a $2D$ shape strictly correlated to the dynamic of the faulty symptom f_{y_1}.

When a fault on the steam flow sensor occurs instead, this faulty symptom will not have any influence on the level of the drum, and consequently the output of the system will not

move from its nominal conditions, i.e. $y_1 = y_1^{SP}$. The configuration of R_b related to this fault condition will be:

$$f_{u_1} \neq 0 \ , \ f_{y_1} = 0 \ \Rightarrow \ \begin{cases} r_{b1} \approx -0.0003 \int_0^t f_{u_1}(\tau) d\tau \\ r_{b2} \approx y_1^{SP} + 0.0003 \int_0^t f_{u_1}(\tau) d\tau \end{cases} \tag{4.66}$$

Hence, both components of $\vec{r}_b$ are affected in the same way by the faulty symptom. As a consequence, after a certain amount of time, depending on the type and intensity of the fault, the trajectory of $\vec{r}_b$ will tend to converge to the subspace S of $\mathbb{R}^2$ denoted as follows:

$$S = \{(r_{b1}, r_{b2}) \in \mathbb{R}^2 \mid r_{b2} = -r_{b1} + y_1^{SP}\} \tag{4.67}$$

that is the straight line having slope -1 and r_{b2}-intercept y_1^{SP}, until the fault's dynamics will have ended. Hence, in this case the fault signature generated by $\vec{r}_b$ will be:

$$\vec{r}_b(t|f_{u_1}) = \vec{L}_b(f_{u_1}) \approx \left\langle -0.0003 \int_0^t f_{u_1}(\tau) d\tau \ , \ y + 0.0003 \int_0^t f_{u_1}(\tau) d\tau \right\rangle \tag{4.68}$$

where the function-valued vector $\vec{L}_b(f_{u_1})$ will result to be a $2D$ shape convergent to the subspace (4.67).

4.3.2 Feedwater System Fault Signatures

According with the scheme in Figure 4.7, for the residual signal generated by the SMO depicted in Section 4.2.2, only the following residual set has been implemented:

$$R_{b_w} : \begin{cases} r_{b1_w}(f_{u_w}, f_{y_w}) = \nu_{eq_w} \approx E_w(f_{u_w}) + f_{y_w} \\ r_{b2_w}(f_{u_w}, y_w) = \nu_{eq_w}^{\perp} = y_w^{mes} - \nu_{eq_w} \approx y_w - E_w(f_{u_w}) \end{cases} \tag{4.69}$$

The trajectories of the residual vector $\vec{r}_{b_w}$, having as components those of the set R_{b_w}, will evolve according to the same reasoning depicted in Section 3.3.3. Therefore, in the following, only the expressions of the residual signatures and of the curve S_w are reported:

$$\vec{r}_{b_w}(t|f_{y_w}) = \vec{L}_{b_w}(f_{y_w}) \approx \langle f_{y_w} \ , \ y_w \rangle \tag{4.70}$$

$$\vec{r}_{b_w}(t|f_{u_w}) = \vec{L}_{b_w}(f_{u_w}) \approx \langle E_w(f_{u_w}), y_w - E_w(f_{u_w}) \rangle \tag{4.71}$$

$$S_w = \{(r_{b1_w}, r_{b2_w}) \in \mathbb{R}^2 \mid r_{b2_w} = -r_{b1_w} + \bar{y}_w\} \tag{4.72}$$

Since also the feedwater system operates at steady state nominal conditions, then also the curve S_w can be considered as a subspace of $\mathbb{R}^2$, that is the straight line having slope -1 and r_{b2_w}-intercept $\bar{y}_w$.

4.4 Experimental Results

In order to corroborate the validity of the proposed FDI framework, hereinafter some results obtained on a set of real data collected from the the Steam Separator Unit of the Serbian Thermal Power Plant TEKOB1 in Kostolac are presented. The parameter configurations used for the practical implementation of the two SMOs discussed in Sections 4.2.1 and 4.2.2

Parameter	Value
$\Lambda = \begin{bmatrix} \Lambda_1 & \Lambda_2 \end{bmatrix}$	$100 \times \begin{bmatrix} 0.5 & 0 & 0 & 0 \\ 0 & 1250 & 75 & 1.5 \end{bmatrix}^T$
$\{A_a\ ,\ B_a\ ,\ C_a\}$	$\{100I_2\ ,\ I_2\ ,\ I_2\}$
$\{k_{11}\ ,\ k_{12}\}$	$\{2\sqrt{10}\ ,\ 20\}$
$\{k_{21}\ ,\ k_{22}\}$	$\{2\sqrt{10}\ ,\ 20\}$

Table 4.1: design parameter values of the steam separator forward path SMO

Parameter	Value
$\Lambda_w = \begin{bmatrix} \lambda_{1_w}\ ,\ \lambda_{2_w} \end{bmatrix}$	$[3\ ,\ 5]$
$\{a_{a_w}\ ,\ b_{a_w}\ ,\ c_{a_w}\}$	$\{-10\ ,\ 1\ ,\ 1\}$
$\{k_{1_w}\ ,\ k_{2_w}\}$	$\{2\sqrt{10}\ ,\ 90\}$

Table 4.2: design parameter values of the feedwater system SMO

Parameter	Value
$\{A_b\ ,\ B_b\ ,\ C_b\}$	$\{100I_2\ ,\ I_2\ ,\ I_2\}$
$\{\lambda_1\ ,\ \lambda_2\}$	$\{2\sqrt{0.01}\ ,\ 0.01\}$

Table 4.3: Levant's differentiator parameter values

are shown in table 4.1 and 4.2, respectively, whereas the parameter configuration used to implement the Levant's differentiator discussed in Section 4.3 is shown in table 4.3. The optimization parameters of the LMI convex optimization problems in (4.27) and (4.42) were found by using the *gevp* solver available in the Matlab Robust Control Toolbox®.

In order to evaluate a broader set of fault configurations, including different kind of failures, simulations were performed by corrupting healthy real data acquired from the plant with suitable multiplicative faults, according to (4.14) and (4.19). The abrupt faults were modeled according to (1.3), whereas the incipient faults according to (1.4), assuming a fault rise time of 24 hours, i.e. $t_r = 86400$ [sec]. Different percentage of faults were considered, by spanning the values of parameters ξ, μ_1, μ_2, ξ_w and μ_w from 0.05 to 1, which means from 5% to 100% of the device's measurement scale. As an example, when considering an incipient fault having intensity equal to 75%, it means that the faulty device will introduce the 100% of error after 32 hours. Furthermore, in order to validate the robustness of the proposed algorithm against noisy measurements, all the real data, already affected by noise, have been further corrupted by a white-gaussian noise suitably designed to simulate the standard level of signal-to-noise ratio for industrial data-acquisition systems, i.e. SNR = 80 [dB] [Pachchigar, 2013].

The four plots in the Figure 4.9 provide a comparison among the actual value the and measurement acquired by the water level and the steam flow sensors, which are the two devices whose fault diagnosis cannot be directly performed by only using the SMO, since both are detected by the same output injection signal. For each measurement, three different percentages of fault intensity are considered: low intensity (25%), denoted by the red color,

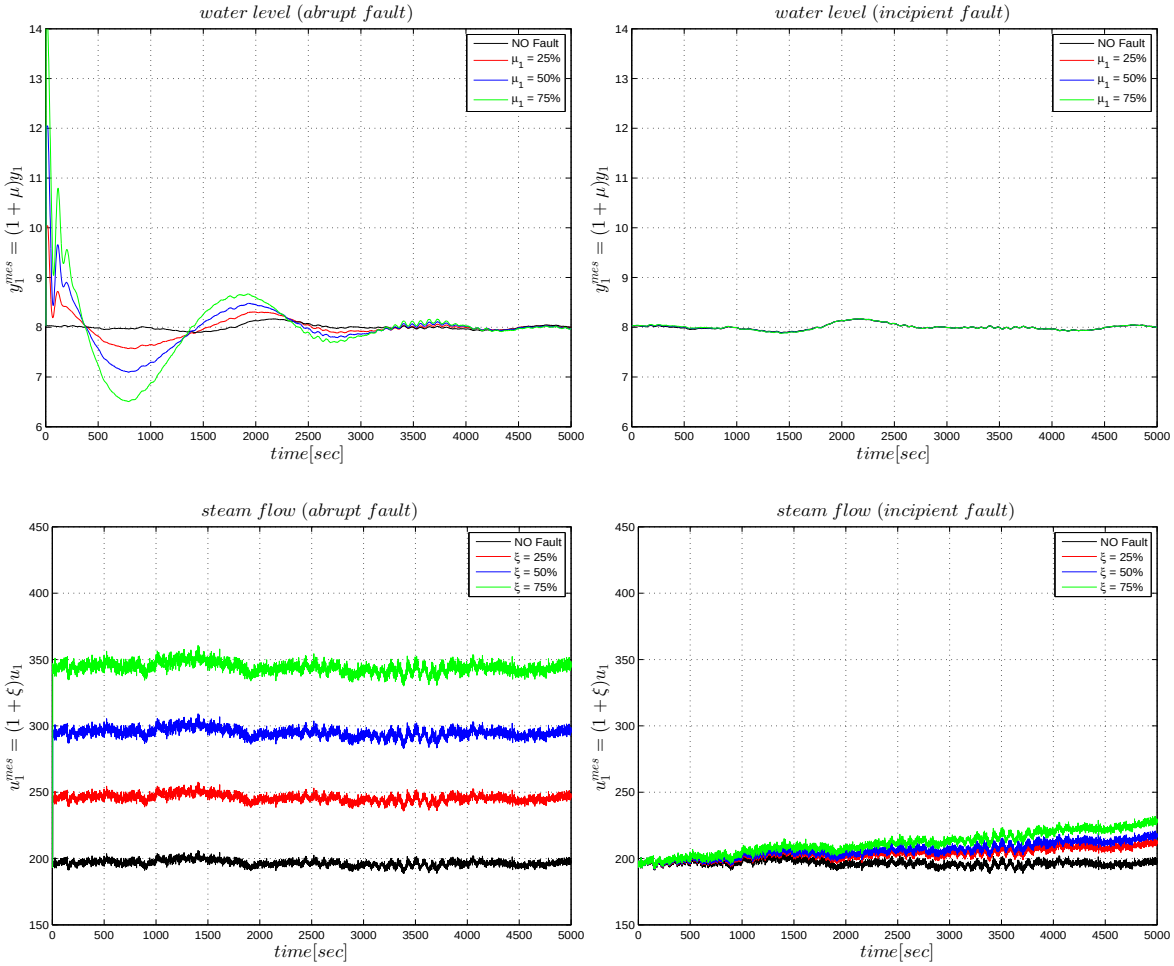

Figure 4.9: Temporal evolution of the water level measurement signal (top) and the steam flow measurement signal (bottom) when different kind of fault occur: abrupt (left) and incipient (right). The fault starts at t=0 [sec].

medium intensity (50%), denoted by the blue color, and high intensity (75%), denoted by the green color. In each case, the fault starts at time $t = 0$ [sec]. The two plots on the top are related to the water level measured signal, i.e. y_1^{mes}, whereas the two plots on the bottom refer to the steam flow measured signal, i.e. u_1^{mes}. These plots highlight how differently the two kind of sensor failures considered in this work, i.e. abrupt fault, on the left, and incipient fault, on the right, corrupt the correct measurement. The black line in each plot reveals the constant dynamic maintained in nominal condition by both input and output sensors, i.e.: $u_1^{mes} = \bar{u}_1 \approx 200\ [m^3/sec]$ and $y_1^{mes} = \bar{y}_1 \approx 8\ [m]$. The other three colored lines instead, allow to rate how much the variation introduced by the abrupt fault is apparent with respect to that introduced by the incipient fault. Moreover, the two plots on the top reflect the erroneous control action performed by the closed loop system when a fault occurs on the output measurement, because of the wrong information provided in this case by the faulty sensor to the PID. Indeed, as reflected in the top-left plot, when abrupt faults occur on y_1^{mes}, after a certain amount of time, which depends on the fault's intensity, the faulty symptom $\mu_1$results to be no more directly appreciable when looking at this measurement signal. Actually, as reflected in the top-right plot, when dealing with incipient faults on y_1^{mes}, no faulty symptom can be appreciated on it. This hiding effect of the faulty symptoms affecting the water level sensor

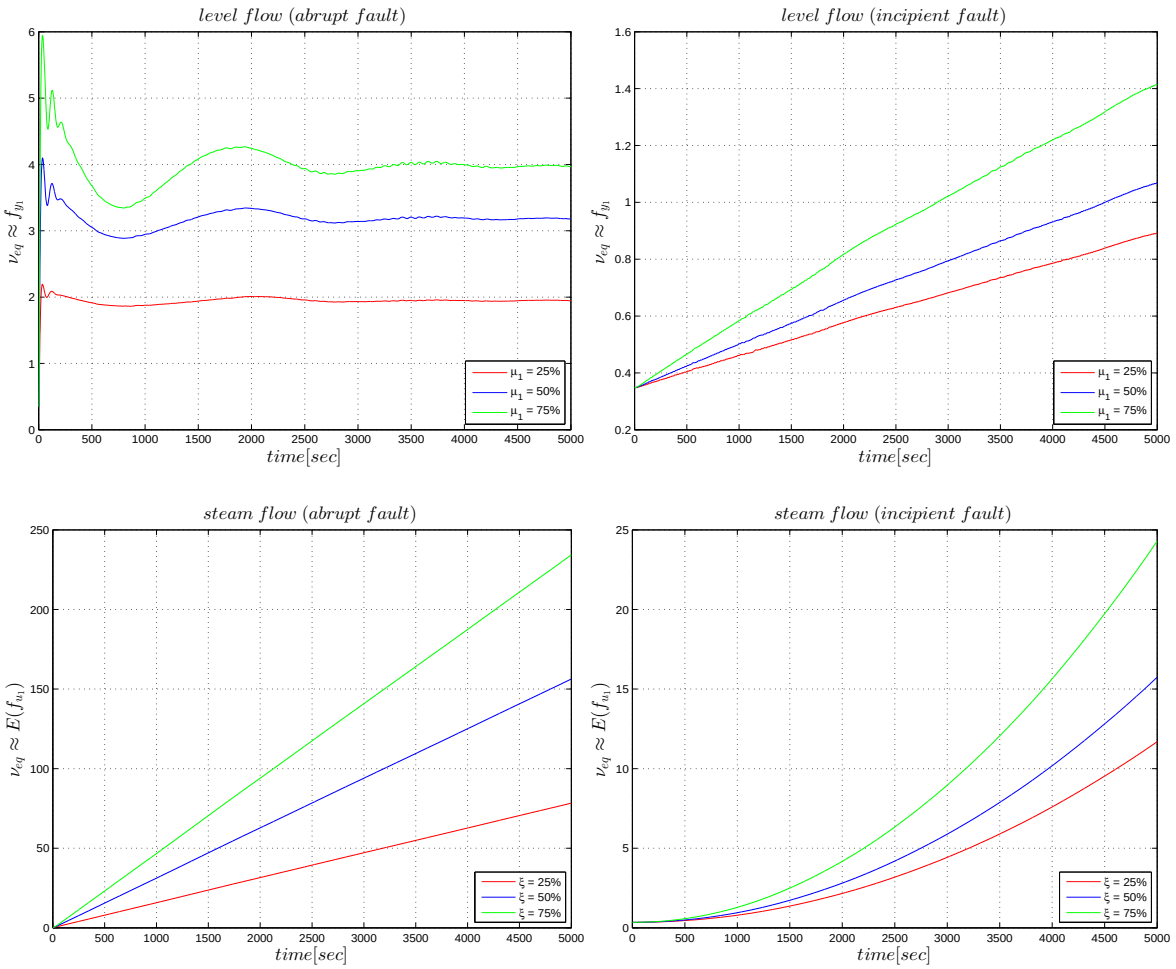

Figure 4.10: Temporal evolution of the output injection signal $v_{eq_1}(t)$ when different kind of fault occur: abrupt (left) and incipient (right) on the water level sensor (top) and on the steam flow sensor (bottom). The fault starts at t=0 [sec].

is a challenging aspect related to this particular FDI application.

The plots of the injection signal v_{eq_1} shown in Figure 4.10 confirm the effectiveness of the proposed fault detection scheme. Indeed, the two plots on the top reveal the reliability of the reconstructed faulty symptom affecting the water level sensor, i.e. abrupt fault, on the top-left, and incipient fault, on the top-right. The two plots on the bottom instead, reflect the temporal evolution of the filtered version of the faulty symptom affecting the steam flow sensor, i.e. abrupt fault, on the bottom-left, and incipient fault, on the bottom-right, according to (4.52). The experimental results therefore, confirm the expected simultaneous sensitivity of the injection signal v_{eq_1} to both water level and steam flow sensor failures, as pointed out in (4.33), and also the fact that a complete fault diagnosis cannot be achieved by only using residuals generated by the SMO. The two plots on the top-right and on the bottom-left in the Figure 4.10 reveal also another challenging aspect of this FDI application, already mentioned in Section 4.3.1 when talking about the fault isolation capabilities of the residual set R_a. Indeed, those two plots reflect the same dynamic, i.e. a ramp signal, generated by the injection v_{eq_1} when an incipient fault occurs on the water level sensor and an abrupt fault affects the steam flow sensor respectively. As a consequence, if a strong incipient fault occurs on the water level sensor, i.e. $\mu_1 \geq 75\%$, or a soft abrupt fault occurs on the steam

flow sensor, i.e. $\xi \leq 25\%$, the two straight dynamics assumed by ν_{eq_1} will be almost the same. Because of this, the capability to discriminate between these two faulty symptoms results to be a very challenging diagnostic request for any FDI system.

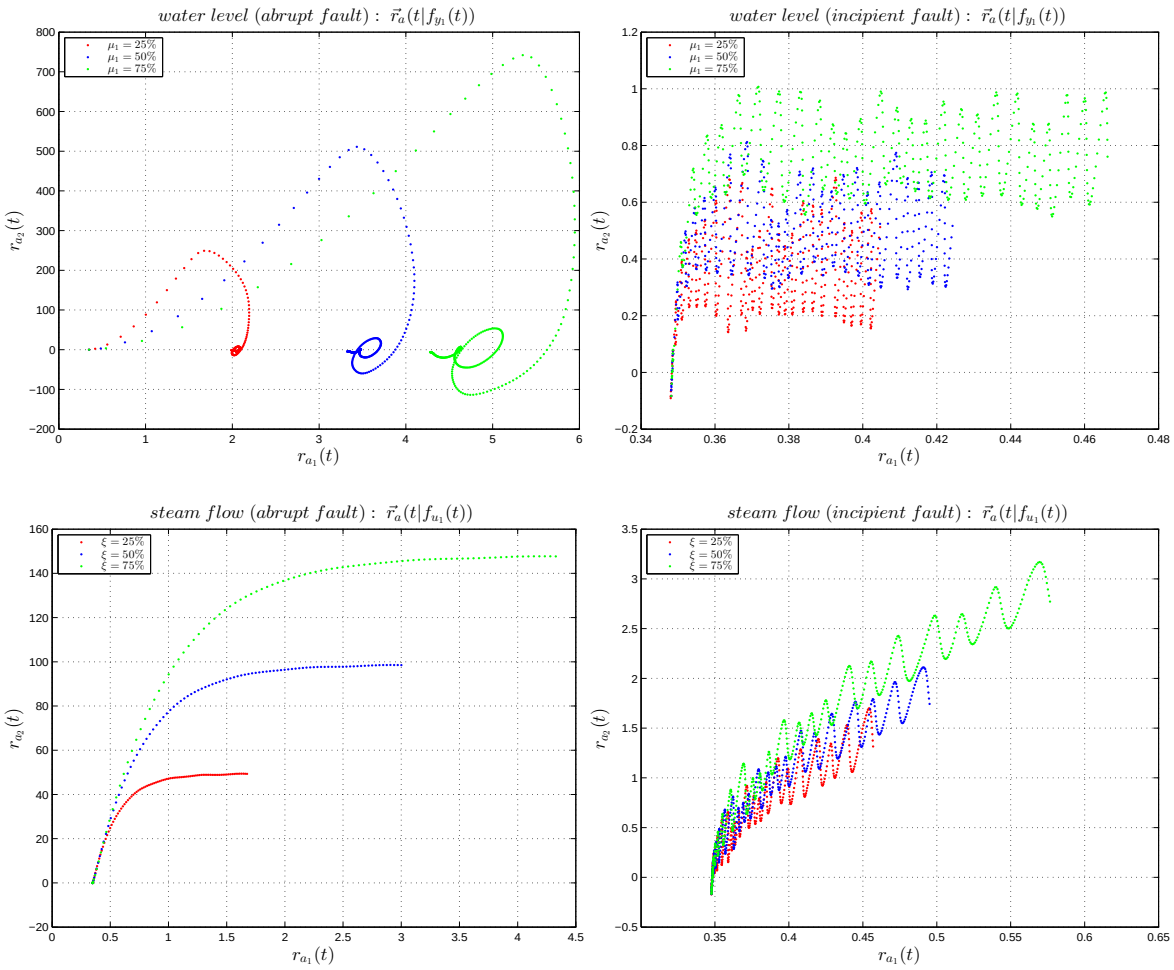

Figure 4.11: Fault Signatures generated by the residual vector $\vec{r}_a$. **Top-Left:** Water level sensor abrupt fault. **Top-Right:** Water level sensor incipient fault.**Bottom-Left:** Steam flow sensor abrupt fault. **Bottom-Right:** Steam flow sensor incipient fault.

In the Figure 4.11 and Figure 4.12 some experimental results are shown, which confirm the effectiveness of the residual evaluation approach designed in Section 4.3 in terms of fault isolation capability. Let consider the Figure 4.11, which illustrates the fault signatures generated by the residual vector $\vec{r}_a$, according to (4.56), when faults affect the water level sensor, i.e. the two plots on the top, and the steam flow sensor, i.e. the two plots on the bottom. Referring to the abrupt faults, i.e. $\vec{r}_a(t|f_{y_1})$ on the top-left, and $\vec{r}_a(t|f_{u_1})$ on the bottom-left, even by a simple visual inspection it results easy to distinguish between the two trajectories depicted by $\vec{r}_a$; as expected also, the two curves $\vec{L}_a(f_{y_1})$ and $\vec{L}_a(f_{u_1})$ result to be not affected by the fault intensity. Referring to the incipient faults instead, i.e. $\vec{r}_a(t|f_{y_1})$ on the top-right, and $\vec{r}_a(t|f_{u_1})$ on the bottom-right, even though these two curves look similar, they still reflect different dynamics, which again do not depend on the fault intensity. Moreover, the shape of the signature related to the incipient fault on the water level reflect similar dynamic properties with respect to the signature of the abrupt fault on the steam flow. These two signatures are different just because of the filtering effect introduced by the Levant's robust differentia-

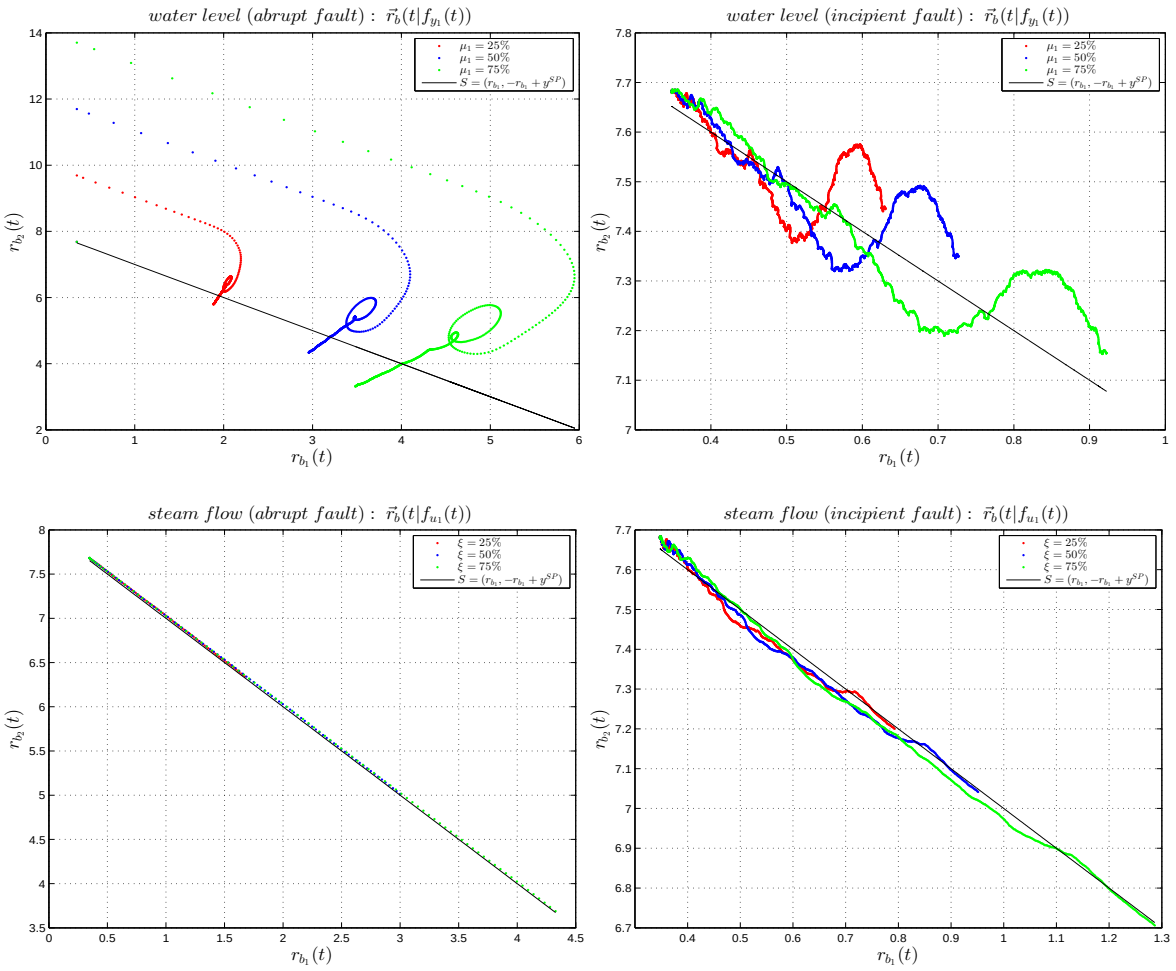

Figure 4.12: Fault Signatures generated by the residual vector $\vec{r}_b$. **Top-Left:** Water level sensor abrupt fault. **Top-Right:** Water level sensor incipient fault.**Bottom-Left:** Steam flow sensor abrupt fault. **Bottom-Right:** Steam flow sensor incipient fault.

tor, according to (4.59). To summarize, the experimental results shown in the Figure 4.11 confirm the capability of the residual set R_a to isolate both abrupt and incipient faults on both the water level and steam flow sensors. The complete fault isolation was obtained also by using the residual set R_b, as shown in the Figure 4.12, which illustrates the fault signatures generated by the residual vector $\vec{r}_b$, according to (4.62). The two signatures on the left, i.e. $\vec{r}_b(t|f_{y_1})$ on the top-left, and $\vec{r}_b(t|f_{u_1})$ on the bottom-left, confirm also for the residual set R_b the high isolation capability when dealing with abrupt faults. The other two signatures on the right instead, i.e. $\vec{r}_b(t|f_{y_1})$ on the top-right, and $\vec{r}_b(t|f_{u_1})$ on the bottom-right, reveal how the two curves $\vec{L}_b(f_{y_1})$ and $\vec{L}_b(f_{u_1})$ can be distinguished, because in this case a discriminative element is available. The comparison term is the straight black line depicted in all the four plots, which represents the subspace $S \in \mathbb{R}$ where, according to (4.67), will tend to lie the trajectory of $\vec{r}_b$ when a fault on the steam flow occurs. The reason why in both cases the trajectory of $\vec{r}_b$ does not lie exactly on the subspace S, is due to the presence of a small error introduced into the observer in order to satisfy the required boundary condition (4.28). Therefore, through the empirical comparison of signatures generated by the residual set R_b, was found a simpler and much effective way to discriminate by visual inspection between faults on the steam flow and water level sensors, even when dealing with faulty symptoms

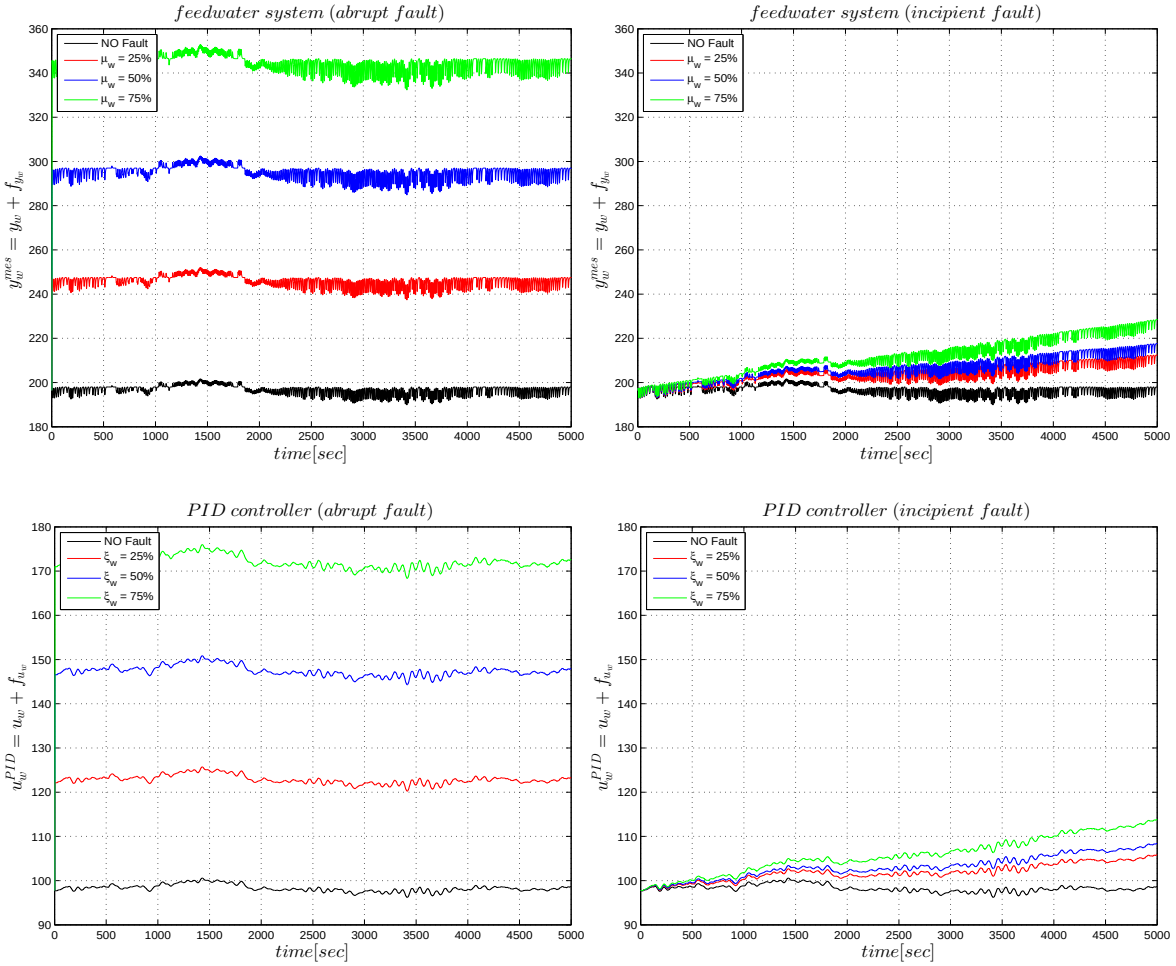

Figure 4.13: Temporal evolution of the controller PID signal (top) and the feedwater system measured signal (bottom) when different kind of fault occur: abrupt (left) and incipient (right). The fault starts at t=0 [sec].

of incipient type. Indeed, in this last case the two corresponding signatures will differ with respect to the number of times the residual vector $\vec{r}_b$ "crosses" the subspace S.

The four plots in the Figure 4.13 provide a comparison among the nominal and faulty values of the two measurements processed by the water flow sensor and the PID controller, respectively. Again, for each signal, three different percentages of fault amplitude, i.e. low, medium and high, are considered. In each case, the fault starts at time $t = 0$ [sec]. The two plots on the top are related to the water flow measured by the sensor installed at the output of the feedwater system, i.e. y_w^{mes}, whereas the two plots on the bottom refer to the set-point send by the PID controller to the feedwater system, i.e. u_w^{PID}. These plots highlight the corruption effects introduced on the actual signal by abrupt faults, on the left, and incipient faults, on the right. The black line in each plot reveals the nominal dynamic of input and output of the feedwater system, i.e.: $u_w^{PID} = \bar{u}_w \approx 100\ [m^3/sec]$ and $y_w^{mes} = \bar{y}_w \approx 200\ [m^3/sec]$, whereas again, the three colored lines allow to rate how much the variation introduced by the abrupt fault is apparent with respect to that introduced by the incipient fault.

Also in this case a complete fault isolation was obtained, as shown in the Figure 4.15, which illustrates the fault signatures generated by the residual vector $\vec{r}_{b_w}$, according to (4.69). The two signatures on the left, confirm also for the residual set R_{b_w} the high isolation capa-

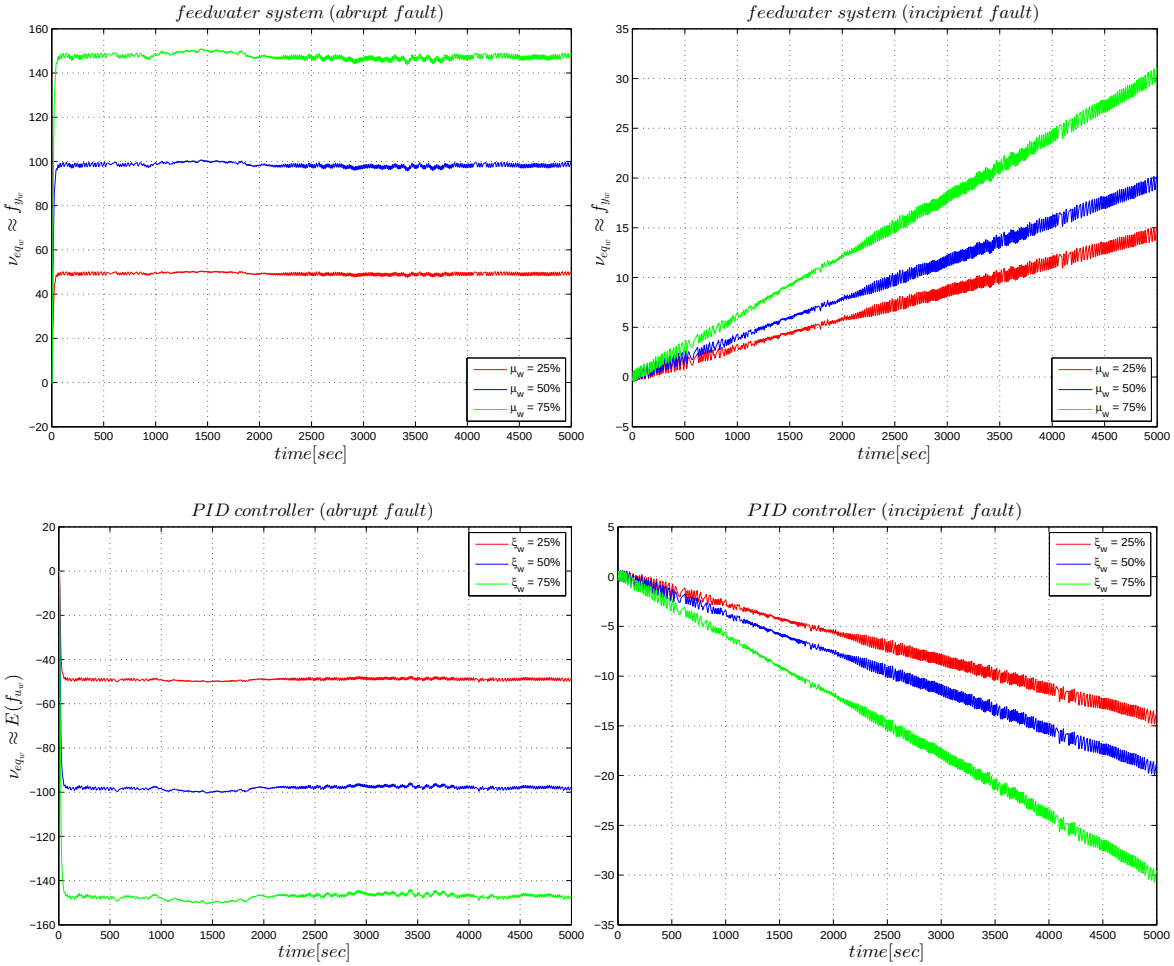

Figure 4.14: Temporal evolution of the output injection signal $v_{eq_w}(t)$ when different kind of fault occur: abrupt (left) and incipient (right) on the feedwater sensor (top) and on the PID controller (bottom). The fault starts at t=0 [sec].

bility when dealing with abrupt faults. The two signatures right, confirm the discriminative capability of R_{b_w} even for incipient faults. Also in this case, the black line depicted in all the four plots, represents the subspace $S_w \in \mathbb{R}$ where will tend to lie the trajectory of $\vec{r}_{b_w}$ when a fault on the input channel occurs, i.e. a fault on the PID controller. Again, the reason why the trajectory of $\vec{r}_w$ does not lie exactly on the subspace S, is due to the presence of a small error introduced into the observer in order to satisfy the required boundary condition (4.43). Then, these experimental results confirm the fault isolation capability also for the residual set R_{b_w}, when dealing with abrupt and incipient faults on the water flow sensor and the PID controller of a feedwater system.

In conclusion, for the considered application, the whole fault isolation can be achieved not only by developing a suitable signature evaluation algorithm, but also in a relatively easy way, by means of a simple visual inspection of the fault signatures from a human experienced operator.

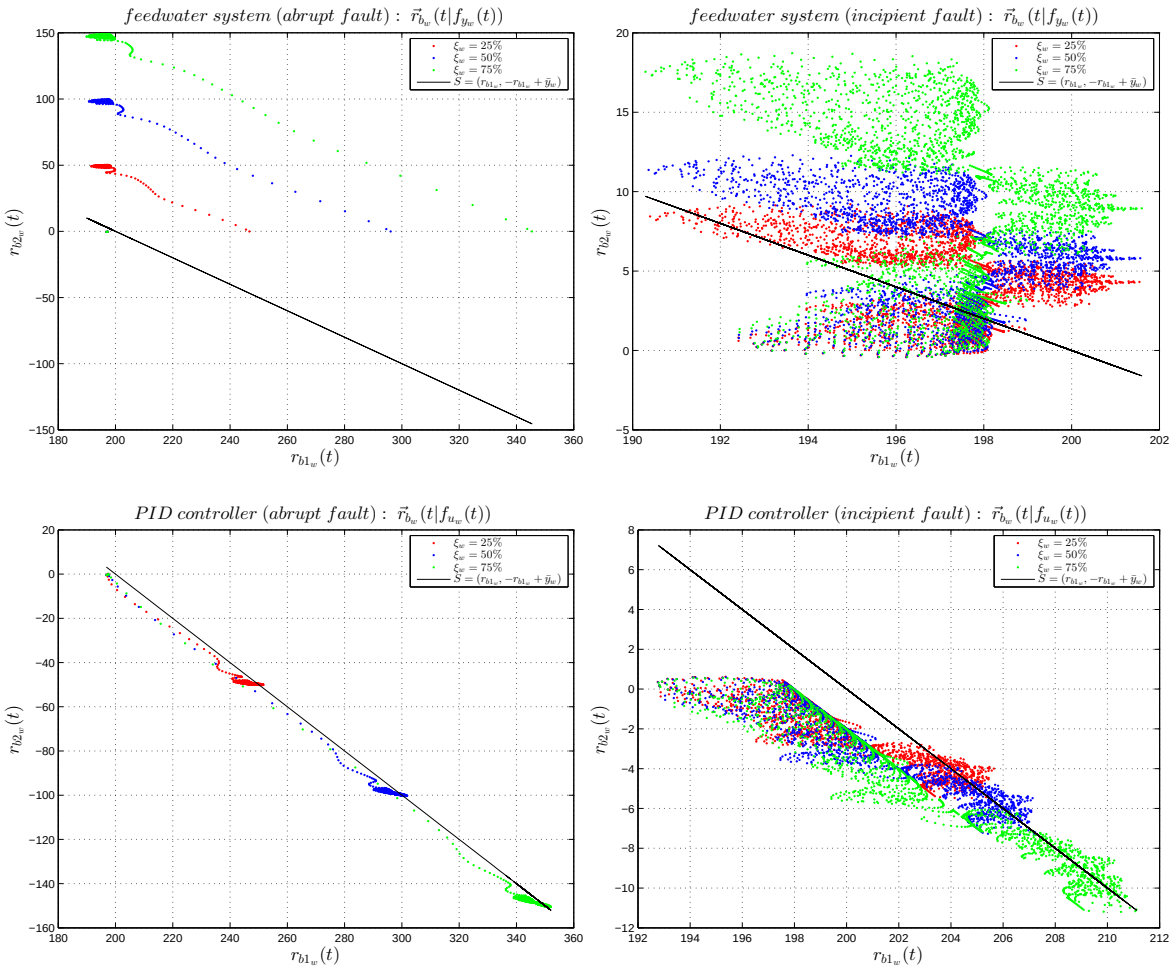

Figure 4.15: Fault Signatures generated by the residual vector $\vec{r}_{b_w}$. **Top-Left:** feedwater sensor abrupt fault. **Top-Right:** feedwater sensor incipient fault.**Bottom-Left:** PID controller abrupt fault. **Bottom-Right:** PID controller incipient fault.

4.5 Conclusion

In this Chapter, the development of an FDD system for a water-steam power plant has been discussed. The design approach discussed in Chapter 3 has been exploited. The proposed hybrid FDI scheme can be divided into two main parts: the residual generator and the residual evaluation stage. The first stage is implemented by using a model-based SMO methodology, while the second one exploits a graphical approach which allows to perform the fault isolation by means of a simple visual inspection of fault signatures. The alternative definition of signature proposed in this research gives the opportunity to implement the whole residual evaluation task also in a completely automated way, by integrating suitable signal based or data-driven techniques. However, this research is still ongoing and experimental results are not yet available for the industrial application considered in this Chapter. Further research is needed also to define a well stated framework able to formally support the advantages given by applying data-mining techniques to a residual generator based on SMOs, which resulted to be an effective fault detector for the considered application. The experimental results confirm for the considered application the opportunity to achieve a full fault isolation even when enough measurements are not available. Indeed, by processing the output injection of the

SMOs, it is possible to identify also faults in the input devices and then get a sufficiently accurate fault classification, overcoming the limitations related to a direct use of the output injection signals as residuals.

Chapter 5

Real-time DDR State-Parameter Estimation

Data Reconciliation is a methodology which exploits process information and mathematical methods in order to automatically correct measurements in industrial processes. When dealing with chemical processes, as explained in [Romagnoli and Sánchez, 2000], errors in process measurements give rise to discrepancies in material and energy balances. In such cases, DR procedures allow to obtain more accurate estimates of process variables that are consistent with a model of the plant's dynamics. This Chapter presents a novel approach to implement a real-time version of DDR along with Parameter Estimation. In the Sections 5.1 and 5.2, two fundamental concepts are introduced, which are the QSS model formulation and the DDR, respectively. Then, in Section 5.3, the novel joint data reconciliation parameter estimation procedure is explained in detail, whereas in Section 5.4 two different state-parameter decoupling strategies are proposed.

5.1 Quasi-Steady-State Model Formulation

The problem to be tackled in this Chapter is that of DR for applications in which the dominant time constant of the dynamic response of the system is much smaller than the period in which disturbances enter the system. As pointed out in Section 2.3.3, under this assumption the system displays QSS behavior. Thus, it can be assumed the process will be essentially at steady state, except for slow drifts or occasional sudden transitions between steady states. In such cases, the estimates should be consistent, that is, they should satisfy the mass and energy balances. Under these assumptions, the vector $\mathbf{f}(\mathbf{x})$ of balance equations, at a particular instant of time k, can be represented as follows in the discrete domain:

$$\mathbf{f}(\mathbf{x}_k) = \mathbf{f}(\hat{\mathbf{x}}_k) + \mathbf{A}_k(\mathbf{x}_k - \hat{\mathbf{x}}_k) = \mathbf{f}(\hat{\mathbf{x}}_k) + \mathbf{A}_k\mathbf{x}_k - \mathbf{A}_k\hat{\mathbf{x}}_k = \mathbf{A}_k\mathbf{x}_k - \mathbf{b}_k \tag{5.1}$$

where:

$$\mathbf{A}_k = \left.\frac{\partial \mathbf{f}(\mathbf{x})}{\partial \mathbf{x}}\right|_{\mathbf{x}=\hat{\mathbf{x}}_k}, \; \mathbf{a}_{ij_k} = \left.\frac{\partial f_i(\mathbf{x})}{\partial x_j}\right|_{\mathbf{x}=\hat{\mathbf{x}}_k}, \; \mathbf{b}_k = \mathbf{A}_k\hat{\mathbf{x}}_k - \mathbf{f}(\hat{\mathbf{x}}_k) \tag{5.2}$$

Hence, the set of constraints can be rewritten as:

$$\mathbf{f}(\mathbf{x}_k) = \mathbf{0} \;\Rightarrow\; \mathbf{b}_k = \mathbf{A}_k\mathbf{x}_k \tag{5.3}$$

Therefore, as stated in [Romagnoli and Sánchez, 2000], the system's dynamics can be modeled by the following three sets of equations, expressed in the discrete domain:

- a set of n transition equations:

$$\mathbf{x}_{k+1} = \mathbf{I}\mathbf{x}_k + \mathbf{w}_k \quad ; \quad k = 0, 1, \ldots \tag{5.4}$$

  where $\mathbf{x}_{k+1}$ and $\mathbf{w}_k$ are the state vector and the process noise vector at time t_k respectively;

- a set of n measurement equations:

$$\mathbf{y}_k = \mathbf{I}\mathbf{x}_k + (\mathbf{v_1})_k \quad ; \quad k = 0, 1, \ldots \tag{5.5}$$

  where $\mathbf{y}_k$ and $(\mathbf{v}_1)_k$ are the output vector and the measurement error vector at time t_k respectively;

- a set of m balance equations:

$$\mathbf{b}_k = \mathbf{A}_k\mathbf{x}_k + (\mathbf{v_2})_k \quad ; \quad k = 0, 1, \ldots \tag{5.6}$$

  where $\mathbf{b}_k$, $\mathbf{A}_k$ and $(\mathbf{v_2})_k$ are the vector containing the estimation of the nonlinear part for each of the balance equations, the matrix related to the linear approximation of the model, and the modeling error vector at time t_k respectively.

According to (2.54), the state and all the error vectors in the model are supposed to be uncorrelated and normally distributed random variables with known covariance matrix, that is:

$$\begin{aligned} \mathbf{x}_k &\sim N[\bar{\mathbf{x}}_0, \mathbf{\Sigma}_0] \\ \mathbf{w}_k &\sim N[0, \mathbf{Q}] \\ (\mathbf{v_1})_k &\sim N[0, \mathbf{R}_1] \\ (\mathbf{v_2})_k &\sim N[0, \mathbf{R}_2] \end{aligned} \tag{5.7}$$

According to (2.38), the DDR is based on a system modeled in its state-space form, which can be expressed as follows in the discrete domain:

$$\begin{aligned} \mathbf{x}_{k+1} &= \mathbf{F}_k\mathbf{x}_k + \mathbf{w}_k \\ \mathbf{z}_k &= \mathbf{G}_k\mathbf{x}_k + \mathbf{v}_k \end{aligned} \tag{5.8}$$

The three equation sets previously defined can be related to this state-space representation by considering an augmented system having a state vector $\mathbf{x}_k$ of dimension n and an observation vector $\mathbf{z}_k$ of dimension $n+m$. Therefore, the following correspondences arise:

$$\begin{aligned} \mathbf{z}_k &= \begin{bmatrix} \mathbf{y}_k \\ \hdashline \mathbf{b}_k \end{bmatrix} \quad ; \quad \mathbf{v}_k = \begin{bmatrix} (\mathbf{v}_1)_k \\ \hdashline (\mathbf{v}_2)_k \end{bmatrix} \\ \mathbf{F}_k &= \mathbf{I} \quad ; \quad \mathbf{G}_k = \begin{bmatrix} \mathbf{I} \\ \hdashline \mathbf{A}_k \end{bmatrix} \end{aligned} \tag{5.9}$$

and consequently, the correlation matrix of the observation error vector $\mathbf{v}_k$ is:

$$\mathbf{R} = \left[\begin{array}{c:c} \mathbf{R}_1 & 0 \\ \hdashline 0 & \mathbf{R}_2 \end{array}\right] \tag{5.10}$$

5.2 Dynamic Data Reconciliation

According to (2.3), the steady-state DR problem can be stated as the following constrained LSE problem:

$$\begin{aligned} &\min_{\mathbf{x}} (\mathbf{y}-\mathbf{x})^T \mathbf{Q}^{-1} (\mathbf{y}-\mathbf{x}) \\ &\text{s.t. } f_j(\mathbf{x}) = 0 \quad , \quad j = 1,\ldots,m \end{aligned} \tag{5.11}$$

where each constraint $f_j(\mathbf{x})$ is a balance equation which has to be satisfied.

The DR problem above is assumed to be operating at steady-state, i.e. only one set of data is available. However, as mentioned in Section 2.1, when the process is sampled regularly, at discrete periods of time, along with the spatial redundancy also the temporal redundancy can be exploited. When static DR methods are used, the estimates of the desired process variables calculated for two different times, t_1 and t_2, are obtained independently, that is, no previous information is exploited in the generation of estimates for other times. In other words, temporal redundancy is ignored and past information is discarded. In the QSS model formulation, as remarked in the previous Section, the process is considered essentially at steady state, except for slow drifts or occasional sudden transitions between steady states. In such cases, the estimates should be consistent, that is, they should satisfy the mass and energy balances.

Let consider the situation at time t_k, and let suppose the predicted values are already available. According to (2.48), the minimum variance estimates of the states can be obtained as the solution of the following minimization problem:

$$\min \mathbf{J}(\mathbf{x}) = [\mathbf{x} - \hat{\mathbf{x}}_{k/k-1}]^T \boldsymbol{\Sigma}_{k/k-1}^{-1} [\mathbf{x} - \hat{\mathbf{x}}_{k/k-1}] + \mathbf{v}_k^T \mathbf{R}_k^{-1} \mathbf{v}_k \tag{5.12}$$

As shown in Section 2.3.2, the solution of this minimization problem simplifies to updating steps of a static KF. For the linear case, the matrices do not depend on $\mathbf{x}$ and the covariance matrix of error can be calculated in advance, without having actual measurements. When the problem is non-linear instead, these matrices depend on the last available estimate of the state vector, and the EKF takes place.

As fully explained in the literature ([Bryson, 1975], [Jazwinski, 1970], [Gelb, 1974]), when dealing with stochastic systems having dynamic linear models and both errors and noises assumed to be all uncorrelated and Gaussian, it can be shown that the KF is an observer-based solution which guarantees an optimal state estimation along with the minimum variance. According to the same general formulation given in [Simon, 2010], [Kamen and Su, 1999], [Friedland, 1969], the equations of the KF in its recursive form can be expressed for the considered case as follows:

$$\hat{\mathbf{x}}_k = \mathbf{F}_k \hat{\mathbf{x}}_{k-1} + \mathbf{K}_k \left(\mathbf{z}_k - \mathbf{G}_k \mathbf{F}_{k-1} \hat{\mathbf{x}}_{k-1} \right) \tag{5.13}$$

where $\hat{\mathbf{x}}_k$ is the state estimation vector at time t_k, whereas $\mathbf{K}_k$ is the so-called *Kalman gain matrix*, which is computed as:

$$\mathbf{K}_k = \boldsymbol{\Sigma}_k \mathbf{G}_k^T \left(\mathbf{G}_k \boldsymbol{\Sigma}_k \mathbf{G}_k^T + \mathbf{R} \right)^{-1} \tag{5.14}$$

$\boldsymbol{\Sigma}_k$ is the so-called *a priori covariance matrix* of the state estimation error $(\mathbf{x}_{k-1} - \hat{\mathbf{x}}_{k-1})$, because it takes into account the observations up to $\mathbf{z}_{k-1}$ but not the current observation $\mathbf{z}_k$,

and it is recursively computed by means of the following so-called *variance equation*:

$$\boldsymbol{\Sigma}_{k+1} = \mathbf{F}_k (\mathbf{I} - \mathbf{K}_k \mathbf{G}_k) \boldsymbol{\Sigma}_k \mathbf{F}_k^T + \mathbf{Q} \tag{5.15}$$

According to [Friedland, 1969], the computation of $\boldsymbol{\Sigma}_{k+1}$ is done in two stages. Indeed, at first the following matrix is computed:

$$\mathbf{T}_k = (\mathbf{I} - \mathbf{K}_k \mathbf{G}_k) \boldsymbol{\Sigma}_k \tag{5.16}$$

Then, $\boldsymbol{\Sigma}_{k+1}$ is obtained as:

$$\boldsymbol{\Sigma}_{k+1} = \mathbf{F}_k \mathbf{T}_k \mathbf{F}_k^T + \mathbf{Q} \tag{5.17}$$

Notice that, $\mathbf{T}_k$ is often called as the a *posteriori covariance matrix* of the state estimation error $(\mathbf{x}_k - \hat{\mathbf{x}}_k)$, because it takes into account all the past observations including the current value $\mathbf{z}_k$. The initial estimates for the KF are computed as follows:

$$\begin{aligned} \hat{\mathbf{x}}_0 &= E[\mathbf{x}_0] \\ \boldsymbol{\Sigma}_0 &= E[(\mathbf{x}_0 - \hat{\mathbf{x}}_0)(\mathbf{x}_0 - \hat{\mathbf{x}}_0)^T] \end{aligned} \tag{5.18}$$

where $E[\cdot]$ is the expectation operator. As stated in [Simon, 2010], if the process noise and the observation error sequences $\mathbf{w}_k$ and $\mathbf{v}_k$ are both Gaussian and uncorrelated, at each time step t_k the KF will minimize the trace of the estimation error covariance matrix $\boldsymbol{\Sigma}_k$.

5.3 Joint Data Reconciliation - Parameter Estimation

The modeling approach considered in this Section allows the implementation of a DDR technique based on a suitable EKF scheme, which includes the estimate of an unknown parameter vector $\boldsymbol{\theta}$ of p elements. Indeed, according to (5.9), the matrix $\mathbf{G}_k$ contains the linear approximation of the steady-state constraints; thus, it depends also on the parameters to be estimated. As it has been done in [Romagnoli and Gani, 1983], in order to estimate the values of those variables which cannot be directly measured, the EKF approach is applied after extending the state vector $\mathbf{x}$, that is by adding to it the parameter vector $\boldsymbol{\theta}$ as follows:

$$\mathbf{x}_A = \begin{bmatrix} \mathbf{x} \\ \hdashline \boldsymbol{\theta} \end{bmatrix} \tag{5.19}$$

The system considered for the EKF implementation, modeled in its state-space form, it becomes in the discrete domain:

$$\begin{aligned} \mathbf{x}_{A_{k+1}} &= \mathbf{M}_k \mathbf{x}_k + \mathbf{w}_{A_k} \\ \mathbf{z}_k &= \mathbf{H}_k \mathbf{x}_{A_k} + \mathbf{v}_k \end{aligned} \tag{5.20}$$

where:

$$\mathbf{x}_{A_k} = \begin{bmatrix} \mathbf{x}_k \\ \hdashline \boldsymbol{\theta}_k \end{bmatrix} \begin{matrix} \updownarrow n \\ \updownarrow p \end{matrix} \quad ; \quad \mathbf{w}_{A_k} = \begin{bmatrix} \mathbf{w}_k \\ \hdashline \mathbf{0} \end{bmatrix} \begin{matrix} \updownarrow n \\ \updownarrow p \end{matrix} \tag{5.21}$$

$$\mathbf{M}_k = \begin{bmatrix} \overset{\longleftrightarrow n}{\mathbf{F}_k} & \overset{\longleftrightarrow p}{\left.\frac{\partial \mathbf{F}_k}{\partial \boldsymbol{\theta}}\right|_{\boldsymbol{\theta}=\hat{\boldsymbol{\theta}}_k}} \\ \mathbf{0} & \mathbf{I} \end{bmatrix} \begin{matrix} \updownarrow n \\ \updownarrow p \end{matrix} = \begin{bmatrix} \mathbf{I}_{[n]} & \mathbf{0}_{[n,p]} \\ \mathbf{0}_{[p,n]} & \mathbf{I}_{[p]} \end{bmatrix} = \mathbf{I}_{[n+p]} \tag{5.22}$$

$$\mathbf{H}_k = \begin{bmatrix} \overset{\longleftrightarrow n}{\mathbf{G}_k} & \overset{\longleftrightarrow p}{\left.\frac{\partial \mathbf{G}_k}{\partial \boldsymbol{\theta}}\right|_{\boldsymbol{\theta}=\hat{\boldsymbol{\theta}}_k}} \end{bmatrix} \updownarrow (n+m) = \begin{bmatrix} \overset{\longleftrightarrow n}{\mathbf{I}_{[n]}} & \overset{\longleftrightarrow p}{\mathbf{0}_{[n,p]}} \\ \mathbf{A_k} & \left.\frac{\partial \mathbf{A}_k}{\partial \boldsymbol{\theta}}\right|_{\boldsymbol{\theta}=\hat{\boldsymbol{\theta}}_k} \end{bmatrix} \begin{matrix} \updownarrow n \\ \updownarrow m \end{matrix} \tag{5.23}$$

Therefore, the recursive equations become:

$$\hat{\mathbf{x}}_{A_k} = \mathbf{M}_{k-1}\hat{\mathbf{x}}_{A_{k-1}} + \mathbf{K}_{A_k}\left(\mathbf{z}_k - \mathbf{H}_k\mathbf{M}_{k-1}\hat{\mathbf{x}}_{A_{k-1}}\right) \tag{5.24}$$

$$\mathbf{K}_{A_k} = \boldsymbol{\Sigma}_{A_k}\mathbf{H}_k^T\left(\mathbf{H}_k\boldsymbol{\Sigma}_{A_k}\mathbf{H}_k^T + \mathbf{R}\right)^{-1} \tag{5.25}$$

$$\boldsymbol{\Sigma}_{A_{k+1}} = \mathbf{M}_k\left(\mathbf{I} - \mathbf{K}_{A_k}\mathbf{H}_k\right)\boldsymbol{\Sigma}_{A_k}\mathbf{M}_k^T + \mathbf{Q}_A \tag{5.26}$$

where:

$$\mathbf{Q}_A = \begin{bmatrix} \overset{\longleftrightarrow n}{\mathbf{Q}} & \overset{\longleftrightarrow p}{\mathbf{0}} \\ \mathbf{0} & \mathbf{0} \end{bmatrix} \begin{matrix} \updownarrow n \\ \updownarrow p \end{matrix} \tag{5.27}$$

is the covariance matrix of the augmented process noise vector $\mathbf{w}_{A_k}$.

The augmented Kalman gain matrix $\mathbf{K}_{A_k}$, and the a priori covariance matrix $\boldsymbol{\Sigma}_{A_k}$ of the augmented state estimation error $(\mathbf{x}_{A_{k-1}} - \hat{\mathbf{x}}_{A_{k-1}})$, are partitioned as follows:

$$\mathbf{K}_{A_k} = \begin{bmatrix} \overset{\longleftrightarrow n+m}{\mathbf{K}_{x_k}} \\ \mathbf{K}_{\theta_k} \end{bmatrix} \begin{matrix} \updownarrow n \\ \updownarrow p \end{matrix} \quad ; \quad \boldsymbol{\Sigma}_{A_k} = \begin{bmatrix} \overset{\longleftrightarrow n}{\boldsymbol{\Sigma}_{x_k}} & \overset{\longleftrightarrow p}{\boldsymbol{\Sigma}_{x\theta_k}} \\ \boldsymbol{\Sigma}_{\theta x_k} & \boldsymbol{\Sigma}_{\theta_k} \end{bmatrix} \begin{matrix} \updownarrow n \\ \updownarrow p \end{matrix} \tag{5.28}$$

where:

- $\boldsymbol{\Sigma}_{x_k}$ is the covariance matrix related to the state estimation error $(\mathbf{x}_k - \hat{\mathbf{x}}_k)$, that is the autocovariance of the state estimation problem
- $\boldsymbol{\Sigma}_{\theta_k}$ is the covariance matrix related to the parameter estimation error $(\boldsymbol{\theta}_k - \hat{\boldsymbol{\theta}}_k)$, that is the auto covariance of the parameter estimation problem
- $\boldsymbol{\Sigma}_{x\theta_k} = \boldsymbol{\Sigma}_{\theta x_k} = \boldsymbol{\Sigma}_{x\theta_k}^T$ is the covariance matrix related to the state $\mathbf{x}_k$ and parameter $\boldsymbol{\theta}_k$ estimation errors, that is the cross-covariance of the joint state-parameter estimation problem.

The initial estimate of the parameter vector $\hat{\boldsymbol{\theta}}_0$ it is assumed to be known at the initial time step t_0 with a given approximation error. This fact implies that $\boldsymbol{\Sigma}_{\theta_0} \neq 0$. Indeed, the assumption $\boldsymbol{\Sigma}_{\theta_0} = 0$ implies the parameter vector $\boldsymbol{\theta}$ is perfectly known at the initial time, thus it will be known thereafter also, that is $\boldsymbol{\Sigma}_{\theta_k} = 0 \ \forall k$, and no parameter estimation but state estimation only will be performed by the EFK. The same consideration applies also to the initial estimate of the state, thus $\boldsymbol{\Sigma}_{x_0} \neq 0$. Another assumption needed to make possible the state-parameter decoupling is to consider $\mathbf{x}$ and $\boldsymbol{\theta}$ to be independent at the initial time step t_0; this fact implies: $\boldsymbol{\Sigma}_{x\theta_0} = \boldsymbol{\Sigma}_{\theta x_0} = 0$.

By computing $\boldsymbol{\Sigma}_{A_{k+1}}$ in two stages, as follows:

$$\mathbf{T}_{A_k} = \left(\mathbf{I} - \mathbf{K}_{A_k}\mathbf{H}_k\right)\boldsymbol{\Sigma}_{A_k} \tag{5.29}$$

then:

$$\boldsymbol{\Sigma}_{A_{k+1}} = \mathbf{M}_k\mathbf{T}_{A_k}\mathbf{M}_k^T + \mathbf{Q}_A \tag{5.30}$$

with the Kalman gain computed as:

$$\mathbf{K}_{A_k} = \mathbf{T}_{A_k}\mathbf{H}_k^T\mathbf{R}^{-1} \tag{5.31}$$

the equations related to the computation of $\boldsymbol{\Sigma}_{x_k}$, $\boldsymbol{\Sigma}_{\theta_k}$ and $\boldsymbol{\Sigma}_{x\theta_k}$ result to be all coupled. Consequently, these covariance matrices cannot be obtained independently, and hence the state and parameter estimation problems cannot be solved separately.

As claimed in [Romagnoli and Gani, 1983], and proved in the appendix of [Friedland, 1969], the *a priori* covariance matrix $\boldsymbol{\Sigma}_{A_k}$ and the *a posteriori* covariance matrix $\mathbf{T}_{A_k}$ can be computed respectively also by means of an equivalent transformation, more suitable for the state-parameter decoupling purpose, which makes use of the auxiliary matrices $\mathbf{U}_{A_k}$, $\mathbf{V}_{A_k}$ and $\mathbf{E}_k$ as follows:

$$\begin{aligned} \boldsymbol{\Sigma}_{A_k} &= \tilde{\boldsymbol{\Sigma}}_{A_k} + \mathbf{U}_{A_k}\mathbf{E}_k\mathbf{U}_{A_k}^T \\ \mathbf{T}_{A_k} &= \tilde{\mathbf{T}}_{A_k} + \mathbf{V}_{A_k}\mathbf{E}_k\mathbf{V}_{A_k}^T \end{aligned} \tag{5.32}$$

Where $\tilde{\boldsymbol{\Sigma}}_{A_k}$ and $\tilde{\mathbf{T}}_{A_k}$ are respectively the *a priori* and *a posteriori* covariance matrices related to the state estimation problem only. The values of $\tilde{\mathbf{T}}_{A_k}$ and $\tilde{\boldsymbol{\Sigma}}_{A_{k+1}}$ are obtained by means of the standard two-stage computation based on the variance equation, that is:

$$\tilde{\mathbf{T}}_{A_k} = \left(\mathbf{I} - \tilde{\mathbf{K}}_{A_k}\mathbf{H}_k\right)\tilde{\boldsymbol{\Sigma}}_{A_k} \tag{5.33}$$

then:

$$\tilde{\boldsymbol{\Sigma}}_{A_{k+1}} = \mathbf{M}_k\tilde{\mathbf{T}}_{A_k}\mathbf{M}_k^T + \mathbf{Q}_A \tag{5.34}$$

being $\tilde{\mathbf{K}}_{A_k}$ the Kalman gain related to the state estimation problem only, which can be computed as:

$$\tilde{\mathbf{K}}_{A_k} = \tilde{\boldsymbol{\Sigma}}_{A_k}\mathbf{H}_k^T\left(\mathbf{H}_k\tilde{\boldsymbol{\Sigma}}_{A_k}\mathbf{H}_k^T + \mathbf{R}\right)^{-1} = \tilde{\mathbf{T}}_{A_k}\mathbf{H}_k^T\mathbf{R}^{-1} \tag{5.35}$$

The value of the auxiliary matrices $\mathbf{U}_{A_{k+1}}$ and $\mathbf{V}_{A_k}$ are obtained by means of a two-stage approach analogous to that used for the computation of $\tilde{\boldsymbol{\Sigma}}_{A_{k+1}}$ and $\tilde{\mathbf{T}}_{A_k}$ as follows:

$$\mathbf{V}_{A_k} = \left(\mathbf{I} - \tilde{\mathbf{K}}_{A_k}\mathbf{H}_k\right)\mathbf{U}_{A_k} \tag{5.36}$$

then:

$$\mathbf{U}_{A_{k+1}} = \mathbf{M}_k \mathbf{V}_{A_k} \tag{5.37}$$

The value of the auxiliary p-dimensional squared matrix $\mathbf{E}_k$ is obtained by means of the following recursive equation:

$$\mathbf{E}_{k+1} = \mathbf{E}_k - \mathbf{E}_k \mathbf{U}_{A_k}^T \mathbf{H}_k^T \left[(\mathbf{H}_k \tilde{\mathbf{\Sigma}}_{A_k} \mathbf{H}_k^T + \mathbf{R}) + \mathbf{H}_k \mathbf{U}_{A_k} \mathbf{E}_k \mathbf{U}_{A_k}^T \mathbf{H}_k^T \right]^{-1} \mathbf{H}_k \mathbf{U}_{A_k} \mathbf{E}_k \tag{5.38}$$

Since $\tilde{\mathbf{T}}_{A_k}$, $\tilde{\mathbf{\Sigma}}_{A_k}$, and $\tilde{\mathbf{K}}_{A_k}$, are all parameter-free matrices, they can be partitioned as follows:

$$\tilde{\mathbf{T}}_{A_k} = \left[\begin{array}{c:c} \tilde{\mathbf{T}}_{x_k} & \tilde{\mathbf{T}}_{x\theta_k} \\ \hdashline \tilde{\mathbf{T}}_{\theta x_k} & \tilde{\mathbf{T}}_{\theta_k} \end{array}\right] = \left[\begin{array}{c:c} \overset{\longleftrightarrow}{n} & \overset{\longleftrightarrow}{p} \\ \hdashline \tilde{\mathbf{T}}_{x_k} & \mathbf{0} \\ \hdashline \mathbf{0} & \mathbf{0} \end{array}\right] \begin{array}{c} \\ \hdashline \updownarrow n \\ \hdashline \updownarrow p \end{array} \tag{5.39}$$

$$\tilde{\mathbf{\Sigma}}_{A_k} = \left[\begin{array}{c:c} \tilde{\mathbf{\Sigma}}_{x_k} & \tilde{\mathbf{\Sigma}}_{x\theta_k} \\ \hdashline \tilde{\mathbf{\Sigma}}_{\theta x_k} & \tilde{\mathbf{\Sigma}}_{\theta_k} \end{array}\right] = \left[\begin{array}{c:c} \overset{\longleftrightarrow}{n} & \overset{\longleftrightarrow}{p} \\ \hdashline \tilde{\mathbf{\Sigma}}_{x_k} & \mathbf{0} \\ \hdashline \mathbf{0} & \mathbf{0} \end{array}\right] \begin{array}{c} \\ \hdashline \updownarrow n \\ \hdashline \updownarrow p \end{array} \tag{5.40}$$

$$\tilde{\mathbf{K}}_{A_k} = \left[\begin{array}{c} \tilde{\mathbf{K}}_{x_k} \\ \hdashline \tilde{\mathbf{K}}_{\theta x_k} \end{array}\right] = \left[\begin{array}{c} \overset{\longleftrightarrow}{n+m} \\ \hdashline \tilde{\mathbf{K}}_{x_k} \\ \hdashline \mathbf{0} \end{array}\right] \begin{array}{c} \\ \hdashline \updownarrow n \\ \hdashline \updownarrow p \end{array} \tag{5.41}$$

Therefore, by taking into account all the partitioned versions of the involved matrices, the following result arises:

$$\tilde{\mathbf{T}}_{x_k} = \left(\mathbf{I} - \tilde{\mathbf{K}}_{x_k} \mathbf{G}_k\right) \tilde{\mathbf{\Sigma}}_{x_k} \tag{5.42}$$

$$\tilde{\mathbf{\Sigma}}_{x_{k+1}} = \mathbf{F}_k \tilde{\mathbf{T}}_{x_k} \mathbf{F}_k^T + \mathbf{Q} \tag{5.43}$$

$$\tilde{\mathbf{K}}_{x_k} = \tilde{\mathbf{\Sigma}}_{x_k} \mathbf{G}_k^T \left(\mathbf{G}_k \tilde{\mathbf{\Sigma}}_{x_k} \mathbf{G}_k^T + \mathbf{R}\right)^{-1} = \tilde{\mathbf{T}}_{x_k} \mathbf{G}_k^T \mathbf{R}^{-1} \tag{5.44}$$

and the following block partitioning arise for the auxiliary matrices:

$$\mathbf{V}_{A_k} = \left[\begin{array}{c} \overset{\longleftrightarrow}{p} \\ \hdashline \mathbf{V}_{x_k} \\ \hdashline \mathbf{V}_{\theta_k} \end{array}\right] \begin{array}{c} \\ \hdashline \updownarrow n \\ \hdashline \updownarrow p \end{array} = \begin{array}{c} \\ n\updownarrow \\ \hdashline \\ p\updownarrow \end{array} \left[\begin{array}{c:c} \overset{\longleftrightarrow}{n} & \overset{\longleftrightarrow}{p} \\ \hdashline \mathbf{I} - \tilde{\mathbf{K}}_{x_k} \mathbf{G}_k & -\tilde{\mathbf{K}}_{x_k} \left.\frac{\partial \mathbf{G}_k}{\partial \boldsymbol{\theta}}\right|_{\boldsymbol{\theta}=\hat{\boldsymbol{\theta}}_k} \\ \hdashline \mathbf{0} & \mathbf{I} \end{array}\right] \left[\begin{array}{c} \overset{\longleftrightarrow}{p} \\ \hdashline \mathbf{U}_{x_k} \\ \hdashline \mathbf{U}_{\theta_k} \end{array}\right] \begin{array}{c} \\ \hdashline \updownarrow n \\ \hdashline \updownarrow p \end{array} \tag{5.45}$$

$$\mathbf{U}_{A_{k+1}} = \begin{bmatrix} \overset{p}{\longleftrightarrow} \\ \mathbf{U}_{x_{k+1}} \\ \cdots\cdots \\ \mathbf{U}_{\theta_{k+1}} \end{bmatrix} \begin{matrix} \updownarrow n \\ \cdots \\ \updownarrow p \end{matrix} = \begin{matrix} n\updownarrow \\ \cdots \\ p\updownarrow \end{matrix} \left[\begin{array}{cc} \overset{n}{\longleftrightarrow} & \overset{p}{\longleftrightarrow} \\ \mathbf{F}_{x_k} & \left.\frac{\partial \mathbf{F}_k}{\partial \boldsymbol{\theta}}\right|_{\boldsymbol{\theta}=\hat{\boldsymbol{\theta}}_k} \\ \cdots\cdots & \cdots\cdots \\ \mathbf{0} & \mathbf{I} \end{array}\right] \begin{bmatrix} \overset{p}{\longleftrightarrow} \\ \mathbf{V}_{x_k} \\ \cdots\cdots \\ \mathbf{V}_{\theta_k} \end{bmatrix} \begin{matrix} \updownarrow n \\ \cdots \\ \updownarrow p \end{matrix} \tag{5.46}$$

Thus:

$$\begin{aligned} \mathbf{V}_{x_k} &= \left(\mathbf{I} - \tilde{\mathbf{K}}_{x_k}\mathbf{G}_k\right)\mathbf{U}_{x_k} - \left(\tilde{\mathbf{K}}_{x_k}\left.\frac{\partial \mathbf{G}_k}{\partial \boldsymbol{\theta}}\right|_{\boldsymbol{\theta}=\hat{\boldsymbol{\theta}}_k}\right)\mathbf{U}_{\theta_k} = \\ &= \mathbf{U}_{x_k} - \tilde{\mathbf{K}}_{x_k}\left(\mathbf{G}_k\mathbf{U}_{x_k} + \left.\frac{\partial \mathbf{G}_k}{\partial \boldsymbol{\theta}}\right|_{\boldsymbol{\theta}=\hat{\boldsymbol{\theta}}_k}\mathbf{U}_{\theta_k}\right) \\ \mathbf{V}_{\theta_k} &= \mathbf{U}_{\theta_k} \end{aligned} \tag{5.47}$$

$$\begin{aligned} \mathbf{U}_{x_{k+1}} &= \mathbf{F}_k\mathbf{V}_{x_k} + \left(\left.\frac{\partial \mathbf{F}_k}{\partial \boldsymbol{\theta}}\right|_{\boldsymbol{\theta}=\hat{\boldsymbol{\theta}}_k}\right)\mathbf{V}_{\theta_k} \\ \mathbf{U}_{\boldsymbol{\theta}_{k+1}} &= \mathbf{V}_{\theta_k} \end{aligned} \tag{5.48}$$

It is worth to note that the auxiliary submatrices $\mathbf{U}_{\theta_k}$ and $\mathbf{V}_{\theta_k}$ are being not updated from their initial value, that is:

$$\mathbf{U}_{\theta_{k+1}} = \mathbf{V}_{\theta_k} \quad \Longrightarrow \quad \mathbf{U}_{\theta_{k+1}} = \mathbf{U}_{\theta_k} \quad \Longrightarrow \quad \mathbf{U}_{\theta_k} = \mathbf{U}_{\theta_0} \tag{5.49}$$

By introducing the auxiliary matrix $\mathbf{S}_k$, defined as:

$$\mathbf{S}_k = \mathbf{G}_k\mathbf{U}_{x_k} + \left(\left.\frac{\partial \mathbf{G}_k}{\partial \boldsymbol{\theta}}\right|_{\boldsymbol{\theta}=\hat{\boldsymbol{\theta}}_k}\right)\mathbf{U}_{\theta_k} \tag{5.50}$$

The following recursive formula arises:

$$\mathbf{V}_{x_k} = \mathbf{U}_{x_k} - \tilde{\mathbf{K}}_{x_k}\mathbf{S}_k \tag{5.51}$$

Then, in terms of partitioned matrices, $\boldsymbol{\Sigma}_{A_k}$ and $\tilde{\mathbf{T}}_{A_k}$ become:

$$\begin{aligned} \boldsymbol{\Sigma}_{x_k} &= \tilde{\boldsymbol{\Sigma}}_{x_k} + \mathbf{U}_{x_k}\mathbf{E}_k\mathbf{U}_{x_k}^T \\ \boldsymbol{\Sigma}_{x\theta_k} &= \tilde{\boldsymbol{\Sigma}}_{x\theta_k} + \mathbf{U}_{x_k}\mathbf{E}_k\mathbf{U}_{\theta_k}^T \\ \boldsymbol{\Sigma}_{\theta x_k} &= \tilde{\boldsymbol{\Sigma}}_{\theta x_k} + \mathbf{U}_{\theta_k}\mathbf{E}_k\mathbf{U}_{x_k}^T \\ \boldsymbol{\Sigma}_{\theta_k} &= \tilde{\boldsymbol{\Sigma}}_{\theta_k} + \mathbf{U}_{\theta_k}\mathbf{E}_k\mathbf{U}_{\theta_k}^T \end{aligned} \tag{5.52}$$

$$\begin{aligned} \mathbf{T}_{x_k} &= \tilde{\mathbf{T}}_{x_k} + \mathbf{V}_{x_k}\mathbf{E}_{k+1}\mathbf{V}_{x_k}^T \\ \mathbf{T}_{x\theta_k} &= \tilde{\mathbf{T}}_{x\theta_k} + \mathbf{V}_{x_k}\mathbf{E}_{k+1}\mathbf{V}_{\theta_k}^T \\ \mathbf{T}_{\theta x_k} &= \tilde{\mathbf{T}}_{\theta x_k} + \mathbf{V}_{\theta_k}\mathbf{E}_{k+1}\mathbf{V}_{x_k}^T \\ \mathbf{T}_{\theta_k} &= \tilde{\mathbf{T}}_{\theta_k} + \mathbf{V}_{\theta_k}\mathbf{E}_{k+1}\mathbf{V}_{\theta_k}^T \end{aligned} \tag{5.53}$$

The initial values of the auxiliary matrices: $\mathbf{U}_{x_0} = \mathbf{0}$, $\mathbf{U}_{\theta_0} = \mathbf{I}$, $\mathbf{E}_0 = \mathbf{I}$, can be obtained by recalling the initial conditions discussed above, which have to be imposed in order make feasible the state-parameter decoupling implementation, that is:

- Initial uncertainty in the state estimation:
  $\Rightarrow \boldsymbol{\Sigma}_{x_0} = \tilde{\boldsymbol{\Sigma}}_{x_0} = E[(\mathbf{x}_0 - \hat{\mathbf{x}}_0)(\mathbf{x}_0 - \hat{\mathbf{x}}_0)^T] \neq \mathbf{0}$
- Initial uncertainty in the parameter estimation:
  $\Rightarrow \boldsymbol{\Sigma}_{\theta_0} \neq \mathbf{0}$
- First estimate of $\mathbf{x}$ and $\boldsymbol{\theta}$ are done independently:
  $\Rightarrow \boldsymbol{\Sigma}_{x\theta_0} = \boldsymbol{\Sigma}_{\theta x_0} = \mathbf{0}$

Indeed, with this choice the following configuration arise:

$$\begin{aligned} \boldsymbol{\Sigma}_{x_k} &= \tilde{\boldsymbol{\Sigma}}_{x_k} + \mathbf{U}_{x_k}\mathbf{E}_k\mathbf{U}_{x_k}^T \\ \boldsymbol{\Sigma}_{x\theta_k} &= \mathbf{U}_{x_k}\mathbf{E}_k \\ \boldsymbol{\Sigma}_{\theta x_k} &= \mathbf{E}_k\mathbf{U}_{x_k}^T \\ \boldsymbol{\Sigma}_{\theta_k} &= \mathbf{E}_k \end{aligned} \tag{5.54}$$

$$\begin{aligned} \mathbf{T}_{x_k} &= \tilde{\mathbf{T}}_{x_k} + \mathbf{V}_{x_k}\mathbf{E}_{k+1}\mathbf{V}_{x_k}^T \\ \mathbf{T}_{x\theta_k} &= \mathbf{V}_{x_k}\mathbf{E}_{k+1} \\ \mathbf{T}_{\theta x_k} &= \mathbf{E}_{k+1}\mathbf{V}_{x_k}^T \\ \mathbf{T}_{\theta_k} &= \mathbf{E}_{k+1} \end{aligned} \tag{5.55}$$

Therefore, the Kalman gain matrix can be expressed in its state-parameter decoupled form, as follows :

$$\begin{aligned} \mathbf{K}_{A_k} &= \overset{n+m}{\longleftrightarrow} \begin{bmatrix} \mathbf{K}_{x_k} \\ \hdashline \mathbf{K}_{\theta_k} \end{bmatrix} \begin{matrix} \updownarrow n \\ \hdashline \updownarrow p \end{matrix} = \begin{matrix} \overset{n}{\longleftrightarrow} & \overset{p}{\longleftrightarrow} \\ n\updownarrow & p\updownarrow \end{matrix} \left[\begin{array}{c:c} \mathbf{T}_{x_k} & \mathbf{T}_{x\theta_k} \\ \hdashline \mathbf{T}_{\theta x_k} & \mathbf{T}_{\theta_k} \end{array}\right] \left[\begin{array}{c} \overset{n+m}{\longleftrightarrow} \\ \mathbf{G}_k^T \\ \hdashline \left(\left.\frac{\partial \mathbf{G}_k}{\partial \boldsymbol{\theta}}\right|_{\boldsymbol{\theta}=\hat{\boldsymbol{\theta}}_k}\right)^T \end{array}\right] \left[\begin{array}{c} \overset{n+m}{\longleftrightarrow} \\ \mathbf{R}^{-1} \end{array}\right] \updownarrow n+m = \\ &= \begin{matrix} \overset{n}{\longleftrightarrow} & \overset{p}{\longleftrightarrow} \\ n\updownarrow & p\updownarrow \end{matrix} \left[\begin{array}{c:c} \tilde{\mathbf{T}}_{x_k} + \mathbf{V}_{x_k}\mathbf{E}_{k+1}\mathbf{V}_{x_k}^T & \mathbf{V}_{x_k}\mathbf{E}_{k+1} \\ \hdashline \mathbf{E}_{k+1}\mathbf{V}_{x_k}^T & \mathbf{E}_{k+1} \end{array}\right] \left[\begin{array}{c} \overset{n+m}{\longleftrightarrow} \\ \mathbf{G}_k^T \\ \hdashline \left(\left.\frac{\partial \mathbf{G}_k}{\partial \boldsymbol{\theta}}\right|_{\boldsymbol{\theta}=\hat{\boldsymbol{\theta}}_k}\right)^T \end{array}\right] \left[\begin{array}{c} \overset{n+m}{\longleftrightarrow} \\ \mathbf{R}^{-1} \end{array}\right] \updownarrow n+m = \\ &= \begin{matrix} \overset{n+m}{\longleftrightarrow} \\ n\updownarrow \\ \hdashline p\updownarrow \end{matrix} \left[\begin{array}{c} \left(\tilde{\mathbf{T}}_{x_k} + \mathbf{V}_{x_k}\mathbf{E}_{k+1}\mathbf{V}_{x_k}^T\right)\mathbf{G}_k^T + \mathbf{V}_{x_k}\mathbf{E}_{k+1}\left(\left.\frac{\partial \mathbf{G}_k}{\partial \boldsymbol{\theta}}\right|_{\boldsymbol{\theta}=\hat{\boldsymbol{\theta}}_k}\right)^T \\ \hdashline \mathbf{E}_{k+1}\mathbf{V}_{x_k}^T\mathbf{G}_k^T + \mathbf{E}_{k+1}\left(\left.\frac{\partial \mathbf{G}_k}{\partial \boldsymbol{\theta}}\right|_{\boldsymbol{\theta}=\hat{\boldsymbol{\theta}}_k}\right)^T \end{array}\right] \left[\begin{array}{c} \overset{n+m}{\longleftrightarrow} \\ \mathbf{R}^{-1} \end{array}\right] \updownarrow n+m \end{aligned} \tag{5.56}$$

Thus, in terms of partitioned matrices:

$$\begin{aligned}\mathbf{K}_{x_k} &= \tilde{\mathbf{T}}_{x_k}\mathbf{G}_k^T\mathbf{R}^{-1} + \mathbf{V}_{x_k}\left[\mathbf{E}_{k+1}\mathbf{V}_{x_k}^T\mathbf{G}_k^T + \mathbf{E}_{k+1}\left(\left.\frac{\partial \mathbf{G}_k}{\partial \boldsymbol{\theta}}\right|_{\boldsymbol{\theta}=\hat{\boldsymbol{\theta}}_k}\right)^T\right]\mathbf{R}^{-1} = \\ &= \tilde{\mathbf{K}}_{x_k} + \mathbf{V}_{x_k}\mathbf{K}_{\theta_k} \\ \mathbf{K}_{\theta_k} &= \left[\mathbf{E}_{k+1}\mathbf{V}_{x_k}^T\mathbf{G}_k^T + \mathbf{E}_{k+1}\left(\left.\frac{\partial \mathbf{G}_k}{\partial \boldsymbol{\theta}}\right|_{\boldsymbol{\theta}=\hat{\boldsymbol{\theta}}_k}\right)^T\right]\mathbf{R}^{-1}\end{aligned} \tag{5.57}$$

The optimum estimation of the state-parameter vector $\hat{\mathbf{x}}_{A_k}$, given the sequence of observations $\{\mathbf{z}_0,\ldots,\mathbf{z}_k\}$, can be obtained by exploiting the well-known filtering recursive formula (5.24), proposed by [Kalman, 1960]. The formula can be partitioned as follows:

$$\begin{aligned}&\left[\begin{array}{c}\hat{\mathbf{x}}_k \\ \hdashline \hat{\boldsymbol{\theta}}_k\end{array}\right] = \left[\begin{array}{c:c}\mathbf{F}_{k-1} & \left.\frac{\partial \mathbf{F}_{k-1}}{\partial \boldsymbol{\theta}}\right|_{\boldsymbol{\theta}=\hat{\boldsymbol{\theta}}_{k-1}} \\ \hdashline \mathbf{0} & \mathbf{I}\end{array}\right]\left[\begin{array}{c}\hat{\mathbf{x}}_{k-1} \\ \hdashline \hat{\boldsymbol{\theta}}_{k-1}\end{array}\right] + \\ &+\left[\begin{array}{c}\mathbf{K}_{x_k} \\ \hdashline \mathbf{K}_{\theta_k}\end{array}\right]\left(\mathbf{z}_k - \left[\begin{array}{c:c}\mathbf{G}_k & \left.\frac{\partial \mathbf{G}_k}{\partial \boldsymbol{\theta}}\right|_{\boldsymbol{\theta}=\hat{\boldsymbol{\theta}}_k}\end{array}\right]\left[\begin{array}{c:c}\mathbf{F}_{k-1} & \left.\frac{\partial \mathbf{F}_{k-1}}{\partial \boldsymbol{\theta}}\right|_{\boldsymbol{\theta}=\hat{\boldsymbol{\theta}}_{k-1}} \\ \hdashline \mathbf{0} & \mathbf{I}\end{array}\right]\left[\begin{array}{c}\hat{\mathbf{x}}_{k-1} \\ \hdashline \hat{\boldsymbol{\theta}}_{k-1}\end{array}\right]\right) = \\ &= \left[\begin{array}{c}\mathbf{F}_{k-1}\mathbf{x}_{k-1} + \left(\left.\frac{\partial \mathbf{F}_{k-1}}{\partial \boldsymbol{\theta}}\right|_{\boldsymbol{\theta}=\hat{\boldsymbol{\theta}}_{k-1}}\right)\hat{\boldsymbol{\theta}}_{k-1} \\ \hdashline \hat{\boldsymbol{\theta}}_{k-1}\end{array}\right] + \\ &+\left[\begin{array}{c}\mathbf{K}_{x_k} \\ \hdashline \mathbf{K}_{\theta_k}\end{array}\right]\left(\mathbf{z}_k - \left[\begin{array}{c:c}\mathbf{G}_k\mathbf{F}_{k-1} & \mathbf{G}_k\left(\left.\frac{\partial \mathbf{F}_{k-1}}{\partial \boldsymbol{\theta}}\right|_{\boldsymbol{\theta}=\hat{\boldsymbol{\theta}}_{k-1}}\right) + \left.\frac{\partial \mathbf{G}_k}{\partial \boldsymbol{\theta}}\right|_{\boldsymbol{\theta}=\hat{\boldsymbol{\theta}}_k}\end{array}\right]\left[\begin{array}{c}\hat{\mathbf{x}}_{k-1} \\ \hdashline \hat{\boldsymbol{\theta}}_{k-1}\end{array}\right]\right)\end{aligned} \tag{5.58}$$

Thus, in terms of partitioned matrices:

$$\begin{aligned}\hat{\mathbf{x}}_k &= \mathbf{F}_{k-1}\hat{\mathbf{x}}_{k-1} + \left(\left.\frac{\partial \mathbf{F}_{k-1}}{\partial \boldsymbol{\theta}}\right|_{\boldsymbol{\theta}=\hat{\boldsymbol{\theta}}_{k-1}}\right)\hat{\boldsymbol{\theta}}_{k-1} + \\ &+\mathbf{K}_{x_k}\left(\mathbf{z}_k - \left[\mathbf{G}_k\mathbf{F}_{k-1}\hat{\mathbf{x}}_{k-1} + \mathbf{G}_k\left(\left.\frac{\partial \mathbf{F}_{k-1}}{\partial \boldsymbol{\theta}}\right|_{\boldsymbol{\theta}=\hat{\boldsymbol{\theta}}_{k-1}}\right)\hat{\boldsymbol{\theta}}_{k-1} + \left(\left.\frac{\partial \mathbf{G}_k}{\partial \boldsymbol{\theta}}\right|_{\boldsymbol{\theta}=\hat{\boldsymbol{\theta}}_k}\right)\hat{\boldsymbol{\theta}}_{k-1}\right]\right) \\ \hat{\boldsymbol{\theta}}_k &= \hat{\boldsymbol{\theta}}_{k-1} + \\ &+\mathbf{K}_{\theta_k}\left(\mathbf{z}_k - \left[\mathbf{G}_k\mathbf{F}_{k-1}\hat{\mathbf{x}}_{k-1} + \mathbf{G}_k\left(\left.\frac{\partial \mathbf{F}_{k-1}}{\partial \boldsymbol{\theta}}\right|_{\boldsymbol{\theta}=\hat{\boldsymbol{\theta}}_{k-1}}\right)\hat{\boldsymbol{\theta}}_{k-1} + \left(\left.\frac{\partial \mathbf{G}_k}{\partial \boldsymbol{\theta}}\right|_{\boldsymbol{\theta}=\hat{\boldsymbol{\theta}}_k}\right)\hat{\boldsymbol{\theta}}_{k-1}\right]\right)\end{aligned} \tag{5.59}$$

As done in [Friedland, 1969], by removing from the equation (5.59) all the components related to the parameter vector $\hat{\boldsymbol{\theta}}_k$, it becomes possible to define as $\tilde{\mathbf{x}}_k$ the parameter-free estimate for the state vector $\hat{\mathbf{x}}_k$:

$$\tilde{\mathbf{x}}_k = \mathbf{F}_{k-1}\tilde{\mathbf{x}}_{k-1} + \tilde{\mathbf{K}}_{x_k}\left(\mathbf{z}_k - \mathbf{G}_k\mathbf{F}_{k-1}\tilde{\mathbf{x}}_{k-1}\right) = \mathbf{F}_{k-1}\tilde{\mathbf{x}}_{k-1} + \tilde{\mathbf{K}}_{x_k}\tilde{\mathbf{r}}_k \tag{5.60}$$

where:

$$\tilde{\mathbf{r}}_k = \mathbf{z}_k - \mathbf{G}_k\mathbf{F}_{k-1}\tilde{\mathbf{x}}_{k-1} \tag{5.61}$$

is defined as the residual of parameter-free estimation.

Proposition 4. *The state vector $\hat{\mathbf{x}}_k$ can be expressed in terms of its parameter-free estimate $\tilde{\mathbf{x}}_k$ and the parameter estimate $\hat{\boldsymbol{\theta}}_k$, as follows:*

$$\hat{\mathbf{x}}_k = \tilde{\mathbf{x}}_k + \mathbf{V}_{x_k}\hat{\boldsymbol{\theta}}_k \tag{5.62}$$

Proof. By substitution of (5.62) in the bracketed term which have in common the expressions of $\hat{\mathbf{x}}_k$ and $\hat{\boldsymbol{\theta}}_k$ in (5.59), and by taking into account that $\mathbf{U}_{\theta_k} = \mathbf{V}_{\theta_k} = \mathbf{I}$, the following expression can be written:

$$\begin{aligned}
&\mathbf{z}_k - \mathbf{G}_k\mathbf{F}_{k-1}\hat{\mathbf{x}}_{k-1} + \mathbf{G}_k\left(\frac{\partial \mathbf{F}_{k-1}}{\partial \boldsymbol{\theta}}\bigg|_{\boldsymbol{\theta}=\hat{\boldsymbol{\theta}}_{k-1}}\right)\hat{\boldsymbol{\theta}}_{k-1} + \left(\frac{\partial \mathbf{G}_k}{\partial \boldsymbol{\theta}}\bigg|_{\boldsymbol{\theta}=\hat{\boldsymbol{\theta}}_k}\right)\hat{\boldsymbol{\theta}}_{k-1} = \\
=&\mathbf{z}_k - \mathbf{G}_k\mathbf{F}_{k-1}\left(\tilde{\mathbf{x}}_{k-1} - \mathbf{V}_{x_{k-1}}\hat{\boldsymbol{\theta}}_{k-1}\right) + \mathbf{G}_k\left(\frac{\partial \mathbf{F}_{k-1}}{\partial \boldsymbol{\theta}}\bigg|_{\boldsymbol{\theta}=\hat{\boldsymbol{\theta}}_{k-1}}\right)\hat{\boldsymbol{\theta}}_{k-1} + \left(\frac{\partial \mathbf{G}_k}{\partial \boldsymbol{\theta}}\bigg|_{\boldsymbol{\theta}=\hat{\boldsymbol{\theta}}_k}\right)\hat{\boldsymbol{\theta}}_{k-1} = \\
=&\underbrace{\left(\mathbf{z}_k - \mathbf{G}_k\mathbf{F}_{k-1}\tilde{\mathbf{x}}_{k-1}\right)}_{=\tilde{\mathbf{r}}_k} - \mathbf{G}_k\underbrace{\left(\mathbf{F}_{k-1}\mathbf{V}_{x_{k-1}} + \frac{\partial \mathbf{F}_{k-1}}{\partial \boldsymbol{\theta}}\bigg|_{\boldsymbol{\theta}=\hat{\boldsymbol{\theta}}_{k-1}}\right)}_{=\mathbf{U}_{x_k}}\hat{\boldsymbol{\theta}}_{k-1} + \left(\frac{\partial \mathbf{G}_k}{\partial \boldsymbol{\theta}}\bigg|_{\boldsymbol{\theta}=\hat{\boldsymbol{\theta}}_k}\right)\hat{\boldsymbol{\theta}}_{k-1} = \\
=&\tilde{\mathbf{r}}_k - \underbrace{\left(\mathbf{G}_k\mathbf{U}_{x_k} + \frac{\partial \mathbf{G}_k}{\partial \boldsymbol{\theta}}\bigg|_{\boldsymbol{\theta}=\hat{\boldsymbol{\theta}}_k}\right)}_{=\mathbf{S}_k}\hat{\boldsymbol{\theta}}_{k-1} = \tilde{\mathbf{r}}_k - \mathbf{S}_k\hat{\boldsymbol{\theta}}_{k-1}
\end{aligned} \tag{5.63}$$

Thus, the expressions of $\hat{\mathbf{x}}_k$ and $\hat{\boldsymbol{\theta}}_k$ can be written also in terms of the parameter-free components $\tilde{\mathbf{x}}_k$ and $\tilde{\mathbf{r}}_k$ as follows:

$$\begin{aligned}
\hat{\mathbf{x}}_k &= \mathbf{F}_{k-1}\left(\tilde{\mathbf{x}}_{k-1} + \mathbf{V}_{x_{k-1}}\hat{\boldsymbol{\theta}}_{k-1}\right) + \left(\frac{\partial \mathbf{F}_{k-1}}{\partial \boldsymbol{\theta}}\bigg|_{\boldsymbol{\theta}=\hat{\boldsymbol{\theta}}_{k-1}}\right)\hat{\boldsymbol{\theta}}_{k-1} + \mathbf{K}_{x_k}\left(\tilde{\mathbf{r}}_k - \mathbf{S}_k\hat{\boldsymbol{\theta}}_{k-1}\right) = \\
&= \mathbf{F}_{k-1}\tilde{\mathbf{x}}_{k-1} + \left[\underbrace{\left(\mathbf{F}_{k-1}\mathbf{V}_{x_{k-1}} + \frac{\partial \mathbf{F}_{k-1}}{\partial \boldsymbol{\theta}}\bigg|_{\boldsymbol{\theta}=\hat{\boldsymbol{\theta}}_{k-1}}\right)}_{=\mathbf{U}_{x_k}} - \mathbf{K}_{x_k}\mathbf{S}_k\right]\hat{\boldsymbol{\theta}}_{k-1} + \mathbf{K}_{x_k}\tilde{\mathbf{r}}_k = \\
&= \mathbf{F}_{k-1}\tilde{\mathbf{x}}_{k-1} + \left(\mathbf{U}_{x_k} - \mathbf{K}_{x_k}\mathbf{S}_k\right)\hat{\boldsymbol{\theta}}_{k-1} + \mathbf{K}_{x_k}\tilde{\mathbf{r}}_k \\
\hat{\boldsymbol{\theta}}_k &= \hat{\boldsymbol{\theta}}_{k-1} + \mathbf{K}_{\theta_k}\left(\tilde{\mathbf{r}}_k - \mathbf{S}_k\hat{\boldsymbol{\theta}}_{k-1}\right) = \left(\mathbf{I} - \mathbf{K}_{\theta_k}\mathbf{S}_k\right)\hat{\boldsymbol{\theta}}_{k-1} + \mathbf{K}_{\theta_k}\tilde{\mathbf{r}}_k
\end{aligned} \tag{5.64}$$

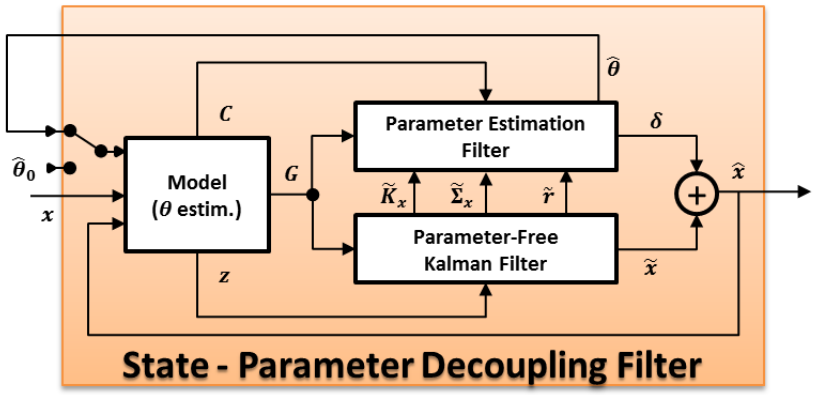

Figure 5.1: Scheme of the Single Channel State-Parameter Decoupling Filter

By substituting in (5.62) the expression of $\hat{\boldsymbol{\theta}}_k$ in (5.64), it can be obtained another expression of $\hat{\mathbf{x}}_k$, written in terms of the parameter-free components $\tilde{\mathbf{x}}_k$ and $\tilde{\mathbf{r}}_k$:

$$\hat{\mathbf{x}}_k = \tilde{\mathbf{x}}_k + \mathbf{V}_{x_k}\left[\left(\mathbf{I} - \mathbf{K}_{\theta_k}\mathbf{S}_k\right)\hat{\boldsymbol{\theta}}_{k-1} + \mathbf{K}_{\theta_k}\tilde{\mathbf{r}}_k\right] \tag{5.65}$$

It is worth to note that (5.64) and (5.65) must be equal in order to be two equivalent expressions of $\hat{\mathbf{x}}_k$ in terms of $\tilde{\mathbf{x}}_k$ and $\tilde{\mathbf{r}}_k$.

Thus:

$$\begin{aligned} &\tilde{\mathbf{x}}_k + \left(\mathbf{V}_{x_k} - \mathbf{V}_{x_k}\mathbf{K}_{\theta_k}\mathbf{S}_k\right)\hat{\boldsymbol{\theta}}_{k-1} + \mathbf{V}_{x_k}\mathbf{K}_{\theta_k}\tilde{\mathbf{r}}_k = \mathbf{F}_{k-1}\tilde{\mathbf{x}}_{k-1} + \left(\mathbf{U}_{x_k} - \mathbf{K}_{x_k}\mathbf{S}_k\right)\hat{\boldsymbol{\theta}}_{k-1} + \mathbf{K}_{x_k}\tilde{\mathbf{r}}_k \\ \Longrightarrow \quad &\tilde{\mathbf{x}}_k = \mathbf{F}_{k-1}\tilde{\mathbf{x}}_{k-1} + \left(\mathbf{U}_{x_k} - \mathbf{K}_{x_k}\mathbf{S}_k - \mathbf{V}_{x_k} + \mathbf{V}_{x_k}\mathbf{K}_{\theta_k}\mathbf{S}_k\right)\hat{\boldsymbol{\theta}}_{k-1} + \left(\mathbf{K}_{x_k} - \mathbf{V}_{x_k}\mathbf{K}_{\theta_k}\right)\tilde{\mathbf{r}}_k \end{aligned} \tag{5.66}$$

To complete the proof, the expression of $\tilde{\mathbf{x}}_k$ in (5.66) must be equal to the definition of $\tilde{\mathbf{x}}_k$ given in (5.60).

Therefore, the two following conditions must apply:

$$\begin{aligned} &\mathbf{K}_{x_k} - \mathbf{V}_{x_k}\mathbf{K}_{\theta_k} = \tilde{\mathbf{K}}_{x_k} \\ &\Longrightarrow \mathbf{K}_{x_k} = \tilde{\mathbf{K}}_{x_k} + \mathbf{V}_{x_k}\mathbf{K}_{\theta_k} \end{aligned} \tag{5.67}$$

$$\begin{aligned} &\mathbf{U}_{x_k} - \mathbf{K}_{x_k}\mathbf{S}_k - \mathbf{V}_{x_k} + \mathbf{V}_{x_k}\mathbf{K}_{\theta_k}\mathbf{S}_k = 0 \\ &\Longrightarrow \mathbf{V}_{x_k} = \mathbf{U}_{x_k} - \left(\mathbf{K}_{x_k} - \mathbf{V}_{x_k}\mathbf{K}_{\theta_k}\right)\mathbf{S}_k \\ &\Longrightarrow \mathbf{V}_{x_k} = \mathbf{U}_{x_k} - \tilde{\mathbf{K}}_{x_k}\mathbf{S}_k \end{aligned} \tag{5.68}$$

Both these constraint are satisfied, thus the proof is successfully completed. □

5.4 Decoupled State-Parameter DDR procedure

5.4.1 Single Channel Estimator

By applying the results obtained in Section 5.3, it is possible to develop the following computational procedure, which allows to implement a parameter-free state estimation $\tilde{\mathbf{x}}$ independent of the parameter vector estimation $\hat{\boldsymbol{\theta}} = [\hat{\theta}_1, \ldots, \hat{\theta}_p]$. The whole procedure can be

splitted in four different sub-programs. The algorithm 1 implements the updating of the all model matrices, by taking as inputs the actual and estimated measurement vector, i.e. $\mathbf{x}$, and $\hat{\mathbf{x}}$, respectively, as well as the estimates of parameters, i.e. $\hat{\boldsymbol{\theta}}$, then it sends as outputs to the state and parameter estimators the observation vector, i.e. $\mathbf{z}$, and the updated model submatrices, i.e. $\mathbf{G}$, and $\mathbf{C} = \partial\mathbf{G}/\partial\boldsymbol{\theta}$. The Algorithm 2 refers to the KF, which performs the parameter-free state estimation, by taking as inputs the observation vector, i.e. $\mathbf{z}$, the model matrix $\mathbf{G}$, and the error and noise covariance matrices, i.e. $\mathbf{R}$, and $\mathbf{Q}$, respectively, then providing as output the state estimation vector $\tilde{\mathbf{x}}$, and the other parameter-free matrices needed by the parameter estimation filter, i.e. the Kalman gain $\tilde{\mathbf{K}}_x$, the covariance matrix $\tilde{\boldsymbol{\Sigma}}_x$, and the residual of parameter-free estimation $\tilde{\mathbf{r}}$. The algorithm 3 implements the filter which performs the estimates of parameters, by taking as inputs the parameter-free components from the KF, i.e. $\tilde{\mathbf{K}}_x$, $\tilde{\boldsymbol{\Sigma}}_x$, and $\tilde{\mathbf{r}}$, the error covariance matrix, i.e. $\mathbf{R}$, and the model's matrices $\mathbf{G}$ and $\mathbf{C}$, then providing as outputs the parameter vector estimation, i.e. $\hat{\boldsymbol{\theta}}$, and the correction term $\delta = \mathbf{V}_x\hat{\boldsymbol{\theta}}$. Finally, the algorithm 4 implements the updating of the state estimation vector, by taking as inputs the estimations provided by the two decoupled filters, i.e. the parameter-free state estimation $\tilde{\mathbf{x}}$, and the correction term δ, then providing as output the vector $\hat{\mathbf{x}}$. The corresponding scheme of this computation procedure is showed in figure 5.1. The covariance matrices $\mathbf{R}$, and $\mathbf{Q}$ are both supposed to be known; thus, they are not considered in this graphical representation, which aims to depict the updating logic of the state-parameter decoupling strategy. In this scheme the computation procedure leads to a two parallel filtering parts, the first one corresponding to the standard KF, which generates the original state estimation $\tilde{\mathbf{x}}$, and the second one implementing the adaptive part, which generates the corrective term δ due to the parameter estimation $\hat{\boldsymbol{\theta}}$. The final state estimation $\hat{\mathbf{x}}$ is then computed by taking into account both the estimation components of the two decoupled filters. As depicted in Figure 5.1, this state-parameter decoupling filter can be seen also as a single channel estimator. This approach results to be effective and useful in many practical applications, because it allows to make the parameter estimation after the "state profile" estimation has been performed. Indeed, the way to solve the estimation problem requiring the initial values both for the state and parameter vectors is to keep constant the parameter vector to a good assumed profile $\hat{\boldsymbol{\theta}}_0$, i.e. to keep closed the parameter estimation channel, and to update for a certain amount of time the state estimation until a good state profile is reached; thus, the parameter estimation channel could be opened and consequently also the parameter vector would start to be estimated.

5.4.2 Multi-Channel Estimator

The direct application of the joint Data Reconciliation-Parameter Estimation procedure developed in Section 5.3 to an industrial system can be done only if a certain amount of restrictive assumptions apply. Indeed, most of the time, the number of parameters which need to be estimated at the same time in an industrial process make unsatisfied the observability property of the corresponding augmented system which should be filtered, that is the necessary condition for the application of this estimation procedure. In such a case, the problem could be solved by reducing the number of components in the parameter vector $\hat{\boldsymbol{\theta}}$ up to obtain a corresponding augmented system which satisfies the observability property. All the remaining parameters which cannot be estimated must be supposed known and constant. In order to overcome this limitation, in this paper a novel approach which makes use of a suitable set of state-parameter decoupling filters has been proposed. The main idea is to split the whole set

Algorithm 1: Update Model ($\boldsymbol{\theta}$ estimation) matrices

Input : $\mathbf{x}, \hat{\mathbf{x}}, \hat{\boldsymbol{\theta}}$
Output: $\mathbf{C}, \mathbf{G}, \mathbf{z}$

$\mathbf{f} \leftarrow \mathit{SteadyStateEqs}(\hat{\mathbf{x}}, \hat{\boldsymbol{\theta}})$
$\mathbf{A} \leftarrow \mathbf{Jacobian}(\mathbf{f}, \hat{\mathbf{x}})$
$\mathbf{B} \leftarrow \mathbf{Jacobian}(\mathbf{f}, \hat{\boldsymbol{\theta}})$
$\mathbf{G} \leftarrow [\mathbf{I}\,;\,\mathbf{A}]$
$\mathbf{C} \leftarrow [\mathbf{0}\,;\,\mathbf{B}]$
$\mathbf{f} \leftarrow \mathit{SteadyStateEqs}(\mathbf{x}, \hat{\boldsymbol{\theta}})$
$\mathbf{A}_m \leftarrow \mathbf{Jacobian}(\mathbf{f}, \mathbf{x})$
$\mathbf{B}_m \leftarrow \mathbf{Jacobian}(\mathbf{f}, \hat{\boldsymbol{\theta}})$
$\mathbf{D} \leftarrow [\mathbf{A}_m\,,\,\mathbf{B}_m]$
$\mathbf{x}_A \leftarrow [\mathbf{x}\,,\,\hat{\boldsymbol{\theta}}]$
$\mathbf{e} \leftarrow \mathbf{D} \cdot \mathbf{x}_A$
$\mathbf{b} \leftarrow (\mathbf{e} - \mathbf{f})$
$\mathbf{z} \leftarrow [\mathbf{x}\,,\,\mathbf{b}]$

Algorithm 2: Update Parameter-Free Kalman Filter

Input : $\mathbf{G}, \mathbf{R}, \mathbf{Q}, \mathbf{z}, k$
Output: $\tilde{\mathbf{K}}_x, \tilde{\boldsymbol{\Sigma}}_x, \tilde{\mathbf{r}}, \tilde{\mathbf{x}}$

if $k = 0$ **then**
  $\tilde{\boldsymbol{\Sigma}}_x \leftarrow \tilde{\boldsymbol{\Sigma}}_{x_0}$
  $\tilde{\mathbf{x}} \leftarrow \mathbf{0}$
end
$\tilde{\mathbf{K}}_x \leftarrow \tilde{\boldsymbol{\Sigma}}_x \mathbf{G}^T (\mathbf{G} \tilde{\boldsymbol{\Sigma}}_x \mathbf{G}^T + \mathbf{R})^{-1}$
$\tilde{\boldsymbol{\Sigma}}_x \leftarrow (\mathbf{I} - \tilde{\mathbf{K}}_x \mathbf{G}) \tilde{\boldsymbol{\Sigma}}_x + \mathbf{Q}$
$\tilde{\mathbf{r}} \leftarrow \mathbf{z} - \mathbf{G}\tilde{\mathbf{x}}$
$\tilde{\mathbf{x}} \leftarrow \tilde{\mathbf{x}} + \tilde{\mathbf{K}}_x \tilde{\mathbf{r}}$

of parameters to estimate in a certain number of subsets. As underlined before, each one of these subsets must to be chosen such as its corresponding augmented system is observable, that is the estimation with a state-parameter decoupling filter would be feasible.

Therefore, given l suitable, i.e. observable, parameter subsets, the whole parameter vector of the model, i.e. $\boldsymbol{\theta}_T$, having a total number of p components, can be splitted as follows:

$$\boldsymbol{\theta}_T = [\boldsymbol{\theta}_1, \ldots, \boldsymbol{\theta}_i, \ldots, \boldsymbol{\theta}_l] \tag{5.69}$$

where:

$$\begin{gathered} \boldsymbol{\theta}_i = [\theta_{i1}, \ldots, \theta_{ip_i}] \quad , \quad i = 1, \ldots, l \\ \textstyle\sum_{i=1}^{l} p_i = p \end{gathered} \tag{5.70}$$

Hence, the parameter vector containing the i-th set of estimates, i.e. $\hat{\boldsymbol{\theta}}_i$, can be denoted as:

$$\hat{\boldsymbol{\theta}}_{T_i} = [\boldsymbol{\theta}_1, \ldots, \hat{\boldsymbol{\theta}}_i, \ldots, \boldsymbol{\theta}_l] \tag{5.71}$$

Algorithm 3: Update Parameter Estimation Filter

Input : $\tilde{\mathbf{K}}_x, \tilde{\mathbf{\Sigma}}_x, \mathbf{G}, \mathbf{C}, \mathbf{R}, \tilde{\mathbf{r}}, k$
Output: $\delta, \hat{\boldsymbol{\theta}}$

if $k = 0$ **then**
  $\mathbf{U}_x \leftarrow \mathbf{0}$
  $\mathbf{E} \leftarrow \mathbf{I}$
  $\hat{\boldsymbol{\theta}} \leftarrow \hat{\boldsymbol{\theta}}_0$
end
$\mathbf{S} \leftarrow \mathbf{G}\mathbf{U}_x + \mathbf{C}$
$\mathbf{V}_x \leftarrow \mathbf{U}_x - \tilde{\mathbf{K}}_x\mathbf{S}$
$\mathbf{U}_x \leftarrow \mathbf{V}_x$
$\mathbf{E} \leftarrow \mathbf{E} - \mathbf{E}\mathbf{S}^T(\mathbf{G}\tilde{\mathbf{\Sigma}}_x\mathbf{G}^T + \mathbf{R} + \mathbf{S}\mathbf{E}\mathbf{S}^T)^{-1}\mathbf{S}\mathbf{E}$
$\mathbf{K}_\theta \leftarrow \mathbf{E}(\mathbf{V}_x^T\mathbf{G}^T + \mathbf{C})\mathbf{R}^{-1}$
$\hat{\boldsymbol{\theta}} \leftarrow \hat{\boldsymbol{\theta}} + \mathbf{K}_\theta(\tilde{\mathbf{r}} - \mathbf{S}\hat{\boldsymbol{\theta}})$
$\delta \leftarrow \mathbf{V}_x\hat{\boldsymbol{\theta}}$

Algorithm 4: Update State Estimation

Input : $\tilde{\mathbf{x}}, \delta$
Output: $\hat{\mathbf{x}}$

$\hat{\mathbf{x}} \leftarrow \tilde{\mathbf{x}} + \delta$

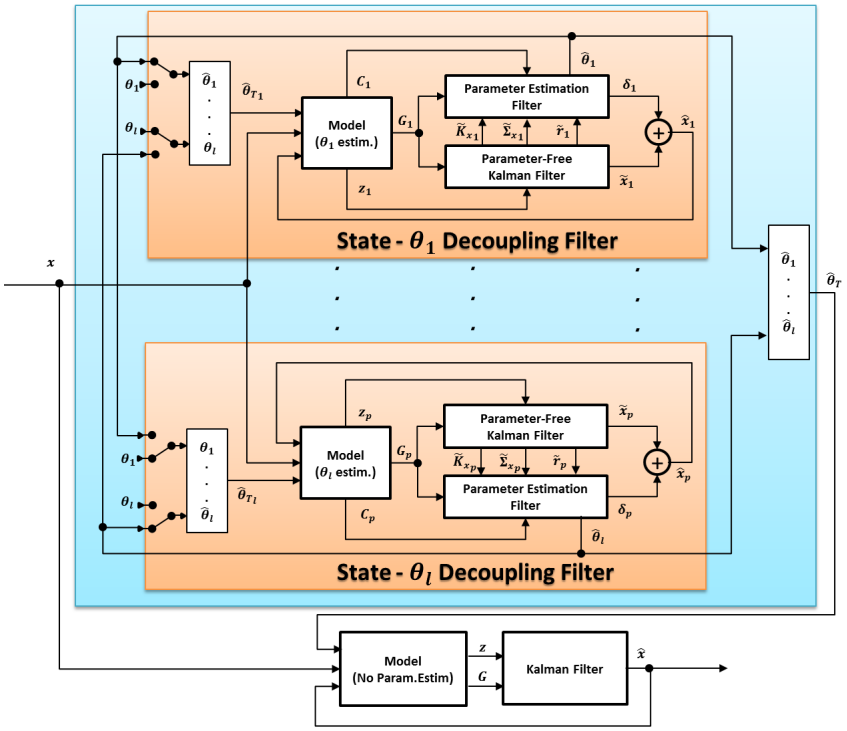

Figure 5.2: Scheme of the l^2-Channels Parameter Estimation with Decoupled KF State Estimation

whereas the estimated parameter vector as:

$$\hat{\boldsymbol{\theta}}_T = [\hat{\boldsymbol{\theta}}_1, \ldots, \hat{\boldsymbol{\theta}}_i, \ldots, \hat{\boldsymbol{\theta}}_l] \tag{5.72}$$

The following modify is then applied to the update of model's matrices procedure implemented inside each of the l state-parameter decoupling filters. Therefore, in a multi-channel estimation scheme, the algorithm 5 is applied in place of the algorithm 1. The only difference between these two codes results in the implementation of the splitting strategy of the parameter vector, which in the algorithm 5 reflects (5.70) and (5.71).

Algorithm 5: Update Model ($\boldsymbol{\theta}_i$ estimation) matrices

Input : $\mathbf{x}, \hat{\mathbf{x}}, \hat{\boldsymbol{\theta}}_{T_i}$
Output: $\mathbf{C}, \mathbf{G}, \mathbf{z}$

$\hat{\boldsymbol{\theta}}_i \leftarrow [\hat{\theta}_{i1}, \cdots, \hat{\theta}_{i_{pi}}]$
$\mathbf{f} \leftarrow SteadyStateEqs(\hat{\mathbf{x}}, \hat{\boldsymbol{\theta}}_{T_i})$
$\mathbf{A} \leftarrow \mathbf{Jacobian}(\mathbf{f}, \hat{\mathbf{x}})$
$\mathbf{B} \leftarrow \mathbf{Jacobian}(\mathbf{f}, \hat{\boldsymbol{\theta}}_i)$
$\mathbf{G} \leftarrow [\mathbf{I}\ ;\ \mathbf{A}]$
$\mathbf{C} \leftarrow [\mathbf{0}\ ;\ \mathbf{B}]$
$\mathbf{f} \leftarrow SteadyStateEqs(\mathbf{x}, \hat{\boldsymbol{\theta}}_{T_i})$
$\mathbf{A}_m \leftarrow \mathbf{Jacobian}(\mathbf{f}, \mathbf{x})$
$\mathbf{B}_m \leftarrow \mathbf{Jacobian}(\mathbf{f}, \hat{\boldsymbol{\theta}}_i)$
$\mathbf{D} \leftarrow [\mathbf{A}_m\ ,\ \mathbf{B}_m]$
$\mathbf{x}_A \leftarrow [\mathbf{x}\ ,\ \hat{\boldsymbol{\theta}}_i]$
$\mathbf{e} \leftarrow \mathbf{D} \cdot \mathbf{x}_A$
$\mathbf{b} \leftarrow (\mathbf{e} - \mathbf{f})$
$\mathbf{z} \leftarrow [\mathbf{x}\ ,\ \mathbf{b}]$

The estimation of the whole parameter vector, i.e. $\hat{\boldsymbol{\theta}}_T$, can then be performed by applying the l^2-Channels state-parameter decoupling filter scheme depicted in Figure 5.2. In this case, a more precise estimate of the state vector, i.e. $\hat{\mathbf{x}}$, can be obtained by applying a standard KF, which directly exploits the better estimates of the whole parameter set. Currently, the research is ongoing to formalize an effective application of this multi-channel scheme. Particularly, a suitable strategy based on the analysis of the observability properties of each of the l dynamic models in needed, to find a correct channel opening sequence, which guarantees the estimation of the whole parameter set. An idea to define the channel opening sequence can be to compute the sensitivity matrix of the system with respect to the parametric variations and, starting from the parameter set which sensitivity index are higher, then to iterate the procedure until the convergence of the estimates is reached.

5.5 Conclusion

In this Chapter, a novel approach to solve the joint data reconciliation along with parameter estimation problem, for systems displaying a quasi-steady-state behavior, has been presented. A decoupled state-parameter DDR procedure which exploits the concepts of QSS model and EKF has been developed. In order to solve the parameter estimation problem,

two different schemes, based on this novel state-parameter decoupling procedure, have been proposed. The single channel scheme aims to achieve the estimation of a parameter set which makes satisfied the observability property of the system. The multi-channel scheme instead, based on an array of l state-parameter decoupling filters of l channels each, resolve to the more challenging estimation problem related to a larger set of parameters, which cause the observability loss of the resulting model. Research is currently ongoing, in order to provide a suitable strategy for the channel opening sequence of the l^2-Channels scheme, based on the observability analysis. Further research is needed also to analytically evaluate the convergence properties of both the proposed schemes, even tough, in principle, they should reflect the same algorithmic efficiency of the EKF approach.

Chapter 6

Practical Application: Pyrolysis Reactor

This Chapter addresses the application of the joint dynamic data reconciliation and parameter estimation procedure for real-time purposes, explained in Section 5.3, to an industrial pyrolysis reactor. The corresponding joint dynamic data reconciliation along with parameter estimation problem was solved by means of the two decoupled filtering approaches discussed in Section 5.4. A real-time version of the state-parameter decoupling filter was implemented at first, to find two independent solutions for the state and parameter estimation problems. The problem of estimating sets of parameters which cause the observability loss of the resulting model was also considered. The performances of both the single and multi-channel estimators have been tested using real data sets collected over a full operational cycle of the plant. In Section 6.1, the pyrolysis process is depicted and a suitable model is provided. Then, in Section 6.2, the experimental results which confirm the validity of the proposed data reconciliation and estimation methods are shown.

6.1 Process Description and Modeling

The pyrolysis reactor is an important processing step in an olefin plant. It is used to crack heavier hydrocarbons such as naphtha, LPG, etc. to lower molecular weight hydrocarbons, such as ethylene. The pyrolysis reactor analyzed in this study consists of two identical sections. Each section of the reactor is commonly referred with the term "side". Each side contains six parallel "coils". A pyrolysis coil is a mechanical component of a cracker furnace where highly endothermic reactions occur to convert hydrocarbons to petrochemicals. The heat required for cracking the hydrocarbons is supplied from the hot flue gas by convention and radiation. Feed gases are divided and passed uniformly through each coil. Steam in also added to each coil, in the required portion, as a cracking media. Cracked gases from each coil in a side are mixed together, and passed through a Transfer Line Exchanger (TLE). The schematic layout of the plant is showed in Figure 6.1.

The reactor's model considered in this research is based on first principles and is the same depicted in the appendix of [Weiss et al., 1996]. The overall hydrocarbon and steam mass flow balance are, respectively:

$$F_{Htot} = \sum_{i=1}^{N} F_{Hi} \tag{6.1}$$

$$F_{Stot} = \sum_{i=1}^{N} F_{Si} \tag{6.2}$$

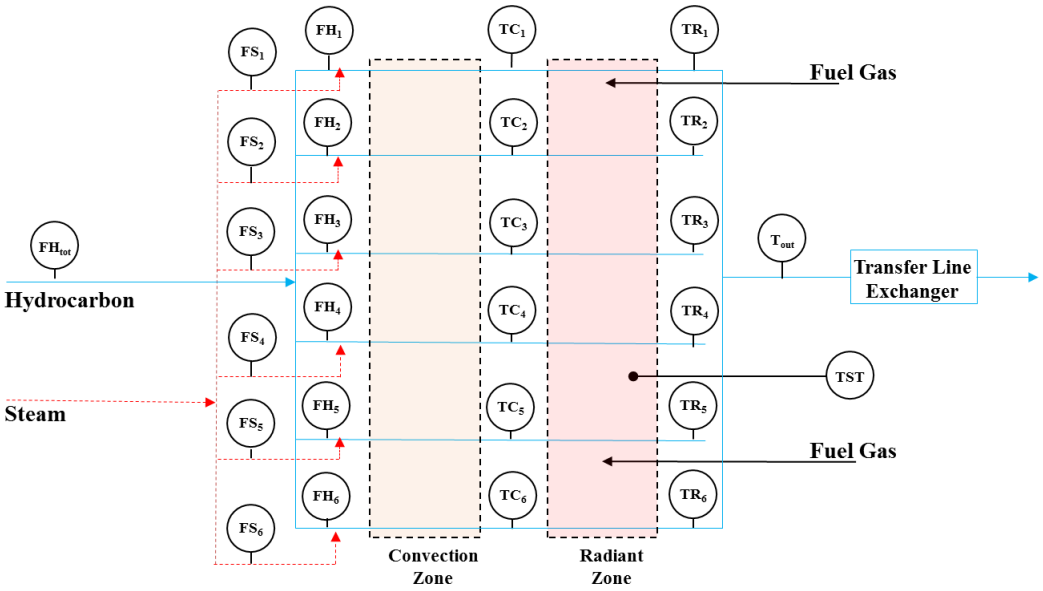

Figure 6.1: Schematic layout of the pyrolysis reactor

and both refers to a total number N = 6 of coils. F_{Htot} is the total flow of hydrocarbons to the reactor; F_{Hi} is the flow of hydrocarbons to the i-th coil; F_{Stot} is the total flow of steam to the reactor; F_{Si} is the flow of steam to the i-th coil. Only the overall flow balance equation related to hydrocarbon, i.e. (6.1), has been taken into account in this model. As in [Weiss et al., 1996], the following assumptions are made:

- all coils on both sides are identical;
- a linear relationship exists between the heat transfer coefficient for the side and the heat transfer coefficient for the coils;
- other effects such as the enthalpy change related to the cracking reactions are taken into account by a specific heat coefficients.

The overall energy balance is given by:

$$UA\left[TST - \frac{(T_{out} + \overline{T_X})}{2}\right] - F_{TM}(T_{out} - \overline{T_X}) = 0 \tag{6.3}$$

where:

- U is the heat transfer coefficient for the reactor side;
- A is the heat transfer area of the reactor side;
- TST is the tube skin temperature;
- T_{out} is the coil outlet temperature;
- $\overline{T_X}$ is the crossover temperature of the reactor side, estimated as the mean value of the crossover temperature measured for each single reactor coil:

$$\overline{T_X} = \sum_{i=1}^{N} T_{Xi} \tag{6.4}$$

- F_{TM} is the thermal mass flow of the reactor side:

$$F_{TM} = F_{Htot}c_h + F_{Stot}c_s \tag{6.5}$$

  where the two coefficients c_h and c_s are the specific heat of hydrocarbon and steam respectively.

The following $N = 6$ equations evaluate the energy balance for each single coil $i = 1,\ldots,N$:

$$U_iA_i\left[TST - \frac{(T_{Oi} + T_{Xi})}{2}\right] - F_{TMi}(T_{Oi} - T_{Xi}) = 0 \tag{6.6}$$

where:

- U_i is the heat transfer coefficient for the i-th reactor coil;
- A_i is the heat transfer area of the i-th reactor coil;
- T_{Oi} is the cracking temperature for the i-th reactor coil;
- T_{Xi} is the crossover temperature for the i-th reactor coil;
- F_{TMi} is the thermal mass flow of the i-th reactor coil:

$$F_{TMi} = F_{Hi}c_h + F_{Si}c_s \tag{6.7}$$

To summarize, the pyrolysis reactor depicted in figure 6.1 has been modeled by using a total number of $m = 8$ balance equations where $n = 27$ measured variables are involved. The resulting vectors of measurements and constraints are structured as follows, respectively: the vector $\mathbf{y} = [y_1,\ldots,y_n]^T$ contains $n = 27$ measurements where:

- y_1 is the total flow of hydrocarbon
- $y_2, \ldots, y_7$ are the flows of hydrocarbons to the single coils
- $y_8, \ldots, y_{13}$ are the flows of steam to the single coils
- $y_{14}, \ldots, y_{19}$ are the crossover temperatures for the single coils
- $y_{20}, \ldots, y_{25}$ are the cracking temperatures for the single coils
- y_{26} is the tube skin temperature
- y_{27} is the coil outlet temperature

whereas the vector $\mathbf{f}(\mathbf{x}) = [f_1(\mathbf{x}),\ldots,f_m(\mathbf{x})]$ contains $m = 8$ balance equations, where:

- $f_1(\mathbf{x})$ is the overall hydrocarbon flow balance equation (6.1)
- $f_2(\mathbf{x})$ is the side energy balance equation (6.3)
- $f_3(\mathbf{x}), \ldots, f_8(\mathbf{x})$ are the single coil energy balance equations (6.6)

It is worth to note that, according to (5.5), all the process variables are measured in this application. Therefore, the state vector $\mathbf{x}$ has the same components of the measurement vector $\mathbf{y}$.

From a theoretical point of view, all the remaining variables of the model, that is: the side and coil heat transfer coefficients U and U_i, the side and coil heat transfer areas A, A_i and the two specific heat coefficients c_h, c_s could be considered in general terms as parameters. Thus, six different parameter vectors could be defined as follows:

$$\begin{aligned} \boldsymbol{\theta}_a &= [U] \\ \boldsymbol{\theta}_b &= [U_1, \ldots, U_N] \\ \boldsymbol{\theta}_c &= [c_h] \\ \boldsymbol{\theta}_d &= [c_s] \\ \boldsymbol{\theta}_e &= [A] \\ \boldsymbol{\theta}_f &= [A_1, \ldots, A_N] \end{aligned} \tag{6.8}$$

Consequently, the vector $\boldsymbol{\theta}_T$ containing the whole set of $p = 16$ potential parameters related to the pyrolysis reactor's model can be defined as follows:

$$\boldsymbol{\theta}_T = [\boldsymbol{\theta}_a, \boldsymbol{\theta}_b, \boldsymbol{\theta}_c, \boldsymbol{\theta}_d, \boldsymbol{\theta}_e, \boldsymbol{\theta}_f] \tag{6.9}$$

Nevertheless, by following the same modeling approach applied in [Weiss et al., 1996], on the basis of the information available about the specific plant considered in this research, some additional assumptions can be made in order to reduce the dimension of $\boldsymbol{\theta}_T$, that is to reduce the number of parameters which need to be estimated. Indeed, the two specific heat coefficients, i.e. c_h and c_s, can be determined by using a rigorous cracking simulator such as PHENICS, while the side and coil heat transfer areas, i.e. A and $A_1, \ldots, A_N$, can be determined as measurement values by analyzing some geometrical properties of the plant. Thus, only the side and coil heat transfer coefficients, i.e. U and $U_1, \ldots, U_N$, remain the parameter which actually need to be estimated in practice, being them unknown quantities which cannot be directly measured.

6.2 Experimental Results

The validity of the joint dynamic data reconciliation and parameter estimation scheme proposed in Chapter 5 has been tested using a real data set collected over a full operational cycle of the considered pyrolysis reactor. At first, the estimation problem where in the pyrolysis process almost all parameters of the reactor's model can be measured, and then supposed to be known and constant, has been considered. The initial values assumed for each single parameter are shown in table 6.1.

In this case, as stated in Section 6.1, only the side and coil heat transfer coefficients cannot be directly measured. Nevertheless, because of their dependence on the coke which build up on the tubes, they can be estimated by applying the single channel state-parameter decoupling filter depicted in Section 5.4.1, by considering $\boldsymbol{\theta} = [\boldsymbol{\theta}_a, \boldsymbol{\theta}_b]$. The figures from 6.2 to 6.6 aim to compare the two different estimation profiles for each of the $n = 27$ state variables, obtained when filtering the plant measurements, i.e. x_i, denoted by the blue line in the plots, by the single channel state-parameter decoupling filter. It is easy to note the better estimations achieved when keeping closed the parameter estimation channel, i.e. $\hat{x}_i$,

Parameter	Value
Heat transfer coeff. (side)	$0,15\ kcal/s\ m^2\ ^\circ C$
Heat transfer coeff. (coil)	$0,15\ kcal/s\ m^2\ ^\circ C$
Specific heat capacity (hydrocarbon)	$0.92\ kcal/kg\ ^\circ C$
Specific heat capacity (steam)	$0.1\ kcal/kg\ ^\circ C$
Heat transfer area (side)	$150m^2$
Heat transfer area (coil)	$25m^2$

Table 6.1: Pyrolysis reactor model parameter values

denoted by the green line in the plots, en respect to the parameter-free state estimation, i.e. $\tilde{x}_i$, denoted by the red line in the plots. The Figure 6.8 shows the performance of the filter in terms of parameter estimation. The entire profile of both the side heat transfer coefficient and all the single coil heat transfer coefficients, denoted by the blue lines in the plots, is coherent with the expected results. Indeed, the almost constant decreasing of each value with respect to time denotes the slow coke build up effect on the coils during the operating cycle of the pyrolysis reactor.

The main limitation related to the reduced number of parameters which could be estimated at the same time, by applying the single channel procedure developed in Section 5.4.1, applies also for the pyrolysis reactor considered in this research. Indeed, the direct application of such an estimation procedure does not allows to estimate at the same time all the potential parameters of the pyrolysis reactor's model, that is all the $p = 16$ components of the vector $\boldsymbol{\theta}_T$ defined in (6.9), but smaller subsets only, which do not cause the loss of observability for the corresponding augmented system. Therefore, by filtering the plant measurements with the single channel state-parameter decoupling filter, the estimation of $\boldsymbol{\theta} = \boldsymbol{\theta}_T$ raised to wrong results, while the following estimations was feasible, separately: $\boldsymbol{\theta} = \boldsymbol{\theta}_a$, $\boldsymbol{\theta} = \boldsymbol{\theta}_b$, $\boldsymbol{\theta} = \boldsymbol{\theta}_c$, $\boldsymbol{\theta} = \boldsymbol{\theta}_d$, $\boldsymbol{\theta} = \boldsymbol{\theta}_e$, $\boldsymbol{\theta} = \boldsymbol{\theta}_f$, $\boldsymbol{\theta} = [\boldsymbol{\theta}_a, \boldsymbol{\theta}_b]$, $\boldsymbol{\theta} = [\boldsymbol{\theta}_e, \boldsymbol{\theta}_f]$. It is worth to note that, for each case, all the remaining parameters of the reactor's model which are not being estimated by the single channel state-parameter decoupling filter, would be set as a suitable constant values. A good estimation of the whole parameter vector $\boldsymbol{\theta}_T$ was raised by filtering the plant measurements with the multichannel state-parameter decoupling filter depicted in paragraph 5.4.2. The Figures from 6.8 to 6.11 aim to corroborate the validity of this claim. These plots show the performance of the multichannel filter in terms of parameter estimation. For each measurable parameter, the corresponding estimation profile is coherent with the measured value reported in table 6.1. Furthermore, for all the heat transfer coefficients, the corresponding estimates are coherent with those obtained by applying a different approach.

Finally, in order to provide a tool software, which could be used also by the plant engineers to monitor in real time all the operating indicators of the pyrolysis reactor, a Graphical User Interface (GUI) written in Python language has been developed. The Figure 6.12 shows a screenshot of this GUI. The main objective of this tool is to implement both a fault detection system and a regeneration cycle time predictor for the reactor, by providing real time updating trends for both reconciled data and important operating parameters of the considered pyrolysis plant, such as the heat transfer coefficients. Currently, the first prototype of this Python GUI implements a real-time version of the single-channel estimation filter, but it can be used only off-line, since it can manage only datasets of measurements stored in excel

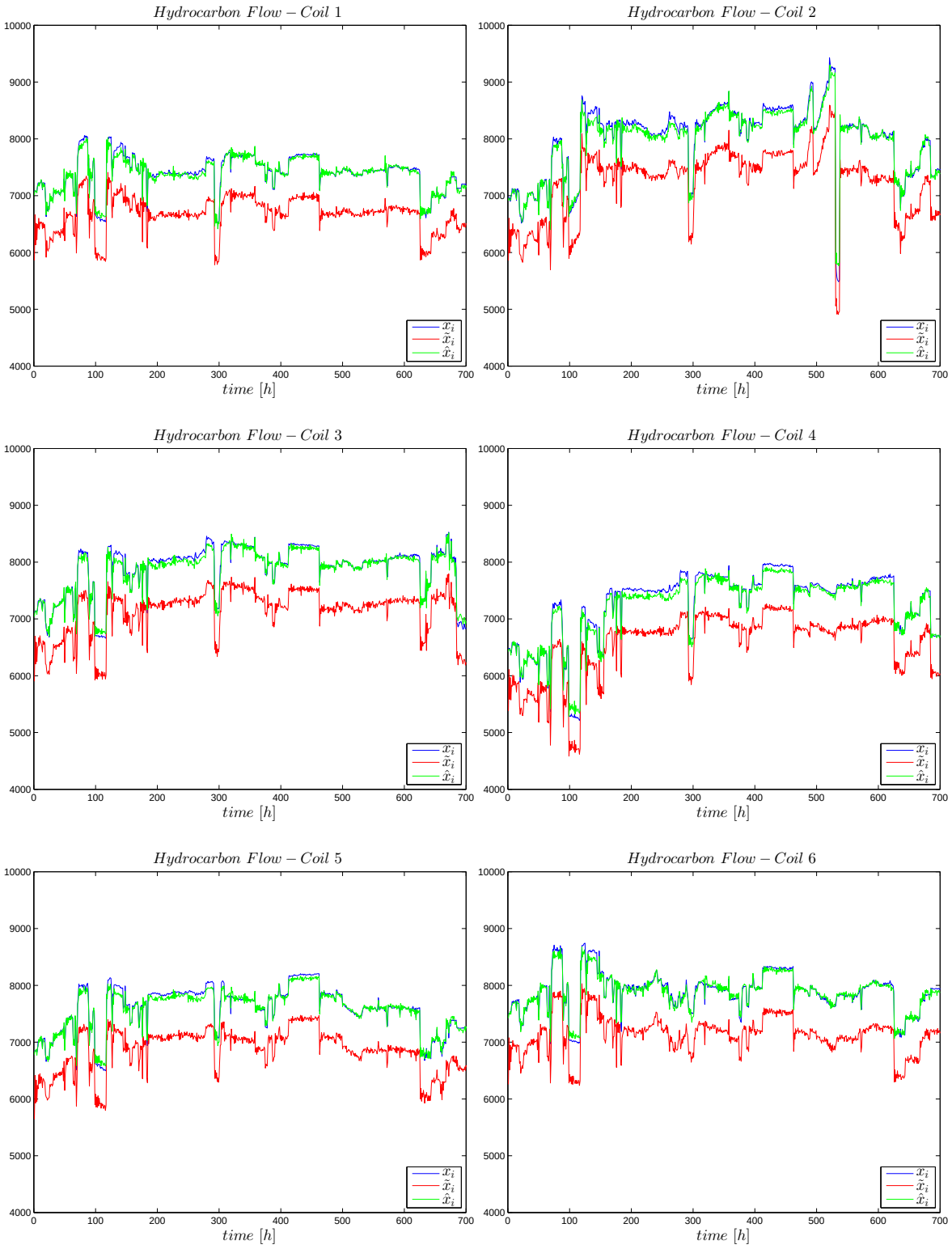

Figure 6.2: Comparison of the estimation profiles obtained for the single coil flows of hydrocarbons when filtering the plant measurements by the single channel state-parameter decoupling filter.

files. For the future, a new version of this tool will be available, which will implement also the multi-channel estimation scheme, and will be able to receive directly from the DCS the

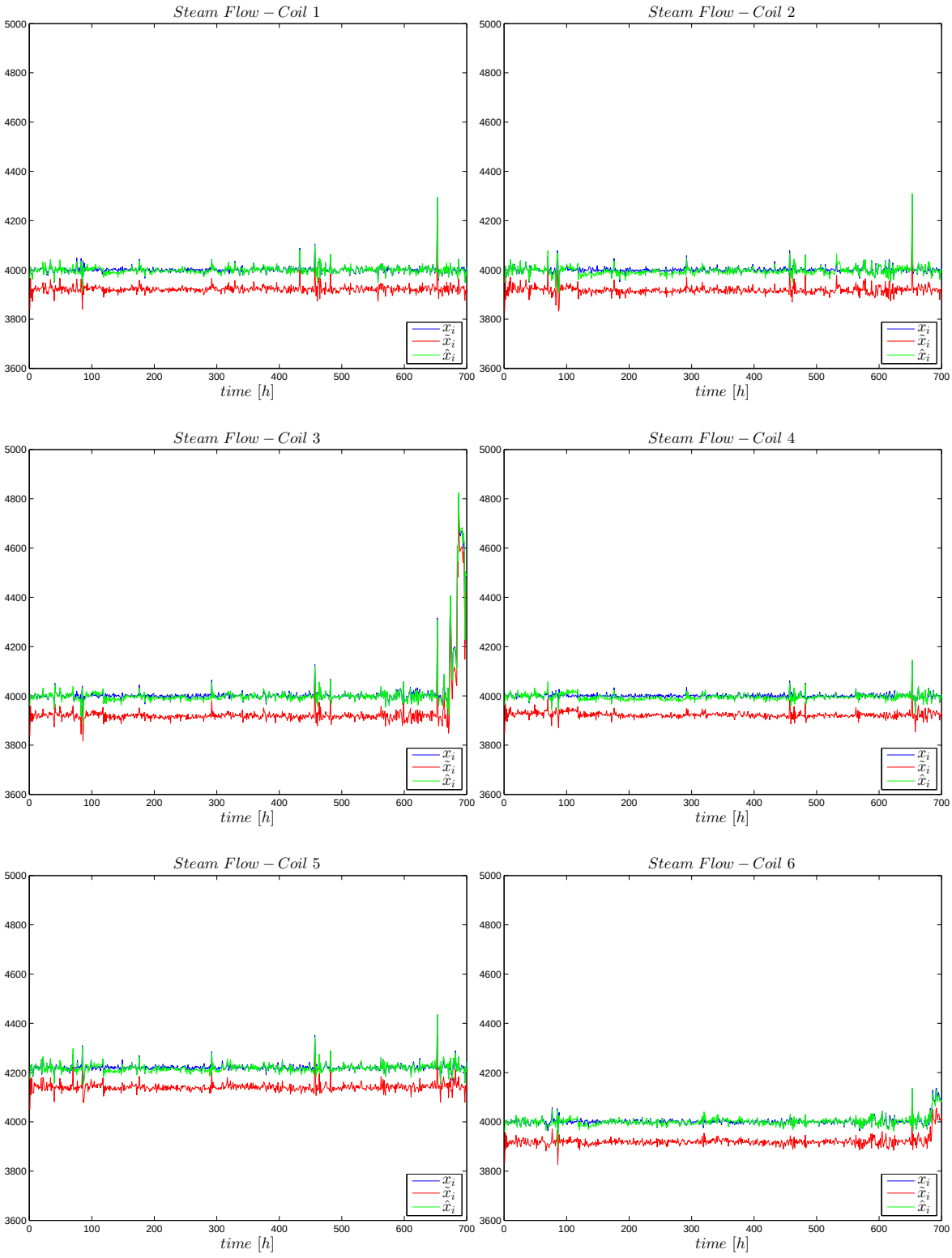

Figure 6.3: Comparison of the estimation profiles obtained for the single coil flows of steam when filtering the plant measurements by the single channel state-parameter decoupling filter.

real-time measurements acquired from the plant, thus, work on-line.

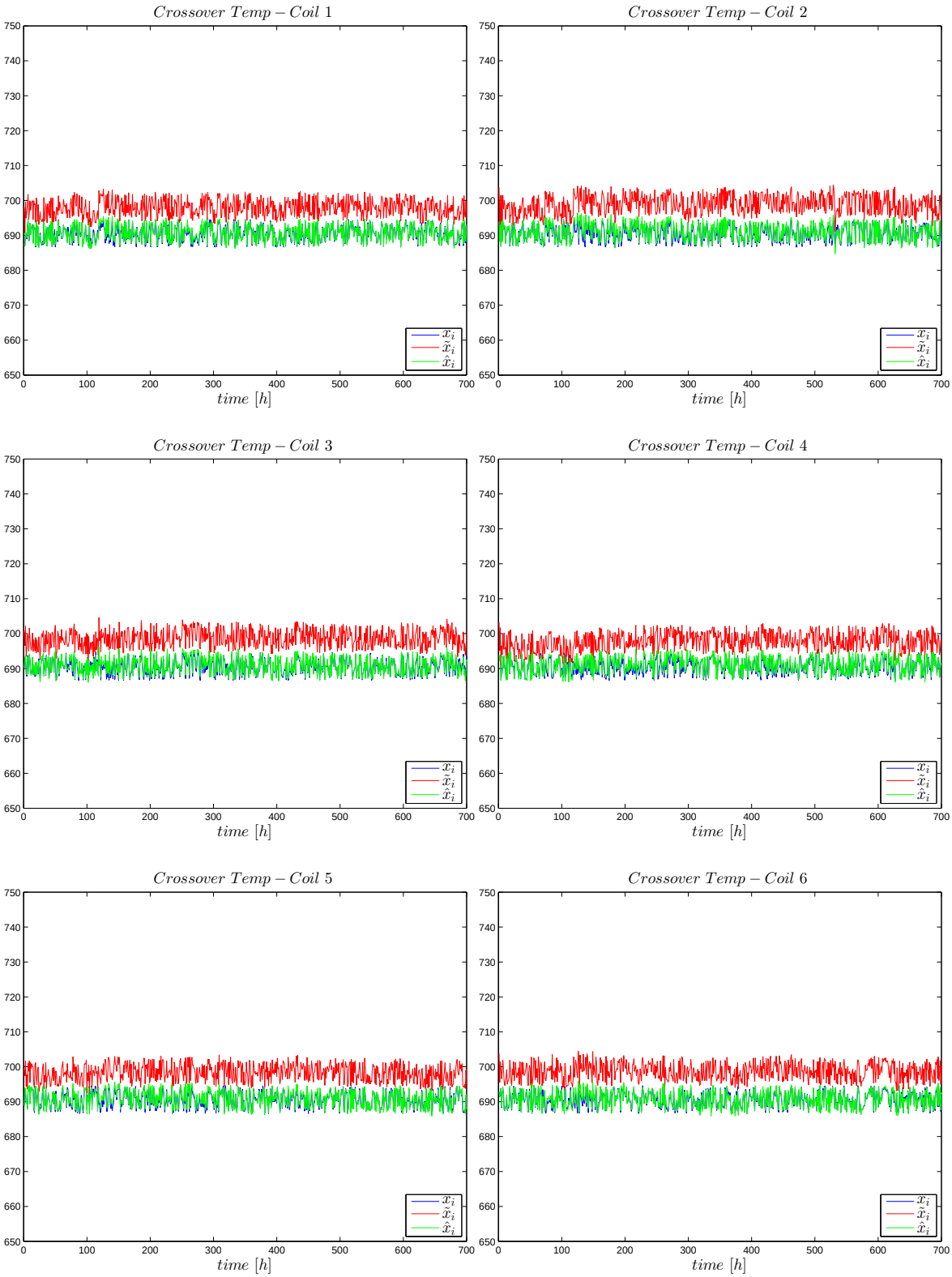

Figure 6.4: Comparison of the estimation profiles obtained for the single coil crossover temperatures when filtering the plant measurements by the single channel state-parameter decoupling filter.

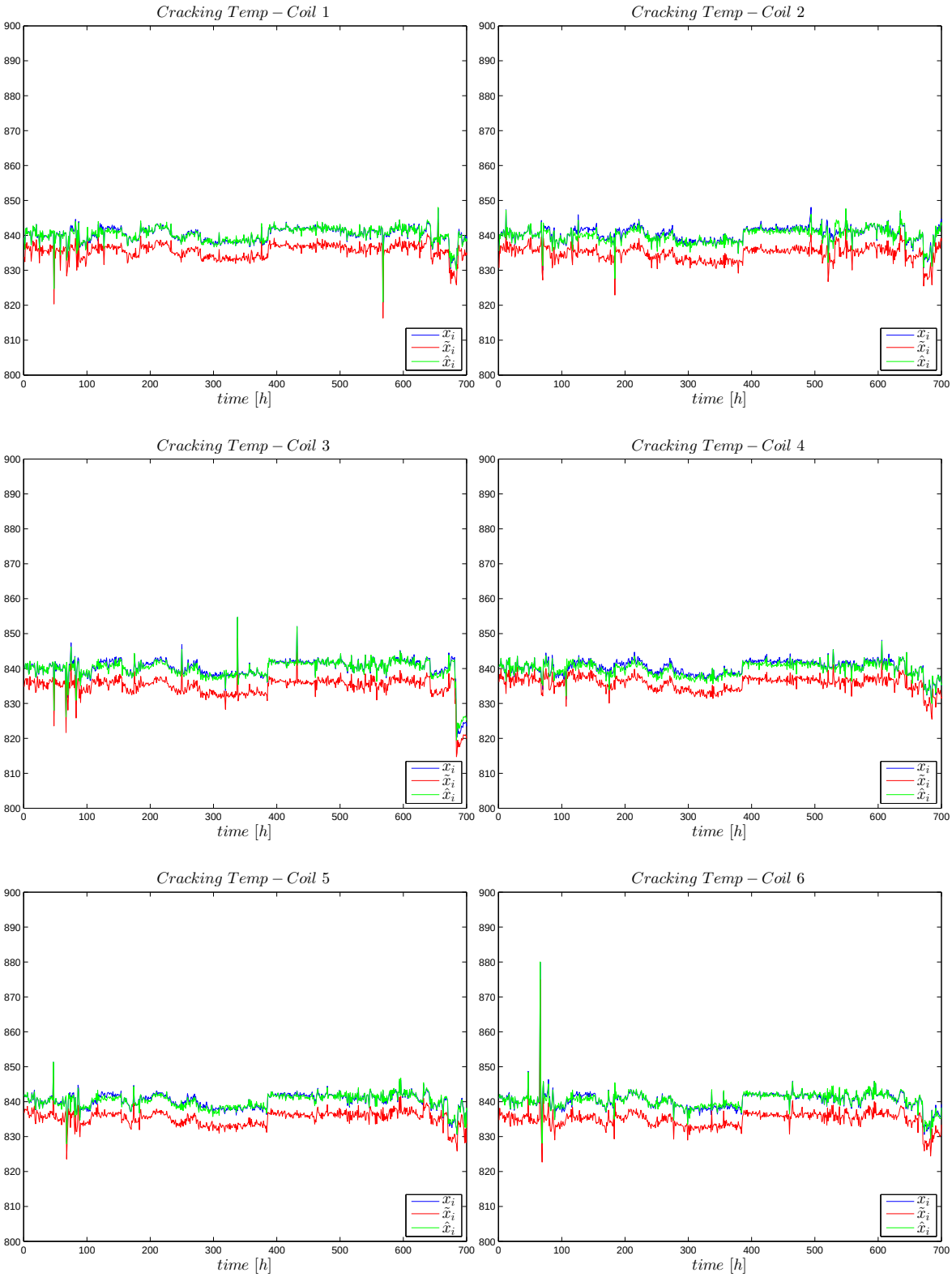

Figure 6.5: Comparison of the estimation profiles obtained for the single coil cracking temperatures when filtering the plant measurements by the single channel state-parameter decoupling filter.

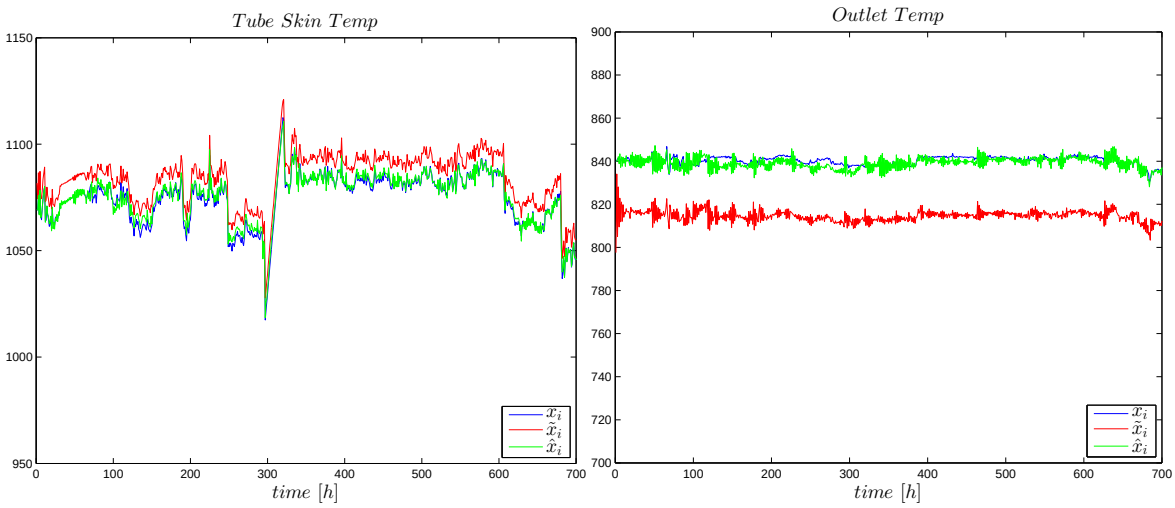

Figure 6.6: Comparison of the estimation profiles obtained for the tube skin temperature and coil outlet temperature when filtering the plant measurements by the single channel state-parameter decoupling filter.

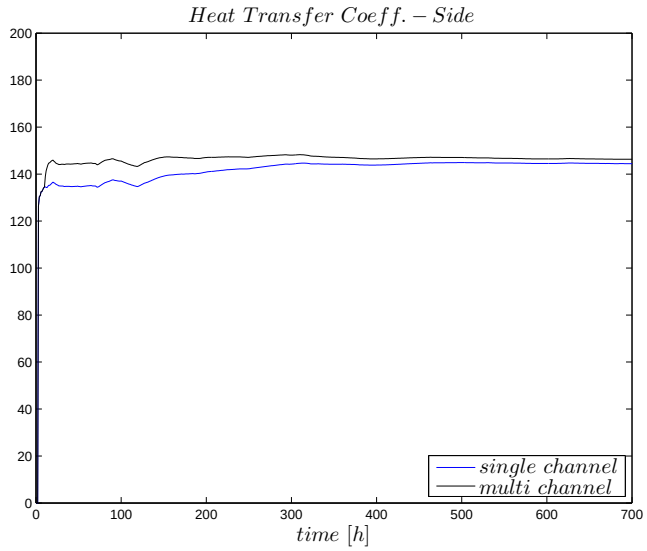

Figure 6.7: Comparison of the estimation profiles of the heat transfer coefficient side obtained when filtering the plant measurements by the single and multiple channel state-parameter decoupling filter.

6.3 Conclusion

In this Chapter, the validity of the novel approach proposed in Section 5.3, to solve the joint data reconciliation along with parameter estimation problem for processes operating in under slowly evolving dynamics, has been tested on an industrial pyrolysis reactor. A steady state model for such a process has been provided. At first, some important indicators of plant malfunctioning which cannot be directly measured, have been considered as parameters. Thus, the corresponding estimation problem has been solved by means of the single channel estimator proposed in Section 5.4.1. The more challenging estimation problem, related to a larger set of parameters which cause the observability loss of the resulting model, has been

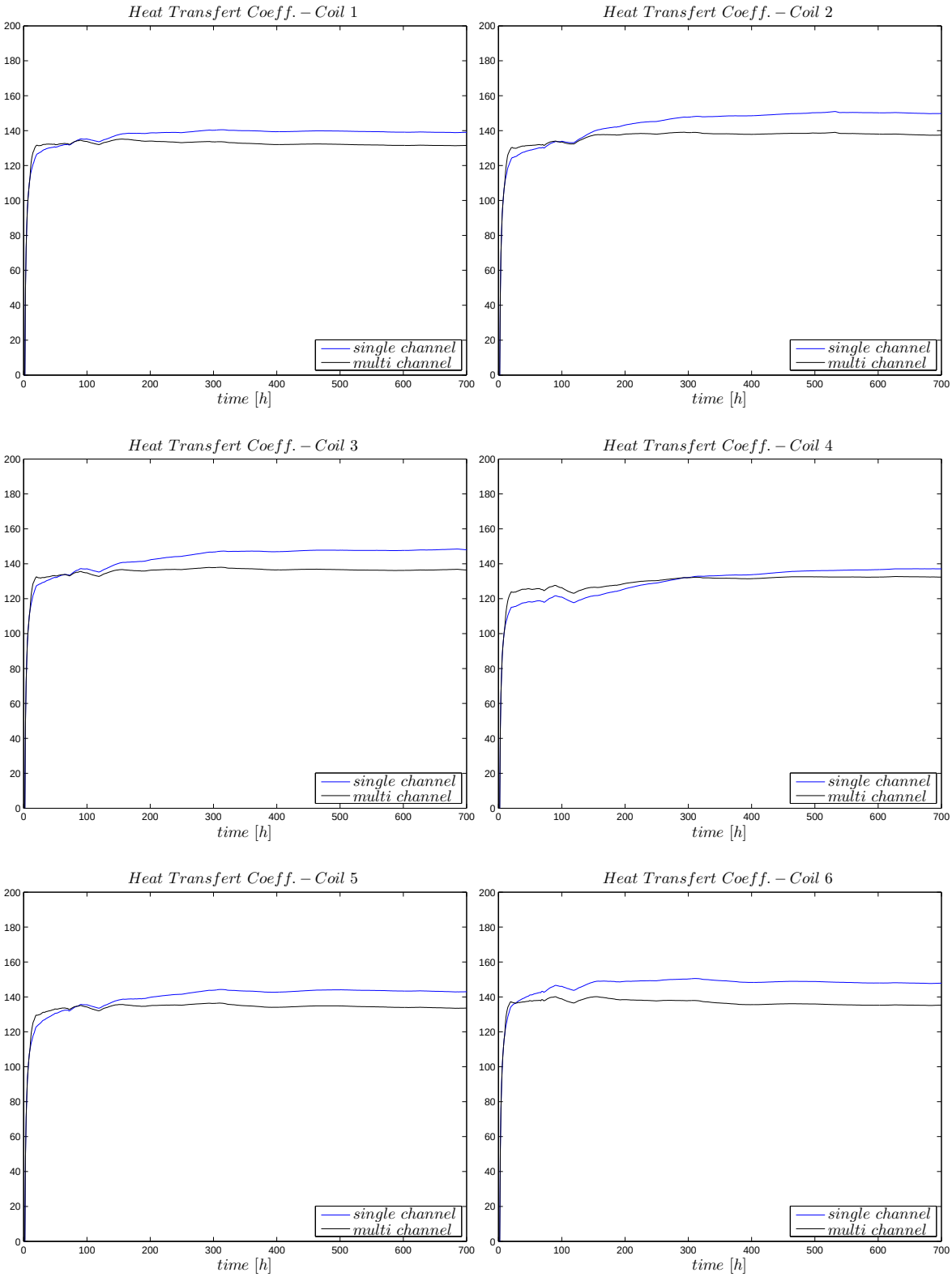

Figure 6.8: Comparison of the estimation profiles of the heat transfer coefficient coils obtained when filtering the plant measurements by the single and multiple channel state-parameter decoupling filter.

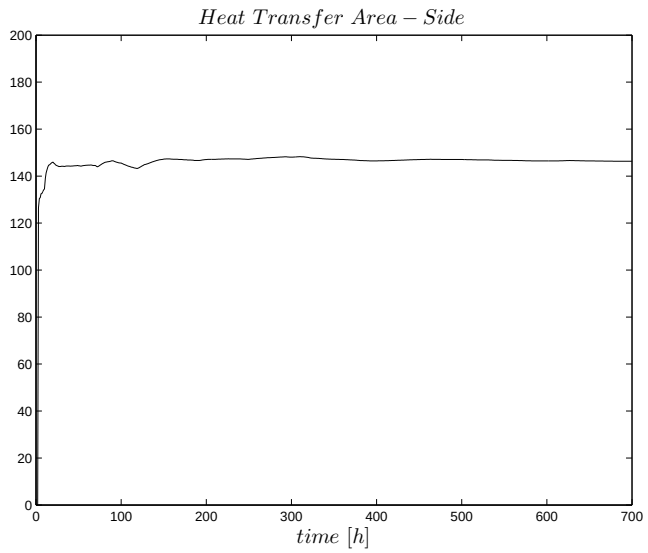

Figure 6.9: Estimation profile of the heat transfer area reactor side obtained when filtering the plant measurements by the multichannel state-parameter decoupling filter.

also considered. The corresponding extended estimation problem has been then solved by exploiting the novel multi-channel scheme, based on an array of state-parameter decoupling filters, depicted in Section 5.4.2. The experimental results on a real data set, collected over a full operational cycle of the pyrolysis plant, confirm the validity of both the single channel and multi-channels schemes. Finally, a GUI implementing a real-time version of the single-channel estimation algorithm, working off-line on datasets of the pyrolysis reactor, has been developed. An improved version of this software application, currently under development, will be provided soon to the plant technicians, to monitor on-line all the operating indicators which allow to determine a better regeneration cycle time of the reactor, and consequently, to reduce the off-line periods of the plant.

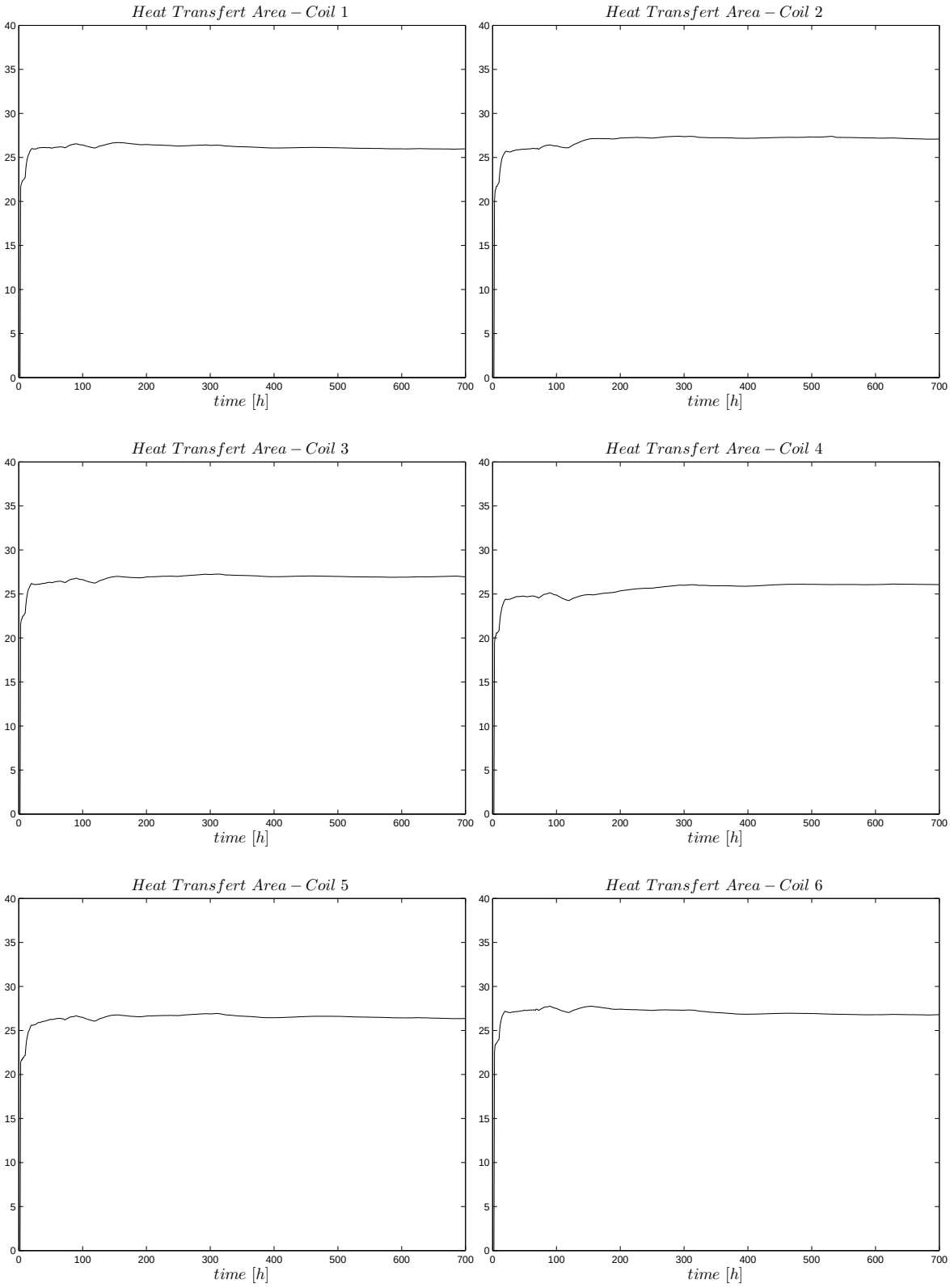

Figure 6.10: Estimation profile of the heat transfer area reactor side and coils obtained when filtering the plant measurements by the multichannel state-parameter decoupling filter.

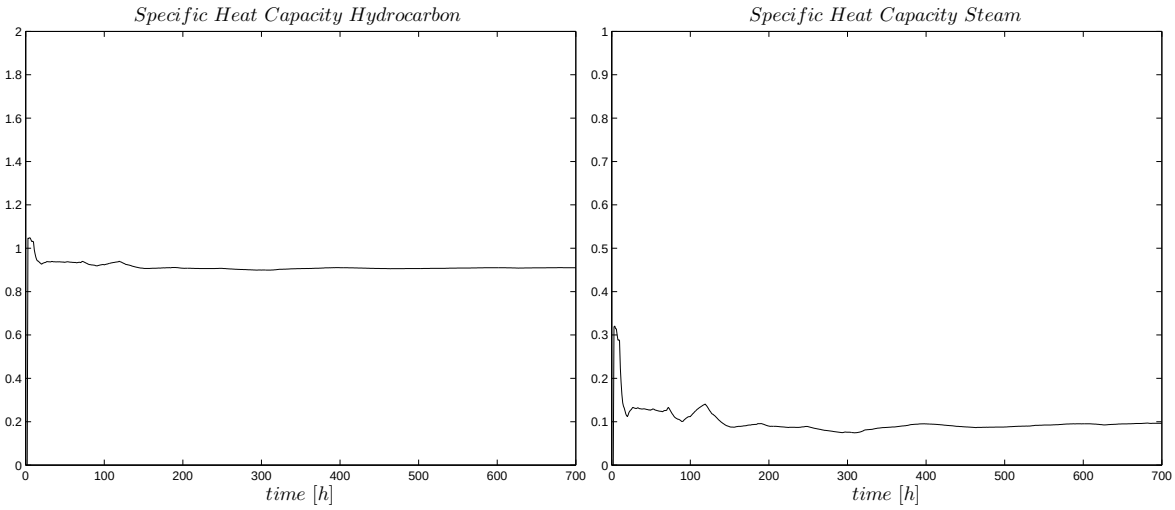

Figure 6.11: Estimation profile of the specific heat transfer capacity coefficient of hydrocarbon and steam obtained when filtering the plant measurements by the multichannel state-parameter decoupling filter.

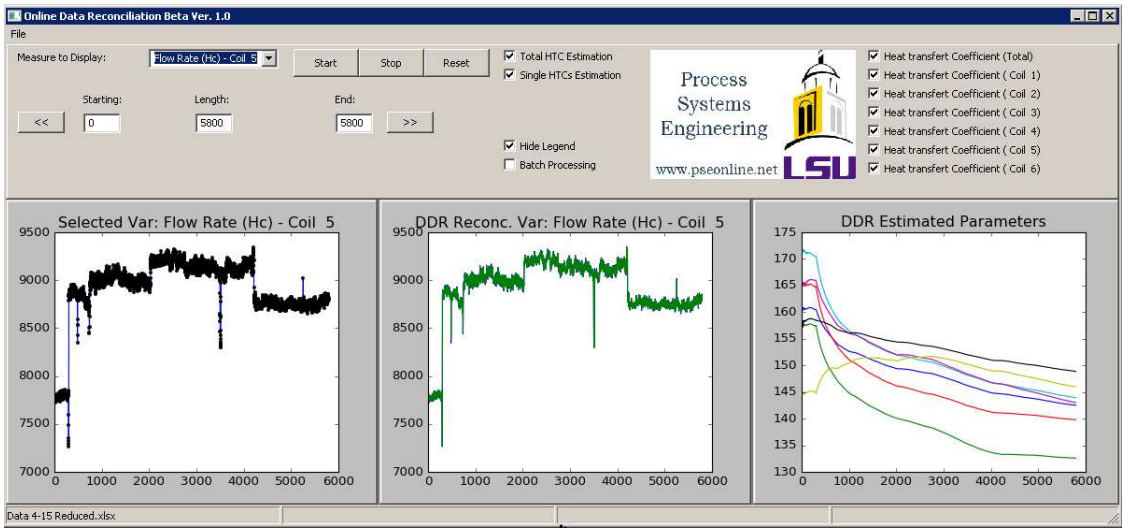

Figure 6.12: Python GUI for the DDR State-Parameter single channel estimation algorithm

Conclusion and Future Work

This dissertation has explored two different issues, both related to the subject of supervision and diagnosis of industrial systems. Within the topic of fault detection and diagnosis, this research has addressed the problem of discriminating between different faults which could affect both sensors and actuators of a generic system. Towards the topic of data reconciliation and parameter estimation instead, the problem of performing jointly and in real-time the reconciliation of measurements and the estimation of the model's parameters has been examined. The first part of the Thesis, has been devoted to introduce some indispensable concepts and the state-of-the-art of these two research areas. Then, the various contributions of this work have been explained and discussed, based on the same order of topics followed in the previous presentation.

In Chapter 1, the main fault diagnosis methodologies, i.e. model-based, signal-based and data-driven methods, including some of their combinations within the more recent hybrid approaches, have been reviewed, by focusing on those aspects which refer to the contributions developed in the Chapters 3 and 4 of is dissertation. Specially, the Beard Fault Detection Filter (BFDF) has been discussed as fault-disturbance decoupling strategy, as well as the use of SMOs as residual generators in the framework of robust diagnostic observers. Furthermore, other key concepts such as structured and directional residual sets, as well as their typical residual evaluation schemes based on the analysis of fault signatures, have been presented.

In Chapter 2, the main approaches to solve the the data reconciliation and parameter estimation problems, both in static and dynamic contexts, have been reviewed, by taking particular attention in discussing those concepts exploited in the contributions presented in the Chapters 5 and 6 of this dissertation. It is worth mentioning that two fundamental model formulations, i.e. LD and QSS, which allow to perform the DDR, have been specifically analyzed.

In Chapter 3, the novel proposal developed in this research to achieve a complete fault diagnosis has been presented. This method is based on an hybrid scheme, where the generation of residuals is performed by exploiting a suitable SMO filtering approach, while their evaluation by extending the concept of residual signature towards a time-varying setting, over a suitably designed augmented residual space. This strategy, which aims to solve the general issue of discriminating between different faults when not enough measurements are available, has been successfully applied on a SISO system, where different faults can affect both the input and output channel, but only a single residual signal can be generated and evaluated by the standard MB approaches. In this proposal, the main limit of the geometric approach to FDI suggested by Beard, related to the lack of robustness with respect to unknown inputs, has been overcome by exploiting the advantages provided by a robust residual generation based on SMOs. The proposed FDD architecture can be considered as a novel hybrid approach, since several different DD or SB methods can be exploited to analyze the time-varying fault signatures, generated in the augmented residual space which is spanned

by suitable residual sets, such as the two suggested in this work. This research is still ongoing. Indeed, currently, two different ways to achieve an automatic residual evaluation, based on a DD and a SB method, respectively, are being investigated, but no experimental results are available yet. Nevertheless, the two draft of proposals have been presented. The formulation of a systematic procedure for finding the optimal set of residuals which make signatures suitable for the fault isolation of a generic MIMO system is another challenging aspect of this proposal still under study. Further research should be done also to investigate the opportunity to apply different diagnostic observers, easier to design with respect to SMO, as residual generators. Furthermore, standing the structural equivalence between observer-based and parity space residual generation approaches, another interesting direction would be the evaluation of the latter as residual generators in the hybrid FDD scheme proposed here.

In Chapter 4, a practical application of the FDD scheme explained in Chapter 3 has been evaluated, based on real data acquired from one of the steam separator units of a thermal power plant. Two SMOs have been designed in order to test different fault configurations and issues, i.e. abrupt and incipient faults, on sensors and actuators, in open loop and closed loop systems. Indeed, each of the two SMOs, refers to a different sub-dynamic of the whole system, having a different feedback setting and a different set of sensors and actuators. The experimental results confirm the capability of such a geometric approach to discriminate among all the considered faulty conditions, even by means of a simple visual inspection of the fault signatures. Since the simulations were performed by corrupting the available healthy data with suitable multiplicative faults, it would be interesting to perform a more challenging evaluation of the developed FDD system, using real faulty data acquired from the plant.

In Chapter 5, the novel procedure which allows to implement jointly and in real-time DDR and parameter estimation has been presented. This method exploits a well-known filtering approach, based on the combination of fundamental concepts such as QSS and KF, and integrates an algorithm which allows to solve separately the problems of estimating state and parameters. Such a state-parameter decoupling procedure was already proposed for the treatment of bias in recursive filtering, but it was never applied for data reconciliation issues. Two different schemes, based on this novel state-parameter decoupling procedure, have been proposed in this Thesis to solve the parameter estimation problem. The single channel scheme allows to estimate a parameter set which makes satisfied the observability property of the considered model. The multi-channel scheme instead, by means of an array of l state-parameter decoupling filters of l channels each, resolve to the more challenging problem of estimating those sets of parameters which cause the observability loss of the resulting model. Research is currently ongoing, in order to provide a suitable formulation of the channel opening sequence for the l^2-Channels scheme, based on the observability analysis. Further research is needed also to analytically evaluate the convergence properties of both the proposed schemes, even tough, in principle, they should reflect the same algorithmic efficiency of the EKF approach.

In Chapter 6, the effectiveness and reliability of the proposal explained in Chapter 5 have been evaluated, by processing real measurements acquired from a pyrolysis reactor. The single-channel state-parameter decoupling filter performed successfully the estimation of some important indicators of the plant's malfunctioning, which cannot be directly measured, but can be considered as parameters. The more challenging estimation problem, related to a larger set of parameters which cause the observability loss of the resulting model, was also considered and solved by exploiting the multi-channel scheme. The experimental results on

different data sets, collected over full operational cycles of the pyrolysis plant, confirmed the validity of both the single channel and multi-channels schemes. A software GUI implementing a real-time version of the single-channel estimation algorithm, working off-line on datasets of the pyrolysis reactor, has been also developed. An improved version of this software application is currently under development, and will be provided soon to the plant technicians, to monitor on-line all the operating indicators which allow to determine a better regeneration cycle time of the reactor, and consequently, to reduce the off-line periods of the plant.

Bibliography

[Abid et al., 2011] Abid, M., Chen, W., Ding, S., and Khan, A. (2011). Optimal residual evaluation for nonlinear systems using post-filter and threshold. *International Journal of Control*, 84(3):526–539.

[Akhenak et al., 2013] Akhenak, A., Duviella, E., Bako, L., and Lecoeuche, S. (2013). Online fault diagnosis using recursive subspace identification: Application to a dam-gallery open channel system. *Control Engineering Practice*, 21(6):797 – 806.

[Aldian Ambark Shashoa et al., 2013] Aldian Ambark Shashoa, N., Kvaščev, G., Marjanović, A., and Djurović, Ž. (2013). Sensor fault detection and isolation in a thermal power plant steam separator. *Control Engineering Practice*, 21(7):908–916.

[Alwi et al., 2011] Alwi, H., Edwards, C., and Tan, C. P. (2011). *Fault detection and fault-tolerant control using sliding modes*. Springer Science & Business Media.

[Angeli and Chatzinikolaou, 2004] Angeli, C. and Chatzinikolaou, A. (2004). On-line fault detection techniques for technical systems: A survey. *INTERNATIONAL JOURNAL OF COMPUTER SCIENCE & APPLICATIONS, VOL*, 1(1):12–30.

[AYDMJ and Duin, 1999] AYDMJ, T. and Duin, R. (1999). Pump failure determination using support vector data description. *Lecture Notes in Computer Science*, pages 415–425.

[Bakshi and Stephanopoulos, 1993] Bakshi, B. R. and Stephanopoulos, G. (1993). Wave-net: A multiresolution, hierarchical neural network with localized learning. *AIChE Journal*, 39(1):57–81.

[Beard, 1971] Beard, R. V. (1971). *Failure Accommodation in Linear Systems Through Self-Reorganization*. PhD thesis, Massachusetts Institute of Technology, Cambridge, MA.

[Bejarano et al., 2011] Bejarano, F., Pisano, A., and Usai, E. (2011). Finite-time converging jump observer for switched linear systems with unknown inputs. *Nonlinear Analysis: Hybrid Systems*, 5(2):174–188.

[Benbouzid, 2000] Benbouzid, M. E. H. (2000). A review of induction motors signature analysis as a medium for faults detection. *IEEE transactions on industrial electronics*, 47(5):984–993.

[Biegler et al., 1986] Biegler, L., Damiano, J., and Blau, G. (1986). Nonlinear parameter estimation: a case study comparison. *AIChE Journal*, 32(1):29–45.

[Bo et al., 2012] Bo, M., Zhi-nong, J., and Zhong-qing, W. (2012). Development of the task-based expert system for machine fault diagnosis. In *Journal of Physics: Conference Series*, volume 364, page 012043. IOP Publishing.

[Bouchard, 2006] Bouchard, D. (2006). Automated time series segmentation for human motion analysis. *Center for Human Modeling and Simulation, University of Pennsylvania*.

[Bouzid and Champenois, 2013] Bouzid, M. B. K. and Champenois, G. (2013). New expressions of symmetrical components of the induction motor under stator faults. *IEEE Transactions on Industrial Electronics*, 60(9):4093–4102.

[Bryson, 1975] Bryson, A. (1975). *Applied Optimal Control: Optimization, Estimation and Control*. Halsted Press book. Taylor & Francis.

[Burnett et al., 1996] Burnett, R., Watson, J., and Elder, S. (1996). The application of modern signal processing techniques for use in rotor fault detection and location within three-phase induction motors. *Signal processing*, 49(1):57–70.

[Cabal-Yepez et al., 2013] Cabal-Yepez, E., Garcia-Ramirez, A. G., Romero-Troncoso, R. J., Garcia-Perez, A., and Osornio-Rios, R. A. (2013). Reconfigurable monitoring system for time-frequency analysis on industrial equipment through stft and dwt. *IEEE Transactions on Industrial Informatics*, 9(2):760–771.

[Carpenter and Grossberg, 1988] Carpenter, G. A. and Grossberg, S. (1988). The art of adaptive pattern recognition by a self-organizing neural network. *Computer*, 21(3):77–88.

[Castaños and Fridman, 2006] Castaños, F. and Fridman, L. (2006). Analysis and design of integral sliding manifolds for systems with unmatched perturbations. *Automatic Control, IEEE Transactions on*, 51(5):853–858.

[Chen and Lu, 2013] Chen, H. and Lu, S. (2013). Fault diagnosis digital method for power transistors in power converters of switched reluctance motors. *IEEE Transactions on Industrial Electronics*, 60(2):749–763.

[Chen and Patton, 1999] Chen, J. and Patton, R. J. (1999). Robust model-based fault diagnosis for dynamic systems.

[Chen et al., 2011] Chen, K.-Y., Long-Sheng, Chen, M.-C., and Lee, C.-L. (2011). Using svm based method for equipment fault detection in a thermal power plant. *Computers in Industry*, 62(1):42–50.

[Chester et al., 1984] Chester, D., Lamb, D., and Dhurjati, P. (1984). Rule-based computer alarm analysis in chemical process plants. In *Proceedings of the Seventh Annual Conference on Computer Technology*, pages 22–29. MICRO-DELCON 84, IEEE.

[Chetouani, 2011] Chetouani, Y. (2011). Change detection in a distillation column based on the generalized likelihood ratio approach. *Journal of Chemical Engineering & Process Technology*.

[Chong et al., 2011] Chong, U.-P. et al. (2011). Signal model-based fault detection and diagnosis for induction motors using features of vibration signal in two-dimension domain. *Strojniški vestnik-Journal of Mechanical Engineering*, 57(9):655–666.

[Chow and Willsky, 1984] Chow, E. and Willsky, A. (1984). Analytical redundancy and the design of robust failure detection systems. *IEEE Transactions on Automatic Control*, 29(7):603–614.

[Chow and Willsky, 1980] Chow, E. Y. and Willsky, A. S. (1980). Issues in the development of a general design algorithm for reliable failure detection. In *Decision and Control including the Symposium on Adaptive Processes, 1980 19th IEEE Conference on*, pages 1006–1012.

[Clark et al., 1975] Clark, R. N., Fosth, D. C., and Walton, V. M. (1975). Detecting instrument malfunctions in control systems. *IEEE Transactions on Aerospace and Electronic Systems*, AES-11(4):465–473.

[Climente-Alarcon et al., 2014] Climente-Alarcon, V., Antonino-Daviu, J. A., Riera-Guasp, M., and Vlcek, M. (2014). Induction motor diagnosis by advanced notch fir filters and the wigner–ville distribution. *IEEE Transactions on Industrial Electronics*, 61(8):4217–4227.

[Dai and Gao, 2013] Dai, X. and Gao, Z. (2013). From model, signal to knowledge: A data-driven perspective of fault detection and diagnosis. *IEEE Transactions on Industrial Informatics*, 9(4):2226–2238.

[Delmaire et al., 1994] Delmaire, G., Cassar, J. P., and Staroswiecki, M. (1994). Comparison of identification and parity space approaches for failure detection in single input single output systems. In *Control Applications, 1994., Proceedings of the Third IEEE Conference on*, pages 865–870 vol.2.

[Desai and Ray, 1984] Desai, M. and Ray, A. (1984). A fault detection and isolation methodology theory and application. In *American Control Conference, 1984*, pages 262–270.

[Ding, 2008] Ding, S. X. (2008). *Model-based fault diagnosis techniques*. Springer.

[Ding et al., 2013] Ding, S. X., Yin, S., Peng, K., Hao, H., and Shen, B. (2013). A novel scheme for key performance indicator prediction and diagnosis with application to an industrial hot strip mill. *IEEE Transactions on Industrial Informatics*, 9(4):2239–2247.

[Ding and Frank, 1990] Ding, X. and Frank, P. M. (1990). Fault detection via factorization approach. *Systems & Control Letters*, 14(5):431 – 436.

[Ding and Frank, 1991] Ding, X. S. and Frank, M. P. (1991). Frequency domain approach and threshold selector for robust model-based fault detection and isolation. In *Proc. IFAC Symp. on Safe Process*, pages 307–312. Baden Baden.

[Döhler and Mevel, 2013] Döhler, M. and Mevel, L. (2013). Subspace-based fault detection robust to changes in the noise covariances. *Automatica*, 49(9):2734 – 2743.

[Dong et al., 2010] Dong, G., Chongguang, W., Zhang, B., and Xin, M. (2010). Signed directed graph and qualitative trend analysis based fault diagnosis in chemical industry. *Chinese Journal of Chemical Engineering*, 18(2):265–276.

[Doraiswami et al., 2010] Doraiswami, R., Diduch, C. P., and Tang, J. (2010). A new diagnostic model for identifying parametric faults. *IEEE Transactions on Control Systems Technology*, 18(3):533–544.

[Ebrahimi et al., 2014] Ebrahimi, B. M., Roshtkhari, M. J., Faiz, J., and Khatami, S. V. (2014). Advanced eccentricity fault recognition in permanent magnet synchronous motors using stator current signature analysis. *IEEE Transactions on Industrial Electronics*, 61(4):2041–2052.

[Edelmayer et al., 1997] Edelmayer, A., Bokor, J., Szigeti, F., and Keviczky, L. (1997). Robust detection filter design in the presence of time-varying system perturbations. *Automatica*, 33(3).

[Edwards et al., 2000] Edwards, C., Spurgeon, S. K., and Patton, R. J. (2000). Sliding mode observers for fault detection and isolation. *Automatica*, 36(4):541–553.

[Efrat et al., 2007] Efrat, A., Fan, Q., and Venkatasubramanian, S. (2007). Curve matching, time warping, and light fields: New algorithms for computing similarity between curves. *Journal of Mathematical Imaging and Vision*, 27(3):203–216.

[Elshenawy and Awad, 2012] Elshenawy, L. M. and Awad, H. A. (2012). Recursive fault detection and isolation approaches of time-varying processes. *Industrial & Engineering Chemistry Research*, 51(29):9812–9824.

[Emami-Naeini et al., 1988] Emami-Naeini, A., Akhter, M. M., and Rock, S. M. (1988). Effect of model uncertainty on failure detection: the threshold selector. *IEEE Transactions on Automatic Control*, 33(12):1106–1115.

[Estima and Cardoso, 2013] Estima, J. O. and Cardoso, A. J. M. (2013). A new algorithm for real-time multiple open-circuit fault diagnosis in voltage-fed pwm motor drives by the reference current errors. *IEEE Transactions on Industrial Electronics*, 60(8):3496–3505.

[Fadda et al., 2015a] Fadda, G., Franceschelli, M., Pilloni, A., Pisano, A., Usai, E., Durovic, Z., Marjanović, A., Papic, V., Tadić, P., and Vujnović, S. (2015a). Robust decentralised estimation for large-scale systems (rodeo). In *Italy Serbia Day: Growth and Development through Science and Technology*, pages 45–50.

[Fadda et al., 2015b] Fadda, G., Pilloni, A., Pisano, A., Usai, E., Marjanović, A., and Vujnović, S. (2015b). Sensor fault diagnosis in water-steam power plant: A combined observer-based/pattern-recognition approach. In *Recent Advances in Sliding Modes (RASM), 2015 International Workshop on*, pages 1–7. IEEE.

[Fadda et al., 2016] Fadda, G., Pilloni, A., Pisano, A., Usai, E., Marjanović, A., and Vujnović, S. (2016). Multiple fault diagnosis by signature recognition of time-varying residuals. In *Control and Fault-Tolerant Systems (SysTol), 2016 3rd Conference on*, pages 245–250. IEEE.

[Faundez-Zanuy, 2007] Faundez-Zanuy, M. (2007). On-line signature recognition based on vq-dtw. *Pattern Recognition*, 40(3):981–992.

[Feng et al., 2013] Feng, Z., Liang, M., and Chu, F. (2013). Recent advances in time–frequency analysis methods for machinery fault diagnosis: a review with application examples. *Mechanical Systems and Signal Processing*, 38(1):165–205.

[Feng and Zuo, 2013] Feng, Z. and Zuo, M. J. (2013). Fault diagnosis of planetary gearboxes via torsional vibration signal analysis. *Mechanical Systems and Signal Processing*, 36(2):401–421.

[Fierrez et al., 2007] Fierrez, J., Ortega-Garcia, J., Ramos, D., and Gonzalez-Rodriguez, J. (2007). Hmm-based on-line signature verification: Feature extraction and signature modeling. *Pattern recognition letters*, 28(16):2325–2334.

[Frank and Ding, 1993] Frank, M. P. and Ding, X. S. (1993). Frequency domain approach to minimizing detectable faults in fdi systems. *Journal Applied Mathematics and Computer Science*, 3(3):417–443.

[Frank, 1993] Frank, P. (1993). Advances in observer-based fault diagnosis. In *TOOLDIAG'93*, volume 3, pages 817–836.

[Frank, 1996] Frank, P. (1996). Analytical and qualitative model-based fault diagnosis a survey and some new results. *European Journal of Control*, 2(1):6 – 28.

[Frank, 1987] Frank, P. M. (1987). *Fault Diagnosis in Dynamic Systems via State Estimation - a Survey*, pages 35–98. Springer Netherlands.

[Frank, 1990] Frank, P. M. (1990). Fault diagnosis in dynamic systems using analytical and knowledge-based redundancy—a survey and some new results. *Automatica*, 26(3):459–474.

[Frank, 1994] Frank, P. M. (1994). Enhancement of robustness in observer-based fault detection. *International Journal of Control*, 59(4):955–981.

[Freire et al., 2013] Freire, N. M., Estima, J. O., and Cardoso, A. J. M. (2013). Open-circuit fault diagnosis in pmsg drives for wind turbine applications. *IEEE Transactions on Industrial Electronics*, 60(9):3957–3967.

[Friedland, 1969] Friedland, B. (1969). Treatment of bias in recursive filtering. *IEEE Transactions on Automatic Control*, 14(4):359–367.

[Gao et al., 2015a] Gao, Z., Cecati, C., and Ding, S. X. (2015a). A survey of fault diagnosis and fault-tolerant techniques part i: Fault diagnosis with model-based and signal-based approaches. *IEEE Transactions on Industrial Electronics*, 62(6):3757–3767.

[Gao et al., 2015b] Gao, Z., Cecati, C., and Ding, S. X. (2015b). A survey of fault diagnosis and fault-tolerant techniques part ii: Fault diagnosis with knowledge-based and hybrid/active approaches. *IEEE Transactions on Industrial Electronics*, 62(6):3768–3774.

[Gao et al., 2007] Gao, Z., Wang, H., and Chai, T. (2007). A robust fault detection filtering for stochastic distribution systems via descriptor estimator and parametric gain design. *IET Control Theory Applications*, 1(5):1286–1293.

[Gelb, 1974] Gelb, A. (1974). *Applied Optimal Estimation*. MIT Press.

[Gertler, 1992] Gertler, J. (1992). Analytical redundancy methods in fault detection and isolation: Survey and synthesis. In ISERMANN, A. and FREYERMUTH, B., editors, *Fault Detection, Supervision and Safety for Technical Processes 1991*, IFAC Symposia Series, pages 9 – 21.

[Gertler, 1995] Gertler, J. (1995). Diagnosing parametric faults: from parameter estimation to parity relations. In *American Control Conference, Proceedings of the 1995*, volume 3, pages 1615–1620.

[Gertler, 1998] Gertler, J. (1998). *Fault Detection and Diagnosis in Engineering Systems*. Electrical Engineering and Electronics. Taylor & Francis.

[Gertler and Singer, 1990] Gertler, J. and Singer, D. (1990). A new structural framework for parity equation-based failure detection and isolation. *Automatica*, 26(2):381 – 388.

[Gertler and Kunwer, 1995] Gertler, J. J. and Kunwer, M. M. (1995). Optimal residual decoupling for robust fault diagnosis. *International Journal of Control*, 61(2):395–421.

[Gill et al., 1986] Gill, P., Murray, W., Sauders, M., and Wright, M. (1986). User's guide for npsol (version 4.0): A fortran program for nonlinear programming. In *Technical Report SOL 86-2, Department of Operations Research, Stanford University*.

[Gong and Qiao, 2013] Gong, X. and Qiao, W. (2013). Bearing fault diagnosis for direct-drive wind turbines via current-demodulated signals. *IEEE Transactions on Industrial Electronics*, 60(8):3419–3428.

[Gritli et al., 2013] Gritli, Y., Zarri, L., Rossi, C., Filippetti, F., Capolino, G.-A., and Casadei, D. (2013). Advanced diagnosis of electrical faults in wound-rotor induction machines. *IEEE Transactions on Industrial Electronics*, 60(9):4012–4024.

[Guo et al., 2014] Guo, Y., Na, J., Li, B., and Fung, R.-F. (2014). Envelope extraction based dimension reduction for independent component analysis in fault diagnosis of rolling element bearing. *Journal of Sound and Vibration*, 333(13):2983–2994.

[He et al., 2013] He, D., Li, R., and Zhu, J. (2013). Plastic bearing fault diagnosis based on a two-step data mining approach. *IEEE Transactions on Industrial Electronics*, 60(8):3429–3440.

[Henley, 1984] Henley, E. (1984). Application of expert systems to fault diagnosis. In *AIChE annual meeting, San Francisco, CA*.

[Hong and Dhupia, 2014] Hong, L. and Dhupia, J. S. (2014). A time domain approach to diagnose gearbox fault based on measured vibration signals. *Journal of Sound and Vibration*, 333(7):2164–2180.

[Hoskins et al., 1991] Hoskins, J., Kaliyur, K., and Himmelblau, D. M. (1991). Fault diagnosis in complex chemical plants using artificial neural networks. *AIChE Journal*, 37(1):137–141.

[Hu and Tsai, 2008] Hu, J.-S. and Tsai, M.-C. (2008). Design of robust stabilization and fault diagnosis for an auto-balancing two-wheeled cart. *Advanced Robotics*, 22(2-3):319–338.

[Isermann, 1984] Isermann, R. (1984). Process fault detection based on modeling and estimation methods: A survey. *Automatica*, 20(4):387 – 404.

[Isermann, 1993] Isermann, R. (1993). Fault diagnosis of machines via parameter estimation and knowledge processingtutorial paper. *Automatica*, 29(4):815 – 835.

[Isermann, 1997] Isermann, R. (1997). Supervision, fault-detection and fault-diagnosis methods an introduction. *Control Engineering Practice*, 5(5):639 – 652.

[Isermann, 2006] Isermann, R. (2006). *Fault-Diagnosis Systems: An Introduction from Fault Detection to Fault Tolerance*. Springer Berlin Heidelberg.

[Isermann and Ballé, 1997] Isermann, R. and Ballé, P. (1997). Trends in the application of model-based fault detection and diagnosis of technical processes. *Control Engineering Practice*, 5(5):709 – 719.

[Jain et al., 2002] Jain, A. K., Griess, F. D., and Connell, S. D. (2002). On-line signature verification. *Pattern recognition*, 35(12):2963–2972.

[Jazwinski, 1970] Jazwinski, A. (1970). *Stochastic Processes and Filtering Theory*. Mathematics in science and engineering. Academic Press.

[Jiang et al., 2014] Jiang, B., Xiang, J., and Wang, Y. (2014). Rolling bearing fault diagnosis approach using probabilistic principal component analysis denoising and cyclic bispectrum. *Journal of Vibration and Control*, page 1077546314547533.

[Joksimović et al., 2013] Joksimović, G. M., Riger, J., Wolbank, T. M., Perić, N., and Vašak, M. (2013). Stator-current spectrum signature of healthy cage rotor induction machines. *IEEE Transactions on Industrial Electronics*, 60(9):4025–4033.

[Jones, 1973] Jones, H. L. (1973). *Failure Detection in Linear Systems*. PhD thesis, Massachusetts Institute of Technology, Cambridge, MA.

[Kalman, 1960] Kalman, R. E. (1960). A new approach to linear filtering and prediction problems. *Transactions of the ASME - Journal of Basic Engineering*, (82 (Series D)):35–45.

[Kamen and Su, 1999] Kamen, E. and Su, J. (1999). *Introduction to Optimal Estimation*. Advanced Textbooks in Control and Signal Processing. Springer London.

[Keogh et al., 2004] Keogh, E., Chu, S., Hart, D., and Pazzani, M. (2004). Segmenting time series: A survey and novel approach. *Data mining in time series databases*, 57:1–22.

[Keogh and Ratanamahatana, 2005] Keogh, E. and Ratanamahatana, C. A. (2005). Exact indexing of dynamic time warping. *Knowledge and information systems*, 7(3):358–386.

[Ketabdar et al., 2005] Ketabdar, H., Richiardi, J., and Drygajlo, A. (2005). Global feature selection for on-line signature verification. In *Proceedings International Graphonomics Society 2005 Conference*.

[Kim et al., 1990] Kim, I.-W., Liebman, M. J., and Edgar, T. F. (1990). Robust error-in-variables estimation using nonlinear programming techniques. *AIChE Journal*, 36(7):985–993.

[Kodavade and Apte, 2012] Kodavade, D. V. and Apte, S. D. (2012). A universal object oriented expert system frame work for fault diagnosis.

[Kvaščev et al., 2011] Kvaščev, G., Marjanović, A., and Djurović, Ž. (2011). Robust adaptive system identification of steam separator process in thermal power plants. volume 15, pages 49–53.

[Lasdon and Waren, 1977] Lasdon, L. and Waren, A. (1977). *Generalized reduced gradient software for linearly and nonlinearly constrained problems*. Graduate School of Business, University of Texas at Austin.

[Lee et al., 2004] Lee, J., Yoon, H.-S., Soh, J., Chun, B. T., and Chung, Y. K. (2004). Using geometric extrema for segment-to-segment characteristics comparison in online signature verification. *Pattern Recognition*, 37(1):93–103.

[Lee et al., 1996] Lee, L. L., Berger, T., and Aviczer, E. (1996). Reliable online human signature verification systems. *Pattern Analysis and Machine Intelligence, IEEE Transactions on*, 18(6):643–647.

[Levant, 1998] Levant, A. (1998). Robust exact differentiation via sliding mode technique. *Automatica*, 34(3):379–384.

[Li et al., 2006] Li, B., Zhang, D., and Wang, K. (2006). Online signature verification based on null component analysis and principal component analysis. *Pattern analysis and applications*, 8(4):345–356.

[Magni, 1995] Magni, J. F. (1995). On continuous-time parameter identification by using observers. *IEEE Transactions on Automatic Control*, 40(10):1789–1792.

[Mah, 2013] Mah, R. S. (2013). *Chemical process structures and information flows*. Elsevier.

[Marteau, 2009] Marteau, P.-F. (2009). Time warp edit distance with stiffness adjustment for time series matching. *Pattern Analysis and Machine Intelligence, IEEE Transactions on*, 31(2):306–318.

[Martí et al., 2014] Martí, L., Sanchez-Pi, N., Molina, J. M., and García, A. C. B. (2014). Combining support vector machines and segmentation algorithms for efficient anomaly detection: A petroleum industry application. In *International Joint Conference SOCO14-CISIS14-ICEUTE14*, pages 269–278. Springer.

[Massoumnia, 1986] Massoumnia, M. A. (1986). A geometric approach to the synthesis of failure detection filters. *IEEE Transactions on Automatic Control*, 31(9):839–846.

[Maurya et al., 2007] Maurya, M. R., Rengaswamy, R., and Venkatasubramanian, V. (2007). A signed directed graph and qualitative trend analysis-based framework for incipient fault diagnosis. *Chemical Engineering Research and Design*, 85(10):1407–1422.

[Ming-Cong et al., 2010] Ming-Cong, D., INOUE, A., and EDAHIRO, K. (2010). Fault detection system design for actuator of a thermal process using operator based approach. *Acta Automatica Sinica*, 36(4):580–585.

[Nakamura et al., 2013] Nakamura, T., Taki, K., Nomiya, H., Seki, K., and Uehara, K. (2013). A shape-based similarity measure for time series data with ensemble learning. *Pattern Analysis and Applications*, 16(4):535–548.

[Nalwa, 1997] Nalwa, V. S. (1997). Automatic on-line signature verification. *Proceedings of the IEEE*, 85(2):215–239.

[Namdari et al., 2014] Namdari, M., Jazayeri-Rad, H., and Hashemi, S.-J. (2014). Process fault diagnosis using support vector machines with a genetic algorithm based parameter tuning. *Journal of Automation and Control*, 2(1):1–7.

[Nan et al., 2008] Nan, C., Khan, F., and Iqbal, M. T. (2008). Real-time fault diagnosis using knowledge-based expert system. *process safety and environmental protection*, 86(1):55–71.

[Nandi et al., 2011] Nandi, S., Ilamparithi, T., Lee, S., and Hyun, D. (2011). Detection of eccentricity faults in induction machines based on nameplate parameters. *Industrial Electronics, IEEE Transactions on*, 58(5):1673–1683.

[Nandi et al., 2005] Nandi, S., Toliyat, H. A., and Li, X. (2005). Condition monitoring and fault diagnosis of electrical motors-a review. *IEEE transactions on energy conversion*, 20(4):719–729.

[Narasimhan and Jordache, 1999] Narasimhan, S. and Jordache, C. (1999). *Data reconciliation and gross error detection: An intelligent use of process data*. Gulf Professional Publishing.

[Orani et al., 2010] Orani, N., Pisano, A., and Usai, E. (2010). Fault diagnosis for the vertical three-tank system via high-order sliding-mode observation. *Journal of the Franklin Institute*, 347(6):923–939.

[Pachchigar, 2013] Pachchigar, M. (2013). Complete sensor-to-bits solution simplifies industrial data-acquisition system design. *Analoge Dialogue: Technical magazine of Analog Devices*, 47(2):21–24.

[Pan et al., 2012] Pan, N., Wu, X., Chi, Y., Liu, X., and Liu, C. (2012). Combined failure acoustical diagnosis based on improved frequency domain blind deconvolution. In *Journal of Physics: Conference Series*, volume 364, page 012078. IOP Publishing.

[Park et al., 1994] Park, J., Rizzoni, G., and Ribbens, W. B. (1994). On the representation of sensor faults in fault detection filters. *Automatica*, 30(11):1793 – 1795.

[Patton et al., 2010] Patton, R. J., Frank, P. M., and Clark, R. N. (2010). *Issues of Fault Diagnosis for Dynamic Systems*. Springer Publishing Company, Incorporated, 1st edition.

[Patton et al., 1989] Patton, R. J., Frank, P. M., and Clarke, R. N. (1989). *Fault Diagnosis in Dynamic Systems: Theory and Application*. Prentice-Hall, Inc.

[Pilloni et al., 2012] Pilloni, A., Pisano, A., Usai, E., and Puche-Panadero, R. (2012). Detection of rotor broken bar and eccentricity faults in induction motors via second order sliding mode observer. In *CDC*, pages 7614–7619.

[Pilloni et al., 2013] Pilloni, A., Usai, E., Edwards, C., Pisano, A., and Menon, P. P. (2013). Decentralized state estimation in connected systems. In *System, Structure and Control*, volume 5, pages 421–426.

[Pillosu et al., 2012] Pillosu, S., Pisano, A., and Usai, E. (2012). Unknown-input observation techniques for infiltration and water flow estimation in open-channel hydraulic systems. *Control Engineering Practice*, 20(12):1374–1384.

[Pisano et al., 2014] Pisano, A., Rapaić, M. R., and Usai, E. (2014). Discontinuous dynamical systems for fault detection. a unified approach including fractional and integer order dynamics. *Mathematics and Computers in Simulation*, 95:111–125.

[Potter and Sunman, 1977] Potter, I. E. and Sunman, M. C. (1977). Thresholdless redundancy management with arrays of skewed instruments. *Integrity in Electronic Flight Control Systems, AGARDOGRAPH-224*, 15:11–25.

[Reilly and Patino-Lea1, 1981] Reilly, P. M. and Patino-Lea1, H. (1981). A bayesian study of the error-in-variables model. *Technometrics*, 23(3):221–231.

[Romagnoli and Gani, 1983] Romagnoli, J. and Gani, R. (1983). Studies of distributed parameter systems: Decoupling the state-parameter estimation problem. *Chemical Engineering Science*, 38(11):1831 – 1843.

[Romagnoli and Sánchez, 2000] Romagnoli, J. and Sánchez, M. (2000). *Data Processing and Reconciliation for Chemical Process Operations*. Process systems engineering. Academic Press.

[Rychetsky et al., 1999] Rychetsky, M., Ortmann, S., and Glesner, M. (1999). Support vector approaches for engine knock detection. In *Neural Networks, 1999. IJCNN'99. International Joint Conference on*, volume 2, pages 969–974. IEEE.

[Sahri and Yusof, 2014] Sahri, Z. B. and Yusof, R. B. (2014). Support vector machine-based fault diagnosis of power transformer using k nearest-neighbor imputed dga dataset. *Journal of Computer and Communications*, 2(09):22.

[Samara et al., 2008] Samara, P. A., Fouskitakis, G. N., Sakellariou, J. S., and Fassois, S. D. (2008). A statistical method for the detection of sensor abrupt faults in aircraft control systems. *IEEE Transactions on Control Systems Technology*, 16(4):789–798.

[Sari, 2014] Sari, A. H. A. (2014). *Data-Driven Design of Fault Diagnosis Systems: Nonlinear Multimode Processes*. Springer Science & Business.

[Seshadrinath et al., 2014] Seshadrinath, J., Singh, B., and Panigrahi, B. (2014). Vibration analysis based interturn fault diagnosis in induction machines. *IEEE Transactions on Industrial Informatics*, 10(1):340–350.

[Shahbazi et al., 2013] Shahbazi, M., Jamshidpour, E., Poure, P., Saadate, S., and Zolghadri, M. R. (2013). Open-and short-circuit switch fault diagnosis for nonisolated dc–dc converters using field programmable gate array. *IEEE Transactions on Industrial Electronics*, 60(9):4136–4146.

[Shahriar et al., 2013] Shahriar, M. R., Ahsan, T., and Chong, U. (2013). Fault diagnosis of induction motors utilizing local binary pattern-based texture analysis. *EURASIP Journal on Image and Video Processing*, 2013(1):1–11.

[Sheibat-Othman et al., 2014] Sheibat-Othman, N., Laouti, N., Valour, J.-P., and Othman, S. (2014). Support vector machines combined to observers for fault diagnosis in chemical reactors. *The Canadian Journal of Chemical Engineering*, 92(4):685–695.

[Shtessel et al., 2013] Shtessel, Y., Edwards, C., Fridman, L., and Levant, A. (2013). *Sliding Mode Control and Observation*. Control Engineering. Springer New York.

[Simani et al., 2010] Simani, S., Fantuzzi, C., and Patton, R. (2010). *Model-based Fault Diagnosis in Dynamic Systems Using Identification Techniques*. Advances in Industrial Control. Springer London.

[Simon, 2010] Simon, D. (2010). Kalman filtering with state constraints: a survey of linear and nonlinear algorithms. *Control Theory & Applications*, 4:1303–1318.

[Sobhani-Tehrani and Khorasani, 2009] Sobhani-Tehrani, E. and Khorasani, K. (2009). *Fault diagnosis of Nonlinear Systems Using a Hybrid Approach*, volume 383. Springer.

[Soualhi et al., 2013] Soualhi, A., Clerc, G., and Razik, H. (2013). Detection and diagnosis of faults in induction motor using an improved artificial ant clustering technique. *IEEE Transactions on Industrial Electronics*, 60(9):4053–4062.

[Stanley and Mah, 1977] Stanley, G. and Mah, R. (1977). Estimation of flows and temperatures in process networks. *AIChE Journal*, 23(5):642–650.

[Staroswiecki et al., 1993] Staroswiecki, M., Cassar, J. P., and Cocquempot, V. (1993). Generation of optimal structured residuals in the parity space. In *12th IFAC World Congress*, volume 8, pages 299–305.

[Sun et al., 2012] Sun, J. P., Gao, M., and Li, Y. L. (2012). Fault prediction method research of the power plant fan. *Advanced Materials Research*, 580:99–104.

[Tadić et al., 2012] Tadić, P., Durovic, Z., Kovacevic, B., and Papic, V. (2012). Fault diagnosis for steam separators based on parameter identification and cusum classification. In *Industrial Technology (ICIT), 2012 IEEE International Conference on*, pages 248–253. IEEE.

[Tan and Edwards, 2002] Tan, C. P. and Edwards, C. (2002). Sliding mode observers for detection and reconstruction of sensor faults. *Automatica*, 38(10):1815–1821.

[Tang et al., 2010] Tang, B., Liu, W., and Song, T. (2010). Wind turbine fault diagnosis based on morlet wavelet transformation and wigner-ville distribution. *Renewable Energy*, 35(12):2862–2866.

[Tjoa and Biegler, 1992] Tjoa, I.-B. and Biegler, L. (1992). Reduced successive quadratic programming strategy for errors-in-variables estimation. *Computers & chemical engineering*, 16(6):523–533.

[Tsai et al., 2013] Tsai, D.-M., Wu, S.-C., and Chiu, W.-Y. (2013). Defect detection in solar modules using ica basis images. *IEEE Transactions on Industrial Informatics*, 9(1):122–131.

[Ungar et al., 1990] Ungar, L., Powell, B., and Kamens, S. (1990). Adaptive networks for fault diagnosis and process control. *Computers & Chemical Engineering*, 14(4-5):561–572.

[Utkin, 1992] Utkin, V. I. (1992). *Sliding Modes in Control and Optimization*, volume 116. Springer.

[Vaidyanathan and Venkatasubramanian, 1992] Vaidyanathan, R. and Venkatasubramanian, V. (1992). Representing and diagnosing dynamic process data using neural networks. *Engineering Applications of Artificial Intelligence*, 5(1):11–21.

[Valko and Vajda, 1987] Valko, P. and Vajda, S. (1987). An extended marquardt-type procedure for fitting error-in-variables models. *Computers & chemical engineering*, 11(1):37–43.

[Venkatasubramanian and Chan, 1989] Venkatasubramanian, V. and Chan, K. (1989). A neural network methodology for process fault diagnosis. *AIChE Journal*, 35(12):1993–2002.

[Venkatasubramanian et al., 2003a] Venkatasubramanian, V., Rengaswamy, R., and Kavuri, S. N. (2003a). A review of process fault detection and diagnosis: Part ii: Qualitative models and search strategies. *Computers & Chemical Engineering*, 27(3):313 – 326.

[Venkatasubramanian et al., 2003b] Venkatasubramanian, V., Rengaswamy, R., Kavuri, S. N., and Yin, K. (2003b). A review of process fault detection and diagnosis: Part iii: Process history based methods. *Computers & Chemical Engineering*, 27(3):327 – 346.

[Venkatasubramanian et al., 2003c] Venkatasubramanian, V., Rengaswamy, R., Yin, K., and Kavuri, S. N. (2003c). A review of process fault detection and diagnosis: Part i: Quantitative model-based methods. *Computers & Chemical Engineering*, 27(3):293 – 311.

[Venkatasubramanian et al., 1990] Venkatasubramanian, V., Vaidyanathan, R., and Yamamoto, Y. (1990). Process fault detection and diagnosis using neural networksi. steady-state processes. *Computers & Chemical Engineering*, 14(7):699–712.

[Viswanadham et al., 1987] Viswanadham, N., Taylor, J., and Luce, E. (1987). A frequency-domain approach to failure detection and isolation with application to ge-21 turbine engine control systems. *Control Theory and Advanced Applications (C-TAT)*, 3(1):45–72.

[Vlachos et al., 2002] Vlachos, M., Kollios, G., and Gunopulos, D. (2002). Discovering similar multidimensional trajectories. In *Data Engineering, 2002. Proceedings. 18th International Conference on*, pages 673–684. IEEE.

[Wang et al., 2008] Wang, X., Kruger, U., Irwin, G. W., McCullough, G., and McDowell, N. (2008). Nonlinear pca with the local approach for diesel engine fault detection and diagnosis. *IEEE Transactions on Control Systems Technology*, 16(1):122–129.

[Watanabe et al., 1989] Watanabe, K., Matsuura, I., Abe, M., Kubota, M., and Himmelblau, D. (1989). Incipient fault diagnosis of chemical processes via artificial neural networks. *AIChE journal*, 35(11):1803–1812.

[Weiss et al., 1996] Weiss, G., Romagnoli, J., and Islam, K. (1996). Data reconciliation: an industrial case study. *Computers & Chemical Engineering*, 20(12):1441 – 1449.

[White and Speyer, 1986] White, J. E. and Speyer, J. L. (1986). Detection filter design: Spectral theory and algorithms. In *American Control Conference, 1986*, pages 1475–1481.

[Whiteley and Davis, 1994] Whiteley, J. R. and Davis, J. (1994). A similarity-based approach to interpretation of sensor data using adaptive resonance theory. *Computers & chemical engineering*, 18(7):637–661.

[Wijayasekara et al., 2014] Wijayasekara, D., Linda, O., Manic, M., and Rieger, C. (2014). Fn-dfe: Fuzzy-neural data fusion engine for enhanced resilient state-awareness of hybrid energy systems. *IEEE transactions on cybernetics*, 44(11):2065–2075.

[Wu and Li, 2009] Wu, S. and Li, Y. F. (2009). Flexible signature descriptions for adaptive motion trajectory representation, perception and recognition. *Pattern Recognition*, 42(1):194–214.

[Wüennenberg, 1990] Wüennenberg, J. (1990). *Observer-based fault detection in dynamic systems*. PhD thesis, University of Duisburg, Fachgebiet Mess- und Regelungstechnik.

[Wünnenberg and Frank, 1987] Wünnenberg, J. and Frank, P. M. (1987). *Sensor Fault Detection via Robust Observers*, pages 147–160. Springer Netherlands.

[Xiang and Yan, 2014] Xiang, L. and Yan, X. (2014). A self-adaptive time-frequency analysis method based on local mean decomposition and its application in defect diagnosis. *Journal of Vibration and Control*, page 1077546314538992.

[Yan and Gao, 2006] Yan, R. and Gao, R. X. (2006). Hilbert–huang transform-based vibration signal analysis for machine health monitoring. *IEEE Transactions on instrumentation and measurement*, 55(6):2320–2329.

[Yan and Edwards, 2007] Yan, X.-G. and Edwards, C. (2007). Sensor fault detection and isolation for nonlinear systems based on a sliding mode observer. *International Journal of Adaptive Control and Signal Processing*, 21(8-9):657–673.

[Yin et al., 2014a] Yin, S., Ding, S. X., Xie, X., and Luo, H. (2014a). A review on basic data-driven approaches for industrial process monitoring. *IEEE Transactions on Industrial Electronics*, 61(11):6418–6428.

[Yin et al., 2014b] Yin, S., Gao, X., Karimi, H. R., and Zhu, X. (2014b). Study on support vector machine-based fault detection in tennessee eastman process. In *Abstract and Applied Analysis*, volume 2014. Hindawi Publishing Corporation.

[Zhang et al., 2013] Zhang, Y., Bingham, C., Gallimore, M., et al. (2013). Fault detection and diagnosis based on extensions of pca. *Advances in Military Technology*, 8(2):27–41.

[Zhang et al., 2014] Zhang, Y., Yang, N., and Li, S. (2014). Fault isolation of nonlinear processes based on fault directions and features. *IEEE Transactions on Control Systems Technology*, 22(4):1567–1572.

[Zhao et al., 2014] Zhao, X., Xue, Y., and Wang, T. (2014). "fault detection of batch process based on multi-way kernel t-pls,. *J. Chem. Pharm. Res*, 6(7):338–346.